INFORMATION TO USERS

This manuscript has been reproduced from the microfilm master. UMI films the text directly from the original or copy submitted. Thus, some thesis and dissertation copies are in typewriter face, while others may be from any type of computer printer.

The quality of this reproduction is dependent upon the quality of the copy submitted. Broken or indistinct print, colored or poor quality illustrations and photographs, print bleedthrough, substandard margins, and improper alignment can adversely affect reproduction.

In the unlikely event that the author did not send UMI a complete manuscript and there are missing pages, these will be noted. Also, if unauthorized copyright material had to be removed, a note will indicate the deletion.

Oversize materials (e.g., maps, drawings, charts) are reproduced by sectioning the original, beginning at the upper left-hand corner and continuing from left to right in equal sections with small overlaps. Each original is also photographed in one exposure and is included in reduced form at the back of the book.

Photographs included in the original manuscript have been reproduced xerographically in this copy. Higher quality 6" x 9" black and white photographic prints are available for any photographs or illustrations appearing in this copy for an additional charge. Contact UMI directly to order.

UMI®

Bell & Howell Information and Learning
300 North Zeeb Road, Ann Arbor, MI 48106-1346 USA
800-521-0600

On the Fretting Wear of Nuclear Power Plant Heat Exchanger Tubes Using a Fracture Mechanics Approach: Theory and Verification

Yemane B. Gessesse

A Thesis

in

The Department

of

Mechanical Engineering

Presented in Partial Fulfillment of the Requirements
for the Degree of Doctor of Philosophy
at
Concordia University
Montreal, Quebec, Canada

August, 1997

ABSTRACT

On the Fretting Wear of Nuclear Power Plant Heat Exchanger Tubes Using a Fracture Mechanics Approach: Theory and Verification

Yemane B. Gessesse, Ph.D.

Concordia University, 1997

The analysis carried out in this research work, showed the inconsistencies observed in trying to identify the tube wear in heat exchangers. It is seen that the associated error could be an order of magnitude higher than the expected value, indicating the possibilities of failure at less than the predicted design life. Hence, the use of the commonly accepted concept of "work rate" as a scaling parameter is found to be questionable.

Wear models available in the open literature, have always been heavy on empirical formulations, because of the complexity of the process. Therefore, it is essential to verify any proposed model experimentally, using controlled parameters. The experimental study conducted for this research work was implemented for the verification of the new theoretical wear model developed. These experiments were carried out on two independent rigs to assert the validity of the new model.

The basis for this model was the extension of the delamination theory of wear for impact conditions (normal and oblique). It was essential to conduct a parametric study using a fracture mechanics approach, to quantify some variables for this model. The finite element method was implemented to study the crack nucleation zones and loading cycles required

for the formation of a crack. It was also implemented to study the probable direction a growing crack will follow, and to estimate the crack propagation rate.

Even though, all the quantities in the new wear model were determined theoretically, it was observed that the prediction of the wear volume using the trend line was close to the prediction of the wear using the experimental one. This discrepancy was adjusted using randomly selected three data points to properly calibrate the crack tip sliding displacement (CTSD). Calibrating the model using three data points or all the data points did not alter the results significantly, for most of the experiments.

In order to reduce the scatter observed while verifying the wear model, it is essential to introduce a characterization parameter. The new wear model is extended to incorporate this characterization, by implementing a force and displacement category multiplier to the work rate. The verification of the characterization process was conducted using the fretting experiments which were carried out on Inconel 600 tubes and stainless steel supports. The wear rate was properly characterized using the new macro/micro contact stress dependant model, developed through a fundamental understanding of the process.

ACKNOWLEDGMENTS

The author would like to express his sincere appreciation and gratitude to his technical supervisors, Dr. M.O.M. Osman and Dr. M.H. Attia, who were extremely helpful during the course of this research work. He has benefited considerably by working under the supervision of these accomplished researchers and feels fortunate to have been given this opportunity.

The financial support of the National Science and Engineering Research Council Grant (# N036 and N318) is gratefully acknowledged. The in kind (experimental setup and instrumentations) support of the Research Division of Ontario Hydro is acknowledged.

Thanks are also due to Mr. P. Schiewller, Mr. H. Huegner and Mr. J. Seeger, who were extremely helpful in machining the experimental setup and providing support as required through out the duration of the long term experiment. The author would like to thank the undergraduate students, T. Thiouvlier, J. Rous and X. Xi for assisting him in the drawings of the experimental setup.

Last but not least, the author would like to thank his spouse, Sylvia Pieper, for her patience and encouragement through many long working nights and weekends.

The author would like to dedicate this thesis to his parents.

TABLE OF CONTENT

LIST OF FIGURES

LIST OF TABLES

LIST OF SYMBOLS

a = the radius of the circular or cylinderical area contact (half Hertzian contact length)

A = apparent area of contact

A_C = peak to peak transverse amplitude of the tube without the restraining gap

A_d = mid-span peak-to-peak displacement

A_G = smaller of A_C or diametral gap

A_i = average surface area of wear for material i

As_{max} = maximum number of contact length for one cycle $[v_s t * s_f/(2af)]$

a_{asp} = asperity contact radius due to maximum Hertzian pressure of p_{0asp}

a_e and b_e = constant determined from the experimental results

a_{wh} = half the total axial contact length (a_{wt})

b = Burger's vector

c = radial clearance between the tube and the support, in.

c_4 = constant for type of contact (sphere on flat surface) and clearance

c_m = material dependant constants

C_e = critical effective crack length

C_{CTSD} = crack generated while being loaded

C_i = column number (i = 1,2,...6)

C_I = constant of integration

C_{rwld} = crack rewelded after the removal of the load

C_{tot} = total crack propagated

d_c = critical depth and diametral clearance

d_r = wear depth-rate

D = tube outside diameter, in.

D_i = displacement value for class i

D_{max} = maximum displacement taken as constant (10μm)

D_i = relative displacement in the i-axis $i = x$ or y

D_R = resultant relative displacement

e = coefficient of restitution

E = modulus of elasticity or Young's modulus

E^* = reduced modulus of elasticity

E_1 = Young's modulus for material 1

E_2 = Young's modulus for material 2

f = frequency of excitation in Hz

$F(t)$ = measured force as a function of time

F_i = normal force for class i

F_{max} = maximum resultant force for each experiment

F_N = dynamic normal contact force between the tube and support plate, lb

F_S = steady contact force between the tube and support plate, lb

F_x = force along the x-axis

F_y = force along the y-axis

F_R = resultant of F_x and F_y

G_i = shear modulus for material i

h = wear depth

h_i = wear depth of material i

h_t = total wear depth

H = material bulk hardness

I = energy of impact

k = yield strength in shear

k_s = specific wear-rate (estimated by means of a reference test under oscillating sliding condition)

k_0 , k_1 and k_2 = constants for corrosion

k_{d1} = dimension correcting factors

k_{d2} = dimension correcting factors

k_i = impact wear constants

k_I = stress intensity factor

k_m = material dependant constants

K = parametric constant

K_s = specific wear rate

K_I = non-dimensional impact wear coefficient

K_i = constant for material i

K_t = wear coefficient for tube, in.^{2}/lb

l = amplitude of oscillation

l_0 = initial condition (inclusion radius)

L = critical crack length

$L_s(t)$ = sliding velocity during contact as a function of time

L_p = pass length

L_b = life of the bearing

L_t = tube length, in.

m = participating mass of the tube

$\bar{m}_c$ = the mass of the cylinder (kg)

m_c = the mass of cylinder per unit length (kg/m)

M = reduced mass of the colliding bodies

n and N = total number of times S is traversed or total number of excitation cycles

n_a = number of asperities

n_{cl} = number of columns of asperities

n_{clmax} = maximum number of asperity columns perpendicular to sliding direction

n_i = number of average surface area (A_i) of worn material i

N_n = total number of cyclic loading for each excitation cycle n

N_0 = The zero wear limit

p = the penetration hardness

$(p)_{ii}$ = percentage of F_i D_i class occurrence

p_m = flow pressure

P_{max} = maximum normal contact force

P_L = pre-load applied to the tube at the support plate kg.

P_0 = maximum load per unit length (N/m)

$\bar{P}_0$ = maximum applied load (N)

r_c = radial clearance

R = equivalent radius of curvature ($1/R_1 \pm 1/R_2$)

R_1 = radius of cylinder (varying with wear)

R_{1org} = original radius of cylinder

R_{2org} = original radius of support

R_i = row number (i = 1,2,...6)

R_S = amplitude of minimum shear load required to maintain the tube stationary kg.

R_w = worn cylinder radius

s = sliding distance

S = sliding distance

S_{ac} = deformed length of cylinder

S_{af} = deformed length of flat

S_{0i} = critical sliding distance for material i

t^* = total time of interest (time of contact or sampling time)

t_s = sliding time

t_1 = starting time of averaging

t_2 = ending time of averaging

t = thickness of tube wall

T = duration of experiment

v_s = sliding velocity

V = relative approach velocity

w = wear volume

w_a = wear volume / asperity contact

w_d = wear volume / distance

w_g = weight of worn material

W_{intf} = overall wear intensity factor

w_r = wear rate (volume/time)

W_m = mean weight of the tube supported at the support plate kg.

W_R = work-rate (work per unit time given by tube-plate relative motion during contact and dynamic contact force)

W_{Rave} = average work-rate

W_{Rni} = work-rate due to normal impact alone

W_{Rsl} = work-rate due to pure sliding alone

$\Delta W(t)$ = average work done over time

$y(x,t)$ = deflection as a function of distance and time

y_o = amplitude of the sinusoidal vibration, in.

α = constant

α_1 to α_6 are constants determined using least square curve fitting technique from experimental data.

β = the surface damage contribution factor given by

β_c = the constant in the crack propagation relationship

γ = experimentally determined wear factor equal to 0.2 or 0.54

γ_R = constant for wear

θ = angle subtending half Hertzian contact a

λ = non-dimensional curvature ratio between 1 and 0.

λ_0 = zero wear curvature ratio

μ = coefficient of friction

ν_1 = Poisson's ratio for material 1

ν_2 = Poisson's ratio for material 2

σ_y = material yield stress in compression

σ_y = yield stress of the material

σ_{max} = maximum contact stress

σ_{fi} = friction stress for material *i*

τ_y = the yield stress in shear (*k*)

τ_{max} = maximum shear stress

ϕ = angle of impact

ω_n = natural frequency Hz

CHAPTER 1

INTRODUCTION

1.1 Significance of Fretting Wear in Heat Exchanger Tubes

Shell and tube steam generators are widely used in nuclear power plants for the production of steam, to run the turbine. The water introduced on the shell side of the generator is at a high temperature and pressure. Tubes supported by baffles or scallop bars inside steam generators are subjected to turbulent cross flow of this pressurized water. The flow induces vibration on the tubes which causes impacting and sliding of these tubes against the baffles and against one another in some instances. These impacting (normal as well as oblique) and sliding occur within the small clearances machined on the support plate for assembly purposes.

The motion of the tubes within the baffle support clearance (in the range of 0.2-0.4 mm radial clearance) is very small. Therefore, the wear occurring is classified as fretting wear, which could be a combination of abrasive, adhesive and fatigue wear mechanisms depending upon the interacting materials and the operating conditions. Fretting wear is defined as the wear of a material caused by elemental oscillatory or cyclical motion (<100-200 μm) of the contacting surfaces relative to one another, in the presence of a normal force [1].

Nuclear power plants have a very stringent safety requirement. Reliability of various

components is critical for the operation of the plant. Since high temperature, high pressure and turbulent flow are characteristic features of various units (steam generators, heat exchangers, condensers, etc.) within the station, it is crucial that operating conditions and design life of these various components are determined accurately. This knowledge will help to avoid accidents and prevent costly emergency shut downs [2].

The phenomenon of tube fretting wear is one of the most critical problems the Pressurized Water Reactor (PWR) industry is presently facing. The problem of tube fretting wear is caused by the reactions occurring between the tube/tube support, due to flow induced tubular vibrations. In the PWR steam generators, the clearance between the tube/tube support is the major cause of these problems. If flow induced vibratory forces are high enough, tube motion within individual tube support structures can lead to disastrous tube and/or support wear. In order to acquire a better understanding of the wear rate, a relationship between the input motion and interaction force and the wear volume should be established.

In the Canadian Deuterium Uranium (CANDU) nuclear power plants, the heat exchanger tubes separate the primary circuit which contains heavy water (subjected to the radio active nuclear fuel), from the secondary circuit containing regular water (Fig. 1). The failure of one of the tubes would result in a power station shut down and expensive repairs. Tube failures in steam generators or heat exchangers may be caused by one or a combination of several wear mechanisms, such as, corrosion, fatigue and sliding as well as impact fretting wear, with a disastrous consequence.

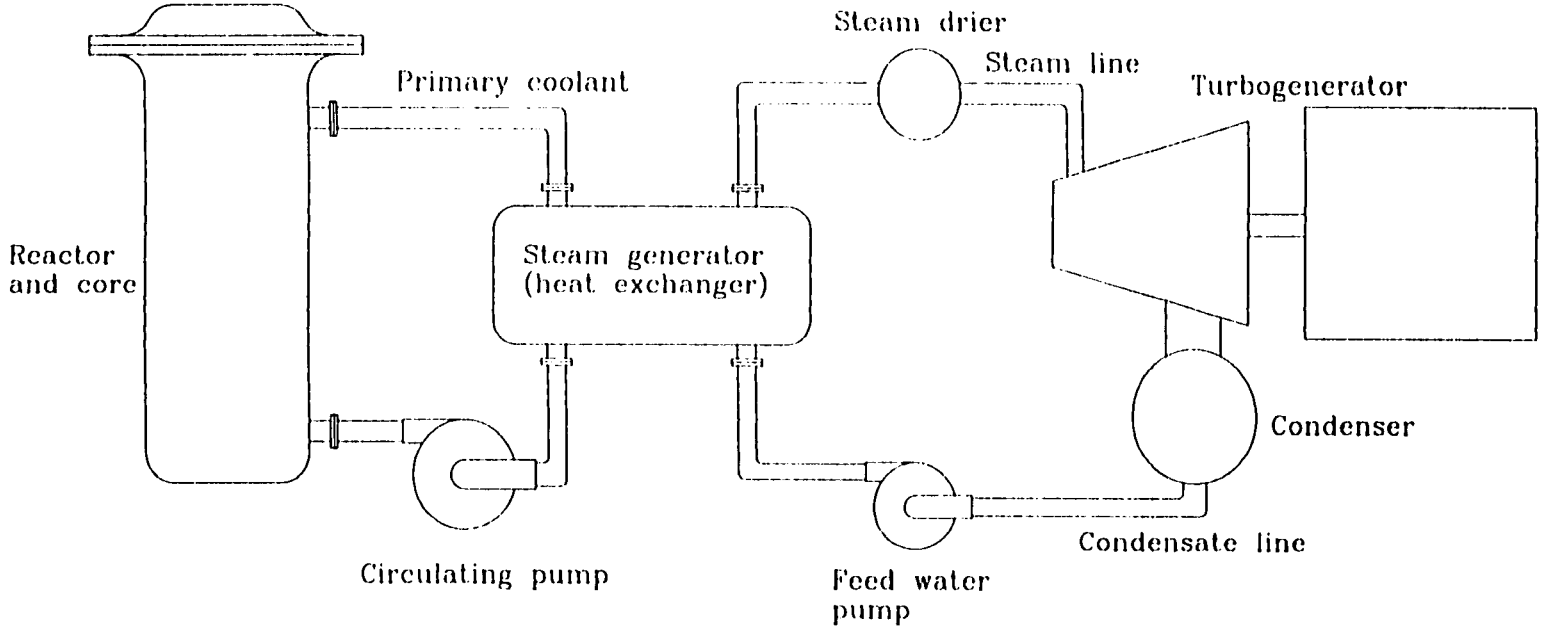

Figure 1.1 Schematic representation of a nuclear power plant

1.2 Mechanisms of Wear

The study of wear mechanisms is a complex phenomenon which requires the knowledge of material science and contact mechanics. In this research work, wear caused by the relative motion of two contacting objects, in the presence of a normal force, will be studied. Theories proposed by different leading researchers which have identified some of the processes involved in the formation of wear will be seen. The various major wear mechanisms proposed and defined, will be discussed in detail in the following chapter, to identify the type of wear mechanism critical in the study of the heat exchanger tubes. Some of the basic wear mechanisms are [3]:

a: adhesive wear

b: abrasive wear

c: delamination wear

d: fatigue wear (shear fracture wear)

e: corrosion or oxidative wear

f: electrical contact wear

Adhesive wear occurs as a result of asperities of different materials cold welding while in contact. Further separation of this two materials will result in the adhesion of material from one onto the other, due to the availability of weak spots at some distance from the contact surface. Repetitive welding of this kind will eventually lead to debris formation in the contact zone subjected to this cyclic conditions. This phenomenon is material dependent as some material combination is conducive to cold welding, more than others.

Abrasive wear is caused by hard constituents or asperities scratching material from the surfaces in contact. It could be due to the hard asperities of the contacting material or a hard particle at the interface. It is not uncommon for oxidized wear debris to get caught in between two wearing materials and cause further damage to both materials, until these debris find themselves outside of the wearing region.

Delamination wear is the process which involves the wear of particles layer by layer. It is governed by fracture mechanics parameters including crack nucleation and crack propagation. Through the action of repetitive loadings of asperities, cracks initiate at the subsurface level and propagate parallel to the surface until they reach a critical length and come to the surface forming wear debris. This type of wear is identified and proposed for sliding relative motion of the contacting materials.

Fatigue wear is defined as the mechanism of wear which includes the cyclical loading of a material above a certain critical stress value. It is associated with asperity contacts on the microscopic level involving repeated deformations resulting in the formation of a wear debris. This type of wear is usually associated with impact type of relative motion of the interacting materials

Corrosion wear is the combination of chemical reactions and rubbing causing the wear or pitting of the surface. Oxidation is a common source of corrosion wear, in most interacting metals creating hard wear particle which might even act as an abrasive, further enhancing the wear process.

Electrical contact wear is the wear which occurs at the contact of electrical junctions, creating high temperature due to high resistance across the contact. The temperature associated with this type of wear might at times reach the boiling point of the metal depending on the amount of gap responsible for the resistance.

Depending upon the materials in contact, magnitude of force, type and magnitude of relative motion and geometry of contact one or all mechanisms of wear could play a role in the debris formation process, compounding the complexity of the problem.

The author of this thesis would like to classify delamination wear and fatigue wear due to impact in the same category, because the mechanism involved in delamination wear and the process involved in the formation of wear during impact involve a similar process where there is crack nucleation followed by crack propagation resulting in a wear debris [4]. Further justification of this proposal is given in the subsequent chapters. Delamination wear was proposed for sliding conditions while fatigue wear is mostly associated with impacting type of motion.

The wear occurring at the interface of the tube/baffle or scallop bar support is known as fretting wear. Fretting wear is defined as the wear by which two surfaces undergo relative oscillatory slip of very small magnitudes while in contact, causing rubbing and eventual formation of a wear debris. Wear due to the impact of heat exchanger tubes is also categorized as fretting because of the limited clearance and elastic compliance causing relative slipping during contact. The fretting wear process consists of the following stages:

dispersion of surface film by oscillating movement; adhesion, plastic deformation, and metal transfer between the contacting surfaces; for some materials, oxidation of the wear particles and formation of an intermediate zone; productions of loose wear particles due to the fretting action; and finally repetition of the cycle. The process could include all the above mentioned mechanisms except electrical contact wear.

The analysis of wear for comparatively low loadings (no plastic deformation on the global level) indicates that the detrimental mechanism of wear, is that which involves critical stress values at the subsurface level, following the fracture mechanics laws for crack nucleation and propagation. Depending upon the type of relative motion between the two wearing materials (sliding, normal impacting and oblique impacting) the wear rate will be different, because of its effects on the wear process. This research work will present a new model for wear, involving low loading conditions for the various contact motions mentioned above.

1.3 Objective

Survey of the available literature indicates that to date a purely analytical model relating wear rate to the various parameters affecting it, does not exist. With the current knowledge of tribology and computation power available at our disposal, we are a few steps closer to achieving this goal. However, some degree of empirical formulation is still required to arrive at a mathematical model predicting the wear between two materials in relative motion. It is, therefore, the aim of this thesis to arrive at a new mathematical model for wear, better suited to handle pure sliding, normal impact as well as the combination of these two.

In addition, the controversy surrounding the issue of accurate characterization of wear rate in nuclear power plant heat exchangers will be investigated. Especially, given the fact that the commonly used characterization parameter does not have a unique relationship with wear-rate. Through the course of this work, a new and improved empirical relationship has been proposed by Hofmann et al. [5]. This semi-empirical model will be utilized on results obtained from experiments conducted in house. In addition, the accuracy of the new stress dependent model derived in this thesis, using a fracture mechanics approach will be verified as well. The second main objective of this research work is to derive a generalized characterization parameter for wear rate which is not sensitive to the type of motion causing the wear.

1.4 Research Outline

The review of some important generalized wear models available in open literature is presented in Chapter 2. The state of the art survey of the different empirical and semi-empirical wear models pertaining to heat exchanger tube wear is also looked at, along with a study of flow induced vibrations of heat exchangers tubes. It is shown that because of the nature of the problem, most of the empirical models proposed are different from each other.

Using some of these accepted empirical formulations and characterization parameters as a basis, the relationship between wear rate and work rate (commonly used characterization parameter in heat exchanger tube wear) are derived for different relative contact motions and geometries in Chapter 3. Comparison of the relationship of wear rate/ work rate of different

geometries and orbital motion are carried out.

A description of the experimental setups is given in Chapter 4. The program developed for data acquisition and analysis using G programming language (LabView) is also described in detail along with some of the listing and analysis of the collected data, in this chapter. Plots describing the average work rate, orbital motion, percentage of force and sliding distance category, and average load rate for all the experiments conducted in this research work, are given as well.

The contact stress conditions are investigated using finite element approach to determine crack nucleation position and number of cyclic loading required to originate a crack from a subsurface inclusion. The subsurface crack propagation is studied using the crack tip sliding displacement to obtain the amount of cyclic loading required to obtain a wear debris. The effect of residual stress and direction of crack propagation for continuously expanding crack are studied as well. All these fracture mechanics analyses are performed in Chapter 5.

The derivation of wear model using the fracture mechanics approach for materials that behave elasto-plastically is presented in Chapter 6. The model is derived for normal impact, oblique impact and sliding conditions by extending the delamination theory of wear, which was originally derived for sliding motion only.

A new wear rate/characterization parameter is introduced in Chapter 7, for various contact conditions and tube orbital motions. As well, analysis of the experimental data is conducted

using the conventional approach, Hofmann's approach and compared with the new characterization parameter. Engel's optimal wear path principle is extended to estimate the depth of wear for the given type of motion, while the new model is used to accurately characterize the wear rate for the various experimental data.

The main conclusions that can be drawn from this work are summarized in Chapter 8. Recommendations for future theoretical and experimental work are also given.

CHAPTER 2

GENERALIZED WEAR MODELS AND SPECIFIC WEAR MODELS FOR NUCLEAR POWER PLANT HEAT EXCHANGER TUBES DUE TO FLOW INDUCED VIBRATIONS

2.1 Introduction

In order to comprehend the wear mechanics evident in a two component body wear, it is crucial that one conducts a survey of the state of the art of generalized wear models derived by the various leading researchers over the past few decades. Several investigators have come up with empirical and semi-empirical wear models pertaining to sliding, impacting and oblique impacting conditions for metals. Most of the above mentioned models owe their empirical formulations to one of two categories. The first one is the basis of these models on the original empirical wear model derived by Archard [6], which is the proportionality of wear on the product of force and sliding distance. The second is for fatigue dominant wear equation which traces its origin to Palmgren's [7] relationship, the proportionality of wear to the product of the cube of the contact force and number of application of this force.

Depending upon the materials, contact force and operating environment any one of the four major wear mechanisms could be at play in the wear process of sliding or impacting objects. However, there seems to be a consensus in the tribology community that for low magnitude contact forces, fatigue of subsurface nature is the main cause of wear between these bodies. The subsurface microstructural analysis conducted by Rice et al. [8,9] gives support to the

theory of fatigue at the subsurface level being detrimental for wear. It indicates that the substructure of the wearing material for both sliding wear and impact wear is similar. The study of fatigue wear was investigated using fracture mechanics for sliding components by some researchers [10-12]. The models described by leading researchers in the field will be discussed briefly and a new model applying to normal and oblique impact, and sliding conditions, taking into account the fatigue relationship, will be proposed and verified using experimental means.

2.2 Wear Models

The mechanics of wear is a complex one which requires the knowledge of mechanical behaviour of materials under cyclical loading, among other properties, inducing the formation of wear debris [13]. To date, the literature survey has indicated the non-existence of a purely analytical wear model predicting accurately the wear volume with respect to energy input parameters of the system. However, there are a few different wear models empirically formulated for various contact conditions (contact geometry and force). The derivations are based on experimental observations and heuristic reasoning. The two most common type of models are sliding wear models and impacting wear models. The classifications described in this chapter will consider sliding wear models as well as fretting wear models in one category and impact (both normal and oblique) wear models in another. The last category is the survey of the wear models developed for a particular application (Heat exchanger tube wear).

2.3 Sliding Wear Models

The magnitude of the contact force in sliding and normally or obliquely impacting objects is critical in determining what type of wear mechanism is critical in the debris formation process. The wear models usually consist of empirical formulations involving the wear volume using the force, sliding distance or number of times the load is applied and material properties. The various important sliding wear models will be listed and investigated in the following section.

2.3.1 Archard's Adhesive Wear Model

After experimenting with sliding bodies, Archard [6] derived an empirical equation for wear relating the volume of worn material to the normal force, relative sliding distance and hardness of the two materials in contact.

Some of the conclusions arrived at by Archard for adhesive type of wear were:

1. The wear rate is proportional to the load
2. The wear rate is independent of the apparent area of contact
3. Provided that K (proportionality constant) and p_m (flow pressure) remain constant, the wear rate is independent of the sliding speed.
4. The theoretical value of the wear rate is independent of the model used to represent the surfaces.

Based on the above assumptions the wear rate equation is given by:

$$w_d = K\frac{F}{3a} \tag{2.1}$$

where,

w_d = wear rate (volume/distance)

K = proportionality constant

F = applied load

a = the Hertzian contact radius given by:

$$a = 1.1\left[\frac{1}{2}FR\left(\frac{1}{E_1}+\frac{1}{E_2}\right)\right]^{1/3} \quad elastic\ contact$$

$$a = \left(\frac{F}{\pi p_m}\right)^{1/2} \quad plastic\ contact \tag{2.2}$$

Archard verified his empirical model using experimental results. The above wear model was valid for heavily loaded members, where there is plastic deformation on a global or local scale. This implies that the wear is predominantly of adhesive nature and that it can be experienced even after a single pass between two members. The Archard's wear model does not apply for impact induced or fretting type of wear as the mechanism differs for this type of contact conditions. Impact or fatigue dominated wear involves an initial incubation period which is normally taken for subsurface crack initiation and propagation until the formation of a debris. Hence, there is no wear during this period.

2.3.2. Fatigue Dominant Sliding Wear Model

Bayer et al. [14], a group of researchers working on the mechanisms of wear at the Endicott

laboratory of IBM, conducted their own sets of experiments and derived wear equations based on experimentally determined fatigue relationship. They first identified the various mechanisms of wear to be load dependant and considered fatigue to be the dominant mechanism for sliding wear between two objects with a relatively low normal load. Rabinowicz [15] has shown that under rolling conditions fatigue wear is more predominant compared to adhesive or abrasive wear. In contrast, the wear occurring at the interface of two relatively sliding metallic objects kept in contact as a result of a comparatively high normal force is predominantly due to adhesive and abrasive mechanisms. The above two wear mechanisms produce debris at a faster rate than fatigue mechanism, because the incubation process associated with fatigue type of wear is relatively high.

Bayer and Ku [16] also support the concept of fatigue wear being the dominant mechanism in the sliding wear of two objects with relatively low levels of load. They identified the various wear mechanisms as:

1. Wear which occurs when the material in the vicinity of the contact region is subjected to a stress which causes plastic flow and material movement away from the contact region giving gross ploughing. Local ploughing is also a repetition of the same phenomenon but on the asperity level.
2. Wear which is a result of transference of material between the two contacting surfaces. Again this phenomenon can occur on a local scale or gross scale depending upon the material and contact conditions.
3. Wear caused due to the abrasive action of worn particles or debris caught in between the mating surfaces, and

4. The wear due to fretting corrosion.

The basic equation for sliding wear is given by the following equation where the pass length L_p has a value equal to the contact length divided by the sliding distance.

$$w = KN(\tau_{max}L_p)^{\frac{9}{2}} \tag{2.3}$$

where,

N = number of impacts

Bayer and Schumacher [17] indicated that fatigue wear results in wear debris with a relatively high aspect ratio. It involves the delamination or flaking of material from the surface due to accumulated cyclical subsurface loading. They have shown that at low maximum shear stress (τ_{max}) levels, between 0.2 and 0.5 of the yield shear stress (τ_y) of the material, the contacts do not involve plastic contact conditions on the global, as well as local asperity level.

Sighting the maximum shear stress theory, which states that plastic flow will occur in a body if the maximum shear stress is greater than the yield stress, they indicated the condition for the avoidance of gross ploughing should be to ensure that the maximum shear stress is always less than the yield stress. Ensuing the above principle, they showed that in order to avoid transfer and local ploughing for one pass, the maximum shear stress should be a fraction of the yield stress, as per the following equation:

$$\tau_{max} < \alpha\tau_y \quad , \quad \alpha < 1 \tag{2.4}$$

Bayer et al. [18] found experimentally that for $\tau_{max} / \tau_y \approx 0.5$ there was zero wear for one pass

of various combinations of materials and lubricants. They also established that based on a value of 0.5 or 0.2 they were able to observe zero wear for 2000 passes. The wear model proposed by Bayer and Ku starts from the Palmgren's equation for fatigue of spherical roller bearing. It gives the relationship prevalent between force and number of passes as:

$$F^3 N = K \tag{2.5}$$

Their basic sliding wear model assumes proportionality of wear to Palmgren's constant. The model is given in equation 2.3 reproduced here to indicate the relationship it has with the applied force F.

$$w = KNF^3 = K_I N(\tau_{max} L_p)^{\frac{9}{2}} \tag{2.6}$$

where,

K_I = constant for impact wear

They derive their model by starting from the above equation and taking the differential formulation of equation (2.6), to eventually arrive at an appropriate wear relationship for the various geometries that could be analysed using this approach.

$$\frac{dw}{w} = \frac{dN}{N} + \frac{9}{2}\frac{d(\tau_{max} L_p)}{\tau_{max} L_p} \tag{2.7}$$

From this differential formulation the wear rate can be characterized for a given contact condition. The initial conditions are determined from the zero wear relationship indicating zero wear for 2000 passes. The derivation of their fatigue wear equation presumes that the wear due to fatigue is proportional to F^3N. It should be noted, that the seemingly linear relationship between wear and number of loading could be deceiving as the stress which is a function of the load and geometry of contact is also dependent on N.

2.3.3. Delamination Theory of Wear

The delamination theory of wear was developed by Suh and his team at M.I.T. [19,20] ensuing their investigations into the wear mechanics of two bodies in sliding contact. They analysed the wear process for two bodies sliding relative to each other and forwarded this theory on the basis of subsurface fatigue being the dominant wear causing phenomenon. The process involved in this type of wear was analysed thoroughly by Jahanmir [11] and was given in a step by step description, explaining the mechanism.

Suh [10,19] developed a mathematical model for sliding wear and indicated that fretting sliding wear is achieved when the amplitude of sliding goes below a certain critical value. In his derivation he utilized the following assumptions:

a. Metals wear layer by layer, each layer consisting of N_w wear sheets.
b. The number of wear sheets per layer is proportional to the average number of asperities in contact at any instance between the slider and the disk.
c. The rate of void and crack nucleation and the critical degree of shear deformation for loose particle formation can be expressed in terms of a critical sliding distance S_0 for a given sliding situation. S_0 is defined as the critical sliding distance required for removal of a complete layer (i.e. N_w wear sheets).

The starting point of this model is the assumption that wear volume is proportional to the sliding distance of the wearing bodies, similar to that of Archard's wear equation. Based on the above assumptions Suh's wear equation for sliding motion is derived and expanded to the following equation by using the dislocation theory of materials and proportionality

relationships between number of asperity contacts and load, and actual area of contact and load. One of the major assumptions was that the number of average area A_t is equal to number of asperity contact.

$$w = \frac{bP_{max}S}{4\pi}\left[\frac{K_1G_1}{\sigma_{f1}S_{01}(1-\nu_1)} + \frac{K_2G_2}{\sigma_{f2}S_{02}(1-\nu_2)}\right] \tag{2.8}$$

where,

S_{0i} = critical sliding distance required to remove one layer of material i

S = total sliding distance

K_i = experimentally determined constant for material i

G_i = shear modulus for material i

σ_{fi} = friction stress for material i

ν_i = poisson's ratio for material i

b = Burger's vector

P_{max} = maximum contact load

It can be observed that, even though, the initial starting point is similar to Archard's adhesive wear equation in its assumption of the wear volume being proportional to the sliding distance, material hardness does not come into play. The other major assumption taken in arriving at the wear equation was that the number of asperity contacts is proportional to the number of average worn area. The experimental work conducted by Suh et al. [19] has, in fact, demonstrated validity of the final wear equation.

Suh and his team at MIT [20] have shown experimentally that this equation is valid by conducting numerous experiments and detailed analytical approach for elasto-plastic

conditions, which has helped to reduce the empirical nature of the problem. Jahanmir and Suh [21,22] carried out an in depth analysis, studying the subsurface stress distribution of two contacting objects, sliding relative to one another, and showed the location of void formation, based on the steady state cumulative residual stresses and applied stresses. The analysis carried out to investigate followed the Merwin and Johnson method [23] which utilized an approximate solution for the point in a semi-infinite body, loaded in compression and tension while being subjected to a rolling/sliding member. The method involved the use of Hooks relationship for stress and strain until the yield criterion according to the von Mises stress is reached and incorporates the Prandtl-Reuss equation to further handle the stress and strain. Unloading of the force will result in the residual stress and strain, values of which can be used for subsequent loading, until the steady state value of the stress and strain is reached. However, the major assumption is that the elastic strain is the total strain used to solve the Prandtl-Reuss equation. It is also seen that the analysis was carried out for plane strain condition, which approximates the asperity contact with cylindrical one instead of a spherical contact. Since a spherical contact which is an axi-symmetric case has a similar stress distribution of a plane strain 2D cylindrical contact, this approach is valid and simplifies the 3D problem.

It was argued that due to large hydrostatic pressure at the contact, void nucleation can only occur below a certain depth, from the surface. The depth of void nucleation from the surface was found to be more for higher forces and friction coefficients. The crack nucleation criteria was following the continuum mechanics approach, which was proposed by Argon et al. [24], which states that the radial stress around an inclusion should reach the particle matrix bond

strength which is equal to the summation of the von Mises (effective) stress and the hydrostatic stress. They used the von Mises yield criterion to check plasticity of the material while it is loaded by the asperity. It was conducted for the determination of void nucleation at the subsurface level, near a cylindrical hard particle. The analysis conducted by these researchers was a fundamental one and attempted to give an understanding to the process involved in fatigue mechanisms. This analysis conducted was based on the assumptions that material properties did not change through the course of application of this cyclic load and that the properties of the inclusion do not affect the stress distribution, beneath the surface of the contact.

Fleming and Suh [25] made use of a subsurface crack propagation equation employing the Paris fatigue crack propagation law, in deriving their sliding wear model initially proposed by Suh [10]. Based on this relationship they derived a wear model by assuming that crack propagation was the wear controlling phenomenon. The analysis considered the fact that in sliding contact the material ahead of the force is in compression (elastic or plastic using the Tresca yield criterion) while the trailing part near the force is in tension (elastic). In this paper they have demonstrated the validity of linear elastic fracture mechanics, even for elasto-plastic conditions. The argument used was that crack propagation can occur only in the tensile region of the loaded zone because the compressive zone will close the crack, enabling the transmission of shear force from one face to the other, and the tensile region is always in elastic contact. The wear model they derived starts from the crack propagation equation given by:

$$\frac{dc}{dN} = \beta(k_I)^n \tag{2.9}$$

where,

c = crack length

N = number of times load is applied

β = constant in the crack propagation equation

k_I = stress intensity factor

n = exponential constant in the crack propagation equation

Using Gupta and Cook's relationship for load and number of asperity contact relationships and simplifying by integrating and substituting, the above equation reduced to a volumetric wear model.

$$w = [\delta k_I^n(\xi H, \mu, d_c, C_e)P_{max}S + C_e]d_c C_e \tag{2.10}$$

where,

w = volume worn

$\delta = \alpha\beta_c$, where β_c is the constant in the crack propagation equation and α is the proportionality constant between number of contacts and load per unit length

ξH = average normal contact force

μ = coefficient of friction

d_c = critical depth

C_e = critical effective crack length

P_{max} = maximum applied load

S = sliding distance

As indicated in the equation, k_f^n is a function of the average normal force, the coefficient of friction, the depth of wear and critical effective crack length. Some of the constants have to be determined experimentally. They recommend the use of 1 for ξ in the absence of any information. β_c and n can be determined from standard fatigue data. The factor α has to be estimated from the surface asperity distribution and fracture mechanics approach was utilized to determine the values of d_c, C_c and k_f.

The above equation indicates that higher value of hardness implies increased wear contrary to previous reports. This is mainly because of the assumption that the normal contact stress is proportional to the hardness of the material. This equation has shown that the load and sliding distance proportionality assumed and arrived at in the delamination theory of wear is valid. There were some assumptions in the derivation which need to be investigated further to expand on this derivation. However, as they have stated time and again, the derivation of a purely analytical equation for wear is not yet feasible due to the complexity of material properties at the subatomic level.

Suh's model, derived for pure sliding conditions is not applicable to the problem of impact wear, without some modifications. It is essential to properly identify the wear mechanisms controlling the process, before applying the principles of delamination theory, to other contact motions. Therefore, further investigation is necessary to develop a generalized wear model for impact as well as sliding conditions, by extending the delamination theory of wear originally developed for sliding only.

2.3.4. Uhlig's Fretting Wear Model

Uhlig and Feng & Uhlig [26,27] developed a sliding fretting wear model (5) which takes into account the chemical effect of the wear process. Depending upon the material combination, they were able to establish that the chemical effect of fretting wear was between 6 to 78% of the actual wear. Thus,

$$w_g = (k_0 F^{1/2} - k_1 F)\frac{N}{f} + k_2 l F N \qquad \textbf{(2.11)}$$

where,

w_g = weight of worn material

F = Normal load

N = total number of cycles (excitation)

f = frequency of the excitation

l = amplitude of oscillation

k_0, k_1 and k_2 = constants

The determination of the constants k_i is carried out, based on the data obtained from experiments conducted for a fixed cycle at various loads. An empirical equation is used to approximate the wear vs pressure relationship between the interacting bodies. As per equation (2.11) the first two terms are due to the chemical effect and the last term is mechanical effect alone. This approach is unique in that it incorporates the effect of corrosion in the wear model, which in some instances could be more than the mechanical effect.

The formulation of this model is highly empirical, involving the determination of several

constants, because of the nature of fretting wear process that they were investigating. The debris formation compounds the wear mechanisms involved, due to the entrapment of particles in between the two contacting bodies initiating abrasive or third body wear in addition to the initial wear causing mechanism.

2.4. Impact Wear Models

Similar to sliding wear, different models have been proposed for impact wear, as well [28,29]. The term impact includes normal and oblique impact motions variation of which is characterized by a sliding component in the case of the latter. The various important wear models developed for impact conditions and published in open literature, will be discussed in this subsection.

2.4.1. Normal and Oblique Impact Wear Model

Engel [30-32] developed an impact wear model, based on the assumption that the above fatigue relationship given for sliding conditions, holds true for impact wear model as well. He then applied the optimal wear path principle which states that the gradual change of the geometric wear scar parameters corresponds to the steepest-descent path for a critical stress related failure parameter. This wear model is capable of handling the wear problem irrespective of the mechanism of wear, as its empirical formulation is based on a purely geometrical approach, and heuristic reasoning relating the worn surface contact to the maximum Hertzian contact length.

Engel [33] and Engel et al. [34] have derived a mathematical model for the impact wear occurring between two objects, based on the optimal wear path principle theory. His assumption was that in the process of wearing a body will try to conform to the shape of the harder surface. The derivation of this wear equation starts from a highly stress dependent impact wear formula given by:

$$w = KN\sigma_{max}^{9} \tag{2.12}$$

where,

w = wear volume

K = constant

N = number of impacts

σ_{max} = contact stress

The derivation assumes that the wear volume is equal to the volume described by the deformation due to Hertzian contact. The impact wear per unit length as arrived at by Engel for soft cylinder impacting against a hard flat surface in terms of the non-dimensional curvature ratio (λ) which is the ratio of the original radius of the cylinder to that of the worn cylinder radius (R_1 / R_w), is given by [34]:

$$w = 7.66\left(\frac{P_0}{E^*}\right)^{3/2}\frac{(1-\lambda)}{\lambda^{3/2}}R_1^{1/2} \tag{2.13}$$

where,

R_1 = worn cylinder radius

P_0 = load per unit length

λ = non-dimensional curvature ratio between 1 and 0.

The reduced modulus of elasticity (E^*) is given by:

$$E^* = \left(\frac{1-\nu_1^2}{E_1} + \frac{1-\nu_2^2}{E_2} \right)^{-1} \tag{2.14}$$

where,

E_1 = Young's modulus for material 1

E_2 = Young's modulus for material 2

ν_1 = Poisson's ratio for material 1

ν_2 = Poisson's ratio for material 2

The derivation of their fatigue wear equation also presumes that the wear due to fatigue is proportional to F^3N. The same argument that was used in the case of the sliding wear model of Bayer et al. can be utilized here, for the non-linear relationship between wear and number of impacts. Also the subsurface stress variation with crack nucleation and propagation developed parallel to the surface should be conducted to verify the formation of wear surface satisfying the optimal wear path principle (i.e. the wear will proceed in a parabolic curve for a cylinder impacting against a flat surface).

2.4.2. Impact Wear Model Based on Force-Sliding Distance Proportionality

Rabinowicz and Hozaki [29] derived a wear model for impact conditions by starting from force sliding distance proportionality (Archard's wear model). This model was derived for high energy impact where the magnitude of the force is sufficient to cause plastic deformation of the contacting surface.

$$w = \frac{KIN}{p} \tag{2.15}$$

where,

w = wear volume

K = non-dimensional impact wear coefficient

I = energy of impact

N = number of impacts

p = the penetration hardness

The validity of this relationship was verified for the contact conditions (high energy impact) using experimental results. Assuming that this equation is valid it does not address the question of properties changing over the duration of energy application (strain hardening). The authors have indicated that low energy impact has a different wear mechanism (fatigue wear). Therefore, the main theme of this research work is to investigate the wear associated with low energy impact both normal and oblique and arrive at a reasonable wear model that will try to address all the questions raised here.

2.5. Survey of Wear Models Pertaining to Heat Exchanger Tubes

The phenomenon of fretting wear is a very complex one. Various researchers have done some work in this field and have tried to come up with empirical or semi-empirical mathematical model for describing the wear process [35-47]. A brief survey listing some of the important wear relationships proposed by the different researchers will be seen in this section.

Ko et al. [37] stated that frequency, total number of cycles, amplitude of motion, normal

pressure, physical characteristics of mating solids and environmental conditions all affect the wear of material. He later went on to investigate the influence of excitation frequency, amplitude, tube baffle clearance and the ratio of tangential to normal component of excitation force under both dry and wet conditions on the fretting wear of Monel 400 tube against plain carbon steel rings.

Ko [38] carried out their experimental investigations using a setup which consisted of two rotary out of balance masses connected to one end of the monel tube. The tube is attached at the centre of a top supporting plate which is rigidly held by four rods sitting on a base plate. The rotor masses are attached to the tube at the bottom, under the base plate. After conducting various tests, he ended up with the result showing that the wear increases exponentially with excitation frequency following his equation and that it also increases with excitation amplitude and diametral clearance. He also found that the amount of wear was dependent on the ratio of Y_{max} to X_{max} of the excitation amplitude, a peak being reached when the ratio is between 2 and 3.

$$w = Ke^{af} \tag{2.16}$$

where,

w = wear volume

f = the excitation frequency Hz

K and a are experimental constants

Ko [38] reported that, with the development of an analytical model for the estimation of impact force for multi-span tubes, he could analyse the effect of impact force on wear in high temperature environments. The necessity for this being that there was no force transducer

capable of working in a high temperature environment at the time. He studied the effect of temperature on wear by conducting his experiments in pressurized water at 265°C in an autoclave and found that the wear increased with temperature. He also stated that there was no direct relationship between mid-span displacement and the root mean square (rms) of the support impact force.

After experimenting with different geometry support plates such as three lobbed broach and triangular lattice bar, Ko [38] was able to conclude that wear decreased with increased circumferential support length. However, the results he obtained as far as the hardness of the material combination was concerned, was inconclusive. Materials with similar hardness wore at different rates depending upon the other mating material. The wear-rate as well as the impact force was found to increase for an increased clearance until a limit is reached where the contact can no longer be maintained. He also reported that an increase in the clearance at the support sometimes caused a change in the type of motion. Eventually, he was able to conclude that it was feasible to predict long-term tube wear using the computer code that he developed, from correlated results between force functions and short-term wear-rates. However, the sensitivity and accuracy of his new proposal remained to be verified using experimental results.

After studying the worn surface finish, Ko et al. [37] inferred that the primary cause of wear in both sliding and impacting is the same. They suggested that the principal mechanism in the wear process is shear and that wear caused by sliding motion between the two objects is more dominant than wear due to relative impact. They came to this conclusion after studying

the low probability of occurrence of impact type high force components as compared to intermediate range rubbing type force component from their experiments. The relationship that they showed for the force component and the wear-rate for two different ranges of forces namely 0-4N and 10-20N for various ratios of the orthogonal excitation forces (F_Y to F_X) indicates that wear-rates were higher for the purely sliding type motion and were the least for highly impacting type motion. It also showed that the force component in the 10-20N range for pure sliding has a high percentage compared to combined sliding and impacting motion.

Blevins [39] did various experimental studies on the mechanism of fretting wear in nitrogen/air atmosphere at room temperature using 410 stainless steel material for the tube and 2-1/4 Cr-1 Mo for the support. His experimental setup consisted of a shaker placed at the middle of a horizontally placed tube which holds the tube specimen at one end. The support plate specimen is attached to a collet at the frame and a pre-loading apparatus is attached near the test zone. Even though excitation was given in a uniaxial direction he had observed that the tube motion at the test zone was in oval orbits.

Based on his experiments, Blevins [39] was able to conclude that the impact fretting wear produced was a result of surface delamination, which was confined to a very thin layer of the wearing specimen. His results also indicated that the wear-rate of the tube and the support plate are approximately equal if they are of the same material and that the wear-rate is not only hardness dependent but also material dependent as materials with similar hardness wear at different rate. His other conclusions were that, increasing the gap between tube and

support plate sharply increases the fretting wear and the rate of fretting wear increases both with frequency and amplitude of tube vibration.

Following his experimental study, Blevins [40] was able to develop an empirical model predicting the wear per cycle of vibration for the test material 2-1/4 Cr,-1 Mo, as follows:-

$$w_r = \alpha_1 f^{\alpha_2} \left(\frac{A_C}{D}\right)^{\alpha_3} \left(\frac{A_G}{D}\right)^{\alpha_4} \left(\frac{t}{D}\right)^{\alpha_5} e^{\alpha_6 (R_s - W_m - P_L)} \qquad \textbf{(2.17)}$$

where,

w_r = weight loss per cycle

f = frequency of vibration (Hz)

A_C = peak to peak transverse amplitude of the tube without the restraining gap

A_G = smaller of A_C or diametral gap

D = diameter of tube

t = thickness of tube wall

R_S = amplitude of minimum shear load required to maintain the tube stationary (kg)

W_m = mean weight of the tube supported at the support plate (kg)

P_L = pre-load applied to the tube at the support plate (kg)

α_1 to α_6 are constants determined using least square curve fitting technique from experimental data.

Equation (2.17) was a good approximation of the fairly scattered experimental data, however, the drawback is that it is highly empirical requiring the determination of six constants. Because of the many experimental constants to be determined, validity of this approach is limited to the particular experiment conducted, and is bound to be material and setup

dependent.

Blevins [43] studied the effect of impact on wear using his experimental setup mentioned earlier [40] on alloy 800H and 2-1/4 Cr-1 Mo steel heat exchanger tubes in loosely held supports in a helium environment at temperatures varying from 20 - 650°C. He developed a model relationship describing the dynamic contact stress for a heat exchanger tube-tube support impact reaction. The major assumption he used was that the contact region was a point contact (sphere on a flat surface) and since Engel [28] has shown that the use of maximum shear was an overly conservative prediction of wear, he used the maximum tensile stress as a prediction of wear and compared the values he obtained analytically with fatigue allowable stresses in ASME Boiler and Pressure Vessel Code for 10^6 cycles.

$$\sigma_{tensile} = c_4 \left[\frac{E^4 f^2 A_d^2 m}{D^3} \right]^{1/5} \qquad \textbf{(2.18)}$$

where,

c_4 = constant for type of contact (sphere on flat surface) and clearance

E = modulus of elasticity

f = frequency of vibration in Hz

A_d = mid-span peak-to-peak displacement

m = participating mass of the tube

D = tube diameter

The microstructure analysis Blevins did, showed that the impact wear occurred by the formation of subsurface cracks parallel to the material surface, indicative of high subsurface stress induced by impact, causing subsequent delamination of the material. The other

observation that he made was that at moderate temperatures (300 to 500°C) the delaminated surface was self welding onto the parent material reducing the amount of wear as compared to room temperature conditions. He also reinforced the theory that reducing vibration amplitude or tube support clearance dramatically reduced the wear-rate at all temperatures.

Connors [41] studied this problem by focusing on the dynamics of the pipe in the fluid and using Archard's wear equation to predict the wear-rate. He analysed the various mechanisms of flow induced vibrations and attributed it to fluid-elastic, turbulence and vortex shedding excitations. Fluid-elastic excitation mechanism is characterized by a critical flow velocity below which vibration amplitudes are small and above which amplitudes increase rapidly causing vibrations near the natural frequencies of the tubes. Turbulence also excites the tubes near their natural frequencies but are narrow band random vibrations with varying amplitudes. Vortex shedding is produced by the wake formed as a result of fluid flow over a tube and has a high amplitude of excitation near the tube's natural frequency.

Connors wear formulae for large- and small-amplitude vibrations are given by equation (2.19) and (2.20) respectively and it assumes that the wear is uniform over the duration of the process and that the support does not wear.

$$w_r = \frac{2\pi\, c\omega_n K_f F_N}{10^{12}} \tag{2.19}$$

where,

w_r = volume wear-rate, $in.^3/s$

c = radial clearance between the tube and the support, in.

ω_n = natural frequency of the tube in the fluid, Hz

K_t = wear coefficient for tube, in.^{2}/lb

F_N = dynamic normal contact force between the tube and support plate, lb

$$w_r = \frac{\pi D K_t \omega_n y_o (2F_S + F_N)}{L_t \times 10^{12}} \tag{2.20}$$

where,

F_S = steady contact force between the tube and support plate, lb

D = tube outside diameter, in.

y_o = amplitude of the sinusoidal vibration, in.

L_t = tube length, in.

Connors concluded that critical wear was a result of fluid-elastic vibration which caused large amplitude excitations. He recommended that it should be avoided in operations, if possible. Vibrations caused due to turbulent flow is generally of smaller amplitude and according to actual observations where fluid-elastic excitations are avoided the wear was relatively smaller. The above equations (2.19 & 2.20) describing the wear-rate were fairly accurate in predicting the life of the steam generator. He mentioned that vortex shedding, however, was not a problem in heat exchangers as it was not occurring due to the close proximity of adjacent tubes.

Levy and Morri [42] developed an oblique impact wear model (16) which is a factor of load, sliding distance, proportionality of wear and mechanical response of the impacting bodies starting from the following relationship taking into account the load-sliding distance proportionality to wear.:

$$w = KN \int_0^s F\,ds \tag{2.21}$$

where,

w = wear volume

K = specific wear rate

N = total number of impacts

$$w = KN\frac{1}{2}MV^2(1+e)[\sin(2\phi) - \mu(1+e)\sin^2(\phi)] \tag{2.22}$$

where,

K = wear coefficient

M = reduced mass of the colliding bodies

V = relative approach velocity

e = coefficient of restitution

μ = coefficient of friction

ϕ = angle of impact

This analysis has a similar approach to Archard's pure sliding wear in that it considers the load sliding distance proportionality. It does not take into consideration effects of impacting and sliding motions.

They verified their model by conducting experimental work on a twin vibrator rig which is capable of delivering repetitive impact of a moving specimen against a stationary target. They analysed the impact wear characteristics of three materials against 310 steel for a range

of temperatures and concluded by saying that their model was valid for a stable wear regime at around 100°C. However, there were errors occurring at elevated temperatures which made the equation not valid. Even though they did not analyse their data in relation to work-rate one can estimate this value from the presently accepted relationship of wear-rate, work-rate and specific work-rate. Therefore their data which was given in their publication gave a brief insight into the wear phenomenon occurring at the contact interface due to oblique impact.

Frick et al. [44] developed a three-dimensional non-linear relationship describing the dynamics of a steam generator tube with clearance at its support and analysed the response of the system using a general purpose finite element program. They defined a quantity known as the work-rate given by equation (2.23) for the tube/support interaction under sliding conditions, however the applicability of this equation to purely impacting conditions was not indicated. Based on their analysis and experimental studies they arrived at a wear model (2.24) relating the wear-rate to the work-rate using Archard's wear equation as a starting point. The empirical derivation of "K" required the performance of some experiments using various materials for impact plus sliding and fretting conditions only, as was carried out by the investigators. The figure given in the report showed that assuming the relationship between wear-rate and work-rate to be linear especially when dealing with combined tube orbital motion, is questionable. The error obtained for this condition was comparatively high except for one particular case (Inconel/carbon steel high temperature and pressure with impact plus sliding excitation).

$$W_R = \frac{\sum_{t=t_1}^{t=t_2} \Delta W(t)}{(t_2 - t_1)} \tag{2.23}$$

where,

W_R = work-rate (work per unit time given by tube-plate relative motion during contact and dynamic contact force)

$\Delta W(t)$ = average work done over time

t_1 = starting time of averaging

t_2 = ending time of averaging

$$w = K(W_R)t \tag{2.24}$$

where,

w = wear volume

K = empirically derived wear coefficient

t = total wear process time

Pettigrew et al. [45] gave a state of the art on flow induced vibrations in nuclear power plant heat exchangers and studied impact fretting wear mechanisms. They stressed the importance of fluid-elastic excitation on cross-flow heat exchanger tube bundles and advised that it be avoided at design stages. They provided an experimental result showing the effect of temperature on wear-rate, conducted in an autoclave, however the plots of this experiment were of different trend to that of Blevins' where he had demonstrated a decrease in the wear-rate with increasing temperature the only difference being his experiments were run in helium medium (support and tube were the same material, alloy 800H) while their's was run in a water medium (tube was incoloy 800 while support was 304 stainless steel and carbon

steel). Possible explanation for this could be that the debris was washed out before it had the chance to self weld hence the growth in wear-rate with increasing temperature.

They give a relationship (2.25) arrived at by Ko et al. [37] for the material combination of Incoloy 800 tubing against Inconel 600 supports, relating the wear-rate directly to forcing function.

$$w_r = a_e F^{b_e} \tag{2.25}$$

where,

w_r = wear-rate (wear for 10^6 cycles)

F = applied force

a_e and b_e = constants determined from the experimental results

For the work-rate calculations they use the continuous form of equation (13) given by Frick et al. [44] which is a product of the normal component of the impact or sliding force and sliding distance, as opposed to Hofmann et al. [5] who consider the measured force which includes both normal and sliding (friction) components.

Fisher et al. [46] tried to relate wear-rate to work-rate (equation 2.26), they made use of the Archard's wear equation as a starting point and indicated that even though the equation showed a linear relationship between wear-rate and work-rate a non-linear relationship might be realized as a result of the dependence of K on work-rate.

$$w_r = K W_R \tag{2.26}$$

where w_r is the volumetric wear rate and is given by:

$$w_r = \frac{k_t}{T}\frac{F_N s}{3p} \tag{2.27}$$

where,

K = constant wear coefficient ($=k_t/3p$)

k_t = constant for wear

p = material bulk hardness

F_N = normal applied force

s = sliding distance

W_R = work rate

They observed that the wear behaviour of the experimental tube and support specimen was not time dependent once steady wear was achieved. There will be an increase in work-rate for an increase in wear-rate as a result of an increment in diametral clearance due to wear. They concluded by saying that the work-rate was an appropriate scaling parameter and that its relationship to wear-rate is non-linear growing exponentially for progressive wear.

Hofmann et al. [47] carried out their experimental studies in a hot temperature (200°C) autoclave with the tube supported at two ends and the experimental support at mid-span. The excitation mechanism was similar to that of Ko's with a slight modification to simulate actual operating conditions as close as possible. Their experiments were carried out for short (10^7 cycles) and long (10^8 cycles) term duration, with measurements taken periodically. Results of their testing showed that wear-rate was higher for sliding alone as compared to impacting only or impacting plus sliding which had comparable value. However, for the testing reported at an rms force of 4.6N operating at 40Hz for a material combination of J 600 tube

against 405 SS hole, there was a difference in the wear-rate of the purely impacting and impact plus sliding contact mechanism. Pure impact had the lowest wear-rate over the entire duration, impact plus sliding had a slightly higher wear-rate while pure oscillating sliding had the highest wear-rate.

In their attempt to relate work-rate to wear-rate they first defined work-rate as the product of the measured force and the sliding distance for both oscillating sliding and impact contact conditions. However, they were at an impasse as far as "work-rate" for purely impacting conditions was concerned, in that there is actually wear due to fatigue while there was no measurable "work-rate".

$$W_R = \frac{\int_0^T F(t) L_s(t) dt}{\int_0^T dt} \tag{2.28}$$

where,

$F(t)$ = measured force as a function of time

$L_s(t)$ = velocity of sliding during contact as a function of time

T = total time of experiment

They suggest that the wear mechanism of a predominantly impact condition consists of two components, namely, the sliding wear caused by small tube displacements during impacting and fatigue wear caused by spalling. They recommend the development of a non-linear relationship between volume wear-rate and these two independent parameters. They attempted to show that the wear mechanism requires the introduction of a third independent

variable (average time of contact) to emphasize the necessity of other parameters and to quantitatively show the effect of various wear phenomena that can occur to a steam generator tube.

The study done by Hofmann et al. [5] stressed that work-rate by itself was not an appropriate characterizing parameter, for wear-rate. They argued that Archard's wear equation derived for sliding wear, can lead to an inaccuracy while considering pure or compound impact. They derived an improved wear-rate equation relating specific wear-rate with average work-rate and an overall intensity factor, which is a combined factor of the weighted work hardening effect of impact force and weighted sliding effect of a predominantly sliding type motion force, on wear. A precondition for the validity of this equation is that, the weighted percentage of work hardening should be less than the weighted percentage of sliding wear.

Hofmann et al. [5] tried to characterize wear rate with respect to predefined energy (work-rate) parameter by taking into account the work hardening effect of impact in oblique impact contact conditions. They identified predominantly impact type and sliding type motions by first creating a class of categories of the impact angle and measuring displacement velocity during this motion. The result of this is a 5 by 5 force displacement scaling parameter. The work-rate equation they used was the same as their equation given by (2.28) except in this case they were using the normal component of the contact force instead of the measured one.

$$w_r = k_3 W_{int} W_{Rave} \tag{2.29}$$

where,

k_3 = specific wear rate (estimated by means of a reference test under oscillating

sliding condition)

W_{int} = overall wear intensity factor

W_{Rave} = average work-rate

The value of the wear intensity factor is given by a ratio of the two weighted percentage factors for sliding wear (wear enhancing) and work hardening (wear reducing) effects for impact motions.

$$W_{int} = \frac{[\Sigma F_i (D_i)^2 (p)_{ii}]^2}{\Sigma k_{d1} (F_i/k_{d2}))^3 (p)_{ii} + \Sigma F_i (D_i)^2 (p)_{ii}} \quad \textbf{(2.30)}$$

where,

$(p)_{ii}$ = percentage of F_i D_i class occurrence

F_i = normal force

D_i = total sliding distance

k_{d1} = material constant

k_{d2} = material constant

Verification of this wear rate equation was shown by the authors for all the experiments conducted and a good agreement was found in all of the cases except for one where the maximum factor the value of predicted to measured wear rate differed was 2.1. However, even though the authors have listed a number of constants to be determined experimentally for the materials used, explanation as to how this constants can be obtained were not specified.

The wear model that they developed takes into account the relationship of the work rate to the wear rate by considering the type of contact motion (impact and sliding). However there

is a fundamental discrepancy in that for normal impact conditions, even though there is almost zero measurable work rate, the value of the wear rate is not. Also, one of the assumptions taken into consideration is Engel's approach, which assumes that wear is proportional to F^3N which as shown earlier is questionable. The other reasoning is that work hardening can be associated with both impacting and sliding contact conditions, and as Fleming and Suh [25] have shown hardening might have a wear enhancing effect on the overall wear process.

The reason why this approach helps in reducing the scatter is that, it recognizes the fact that wear rate for a predominantly impact motion, is relatively smaller than for a predominantly sliding type of motion. The model accounts for this effect by using the weighted percentage values, which scales the work rate down for impact motions.

The recent analysis carried out by Hofmann et al. [48], focused on the characterization of wear in heat exchanger tubes, due to impact alone. Indicating the inapplicability of the model developed by Hofmann et al. [5], they went on to investigate the possible effects of accelerated corrosion because of electrochemical activation of the metallic surface. They conducted their own set of experiments and showed that the conventional work rate characterization fails in reducing the scatter. They showed that this error can be reduced by categorizing the amount of sliding per contact, into different classes and using the impact force as a characterization parameter. They used this approach after, showing that the amount of corrosion current is in direct proportion to the measured impact force.

2.6. Flow Induced Vibrations

Axisa et al. [49] performed a dynamic analysis on a multi-span heat exchanger tube to study its vibro-impact response. The tube was given an impact excitation at its mid-span and the response of the system was analysed at the support with clearance. Their investigations showed that at moderate vibration levels, mid-span displacement of the tube was proportional to the excitation amplitude and its support clearance. However, it also revealed that impact forces averaged over a cycle of vibration were almost proportional to excitation and less dependent on support clearance.

Rao et al. [50] did an analytical investigation into the prediction of vibratory response of a non-linear multi-span heat exchanger tube with clearance at the supports using finite-element approach. They used their model to predict the various wear related parameters such as maximum and rms reaction force, maximum and rms z displacement, sliding distance, percentage contact time, average contact time and work-rate. They utilized readily available data, on heat exchanger tube wear, from previously conducted experiments and found close agreement with their predicted values.

Even though the dynamics of the tubes is important from the wear determination aspect, the main objective of this research work is to analyse the intensive work done on the mechanical aspect of wear of tubes in heat exchangers. Hence, in order to study the surface interaction of the tube and its support, for different orbital motions, for correct characterization of the wear, survey of the limited available literature dealing with the concept of wear rate/work

rate was stressed upon.

2.7 Conclusion

The state of the art survey given on the various wear models, generalized as well as those particular for heat exchanger tubes indicates the different schools of thought. Since all the reports are supported by experimental results and most of the models are different from each other, the only reasonable explanation for the validity of this equations is that they are dependent on the dynamics of the particular system used by the individual researcher. Hence, this is a further indication that accurate generalized wear models are not available to be implemented for the analysis and design of a heat exchanger tube.

The next chapter will examine the validity of the wear characterization parameter, work-rate, using the stress dependent empirical formulations forwarded by Schumacher and his research associates and Engel and his research associates.

CHAPTER 3

ASSESSMENT OF THE WORK RATE PARAMETER TO CHARACTERIZE IMPACT AND/OR SLIDING FRETTING WEAR

3.1 Introduction

The characterization of wear is, without doubt, one of the most controversial issues facing researchers in the tribology community, working in the field of heat exchanger tube wear. Conditions such as normal impacting, oblique impacting and pure sliding contacts add to the complexity of the problem by changing the method of energy characterization and wear mechanisms. The different empirical formulations, covered in the previous section indicate that, depending upon the researcher and circumstances under which the experiment was conducted, the models derived vary from each other considerably. [102, 104] (Author's Ref.)

There are various mathematical models derived for analysing sliding wear or impacting wear separately. To date, there is no model capable of handling both sliding and impacting wear at the same time, implying the mechanism of wear for the two contact conditions are different. However, most of the different researchers working in wear mechanics have shown that fatigue is the detrimental wear mechanism causing the bulk of the debris formation under the various contact conditions, if the force associated with the wear does not cause plastic deformation on both the global and local scale [14]. Bearing in mind the above observation, this chapter will attempt to characterize wear based on conventional input parameters.

The conventional method used for characterizing wear rate is work rate. It is currently the common energy input parameter accepted and used by most researchers in the field. Seeing that the work rate is a product of the normal force and sliding distance per unit time, this definition will be assumed valid for the analysis of wear both in sliding and impacting contact conditions. Even though there is no measurable work rate in pure impact, the relative elastic compliance of the contacting bodies will be considered as the overall sliding distance for calculating the work rate.

The generalized fatigue wear model developed by Bayer et al. [14,18] for sliding wear and by Engel and Engel et al. [30-34] for normal and oblique impact have similar conceptual approach for both cases. The differential formulation of both wear models is based on the assumption that fatigue is the dominant mechanism causing the wear. These wear models will be utilized to investigate wear rate / work rate relationship, occurring between a cylinder and a flat surface and a cylinder in a conforming surface, for the three relative motions namely sliding, normal impacting and oblique impacting. The analysis will consider a low energy contact condition (contact force does not cause plastic deformation both on the global and local scale) for the three contact case studies.

The wear models derived for sliding and impact motions is based on the assumption that fatigue wear is the dominant mechanism. Based on this assumption the wear model formulation starts from the Palmgren's relationship [7] for spherical roller bearing life, giving the life of the bearing to be proportional to the product of the cube of the contact force and the number of cycles.

the life of the bearing to be proportional to the product of the cube of the contact force and the number of cycles.

$$L_b \propto F^3 N \tag{3.1}$$

where,

L_b = life of the bearing

F = maximum normal contact force

N = number of F cycles

The approach used by Bayer and Engel presumes the wear volume to be proportional to F^5N, as they have taken fatigue to be the dominant wear mechanism. Their results have been verified experimentally, as listed in their published reports. Therefore, based on their assumptions and relationships, it will be shown that the wear rate / work rate relationship does not follow a particular trend which makes work rate an ineffective identifying parameter. This means that the non-uniqueness of this parameter will be established, ensuring the need for a better model and characterizing parameter. The first model derived will be a cylinder impacting a flat hard (flat surface does not wear) surface at an angle of 90°.

3.2 Pure Impact Wear Model (Cylinder on a Flat Surface)

The first analysis investigates the wear occurring between a cylinder and a flat surface undergoing repetitive normal impacting (Figure 3.1 a-b). In order to calculate the wear rate, one needs to start from the general wear model as given by Engel [28]. The differential formulation of the fatigue wear model which is obtained by taking the partial derivative of the wear with respect to number of impacts and contact stress (σ) is given:

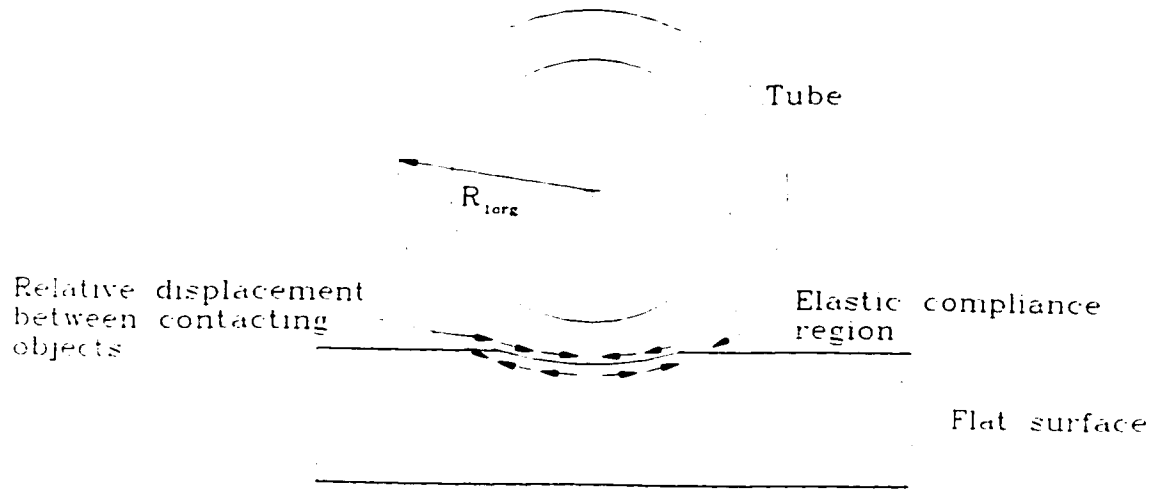

a)

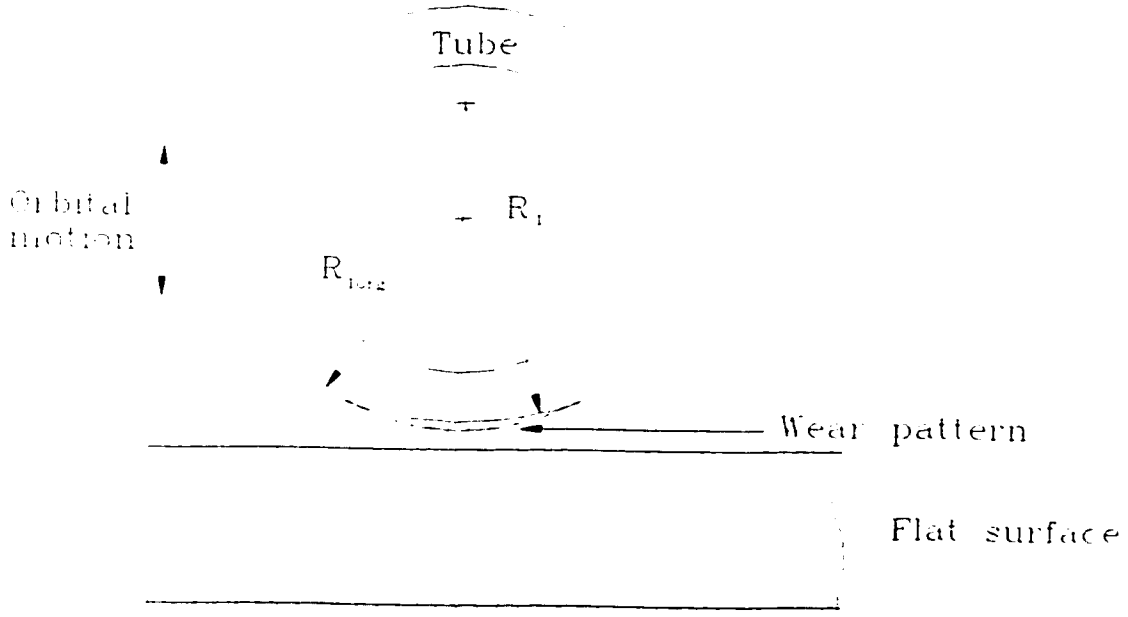

b)

Figure 3.1 Impact of a tube on a flat surface a) contact conditions and b) wear pattern

$$w = k_i P_{max}^3 N = K\sigma^9 N$$

$$dw = \frac{w dN}{N} + 9w\frac{d\sigma}{\sigma} \tag{3.2}$$

where,

k_i = experimental constant

Rearranging the differential of the stress dependent wear equation by expressing w and σ in terms of R_{1org} and R_1 and simplifying by substituting, one obtains the equation relating the number of impacts and non-dimensional radius parameter $\lambda(R_{1org}/R_1)$ is given by equation (3.3) [28]:

$$N = N_0 \frac{(1-\lambda)/(1-\lambda_0)}{\lambda^6/\lambda_0^6} = k_N\left(\frac{1-\lambda}{\lambda^6}\right) \tag{3.3}$$

where,

N = number of impacts for λ curvature ratio

N_0 = zero wear limit

λ_0 = zero wear curvature ratio

It is essential that λ be expressed as a function of N, in order to simplify the analysis. Hence, this task can be performed by inserting some values for λ between zero and one, in the above equation and by estimating an equation using the least square approximation method. It can be seen that the approximation is dominated by the sixth power relationship of the denominator λ to N, within the range of λ, especially for higher values of wear, eventually giving:

$$\lambda \approx \left(\frac{k_N}{N}\right)^{\frac{1}{6}} = \left(\frac{k_N}{N}\right)^{0.17} \tag{3.4}$$

The constant k_N is obtained from the zero wear conditions using:

$$k_N = \frac{N_0 \lambda_0^6}{1-\lambda_0} \tag{3.5}$$

where the number of impact for zero wear (N_0) is determined from the following equation:

$$N_0 = 2000\left(\frac{\gamma \sigma_y}{\sigma_{max}}\right)^9 \tag{3.6}$$

where,

γ = Engle's [18] experimentally determined wear factor equal to 0.2 or 0.54

σ_y = material yield stress in compression

σ_{max} = maximum contact stress including stress concentration factor

The values of N_0 and λ_0 can be determined using Engel's [34] graphical method known as master curve shifting approach, or can be determined more accurately by using the following geometrical relationship which relates the wear depth to the continuously varying radius of curvature of the worn surface, derivation of which is given in Appendix A:

$$R_1 = R_{1org} - h + \frac{R_{1org}h - 0.5h^2}{R_{1org} - h - \sqrt{R_{1org}^2 - a^2}} \tag{3.7}$$

where the Hertzian contact length a is:

$$a = \sqrt{4P_0 R/(\pi E^*)} \tag{3.8}$$

and,

$$\frac{1}{R} = \frac{1}{R_1} + \frac{1}{R_{2org}} \quad \Rightarrow \quad R = R_1 \tag{3.9}$$

where,

P_0 = Maximum load per unit length

R_{1org} = original radius of cylinder

R_{2org} = original radius of flat surface (∞)

R_1 = worn radius

The reduced Young's modulus is given by:

$$E^* = \left(\frac{1-\nu_1^2}{E_1} + \frac{1-\nu_2^2}{E_2} \right)^{-1} \tag{3.10}$$

Using the above relationships, h (the wear depth) can be expressed in terms of R_1 as follows:

$$h = R_{1org} - R_1 + \sqrt{R_1^2 - \frac{4P_0R_1}{\pi E^*}} - \sqrt{R_{1org}^2 - \frac{4P_0R_1}{\pi E^*}} \tag{3.11}$$

The wear rate ($m^3/m/s$) averaged over the entire duration of the experiment (T) can be obtained by dividing the wear equation for soft cylinder wearing against hard flat surface, given as [28]:

$$w_r = \frac{w}{T} = \frac{0.96}{T} \left(\frac{P_0}{E^*} \right)^{3/2} \frac{(1-\lambda)}{\lambda^{3/2}} R_{1org}^{1/2} \tag{3.12}$$

The above equation gives the wear rate as a function of the force, the reduced Young's modulus, the non-dimensional curvature ratio and the original radius of the cylinder. The next step, at this stage, is to calculate the work rate to use it in the above equation for characterizing the wear. In order to calculate the work rate, the relative deformation (elastic compliance) of the cylinder and flat surface during the application of the force is considered as the overall sliding distance. Even though the contact surface consists of sticking and slipping segments, it will be assumed that the overall relative sliding distance can be

expressed as the difference in length of the two surfaces. Using the Hertz elastic theory of contact, the half length of the cylinder and flat surface in contact is given by:

$$a(t) = \left(\frac{4P(t)R_1}{\pi E^*} \right)^{1/2} \tag{3.13}$$

The variation of the impact force can be assumed to be sinusoidal:

$$P(t) = P_0 \sin\left(\pi \frac{t}{t^*} \right) \tag{3.14}$$

The contact time t^* for a cylinder impacting against a flat surface can be derived by starting from Poritsky's [51] elastic deformation equation. He describes the elastic deformation of the flat surface using two equations, one valid for x/a between 1 and 10 and the other valid for the surface variation between the centre and Hertzian contact length (a) which is given by:

$$y(x,t) = \frac{-4P(t)}{\pi E^*} \left[\left(\frac{x}{a} \right)^2 + K \right] \tag{3.15}$$

The constant K is determined from the assumption that at $x/a = 10$ (Fig. 8 of ref. [51]) the displacement is zero ($K = -3.5$). Since maximum deflection occurs at the centre of contact, taking the variable x to be zero at the time when P is a maximum gives:-

$$y(0,t^*/2) = \frac{14P_0}{\pi E^*} \tag{3.16}$$

During impact, the force varies with respect to time and so does the deflection. Bearing in mind that the maximum deflection occurs at $x = 0$, it is evident that the above equation (3.16) gives the overall displacement of the flat surface in the y-direction. The total approach between the two bodies can be calculated by adding the compliance of the cylinder to this value. The compliance of the cylinder can be calculated from the geometrical properties of

the cylinder and from the value of y at $x = a$. It can be seen that the total elastic compliance of the cylinder is the radius of the cylinder minus the y value at $x = a$ minus the difference of the y value at $x= 0$ and $x=a$. Taking the summation of the approach of the cylinder as well the approach of the flat surface the total approach of the two objects is given by:

$$y(t) = \frac{5P(t)}{\pi E^*} + R_{1org} - \sqrt{R_{1org}^2 - 4P(t)R_{1org}/\pi E^*} \tag{3.17}$$

The above equation can be reduced to the following by least square approximation using appropriate values for the constants.

$$y(t) = k_t P(t) \tag{3.18}$$

where,

$k_t = 1.96 * 10^{-11} ms^2/kg$

In order to derive the duration of impact one can follow a similar procedure given by Weber et al. [52] derived for two cylinders impacting with each other. Assuming the cylinder has a mass m per unit length and is impacting the surface with a velocity V one obtains,

$$m_c \frac{dV(t)}{dt} = -P_0(t) \tag{3.19}$$

After impact has commenced, the velocity and acceleration are given by:

$$\frac{dy(t)}{dt} = V(t) \quad and \quad \frac{d^2y(t)}{dt^2} = \frac{dV(t)}{dt} = -\frac{P(t)}{m_c} \tag{3.20}$$

From the above relationship one obtains a second order homogenous linear differential equation:

$$\frac{d^2y(t)}{dt^2} + \frac{y(t)}{m_c k_t} = 0 \tag{3.21}$$

Solution for the above homogeneous differential equation can be obtained by assuming that the maximum displacement will occur at half the contact time, i.e. at $t = t^*/2$, $y(t^*/2) = y_0$ and that contact starts just after time $t = 0$, i.e. at $t = 0$, $y(0) = 0$.

$$y = y_0 \sin\left(\frac{1}{\sqrt{m_c k_t}} t\right) \tag{3.22}$$

The total impact duration is, therefore, given by:

$$t^* = \pi\sqrt{m_c k_t} = 1.39 * 10^{-5}\sqrt{m_c} \tag{3.23}$$

where,

m_c = the mass of cylinder per unit length (kg/m)

It is interesting to note that the time of contact is not a factor of the force, but rather the mass and elastic properties of the two contacting bodies. The angle which subtends half the Hertzian contact length is given by:

$$\theta(t) = \sin^{-1}\left(\frac{a(t)}{R_1}\right) \tag{3.24}$$

Taking into consideration the elastic deformation at the contact surface the quantity S_y derived in appendix B (to demonstrate that the difference between original distance and deformed distance, is extremely small making measurement impossible), is added on to the length of the flat surface and subtracted from the cylindrical surface in contact. This implies that the total length reduction or addition for the cylinder is given by:

$$S_{ac}(t) = \theta(t) R_1 - S_y(t) \tag{3.25}$$

and the flat surface is given by:

$$S_{af}(t) = S_y(t) - a(t) \tag{3.26}$$

Therefore, the overall relative length variation is given by the following equation which gives

the relative instantaneous sliding distance between this two surfaces in contact.

$$S(t) = S_{ac}(t) + S_{af}(t) = \theta(t) R_1 - a(t) \tag{3.27}$$

Since the impact force is of a sinusoidal nature for each loading, it is apparent that the elastic compliance is also a function of time. Hence, the work-rate which is defined as a product of normal force and tangential sliding distance per unit time has to be integrated over the contact time t^* to calculate the work rate during impacting:

$$W_{Rni} = \frac{2N}{Tt^*} \int_0^{t^*} S(t)\, P(t) dt = \frac{2NP_0}{T} \bar{S}_1 \tag{3.28}$$

where,

$$\bar{S}_1 = \frac{1}{t^*} \int_0^{t^*} \left[R_1 \sin^{-1} \sqrt{\frac{4P_0 \sin\left(\pi \frac{t}{t^*}\right)}{R_1 \pi E^*}} - \sqrt{\frac{4P_0 R_1 \sin\left(\pi \frac{t}{t^*}\right)}{\pi E^*}} \right] \sin\left(\pi \frac{t}{t^*}\right) dt \tag{3.29}$$

Since the above equation does not have a closed form solution, a numerical integration scheme is utilized to calculate the values. Inserting this equation into the wear-rate equation of (3.12) the final equation relating wear-rate and work-rate is given by:

$$w_r = 0.48 \frac{(P_0 R_{1org})^{1/2}}{(E^*)^{3/2}} \frac{\lambda^{9/2}}{\bar{S}_1 k_N} W_{Rni} \tag{3.30}$$

which can be written without λ as:

$$w_r = \frac{0.48}{\bar{S}_1 N^{1/6} k_N^{3/12}} \frac{(P_0 R_{1org})^{1/2}}{(E^*)^{3/2}} W_{Rni} \tag{3.31}$$

The wear-rate equation can be expressed in terms of the number of impacts as:

$$w_r = \frac{0.96\sqrt{R_{1org}}}{T} \left(\frac{P_0}{E^*}\right)^{3/2} \left(\frac{N}{k_N}\right)^{3/12} = \frac{0.96 f_n \sqrt{R_{1org}}}{N^{9/12} k_N^{3/12}} \left(\frac{P_0}{E^*}\right)^{3/2} \tag{3.32}$$

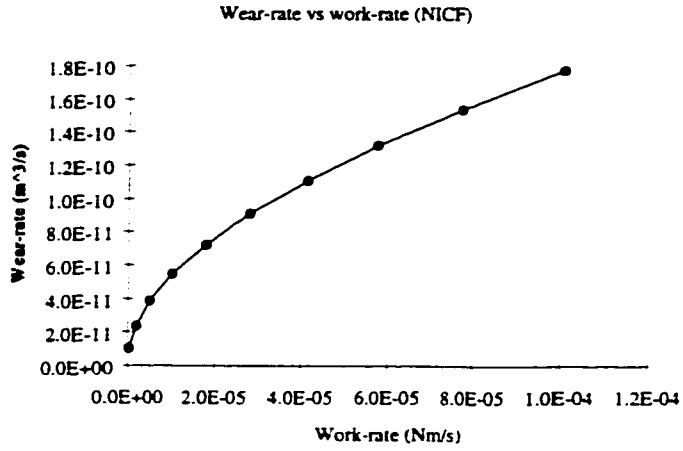

a

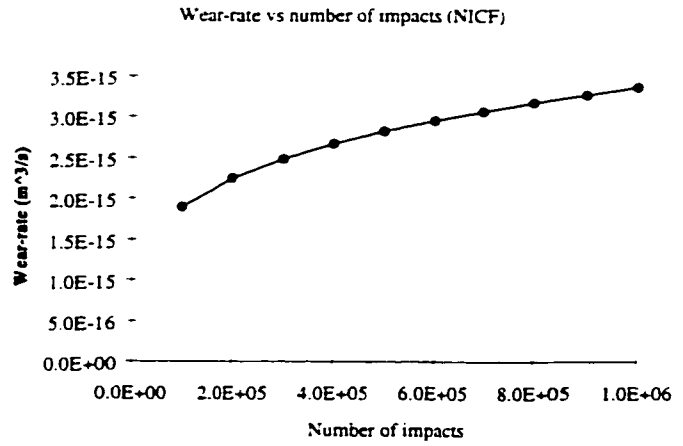

b

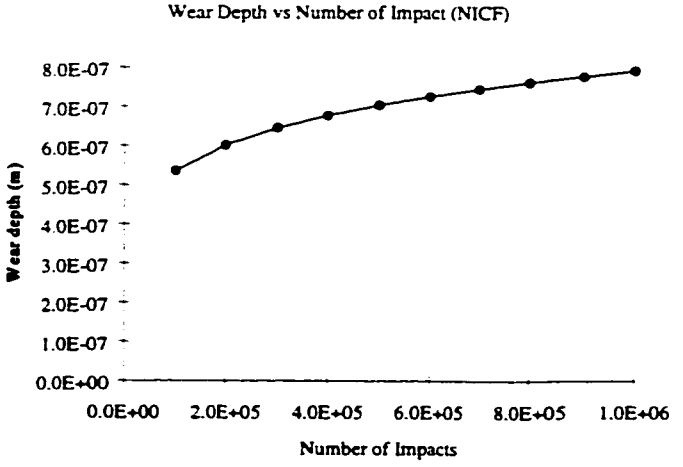

c

Figure 3.2 Wear characteristics of a cylinder normally impacting on a flat surface

The wear depth is an important quantifying parameter when dealing with the wear of a tube. Therefore, it is essential to obtain h in terms of the non-dimensional ratio λ. This is achieved by substituting values of R_l in the eq.. relating h to R_l to obtain the following:

$$h = R_{1org} - \frac{R_{1org}}{\lambda} + \sqrt{\left(\frac{R_{1org}}{\lambda}\right)^2 - \frac{4PR_{1org}}{\lambda\pi E^*}} - \sqrt{R_{1org}^2 - \frac{4PR_{1org}}{\lambda\pi E^*}} \qquad (3.33)$$

But λ itself is approximated as a function of N as per equation (3.4). Therefore, h can be expressed as a function of N as follows:

$$h = R_{1org} - \frac{R_{1org}}{(k_N/N)^{1/6}} + \sqrt{\left(\frac{R_{1org}}{(k_N/N)^{1/6}}\right)^2 - \frac{4PR_{1org}}{(k_N/N)^{1/6}\pi E^*}} - \sqrt{R_{1org}^2 - \frac{4PR_{1org}}{(k_N/N)^{1/6}\pi E^*}} \qquad (3.34)$$

The variation of the wear rate / work rate, wear rate / number of impacts and wear depth / number of impact relationships is derived and plotted in Figures. (3.2a-c) as follows. The maximum loading was varied from 2000 - 20000 N/m, while keeping the number of impacts and time of application constant at $1.0*10^6$ and $3.6*10^4$ sec., respectively. The stress concentration factor is considered as unity for the purposes of analysis and is maintained the same for all the cases. The characterization of wear rate and wear depth using work rate and number of impacts is very important in determining the wear of the tube in general. Similar analysis is performed for oblique impact conditions for a cylinder against a flat surface. The results of all the plots are discussed comparatively in section 3.8.

3.3 Compound Impact Wear Model (Cylinder on a Flat Surface)

The compound or oblique impact model is derived for a flat surface and a cylindrical object moving at equal velocities perpendicular to each other. This implies that the angle of impact

is 45° (Figure 3.3), chosen as a typical case, for the purpose of analysis. The motion between the bodies can be analysed by assuming quasi-static Hertzian contact conditions for the duration of the impact. It is evident that due to the motion of the two objects there is relative sliding due to rigid body movement as well as elastic compliance, which is of Hertzian nature. The normal impact component can be superposed to the sliding component formulation of which starts from the work rate relationships. The work-rate can be derived by summing the component due to elastic compliance (normal impact) and component due to sliding (tangential component of velocity).

$$W_R = W_{Rni} + W_{Rsi} \tag{3.35}$$

The work-rate due to normal impact has already been derived in the previous section. The work-rate due to compound impact is derived by integrating the time dependant contact force over the slipping time t^*. As in the previous case, the load variation is assumed to be sinusoidal over the duration of contact, having a maximum value of P_0.

$$W_{Rsi} = \frac{N}{T}\int_0^{t_s} P_0 \sin\left(\frac{\pi t}{t^*}\right) v_s dt = \frac{NP_0 v_s t^*}{T\pi}\left[1-\cos\left(\pi\frac{t_s}{t^*}\right)\right] \tag{3.36}$$

where, the slipping time t_s is given by [28]:

$$t_s = \frac{t^*}{\pi}\cos^{-1}\left(1-\frac{\pi m v_s}{\mu P_0 t^*}\right) = \frac{t^*}{\pi}\cos^{-1}(1-f) \tag{3.37}$$

Engel [31] has shown that the values of f describe the slipping motion. Lower values mean little or no slipping while higher values imply higher slipping. He categorized the value as follows indicating the amount of slipping:

$f = 0$ implies no slipping

$0 < f < 2$ implies moderate slipping following the above relationship

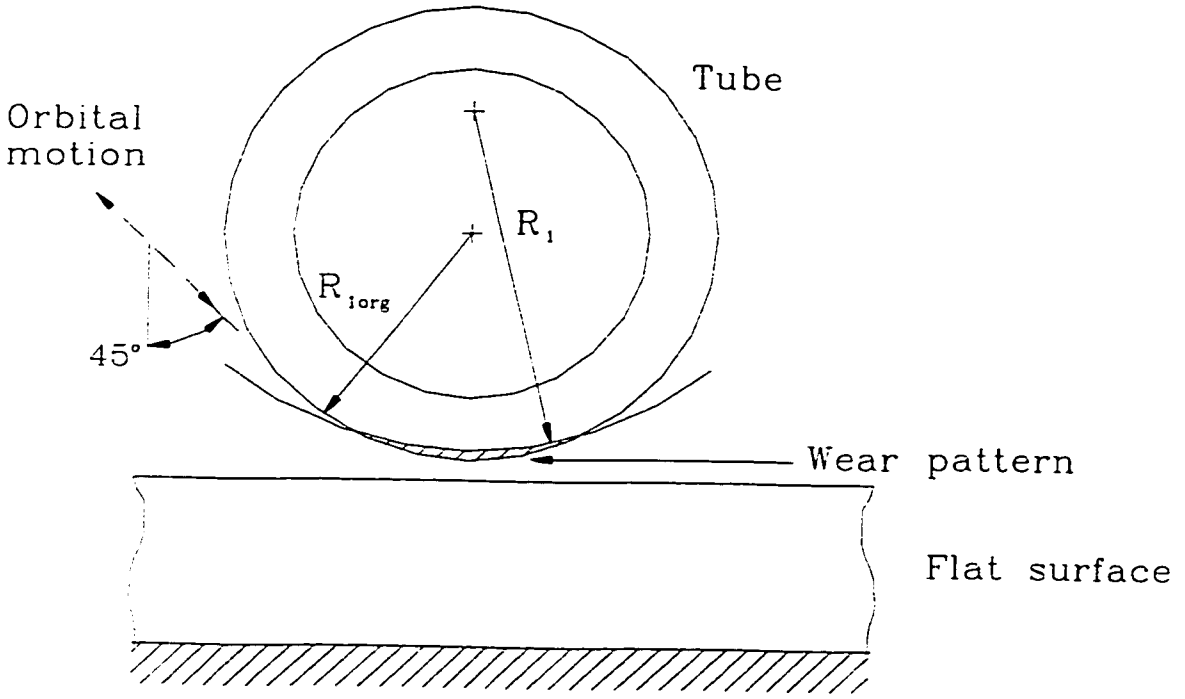

Figure 3.3 Wear pattern of a cylinder obliquely impacting on a flat surface

$f \geq 2$ implies $t_s = t^*$

The total work rate for compound impact is a sum of the normal and sliding components as indicated earlier and is given by:

$$W_R = \frac{2NP_0}{T}\left(\bar{S}_1 + \frac{v_s t^* c_s}{2\pi}\right) \tag{3.38}$$

where,

$$c_s = 1 - \cos\left(\pi t_s / t^*\right) \tag{3.39}$$

Inserting the value of the compound impact work rate equation into the wear-rate equation, the relationship between work rate and wear rate is given by:

$$w_r = \frac{0.48}{(\bar{S}_1 + v_s c_s t^*/2\pi) N^{1/6} k_N^{3/12}} \frac{(P_0 R_1)^{1/2}}{(E^*)^{3/2}} W_R \tag{3.40}$$

The wear-rate equation is given as a function of number of impacts by:

$$w_r = \frac{0.96 f_n \sqrt{R_{1org}}}{N^{9/12} k_N^{3/12}} \left(\frac{P_0}{E^*}\right)^{3/2} \tag{3.41}$$

The wear depth as a function of number of impacts is determined from the same equation utilized in the previous section. The only difference in this case is that the value of k_N will not be the same.

$$h = R_{1org} - \frac{R_{1org}}{(k_N/N)^{1/6}} + \sqrt{\left(\frac{R_{1org}}{(k_N/N)^{1/6}}\right)^2 - \frac{4PR_{1org}}{(k_N/N)^{1/6}\pi E^*}} - \sqrt{R_{1org}^2 - \frac{4PR_{1org}}{(k_N/N)^{1/6}\pi E^*}} \tag{3.42}$$

Where k_N is determined after finding the number of impacts for zero wear using the following relationship given by Engel [28]:

$$N_0 = \frac{2000}{1+\beta}\left(\frac{\gamma \sigma_y}{\sigma_{max}}\right)^9 \tag{3.43}$$

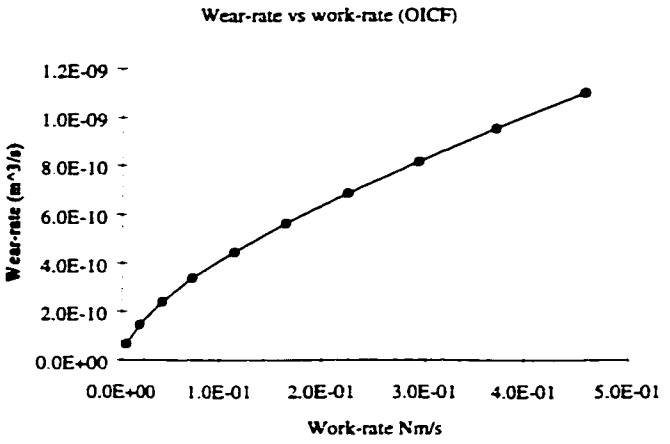

a

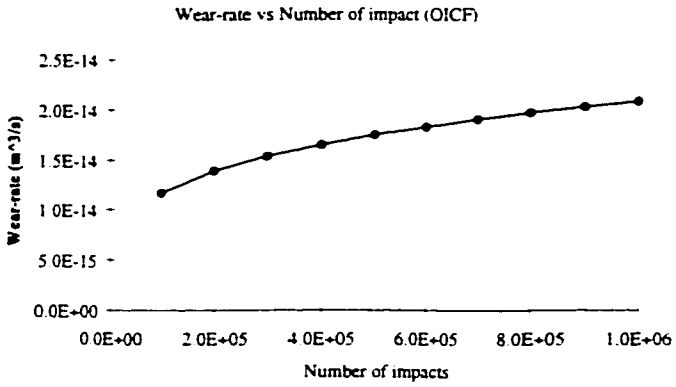

b

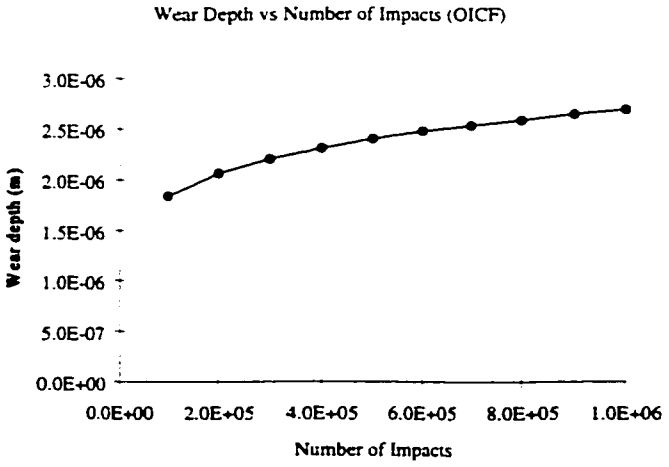

c

Figure 3.4 Wear characteristics of a cylinder obliquely impacting on a flat surface

where,

β = the surface damage contribution factor given by:

$$\beta = \left(\frac{\mu}{0.31}\right)^9 \frac{\int_0^{\cos^{-1}(1-f)} \sin^9\xi d\xi}{\int_0^{\pi} \sin^9\xi d\xi} = \left(\frac{\mu}{0.31}\right)^9 \frac{\int_0^{\cos^{-1}(1-f)} \sin^9\xi d\xi}{0.8127}, \qquad (0<f<2) \tag{3.44}$$

Then,

$$\beta = \frac{\mu^9}{2.15*10^{-5}}\left[(1-f)\left(-\frac{1}{9}s_c^8 - \frac{8}{63}s_c^6 - \frac{16}{105}s_c^4 - \frac{64}{315}s_c^2 - \frac{128}{315}\right) + \frac{128}{315}\right] \tag{3.45}$$

or,

$$\beta = \frac{f}{2}\left(\frac{\mu}{0.31}\right)^9, \qquad (f>2) \tag{3.46}$$

where,

$s_c = \sin[\cos^{-1}(1-f)]$

and the value of λ_0 is found using the relationship between the wear depth and radius of curvature as given in the previous section. After determining the value of R_1 (h_0) it can be used to find the value of λ_0 which will help to calculate the constant as follows:

$$k_N = \frac{N_0 \lambda_0^6}{1-\lambda_0} \tag{3.47}$$

Using the above relationships of work rate / wear rate, wear rate / number of impacts and depth of wear / number of impacts the general trend of wear is shown as per the plots given in figures 3.4a-c. It should be noted that the wear characterization follows a similar trend as

in the normal impact case because the equation formulating the above relationships is the same and the constants are also the same. The oblique angle is assumed to be 45° and is maintained for the various magnitudes of load by using Engel's velocity / impact load relationship for cylinders given in [28]. The only difference is in the introduction of the surface damage contribution factor β which controls the number of impact for zero wear.

3.4 Pure Sliding Wear Model (Cylinder on a Flat Surface)

The various relationships derived in the previous sections for normal and oblique impact were based on the wear model arrived at by Engel et al. [30]. In this section, the relationships for pure sliding motion (Figure 3.5) is derived based on the wear model proposed by Bayer et al. [16-18]. As in the previous case, the major assumption is based on the proportionality of wear volume to Palmgren's famous fatigue relationship. Solving for the solution of the differential, by expressing the wear as a product of the shear stress, pass length and number of pass lengths traversed (n), in terms of the variable depth h, will give the wear for the particular geometry.

$$w = KN(\tau_{max} L_p)^{\frac{9}{2}}$$

$$dw = \frac{w}{N} dN + \frac{9}{2} \frac{w}{(\tau_{max} L_p)} d(\tau_{max} L_p) \qquad \textbf{(3.48)}$$

where,

K = constant of wear

N = number of cycles

τ_{max} = maximum shear stress

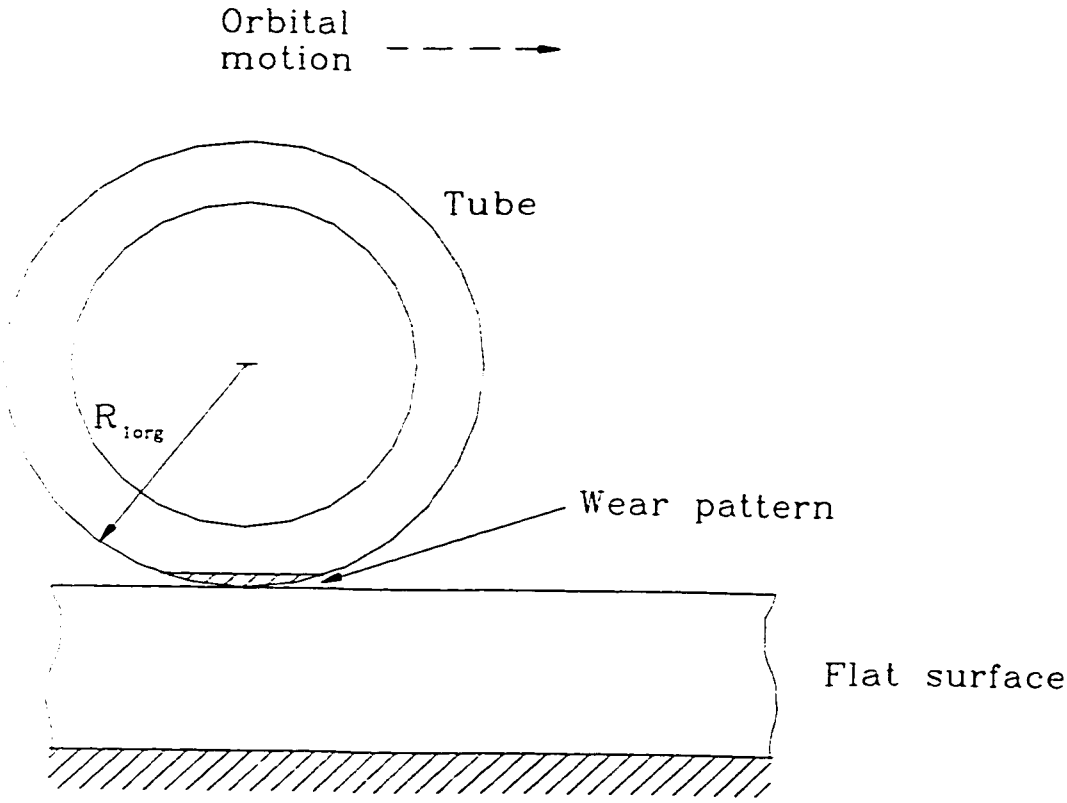

Figure 3.5 Wear pattern of a cylinder sliding on a flat surface

L_p = pass length

The derivation of τ_{max} depends on the maximum contact pressure and is given by equation (3.49) for sliding of a cylinder on a flat surface, perpendicular to its axis [16].

$$\tau_{max} = k_s \sigma_{max} \sqrt{\frac{1 + 4\mu^2}{4}} \tag{3.49}$$

where,

k_s = stress concentration factor

μ = coefficient of friction

σ_{max} = maximum contact stress

The stress is based on the assumption that the zero wear limit has been reached. Hence, the maximum pressure is simply the load divided by the total contact surface area:

$$\sigma_{max} = \frac{P_0}{A} = \frac{P_0}{1 \cdot L_p} = \frac{P_0}{\sqrt{8 R_{1org} h}} \tag{3.50}$$

Assuming the wear area is triangular (approximation) the volume worn per unit length is:

$$w = \sqrt{2 R_{1org} h^3} \tag{3.51}$$

Taking the differential with respect to h:

$$dw = \frac{3}{2}\sqrt{2 R_{1org} h}\, dh \tag{3.52}$$

The next step is finding the differential formulation of the product of the maximum shear stress and the pass length. The differential is taken with respect to the wear depth, h giving:

$$\frac{d(\tau_{max} L_p)}{dh} = \frac{d\left(k_s P_0 \sqrt{\frac{(1+4\mu^2)}{4}} \right)}{dh} = 0 \tag{3.53}$$

Since N is given by the product of the sliding distance (S) and number of times the cylinder traverses this contact (n) over the instantaneous contact length (L), the differential dN can be expressed as:

$$N = \frac{Sn}{\sqrt{8R_{1org}h}} \tag{3.54}$$

Taking the partial differential with respect to n and h:

$$dN = \frac{\partial N}{\partial h}dh + \frac{\partial N}{\partial n}dn = -\frac{Sn}{2\sqrt{8R_{1org}h^3}}dh + \frac{S}{\sqrt{8R_{1org}h}}dn \tag{3.55}$$

Substituting this quantities into the wear differential equation one obtains:

$$\frac{3}{2}\sqrt{2R_{1org}h}\,dh = \frac{\sqrt{2R_{1org}h^3}}{nS}\sqrt{8R_{1org}h}\left[\frac{S}{\sqrt{8R_{1org}h}}dn - \frac{Sn}{2h\sqrt{8R_{1org}h}}dh\right] \tag{3.56}$$

Simplifying and integrating the above equation one obtains:

$$\int\left(\frac{3}{2h} + \frac{1}{2h}\right)dh = \int\frac{1}{n}dn \quad \Rightarrow \quad h^2 = C_1 n \tag{3.57}$$

where

C_1 = constant of integration

The determination of C_1 is done for the zero wear (maximum depth h_0, which is half the original roughness) of the surface and the zero wear limit is calculated using the following equation:

$$N_0 = 2000\left(\frac{\gamma_R \tau_y}{\tau_{max}}\right)^9 \tag{3.58}$$

The average work-rate equation is given by:

$$W_R = \frac{P_0 N\sqrt{8R_{1org}h}}{T} = \frac{P_0 Sn}{T} \tag{3.59}$$

where,

S = sliding distance

N = total number of times the pass length is traversed

n = total number of times S is traversed

T = total time duration for the wear

P_0 = maximum normal load

R_{1org} = original radius of cylinder

h = wear depth

The average wear-rate equation is given by:

$$w_r = \frac{\left(2R_{1org}h^3\right)^{\frac{1}{2}}}{T} = \frac{\left[2R_{1org}\left(\sqrt{C_l n}\right)^3\right]^{\frac{1}{2}}}{T} \tag{3.60}$$

The wear-rate can be expressed as a function of time as:

$$w_r = \frac{f\sqrt{2R_{1org}}C_l^{3/4}}{n^{1/4}} \tag{3.61}$$

where,

f = frequency of excitation

The wear-rate is related to the work-rate by the following equation:

$$w_r = \frac{\left[2R_{1org}\left(\sqrt{C_l n}\right)^3\right]^{\frac{1}{2}}}{T}\frac{T}{P_0 Sn}W_R = \frac{\sqrt{2R_{1org}}C_l^{3/4}}{P_0 Sn^{1/4}}W_R \tag{3.62}$$

The depth wear rate, which is important in terms of identifying the safe operation of tubes, is given by:

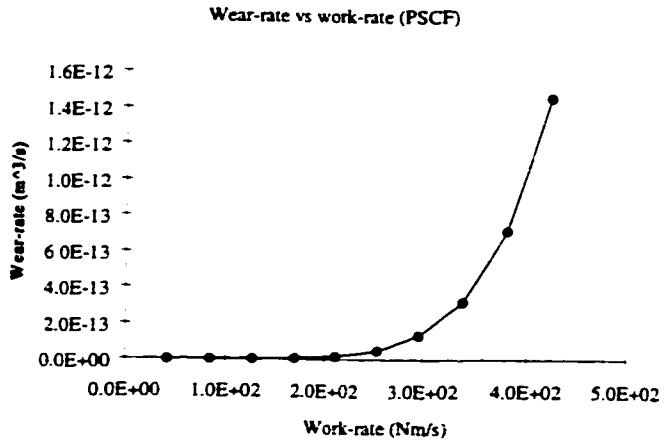

a

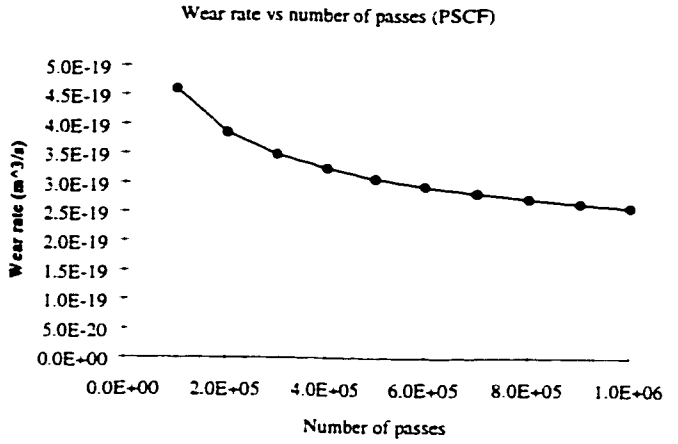

b

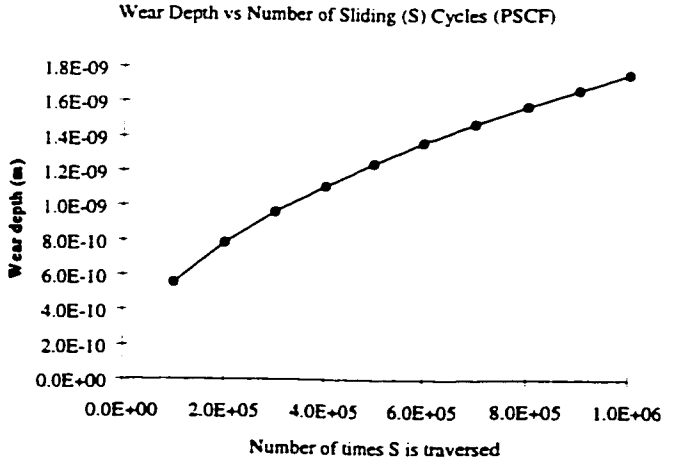

c

Figure 3.6 Wear characteristics of a cylinder purely sliding on a flat surface

$$h = \sqrt{C_1 n} \tag{3.63}$$

By varying the value of P_0 one can observe the variation of wear-rate to work-rate bearing in mind that C_1 the constant of integration is dependent on P_0. The variation of the wear rate over time and the depth rate over time are shown in figures. 3.6a-c. The variation of these two quantities is plotted by changing the number of times the pass length S which is 7.62E-04 m is traversed by keeping the maximum contact load at 2000 N/m.

3.5 Normal Impact Wear Model (Cylinder in a Cylinder)

The wear model of a cylinder within a cylinder (Figure 3.7) is analysed by making use of approximate wear volume equation and using this equation in the differential wear model as in the previous cases. According to the optimal wear path principle the wear curvature surface is equal to the geometric Hertzian contact of the two objects and proceeds in a manner which will conform this curvature of the wearing object to the hard object's curvature [28]. Therefore a geometrical approach is adopted to find the variation of a (half the Hertzian contact length) with respect to the wear depth h as the radius of curvature of the wearing body proceeds automatically conforming with the slightly larger diameter hole. The following relationship gives this variation as (Appendix B):

$$R_1 = R_{1org} - h + \frac{R_{1org}h - 0.5h^2}{R_{1org} - h - \sqrt{R_{1org}^2 - a^2}} \tag{3.64}$$

where,

$$a = \sqrt{\frac{4P_0 R_{2org}}{\pi E'} \frac{R_1}{(R_{2org} - R_1)}} \tag{3.65}$$

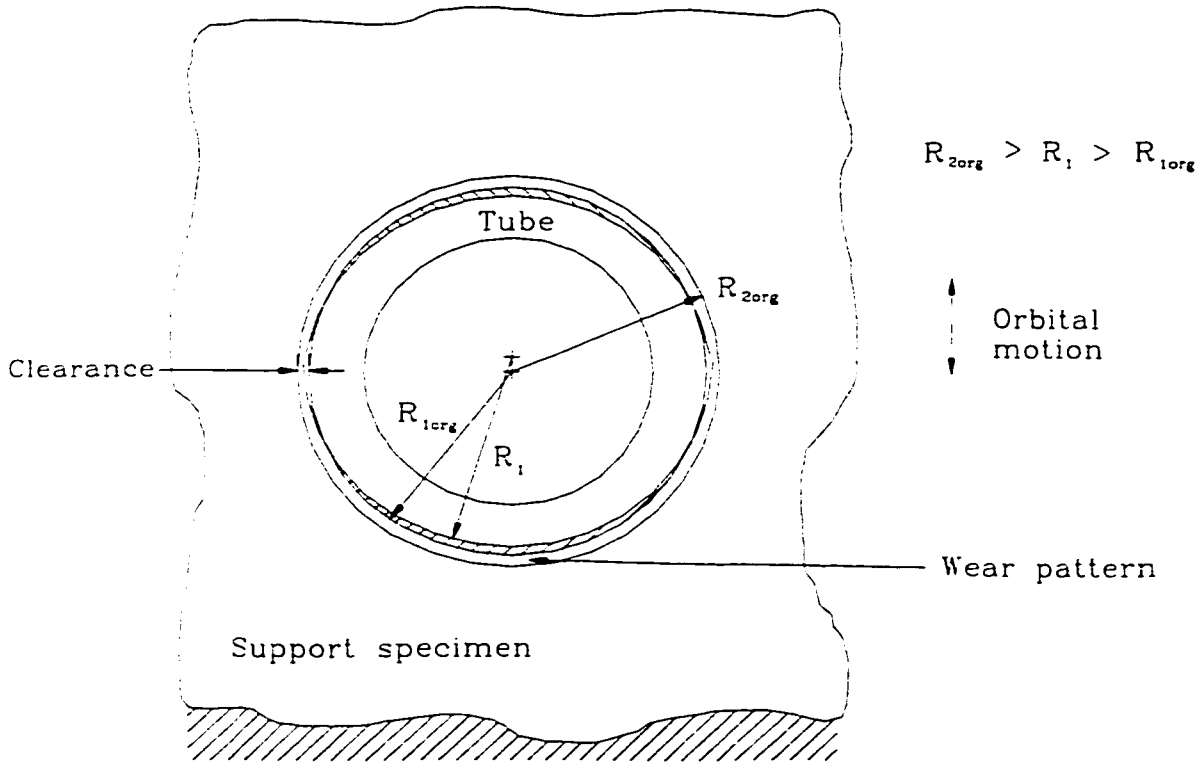

Figure 3.7 Wear pattern of a cylinder impacting in a conforming surface

The value h can be expressed in terms of the variable R_1 and some other constants as follows:

$$h = R_{1org} - R_1 - \sqrt{R_{1org}^2 - \frac{4P_0R_{2org}R_1}{\pi E^*(R_{2org} - R_1)}} + \sqrt{R_1^2 - \frac{4P_0R_{2org}R_1}{\pi E^*(R_{2org} - R_1)}} \quad \textbf{(3.66)}$$

From the above equations there is a unique relationship between h and R_1 and there is one between a and R_1. The value of R_1 varies from R_{1org} to R_{2org} meaning the validity of this wear model is limited until there is absolute conformance of the two bodies. Therefore, using the above relationships, an exponential equation is obtained by approximating a in terms of h, minimizing the error as follows:

$$a \approx 0.22h^{0.42} \quad \textbf{(3.67)}$$

where h is in meters. Substituting this value into the volume of wear using the parabolic geometry of wear relationship:

$$w = \frac{4}{3}ah = 0.29h^{1.42} \Rightarrow \frac{dw}{dh} = 0.41h^{0.42} \quad \textbf{(3.68)}$$

Assuming conformance of the surface as a result of the two radii being almost identical the maximum contact stress including the stress concentration factor (k) is taken as the pressure over the projected area times stress concentration factor.

$$\sigma_{max} = \frac{kP_0}{2a \cdot 1} = \frac{kP_0}{0.44h^{(0.42)}} \Rightarrow \frac{d\sigma_{max}}{dh} = -\frac{0.19kP_0}{h^{1.42}} \quad \textbf{(3.69)}$$

substituting this above relationship in the following differential:

$$\frac{dw}{w} = \frac{dN}{N} + \frac{9d\sigma_{max}}{\sigma_{max}} \quad \textbf{(3.70)}$$

Substituting and simplifying the above relationship gives, the solution is obtained by integrating the above as:

$$\int 1.49\frac{dh}{h} = \int \frac{dN}{N} \quad \Rightarrow \quad h^{1.49} = C_I N \tag{3.71}$$

The value of C_I is determined from the zero wear impact model N_0 for a zero wear depth (h_0) of 0.0005 mm:

$$N_0 = 2000\left(\frac{\gamma\sigma_y}{\sigma_{max}}\right)^9 \tag{3.72}$$

where,

γ = constant for wear

σ_y = yield stress of the material

σ_{max} = maximum contact stress

Using the value of 0.0005mm for h_0 one can obtain the constant C_I from:

$$C_I = \frac{h_0^{1.49}}{N_0} \tag{3.73}$$

The work rate can be approximately determined by assuming the relative sliding distance to be the difference of the elastic compliance of the two bodies. It is taken as a product of, the difference between the average radius and wearing radius of cylinder plus the difference between the original radius of conforming hole and wearing radius of cylinder, and the contact angle. Thus,

$$\theta(t,h)\left(\frac{R_1 + R_{2org}}{2} - R_1\right) + \theta(t,h)\left(R_{2org} - \frac{R_1 + R_{2org}}{2}\right) = \theta(t,h)(R_{2org} - R_1) \tag{3.74}$$

giving the work rate as:

$$W_{Rni}(h) = \frac{2NP_0}{Tt^*}\int_0^{t^*}\sin\left(\frac{\pi t}{t^*}\right)\sin^{-1}\left(\frac{a(t,h)}{R_1(h)}\right)[R_{2org} - R_1(h)]dt = \frac{2NP_0}{T}\bar{S}_2 \tag{3.75}$$

where,

$$a(t,h) = \sqrt{\frac{4P(t)R(h)}{\pi E^*}} \tag{3.76}$$

and,

$$R(h) = \frac{R_{2org}R_1}{R_{2org}-R_1} \tag{3.77}$$

In the above equation, a is a function of both time (t) and wear depth (h) as the one of the radius is wearing. The need for classifying h and t separately arose due to the wear depth being negligibly small within the contact time t^*. Hence, the above integration can be performed by assuming h to be constant in the interval of this contact time. The contact time for a cylinder impacting against a conforming cylinder can be derived by starting from Dubowsky's [53] elastic deformation equation:

$$y(t,h) = \frac{\bar{P}(t)}{2a_{wh}E^*}\ln\left(\frac{8a_{wh}E^*e}{R(h)\bar{P}(t)}\right) \tag{3.78}$$

where,

a_{wh} = half of the axial contact width

$\bar{P}(t)$ = the applied load (N)

Assuming h to be constant in the time interval 0 to t^* and taking the force variation to be sinusoidal, one obtains:

$$y(t) = \frac{\bar{P}_0\sin(\pi t/t^*)}{2a_{wh}E^*}\ln\left(\frac{8a_{wh}^3E^*e}{R\bar{P}_0\sin(\pi t/t^*)}\right) \tag{3.79}$$

In order to derive the duration of impact one can follow a similar procedure employed in section 3.2. Assuming the cylinder has a mass $\bar{m}_c$ (kg) and is impacting the surface with a

velocity V one obtains:

$$\bar{m}_c \frac{dV(t)}{dt} = -\bar{P}(t) \tag{3.80}$$

After impact between the cylinder and the flat surface has commenced, the relative velocity is as shown earlier given by:

$$\frac{dy(t)}{dt} = V(t) \tag{3.81}$$

taking second derivative of y:

$$\frac{d^2y(t)}{dt^2} = \frac{dV(t)}{dt} = -\frac{\bar{P}(t)}{\bar{m}_c} \tag{3.82}$$

which gives at $t = t^*/2$:

$$\frac{d^2y(t^*/2)}{dt^2} = \frac{\bar{P}_0\pi^2}{2a_{wh}E^* t^{*2}}\left[1 - \ln\left(\frac{8a_{wh}^3E^*e}{R\bar{P}_0}\right)\right] = -\frac{\bar{P}_0}{\bar{m}_c} \tag{3.83}$$

This implies that:

$$t^* = \pi\sqrt{\frac{\bar{m}_c}{2a_{wh}E^*}\ln\left(\frac{8a_{wh}^3E^*}{R\bar{P}_0}\right)} \tag{3.84}$$

The value of the half axial contact width a_{wh} is 0.0005m which corresponds to half the width of the scallop bar support. The wear rate / work rate relationship is given by the following equation:

$$w_r = \frac{0.67a(t^*/2,h)h}{NP_0\bar{S}_2(h)}W_{Rni}(h) = \frac{0.15C^{0.95}}{N^{0.05}P_0\bar{S}_2(h)}W_{Rni}(h) \tag{3.85}$$

The wear-rate as a function of time is given as:

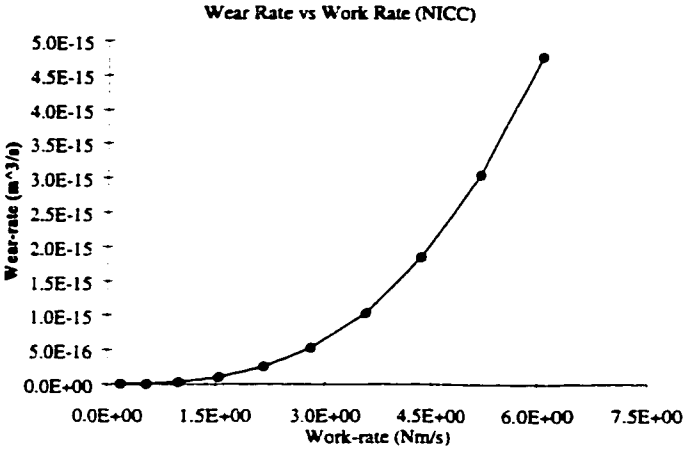

a

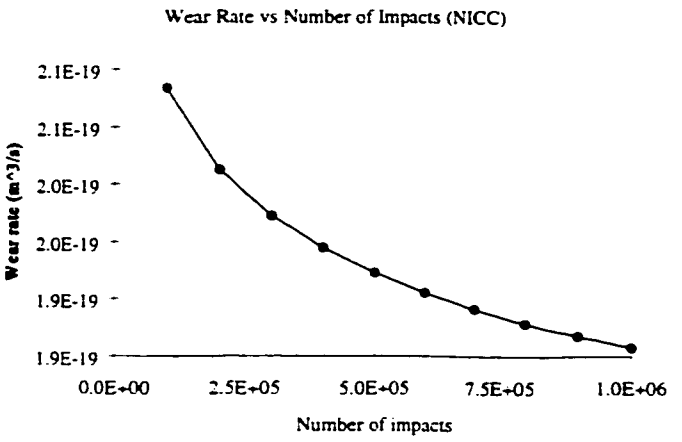

b

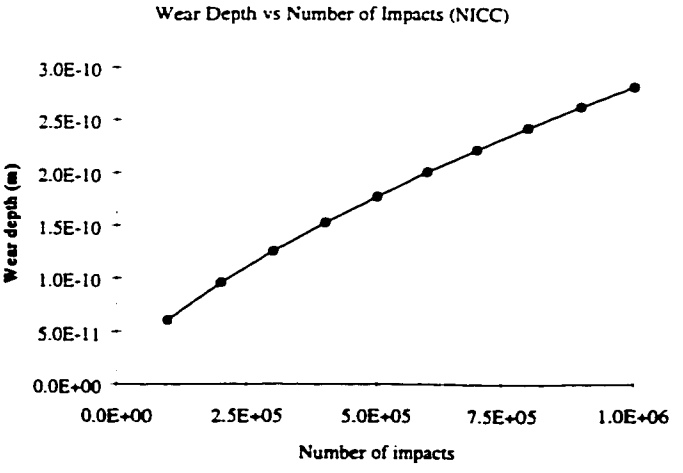

c

Figure 3.8 Wear characteristics of a cylinder normally impacting on a conforming support

$$w_r = \frac{0.22 f_n C_l^{0.95}}{N^{0.05}} \tag{3.86}$$

The wear depth h is given by:

$$h = (C_l N)^{\frac{1}{1.49}} \tag{3.87}$$

The last three relationships are used to plot the variations of wear rate vs work rate, wear rate vs frequency of excitation and depth of wear vs number of impact. Even though R is a function of wear depth (h), the numerical integration is performed by assuming h to be constant in the time interval 0 to t^*. This is a justified assumption as the wear depth h does not vary in the contact time t^* while impacting. The quantity varied in order to plot (figures 3.8a-c) the wear rate / work rate relationship is the load which is from 2000 - 20000 N/m. and for the wear rate and wear depth is number of impact.

3.6 Oblique Impact Wear Model (Cylinder in a Cylinder)

The derivation for the oblique impact (Figure 3.9) wear model is the same as the normal impact however the only difference is that the initial condition will be different and the work rate equation will involve a sliding component.

$$w = \frac{4}{3} a h = 0.29 h^{1.42} \tag{3.88}$$

The relationship between h and N is given same as in the previous case by:

$$h^{1.49} = C_l N \tag{3.89}$$

The constant of integration is obtained from the zero wear characteristics h_0 and N_0. Value

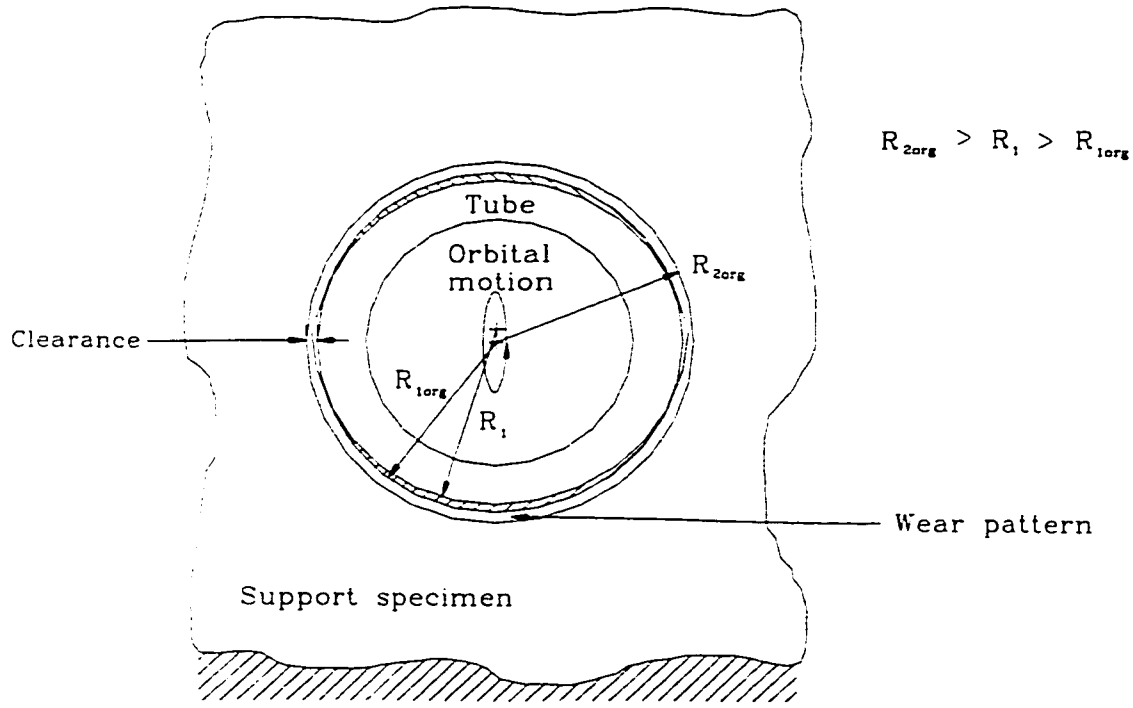

Figure 3.9 Wear pattern of a cylinder obliquely impacting in a conforming surface

of the zero surface wear can be taken as 0.0005mm which is taken as the same from all the previous cases, and value of N_0 can be obtained from the following equation:

$$N_0 = \frac{2000}{(1+\beta)}\left(\frac{\gamma\sigma_y}{\sigma_{max}}\right)^9 \tag{3.90}$$

where the surface damage contribution factor is given by:

$$\beta = \left(\frac{\mu}{0.31}\right)^9 \frac{\int_0^{\cos^{-1}(1-f)} \sin^9\xi d\xi}{0.8127}, \qquad (0<f<2) \tag{3.91}$$

or

$$\beta = \frac{f}{2}\left(\frac{\mu}{0.31}\right)^9, \qquad (f>2) \tag{3.92}$$

The values of t_s is the same as given in section 3.3 by equation (3.37). The work-rate can be similarly derived by:

$$W_R = W_{Rni} + W_{Rsi} \tag{3.93}$$

The work-rate due to normal impact has already been derived in the previous section where as the work-rate due to compound impact is derived as follows assuming the load variation is sinusoidal over the duration of contact, having a maximum value of P_0:

$$W_{Rsi} = \frac{N}{T}\int_0^{t_s} P_0 \sin\left(\frac{\pi t}{t^*}\right) v_s dt = \frac{NP_0 v_s t^*}{T\pi}[1-c_s] \tag{3.94}$$

where,

$$c_s = 1-\cos\left(\pi t_s/t^*\right)$$

Therefore,

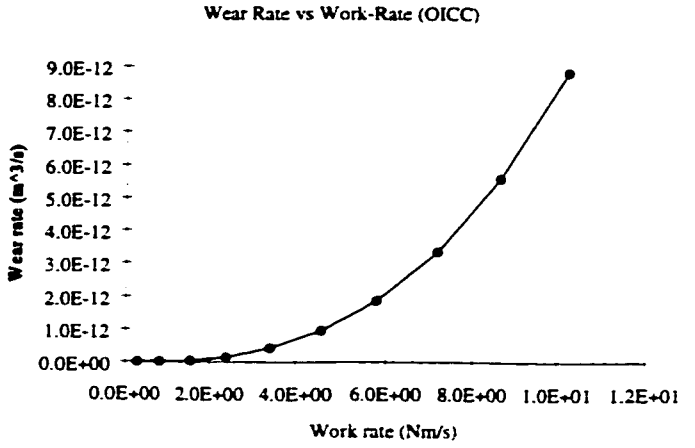

a

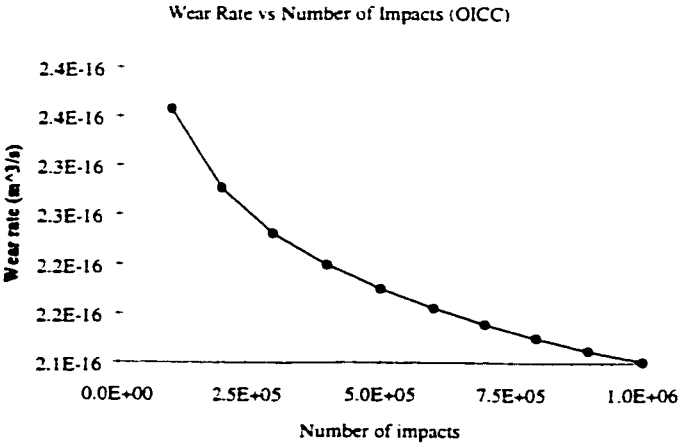

b

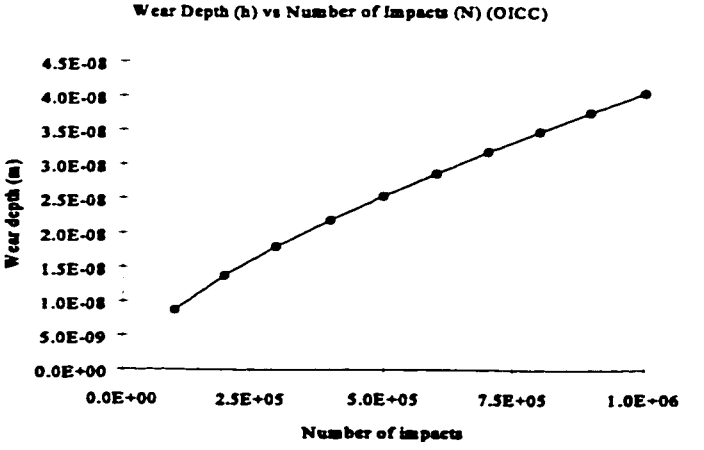

c

Figure 3.10 Wear characteristics of a cylinder obliquely impacting in a conforming support

$$W_R = \frac{2NP_0}{T}\left(\bar{S}_2 + \frac{v_s t^* c_s}{2\pi}\right) \tag{3.95}$$

Inserting this into the wear-rate equation above the relationship between work-rate and wear-rate is given by:

$$w_r = \frac{0.67\,a(t^*/2,h)h}{NP_0[\bar{S}_2(h) + v_s c_s t^*/2\pi]} W_{Rni} = \frac{0.15\,C_l^{0.95}}{N^{0.05}P_0[\bar{S}_2(h) + v_s c_s t^*/2\pi]} W_{Rni} \tag{3.96}$$

The wear-rate can be obtained as a function of time and is given by:

$$w_r = \frac{0.22 f_n C_l^{0.95}}{N^{0.05}} \tag{3.97}$$

Similarly, the wear depth vs number of impact can be plotted from the following relationship:

$$h = (C_l N)^{\frac{1}{1.49}} \tag{3.98}$$

The wear characterization is performed using the above three equations which relates the wear rate to work rate, the wear rate to number of impacts and the wear depth to number of impacts (Figure 3.10). The constants are similar as in the previous cases and the variables are also similar. As in the oblique impact of cylinder on flat, the oblique angle is maintained at 45° for the various magnitude of loads while impacting.

3.7 Pure Sliding Wear Model (Cylinder in a Cylinder)

The model for pure sliding wear (Figure 3.11) is derived by assuming that radius of cylinder will reduce by a length equal to the wear depth evenly. All the equations being valid for the

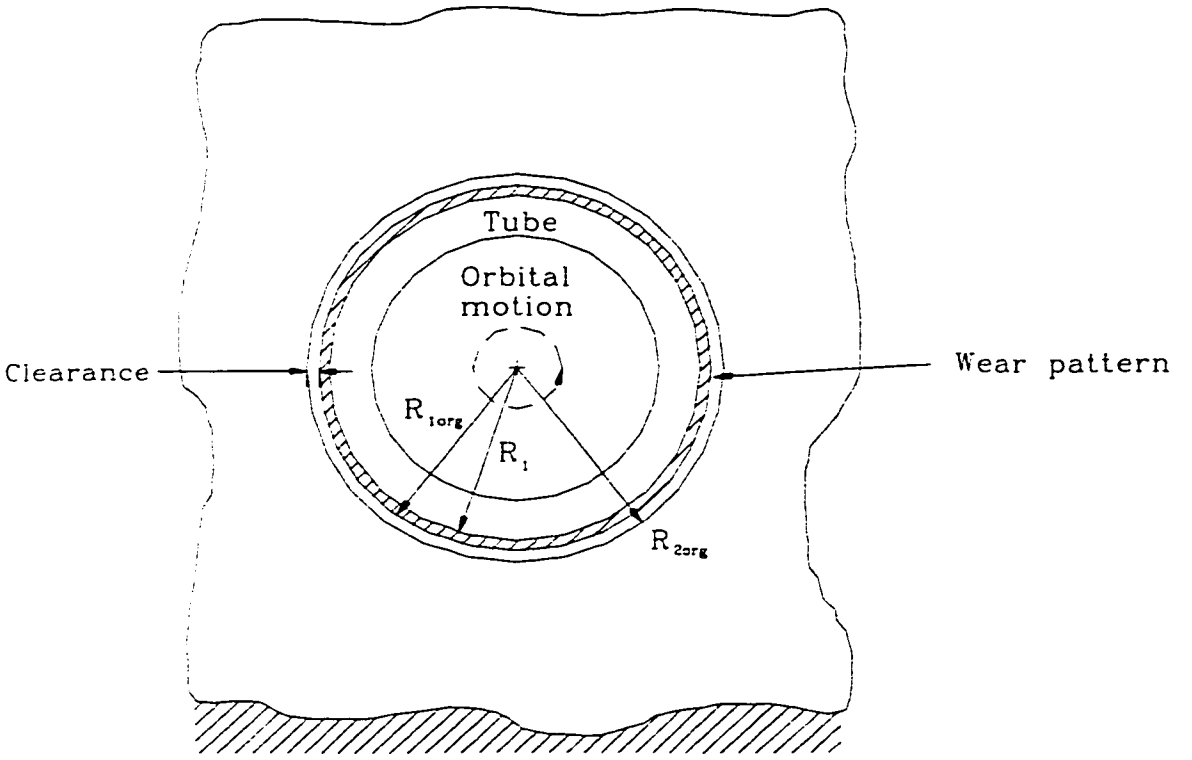

Figure 3.11 Wear pattern of a cylinder sliding in a conforming surface

cylinder on flat the basic difference is in the equivalent radius of the Hertzian contact model is therefore, given as:

$$R = \frac{R_{2org}(R_{1org} - h)}{R_{2org} - R_{1org} + h} \tag{3.99}$$

This implies that the above value of R is used in the equation of half the Hertzian contact width a. The maximum shear stress for sliding objects which are conforming is given in the Handbook of Analytical Design [16] by the formula :

$$\tau_{max} = k_s \frac{2P_0}{\pi a}\left(\frac{1+\mu}{2}\right) \tag{3.100}$$

Taking the differential with respect to the depth h in order to substitute into the sliding wear differential equation one obtains:

$$\frac{d(\tau_{max} L_p)}{dh} = \frac{d\left[k_s \frac{4P_0}{\pi}\left(\frac{1+\mu}{2}\right)\right]}{dh} = 0 \tag{3.101}$$

The wear volume is assumed to be the rectangular area defined by the hertz contact width $2a$ (L) and the wear depth h. Therefore it is given by the following equation:

$$w = 2ha = 2h\sqrt{\frac{4P_0}{\pi E^*}\left[\frac{R_2(R_1 - h)}{R_2 - R_1 + h}\right]} \tag{3.102}$$

Substituting the differential of the wear volume and the maximum shear stress and integrating the final differential wear equation one obtains a simplified equation relating the wear depth (h) and number of passes (N).

$$\frac{h\sqrt{|R_1 - h|}}{\sqrt{|R_1 - R_2 - h|}} = C_1 N \tag{3.103}$$

where ,

C_I = constant of integration

which can be approximated by:

$$N = \frac{0.95h^{0.84}}{C_I} \Rightarrow h = \left(1.05C_I N\right)^{1.19} \tag{3.104}$$

The zero wear model is utilized to find the wear for a value of 0.0005mm for h_0 and it is expressed by $N_0 = 2000\left(\gamma_R \tau_y / \tau_{max}\right)^9$ as shown in the previous sections. Using this relationship the constant of integration C_I can be determined for 0.0005mm of h_0 implying:

$$C_I = \frac{h_0\sqrt{|R_1 - h_0|}}{N_0\sqrt{|R_1 - R_2 - h_0|}} \tag{3.105}$$

The work rate equation can be given by:

$$W_R = \frac{NP_0\int_0^{2a}\sin\left(\frac{\pi x}{2a}\right)dx}{T} = \frac{4aNP_0}{\pi T} \tag{3.106}$$

The wear rate / work rate relationship is given by:

$$w_r = \frac{2ha}{T}\frac{\pi T}{4P_0 Na}W_R = \frac{\pi h}{2P_0 N}W_R \tag{3.107}$$

but h and N are dependent on each other giving:

$$w_r = \frac{\pi(1.05C_I N)^{1.19}}{2P_0 N}W_R = \frac{1.67C_I^{1.19}N^{0.19}}{P_0}W_R \tag{3.108}$$

The wear-rate as a function of time is given by:

$$w_r = \frac{2f_n(1.05C_I N)^{1.19}}{N}\sqrt{\frac{4P_0}{\pi E^*}\left[\frac{R_2[R_1 - (1.05C_I N)^{1.19}]}{R_2 - R_1 + (1.05C_I N)^{1.19}}\right]} \tag{3.109}$$

which is simplified to:

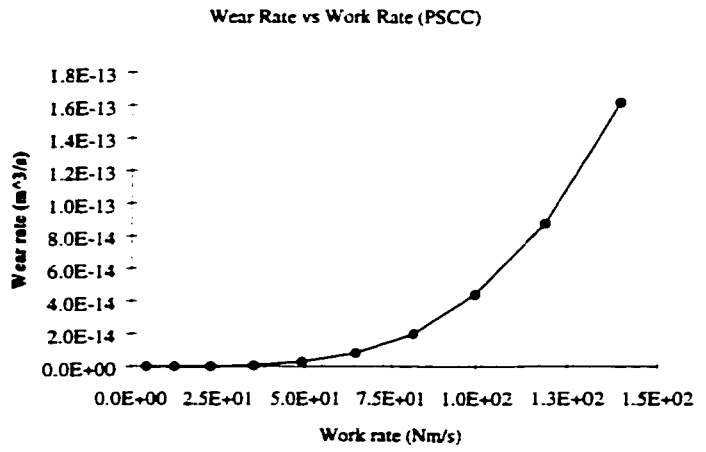

a

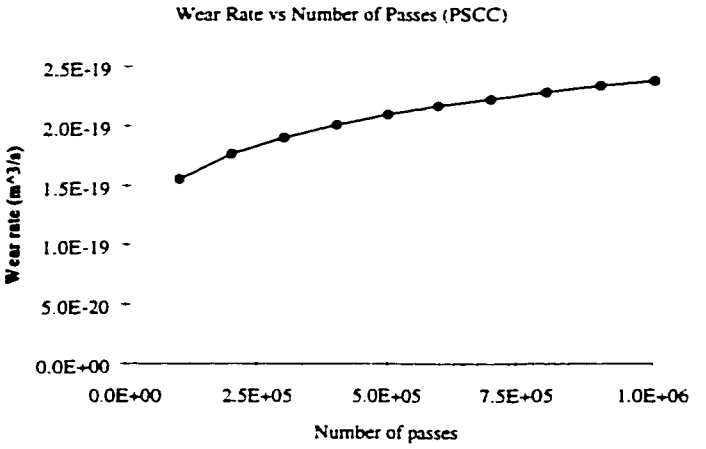

b

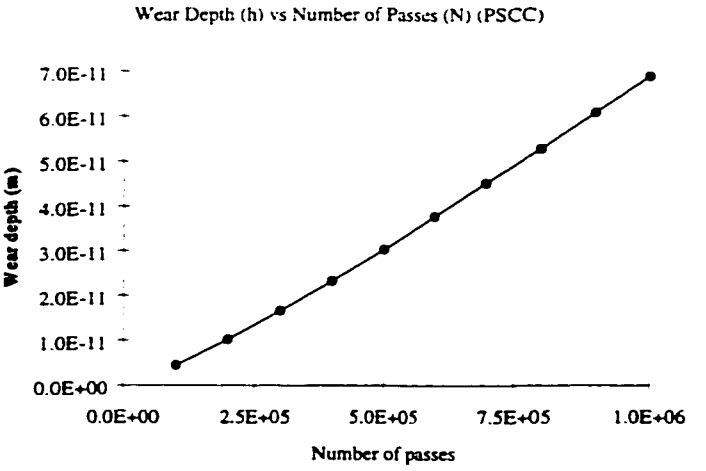

c

Figure 3.12 Wear characteristics of a cylinder purely sliding in a conforming support

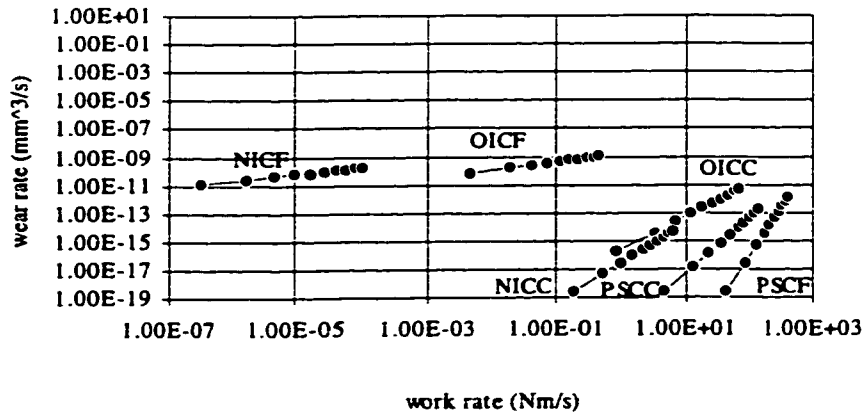

Figure 3.13 Wear rate vs work rate (log-log) plot

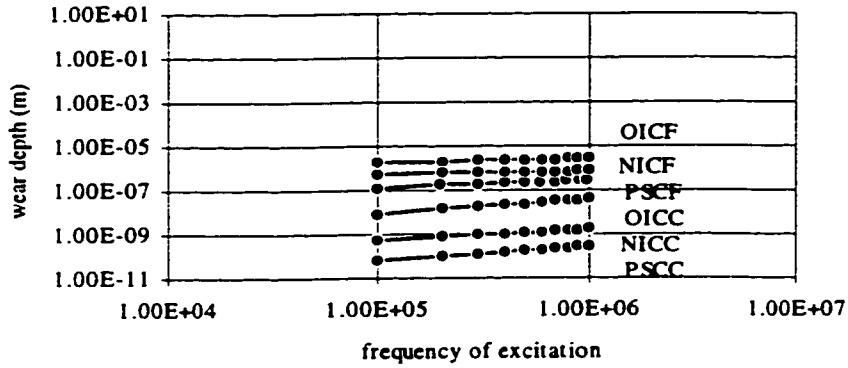

Figure 3.14 Wear depth vs total number of excitation (log-log) plot

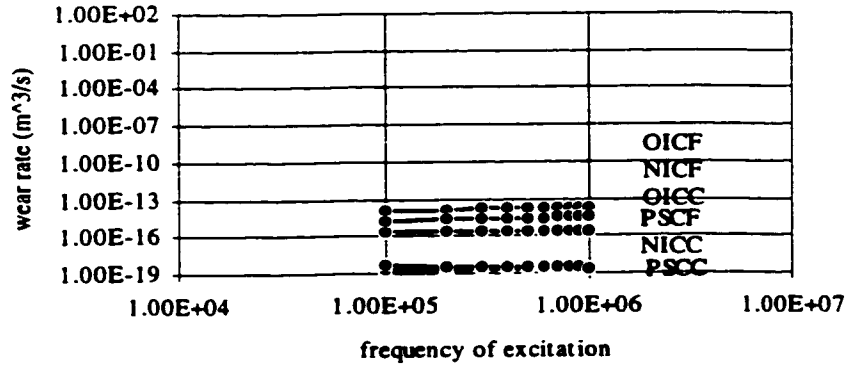

Figure 3.15 Wear rate vs total number of excitation (log-log) plot

$$w_r = 2.4 f_n C_l^{1.19} N^{0.19} \sqrt{\frac{P_0}{E^*}\left[\frac{R_{2org}[R_{1org} - (1.05 C_l N)^{1.19}]}{R_{2org} - R_{1org} + (1.05 C_l N)^{1.19}}\right]} \quad \textbf{(3.110)}$$

The wear depth / number of pass length traversed relationship is given by:

$$h = 1.06 (C_l N)^{1.19} \quad \textbf{(3.111)}$$

The wear model for this case is derived based on a region defined by the Hertzian contact length ($2a$) on the circumference of the tube, i.e. even though the wear in sliding is over the entire circumference, the characterization will be done on the region mentioned because in one cycle the region will be loaded only once. The stress concentration factor was assumed to be unity for the purpose of comparison with all the other case. In order to calculate the wear rate / work rate relationship the load P_0 was varied from 2000-20000 N/m. This implies that constant of integration C_l which is dependant on the force was also varying correspondingly. However, to calculate the wear rate and wear depth variation (Figure 3.12) the only variable was number of passes N, which corresponds to the total number of cycles while the load was kept constant at 2000 N/m.

3.8 Discussion

Taking the interaction between a cylinder and a flat surface the wear rate / work rate relationship indicates that even though there is a comparatively higher work rate value for pure sliding conditions, the wear rate values are relatively higher for normal and oblique impact conditions. Provided the contact force is not varied over the duration of the application one can observe that the wear rate and wear depth of the cylinder over the span of the simulation are seen to be highest for oblique impact, followed by normal impact and

pure sliding conditions. The comparisons were performed for the same force magnitudes, hence indicating the relative effect of impact and sliding contact conditions.

The analysis of a cylinder in a conforming surface for the three contact conditions, indicates similar characteristics like the above. In this case also, the wear rate associated with sliding is slightly less than normal impact. It should be noted that even though wear rate / work rate relationships are derived theoretically, experimental investigations of the wear associated with impact can not be characterized using work rate, as this quantity can not be accurately measured. The effect of normal impact is seen to be quite dominant according to the relationship. This phenomenon can especially be observed in cases where number of impacts or passes are related to wear depth.

The derivation of the wear model by Bayer et al. [14] has introduced the use of stress concentration factor for the end contacts. Accordingly, the author of this thesis has chosen to introduce a similar factor to the wear model given by Engel et al. [30] and have taken this value as unity for comparison purposes. This factor is detrimental to the quantity of wear occurring, therefore since the geometry of the contacting bodies was similar for the various contact conditions it is not unreasonable to assume the same value for all the cases.

The plot of Figures 3.13-15 indicate that the concept of uniqueness for the wear rate work rate relationship is not justified. It shows that based on the type of contact and geometry of interacting materials there could be different wear rates for the same amount of work rate. It can also be seen that the wear associated with impact can not be ignored as it might have

comparable amount of material wear depending on the amount of load and number of application. The main reason for this is that according to Bayer's sliding wear model the ratio of the maximum shear stress to the yield stress in shear is comparatively lower than the ratio of maximum contact stress to the yield stress in compression. The zero wear value which has a greater control on the magnitude of wear is highly sensitive to the stress ratio mentioned and stress concentration factor, as it is the 9^{th} power of the quantity which controls the wear.

3.9 Conclusion

The analysis performed using proven wear models shows that the characterization of wear can not be done using work rate as a scaling parameter. The derivation carried out for characterizing wear of various geometries and contact conditions with respect to work rate indicates that the relationship between these two quantities is not unique and that it is not linear as well. There were cases where extremely small (nearly zero) work rate quantities were resulting in significant wear rates equivalent to those of relatively higher work rate values. The above relationships derived for various contact conditions seem to point out the discrepancy with regards to wear characterization, discussed earlier. It is therefore important to realize the fact that subsurface phenomenon is highly critical to the wear occurring in between two contacting objects under relatively low load and derive a new model which addresses this factor and recognizes the need for a generalized wear model capable of handling all the various contact motions. After the derivation of this model the appropriate characterizing parameter can be clearly defined.

CHAPTER 4

EXPERIMENTAL SETUP AND ANALYSIS OF RESULTS

4.1 Fretting Wear Rig

The wear mechanics of two contacting objects in relative motion is dependent on various factors as described in the previous chapters. Therefore, the conducting of experimental investigations is crucial for the assertion of the validity of the mathematical models. Based on this reasoning, the fundamentals of a regulated experimental analysis are identified by properly classifying the controlled input parameters and resulting effects, essential to this research work. [104] (Author's Ref.)

The requirements of the experimental setup are simplified such that the motions imparted to the tube, the amount of contact force generated and the frequency at which this force is applied are controlled. Hence, inherent specifications of the setup are:

1) It should be a fairly rigid setup, because of the excitation loads associated

2) Precise control of forcing input for repeatability

3) The use of non corrosive materials to reduce the effect of chemical wear

4) Accurate data collection of the applied force and measured displacement

5) The environment in which there is an interaction between the tube specimen and support ring specimen should be as close as possible to the actual operating conditions of a heat exchanger.

Taking these five points as a guideline, the attainable objectives are identified and the design of the setup carried out, without compromising the fundamentals of the research work. The design of the setup had to be built around available transducers in order to avoid unnecessary cost. Factors influencing this design were classified into two predominant categories, environmental conditions and forcing input. It was also essential to have easy access to the interaction zone, as the tube and support specimen had to be changed for every experiment. Because of the nature of the experiment, which is of a relatively long duration, (168 hrs at 14 Hz) it was also important to prevent the fretting of vital components of the setup. This may alter the structural integrity and dynamic response of the system in the long run.

The conceptual design of the rig was initiated by categorizing the components required for the predetermined functions. Then the problem was reduced to bringing these components together in their appropriate position, using a rigid setup which satisfies most of the imposed requirements and restrictions. Hence, the various important components are classified into five major parts which are listed as:

1) Accurate positioning of the contact zone should be in place
2) The proper force and displacement measurement apparatus should be utilised
3) Appropriate motion and force controller should be designed
4) The material interaction zone should be in water, to simulate realistic conditions
5) Data acquisition and processing should be implemented

Even though, there was a test rig borrowed from the fretting laboratory of Ontario Hydro Technologies (OHT-rig), which satisfied the above requirements, it was deemed essential to design another test apparatus (ConU-rig) for the purpose of the exclusion of the dynamic

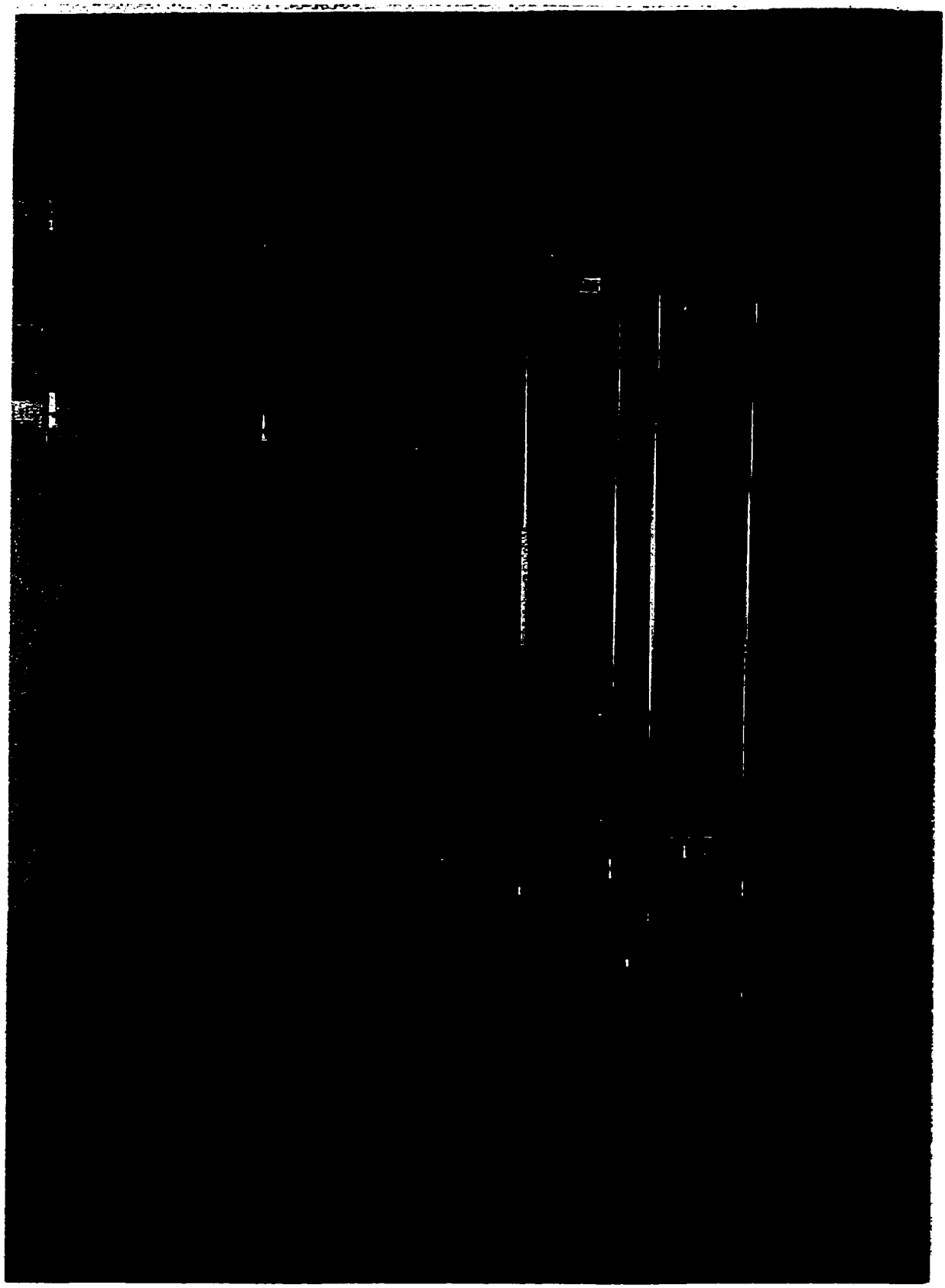

Figure 4.1 Fretting wear rig designed and built at Concordia University

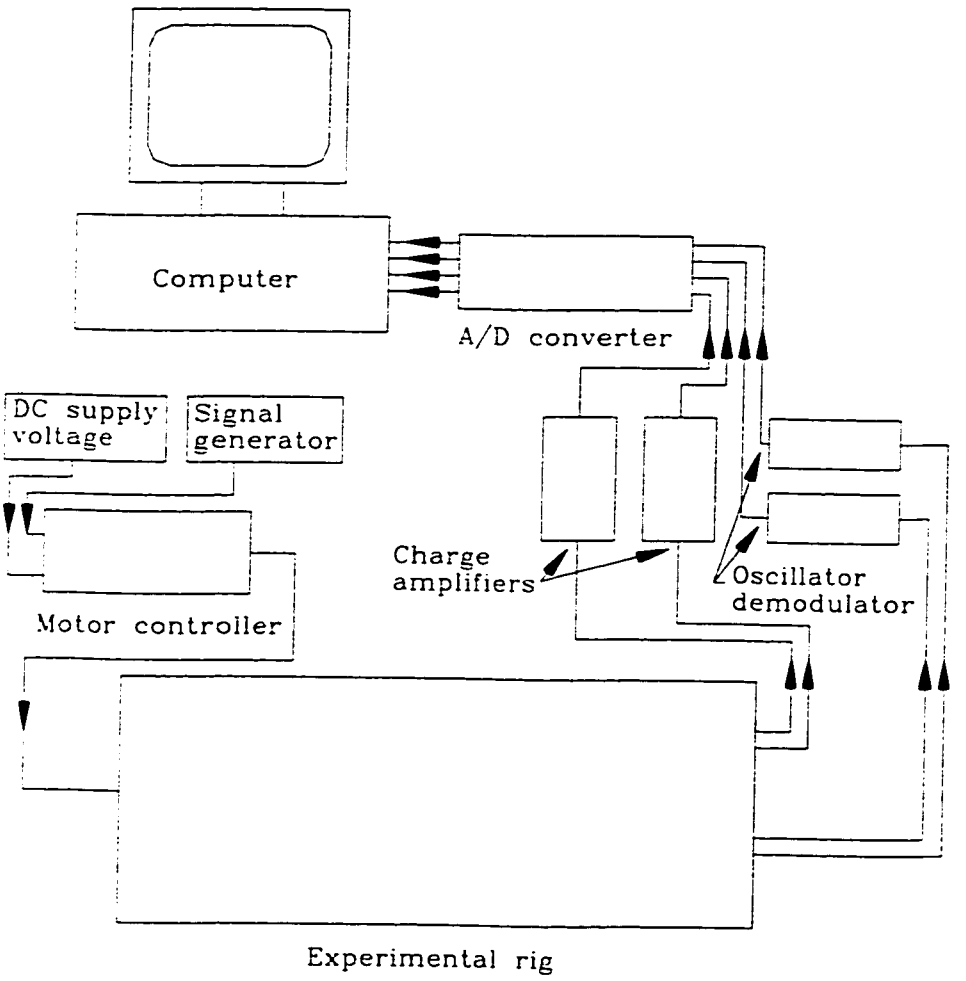

Figure 4.2) Block diagram of fretting wear rig built at Concordia University

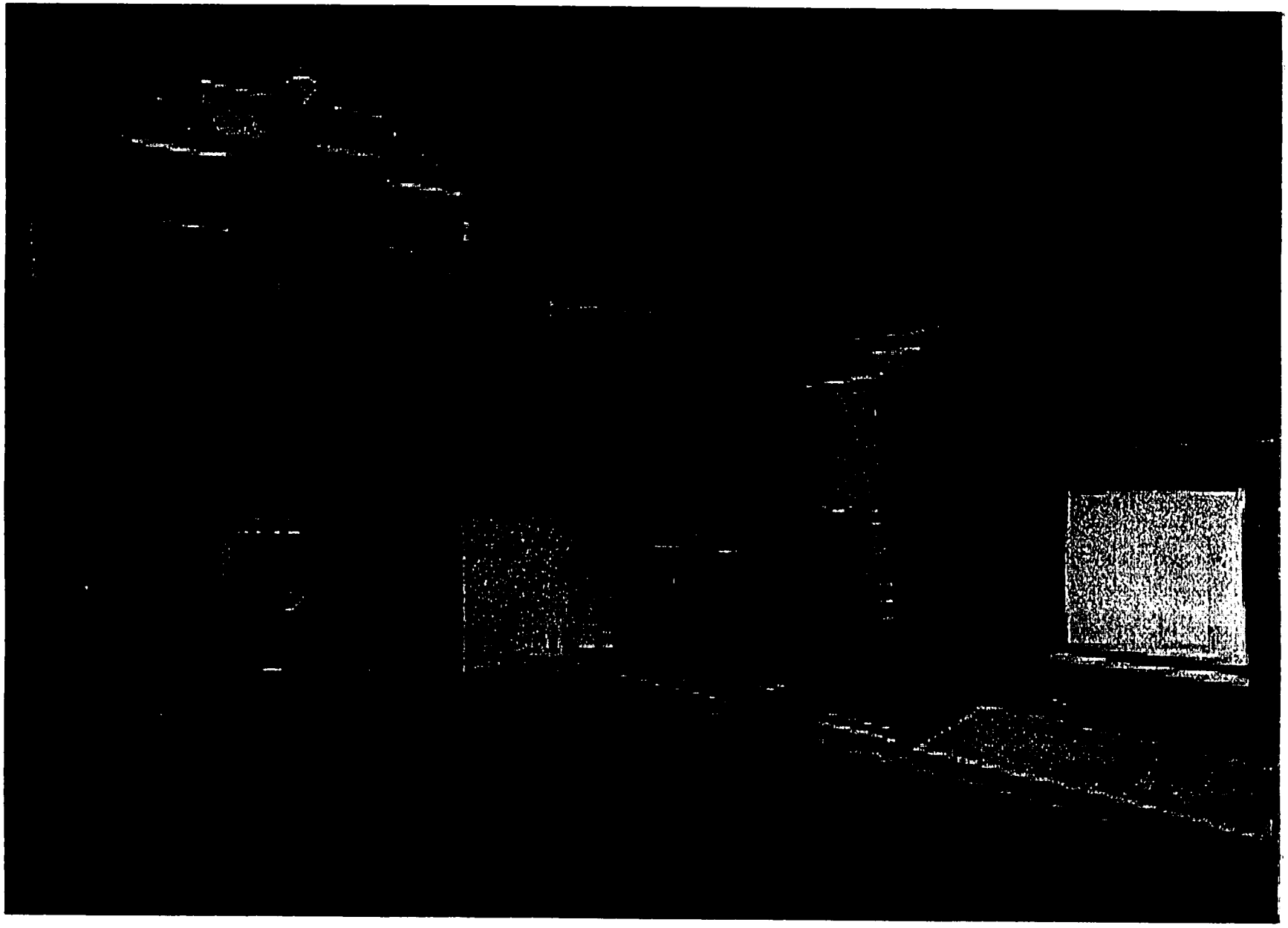

Figure 4.3 Fretting wear rig borrowed from Ontario Hydro

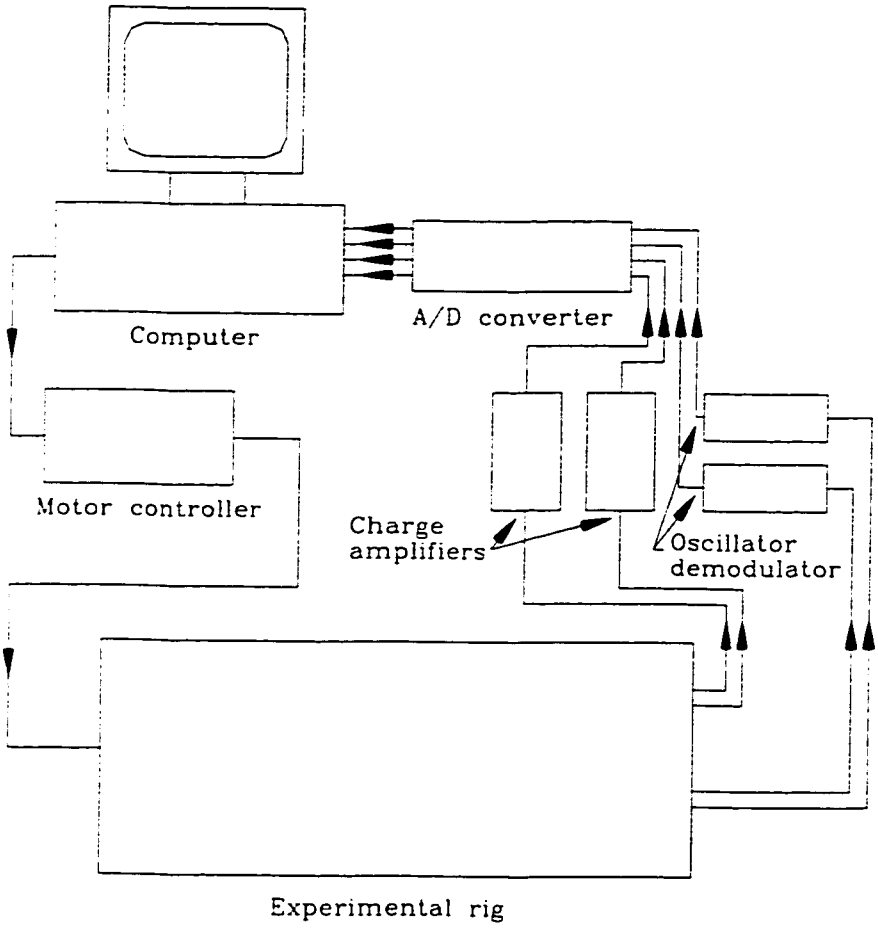

Figure 4.4) Block diagram of fretting wear rig borrowed frm Ontario Hydro

effects. The design of the new rig (Figures 4.1 and 4.2) is similar to the single span room temperature fretting wear rig designed by Dr. Attia (Figures 4.3 and 4.4). This setup was used for conducting some of the experiments, while the remaining ones were conducted on the ConU-rig. Details of the experiments conducted is given in Table 4.2. Results of the experiments on both the OHT-rig and the ConU-rig are used to verify the mathematical model, derived to predict the wear rate.

4.1.1 Positioning Device

The correct positioning of the experimental zone is crucial before starting the experiments. Bearing in mind that the radial clearance between the tube and support is only 0.15 mm, it is not uncommon to position the specimen holder off its central position due to the inherent assembly error, every time a new experiment is begun. Therefore, to reduce the unknowns of the experiment and to ensure repeatability it is recommended that the position of the specimen should be at the centre of the holder, before the start of each experiment. This setup works in tandem with the proximity sensing device to ensure the relative position of the tube specimen with respect to the support ring specimen, and to periodically monitor the position, while force measurements are taken. Therefore, in order to make use of this setup, there should be an accurate positioning attachment incorporated.

This positioning device is implemented in the form of an X-Y table, located at the top of the setup, to vary the placement of the specimen near the contact zone. The motion of this table is controlled using two lead screws, fitted with a knurled knob at the end, to generate the

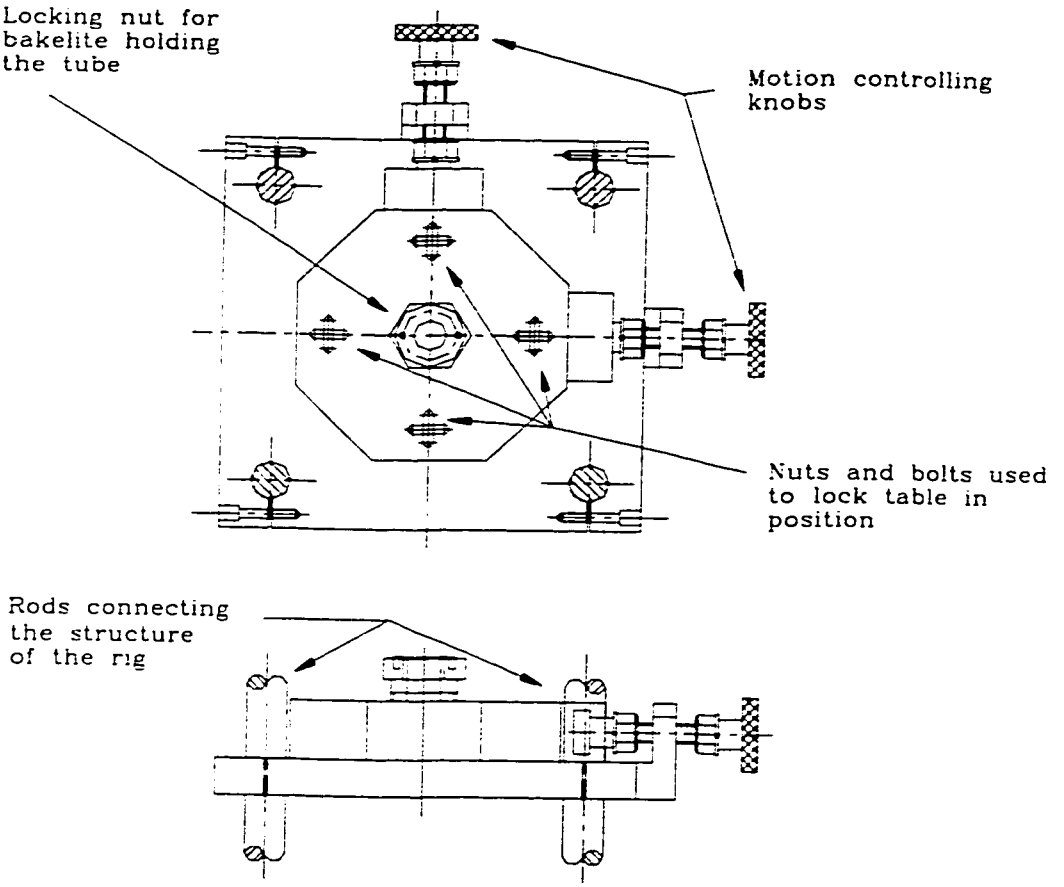

Figure 4.5 Sub-assembly drawing of the positioning device

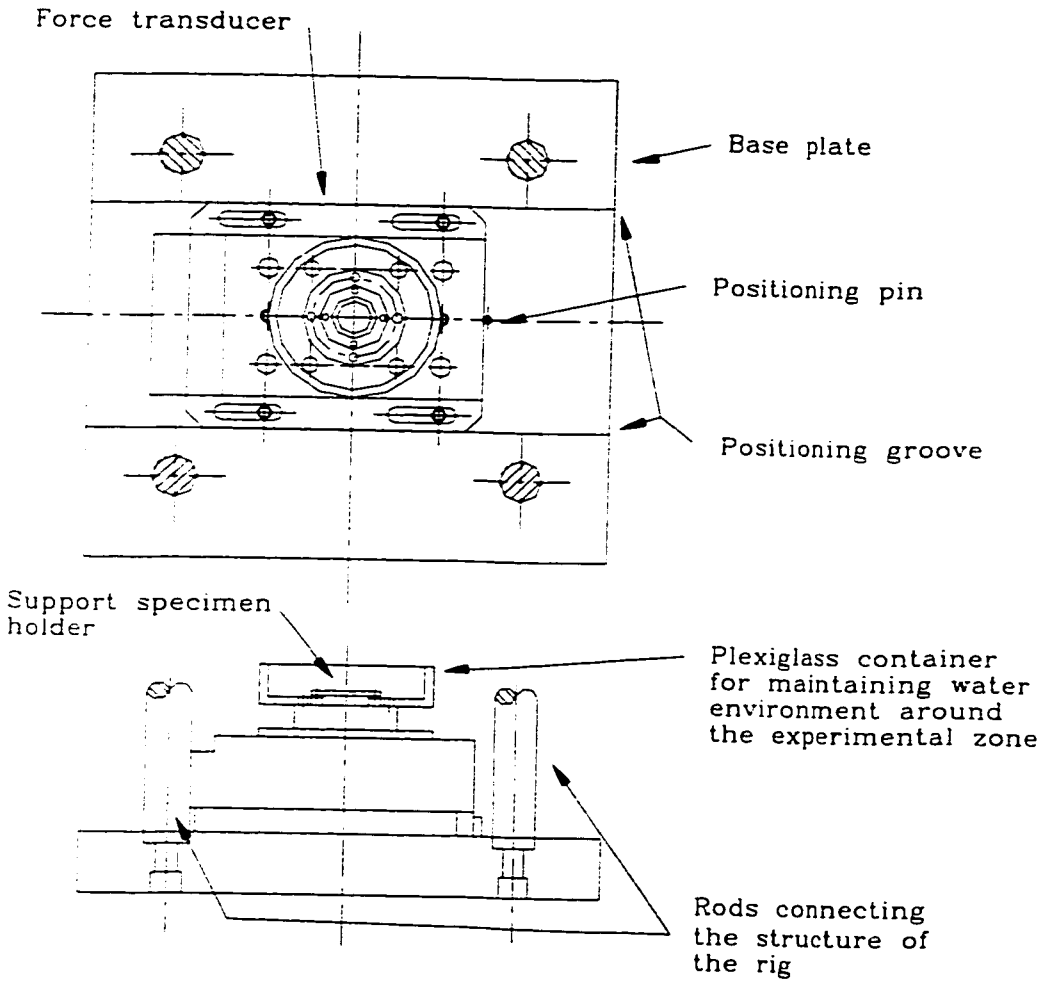

Figure 4.6 Sub-assembly drawing of the force transducer and specimen mount

necessary displacement for accurate placement of the tube. A sub-assembly drawing of this setup, given in Figure 4.5, indicates the operation of this table.

4.1.2 Force and Displacement Transducers

The force sensor is a Kistler 3-axes piezoelectric transducer, used for measuring forces in the three orthogonal direction. It is a very rigid sensor with a correspondingly high resonant frequency, in order to measure very rapidly varying force changes. A proportional electrical charge is setup in the platform for each of the three force components. These charge signals are converted and amplified using a charge amplifier, and the output data is fed into the computer in the form of voltage. The computer is equipped with a data acquisition card which converts the analog signal to digital signal and stores it in a file for further processing.

The Kistler load plate is capable of measuring up to 5 kN in all the three axes, which is far more than the maximum anticipated load of 200 N. Only two directions, x and y are used to measure the force signal. The calibration was already done using a pulley and known weights, to ensure accurate results of the measured force. An impact hammer was used in this case, to check the calibration, and was in good agreement with the results provided from the first method. The magnitude of the excitation was varied to cover a wider range in the calibration process. Following this procedure an almost linear relationship was obtained.

The sub-assembly drawing of Figure 4.6 shows how the force transducer is attached in the experimental setup. The calibration was done on the assembled setup to acquire better

accuracy of the results.

The other essential component of the setup is the displacement measuring apparatus. The function of a non-contact displacement measuring sensor (Figure 4.7) used in this experiment is to monitor the position of a target relative to some reference plane. The magnitude of the analog output is dependent upon the relative position of the target, within the sensor's electromagnetic field. The displacement transducer is a Kaman non-contact sensor, which has a maximum span of 1.016 mm (0.04") and a required minimum offset of 0.127 mm (0.005"). The calibration was conducted using a micrometer setup on the target surface, which was made from the same material as that used for the experiments. Signals from the non-contact sensors were conditioned in the oscillator demodulator, and then fed to two of the four channels, on the data acquisition card.

The calibration procedure is as follows:

1) The target is positioned in place using a micrometer setup and a spacer with a combined thickness of the maximum displacement plus the offset.
2) The gain control is then adjusted until the desired full scale voltage is obtained.
3) The next step is to position the target at zero displacement plus offset, and to adjust the zero control such that the output voltage reading goes down to 0 V dc.
4) Following this, the target is positioned mid way between the full scale displacement plus offset and the zero displacement plus offset. Then, the gain control is adjusted until the output voltage reading is half of the full scale.
5) The target is repositioned at full scale displacement plus offset and the reading of the

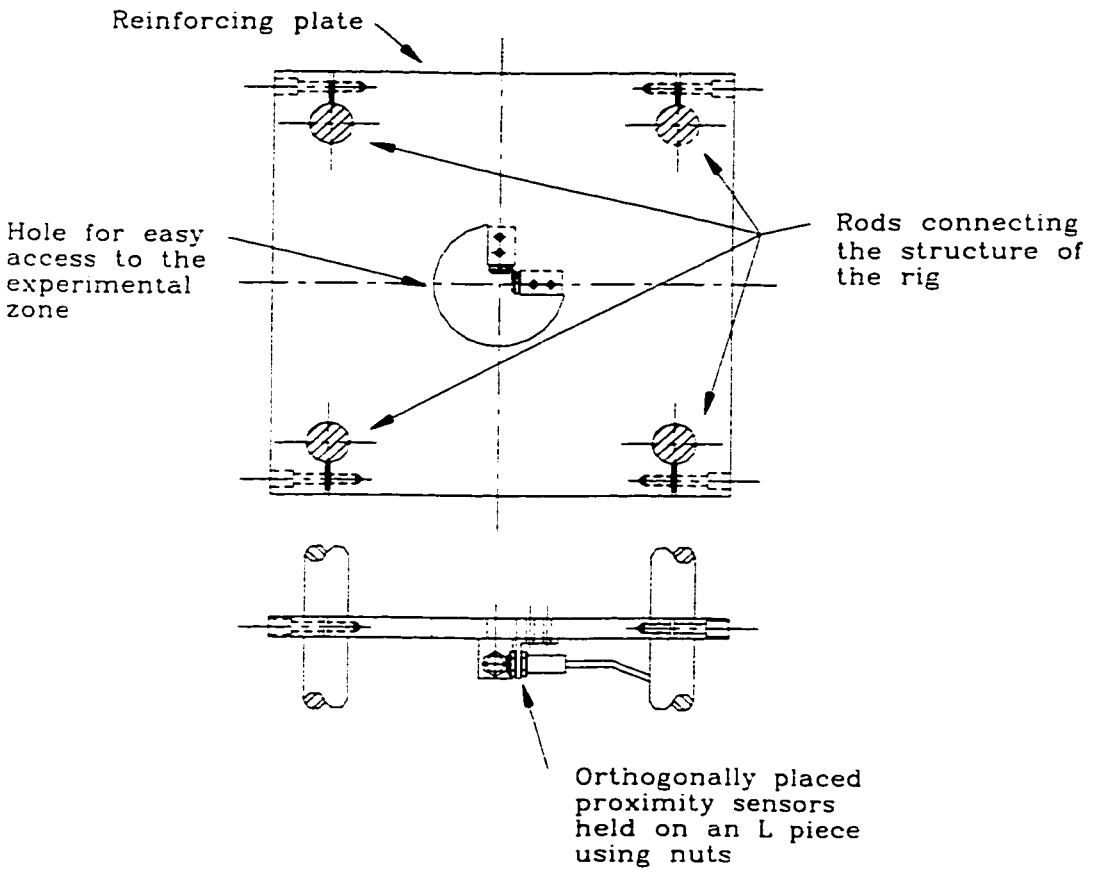

Figure 4.7 Sub-assembly drawing of the proximity sensor attachment

output voltage is noted down. The difference is taken as the output reading minus the desired reading already set in the second step. Then the linearity control is adjusted coarse and then fine, until the adjusted output reading is equal to the desired reading minus the difference. For example, if the output voltage reading is 1.300 volts and the desired value is 1.000 volts then the linearity control is adjusted until the voltage reads 1.000-(1.300-1.000), or 0.700 V. Similarly, if the output reads 0.800 then the required value is 1.000-(0.800-1.000), or 1.200 V.

6) Steps 3 to 5 are repeated as many times as required, until the desired output voltage is obtained at each position. Accurate calibration will remove the necessity of further variations to the zero, gain and linearity controls.

Following this procedure, the calibration for the particular specimen was set at 1 V/mm and a minimum offset of 0.127 mm (0.005") implemented, for the proximity sensor measurement device.

4.1.3 Motion Controller

The motion is controlled through inertial force input. This input to the system is carried out using two stepper motors and their controller, to attain different combination of Fx and Fy ratio, as listed in Table 4.1. Variation of the ratio was implemented by attaching different weights at the end of the arm and rotating the two motors in opposite directions (Figure 4.8). Motors rotating in the same direction with the same speed will give pure sliding motion.

The equation describing the force generated by the rotating unbalance is a function of the

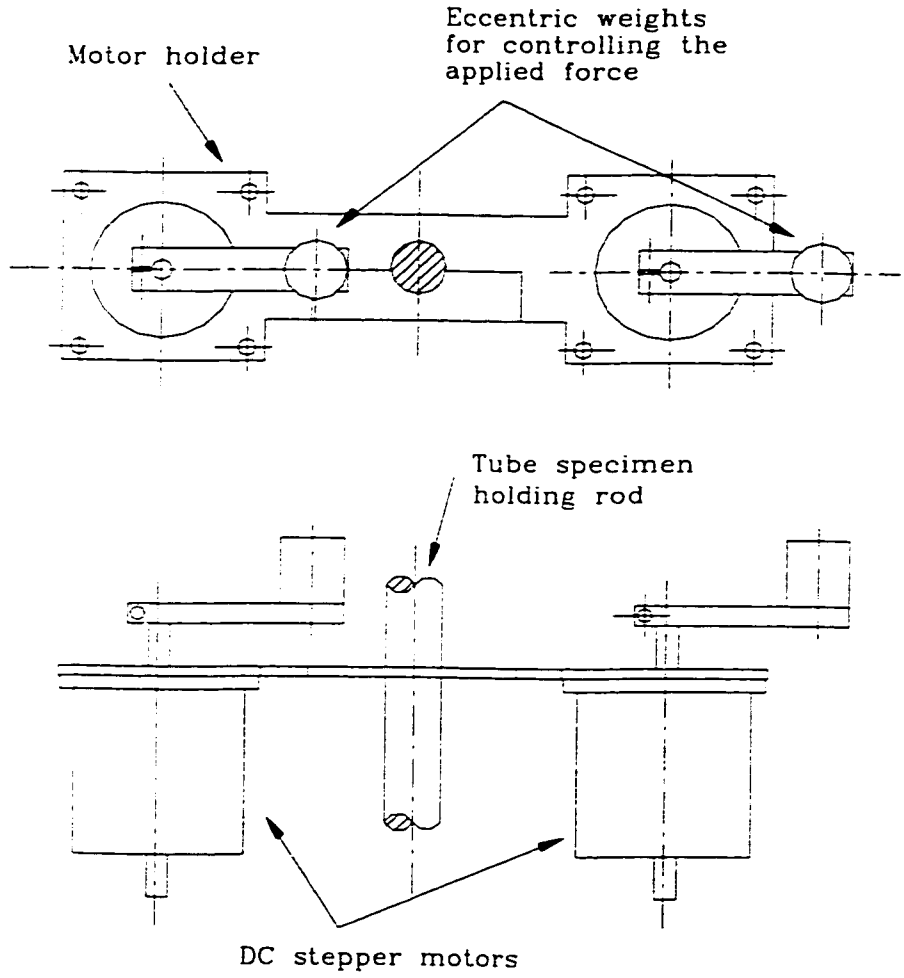

Figure 4.8 Sub-assembly drawing of the excitation mechanism

unbalance mass, its position and its angular velocity. For the type of arrangement used in this setup the total instantaneous radial force is given by:

$$F_t = \sqrt{[M_1 R_1 \omega_1^2 c_{\omega 1} + M_2 R_2 \omega_2^2 c_{\omega 2}]^2 + [M_1 R_1 \omega_1^2 s_{\omega 1} + M_2 R_2 \omega_2^2 s_{\omega 2}]^2} \qquad \textbf{(4.1)}$$

where,

$c_{\omega i} = \cos(\omega_i t)$ $i = 1,2$

$s_{\omega i} = \sin(\omega_i t)$ $i = 1,2$

Table 4.1 Details of the force excitation mechanism

No.	Mass 1*	Mass 2*	Force x	Force y	Force ratio
1	100 gm	100 gm	0	63.19	0
2	100 gm	90 gm	2.77	60.42	0.05
3	100 gm	41 gm	16.35	46.84	0.35
4	100 gm	10 gm	23.84	34.36	0.60
5	100 gm	0 gm	27.72	35.48	0.78
6**	100 gm	100 gm	63.19	63.19	1

* Mass number designation refers to the amount of mass mounted on each motor
** This indicates that the rotation of the motor is in the same direction

The restrictions to the above equation are that $\omega_2 = \omega_1$ or $\omega_2 = -\omega_1$. For the first case i.e. both motors rotating in the same direction with the same speed the total generated force is of sliding type (case No. 6) and given by:

$$F_t = (M_1 R_1 + M_2 R_2)\omega_1^2 \qquad \textbf{(4.2)}$$

The above equation describes the magnitude of the radial force at any angular orientation of the system. For the second case, i.e. the motor running in opposite direction but at the same speed the total generated force (case No. 1-5) is given as a function of time as:

$$F_t = \omega_1^2 \sqrt{[(M_1 R_1 + M_2 R_2)\cos(\omega_1 t)]^2 + [(M_1 R_1 - M_2 R_2)\sin(\omega_1 t)]^2} \quad (4.3)$$

The first term under the square root refers to the force along one axis and the second one refers to the force along an orthogonal axis. The angle at which the force is applied is given by the inverse tangent of the first term divided by the second term. The values of $M_i R_i$ is not only the effect due to the concentrated mass, but also that of the holder which has to be integrated over the entire length. Therefore, equation (4.4) gives the total value of $M_i R_i$ in terms of the thickness (t), width (b), density (ρ) and effective length (r_{max}-r_{min})of holder.

$$M_i R_i = \int_{r_{min}}^{r_{max}} r t b \rho \, dr + m_i r_i = (r_{max}^2 - r_{min}^2)\frac{tb\rho}{2} + m_i r_i \quad (4.4)$$

4.1.4 Interaction zone

The tube and support specimen interaction location has to be near the base of the setup, to accommodate the force transducer available. It is crucial for the design of this sub-assembly to be less than 25 mm in height, from the face plate of the load sensor, because of transducer restrictions (Figure 4.6). In addition, to simulate the actual operating conditions as close as possible, it is essential to have the contact occurring in water. For the purpose of reducing the chemical effects on the wear, only distilled water is used.

4.1.5 Data acquisition and processing

The data acquisition is done through a computer equipped with a National Instrument data acquisition card and a windows based interface programming software known as LabView.

The data acquisition card is capable of collecting data, for four channels (two forces and two displacements) simultaneously sampled, at a rate of 20 kHz. A total of 6 sec worth of information is collected at an interval of four hours. Each file is saved in the form of binary file taking up a total of 1.92 Mbyte of hard disk space. The program developed for this purpose is capable of carrying out this function once every 4 hours (or any desired time) using the clock of the CPU, until the experiment is finished (Figure 4.9).

Each experiment is run at a frequency of 14 Hz for seven days resulting in a total of nearly $8.5*10^6$ excitation cycles. Therefore, the total number of space taken up by the raw data was about 81 Mbyte on the hard disk for each experiment. Because of the size of the experimental data, an optical disk is used to store the information after the completion of each experiment, and the hard disk space reclaimed by deleting the raw data. This data had to be further analysed off-line to give the interpretation of the results.

The data processing software is developed using the G code of LabView and a number of information is obtained for each run. The analysis of each set of data took about six hours of total computer time. The first procedure is to read the four signals, two displacement and two forces. These signals are scaled appropriately using the sensitivity values and the signal is filtered using a digital Butterworth filter. The difference of the displacement signals between two consecutive measurements is taken and stored in two, one dimensional arrays. The filtered force signal however, is converted into magnitude force by taking the square root of the sum of the two squared forces (Fx and Fy) and also stored in two, one dimensional arrays. The subsequent step of the analysis is the multiplication of the average force by the

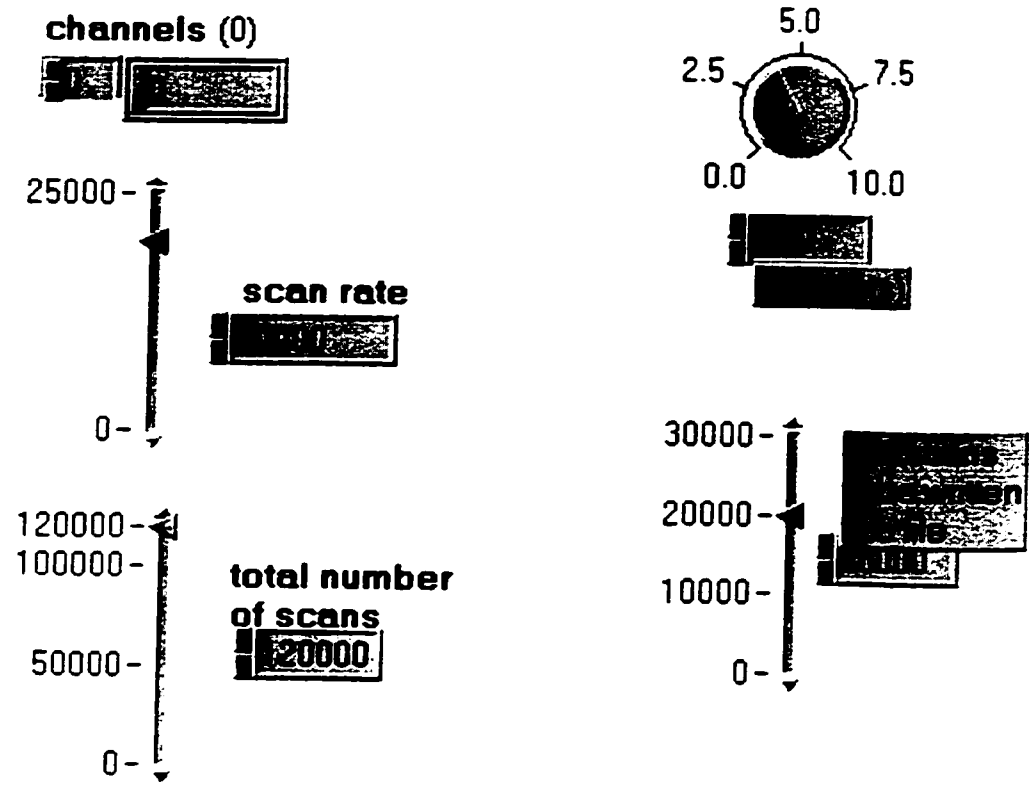

a

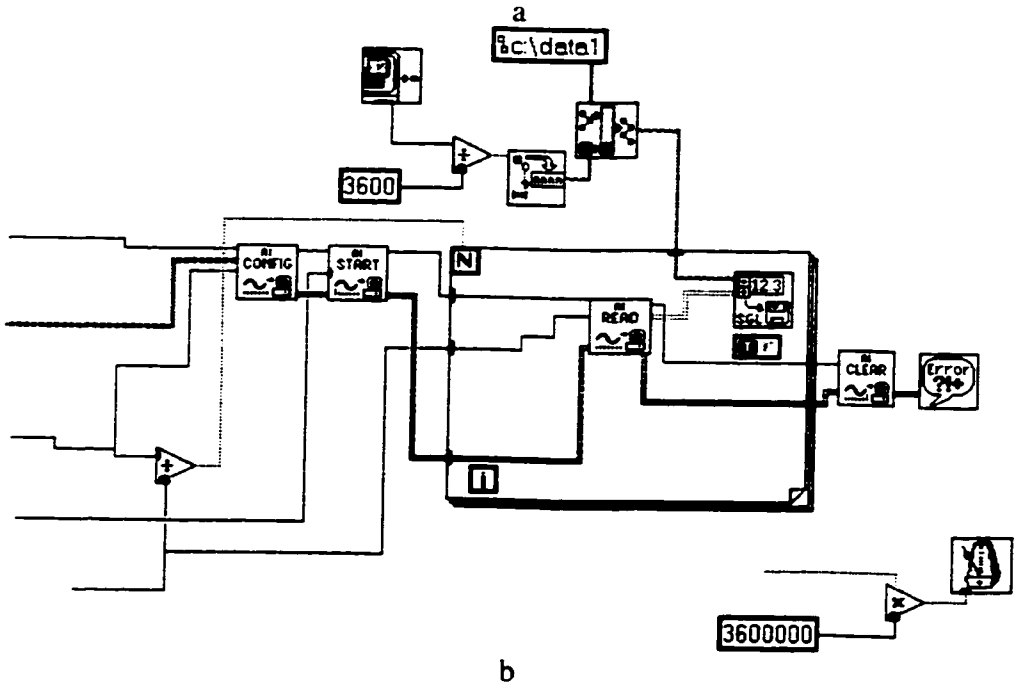

b

Figure 4.9 a-b Front panel and wiring diagram of data acquisition program

corresponding displacement. A segment in the program is also developed to categorize the different percentage occurrences of force and displacement. It takes the maximum force and displacement and divides it into six, giving a six by six matrix, resulting in a total aggregate of thirty six percentage values (to be used in the characteriztion equation of Chapter 7). The program is also developed such that the work rate can be calculated using the approach of Hofmann et al.[5]. However, since there were some experimental constants to be determined depending upon the material used, the modified work rate value was obtained using the percentage matrix distribution and the calculated work rate in a spreadsheet program.

4.2 Error Analysis

The calibration conducted for the transducers and measurement equipments produced some errors, though not significant. Results obtained from the impact hammer were compared to the values obtained from the force transducer. The comparisons were carried out for the forces in the x and y directions separately and the error for the total force was obtained from the vectorial summation of the individual force (F_x and F_y) errors (Appendix C). The total error with a confidence level of 95% (2σ) was found to be 12.03 N. This was obtained for the range of force measurement considered from 17 N to a maximum of 261 N.

The displacement measurement apparatus was also calibrated using standard spacers. The two orthogonally placed proximity sensors were calibrated separately, and the maximum percentage error near the zone of interest, obtained. The maximum radial clearance of the tube and the specimen was given to be 0.02 mm and the original setting of the tube within

the specimen was around 0.627 mm (mid-span of the proximity sensors) from the tip of the non-contact sensor. This implies that the motion of the tube is from 0.607 to 0.647 mm. It was determined that the total error was 0.7 μm, with a confidence level of 95%.

The weight measurement was carried out using a digital scale, which is sensitive to four significant digits and capable of measuring from 0.0000 to 100.0000 g. The total weight loss measurement was relatively small, ranging from 0.0002 to 0.0227 g. Therefore it was essential to conduct a repeatability measurement of the specimen, both before and after the experiment. The results obtained for this test were extremely good, deviating by a maximum value of only 0.0001 g. Based on this maximum value, the error for a 95% confidence level was obtained to be 0.0002 g.

4.3 Experimental Results

In this chapter, some of the relevant results implemented in the validation of the wear model developed in Chapter 6, are observed (Figures 4.10 - 4.23). The orbital motion of the tube at the start, middle and end of the experiments are plotted to observe the variations, if any. The time history of the work rate ($\int P(t)s(t)dt/T$) is also plotted, so is the mean force (load) rate (F_m) which is defined as $\int P(t)dt/T$. In addition, the percentage distribution of the force and displacement combinations are plotted in a 3D graph.

A number of deductions can be inferred from the graphical representations displayed for the different experiments. It can be observed from the plots that there is not an appreciable

difference in the average work rate and mean force rate over the duration of the experiment except in the case of experiment number 5. It was also observed that the motion did not change over the seven days duration appreciably, especially in the case of sliding and oblique impact. It can also be observed that the force or energy level associated with impact is relatively lower on the overall compared to sliding. This is apparent from the 3D percentage graph (to be used in Chapter 7) representing the load and sliding distance combinations.

Table 4.2 Experimental results

Expt. No.	F_x/F_y	Experimental setup	Duration (hours)	Weight loss (g)	Figure No.
1	0.0	OHT-rig	168	0.0031	4.10
2	0.35	OHT-rig	168	0.0090	4.11
3	1.0	OHT-rig	168	0.0227	4.12
4	1.0	OHT-rig	168	0.0211	4.13
5	0.0	OHT-rig	168	0.0059	4.14
6	0.35	OHT-rig	168	0.0124	4.15
7	0.78	OHT-rig	168	0.0085	4.16
8	Os.+1.5kg*	OHT-rig	168	0.0002	4.17
9	Os.+3.0kg*	OHT-rig	240	0.0010	4.18
10	0.35	ConU-rig	168	0.0012	4.19
11	0.6	ConU-rig	168	0.0026	4.20
12	0.0	ConU-rig	168	0.0005	4.21
13	0.05	ConU-rig	168	0.0016	4.22
14	0.05	OHT-rig	168	0.0013	4.23

* Os. indicates oscillatory sliding with the constant applied normal force

Table 4.2 indicates some of conditions implemented in the experiments conducted for this thesis. The type of orbital motion, the setup used, the total duration of the experiment, the total weight loss and the figure number corresponding to each experiment are given in this table. There were a total of fourteen experiments conducted for this research work, excluding the ones conducted for the commissioning process of both experimental setups. Even though, the total duration of each experiment is seven to ten days per experiment, there were a number of obstacles that were encountered during the course of this research work. It should be noted that the total duration of the experimental work took nearly a full year to design, setup and conduct all the experiments, carried out on the rig built at Concordia University.

All the necessary precautions were taken to ensure repeatability of the experiments. This was crucial because of the calibration and verification process for the proposed wear model in Chapter 6. This model is derived following the fracture mechanics analysis conducted in Chapter 5. This model is further implemented to accurately characterise the wear rate incorporating the 3D force-displacement percentage distribution. This verification of the characterization parameter is implemented in Chapter 7 of this thesis. In addition, the uniqueness of the solution is also investigated in this chapter.

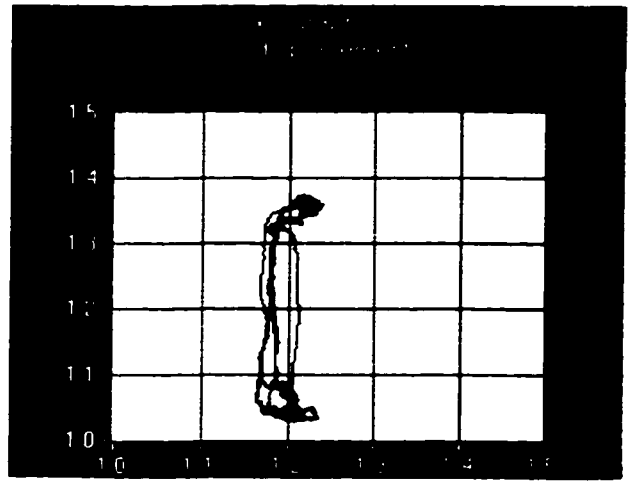

a

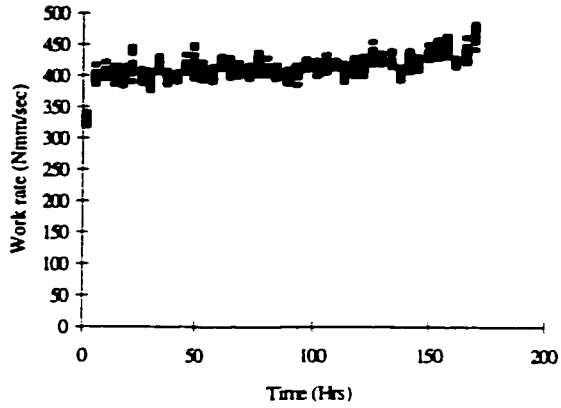

d

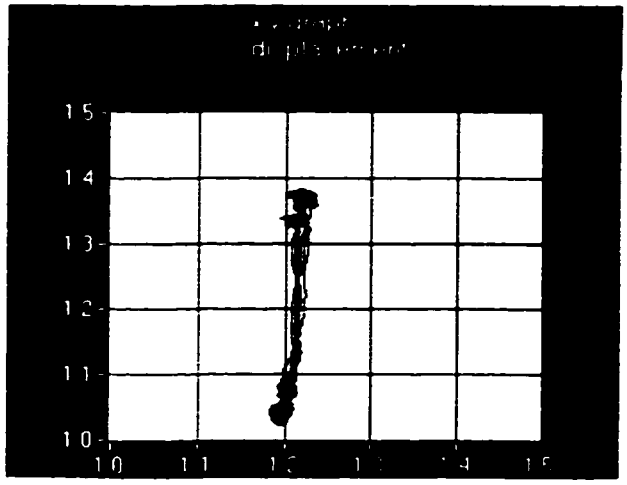

b

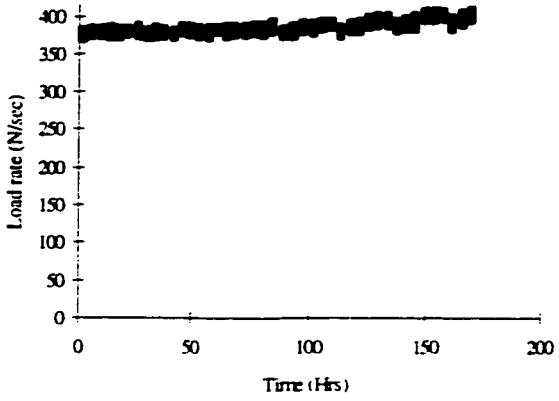

e

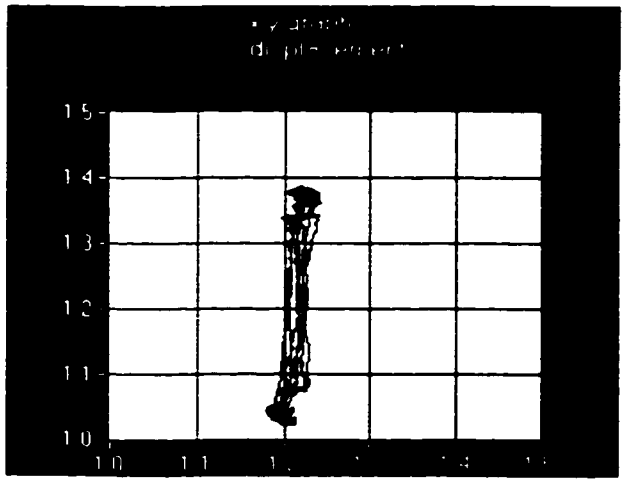

c

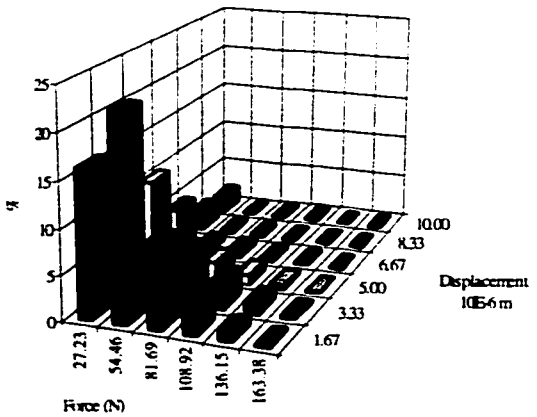

f

Figure 4.10 a-f) Experimental data analysis for a normally impacting motion

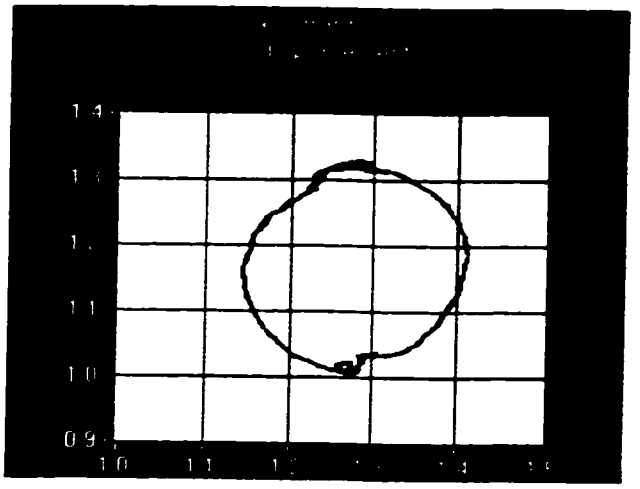

a

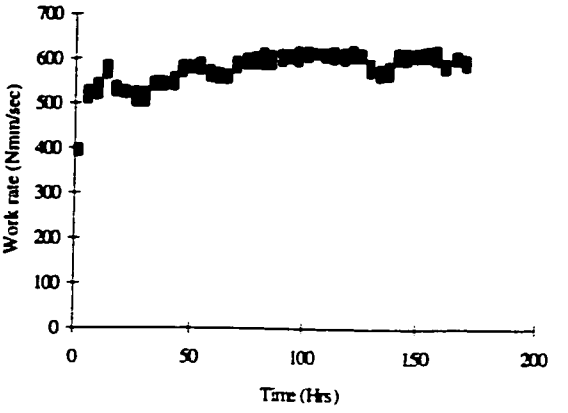

d

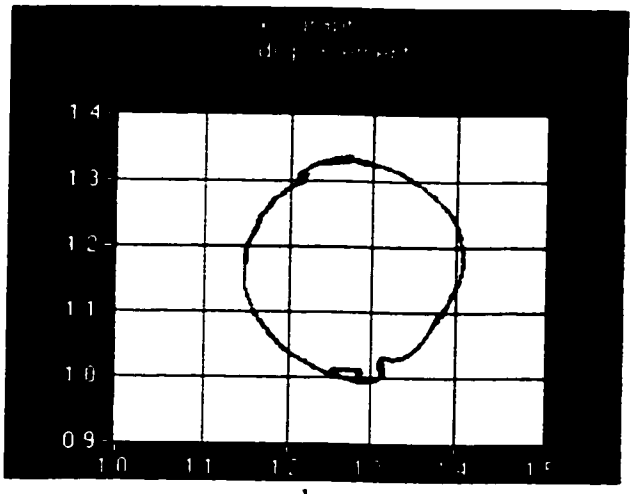

b

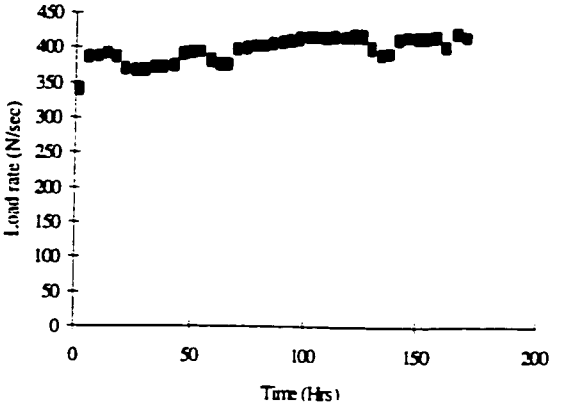

e

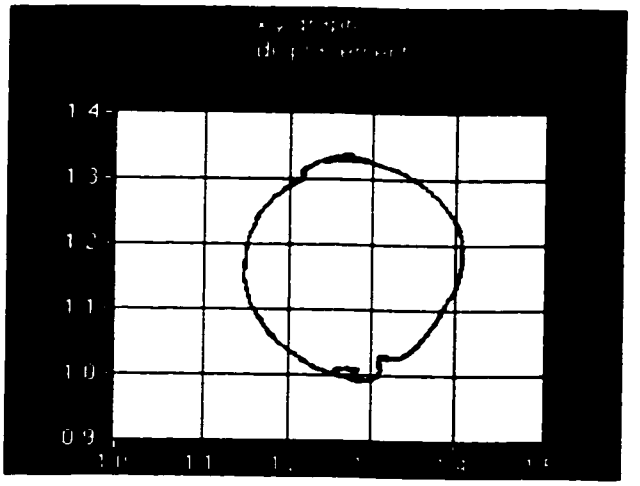

c

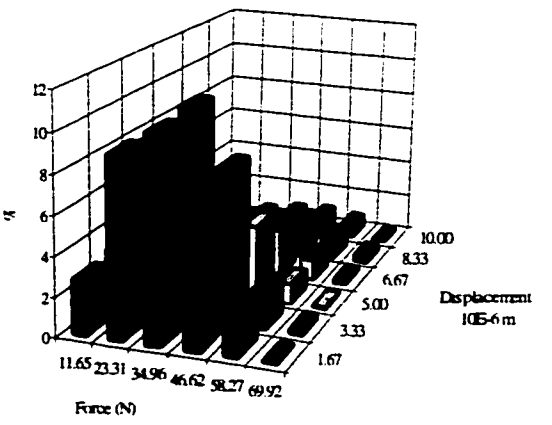

f

Figure 4.11a-f) Experimental data analysis for Fx/Fy = 0.35 (oblique ratio)

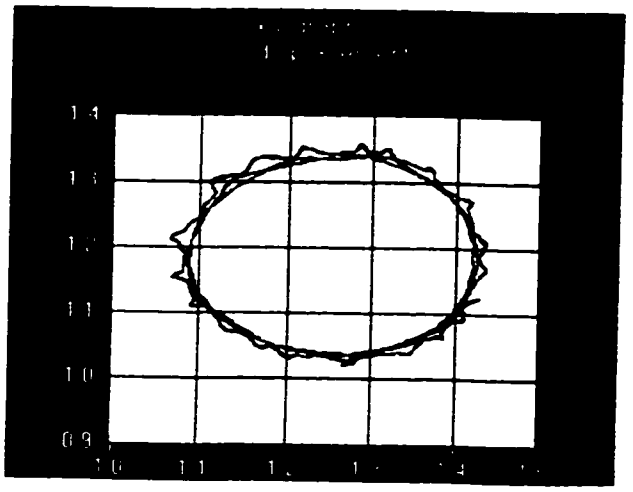

a

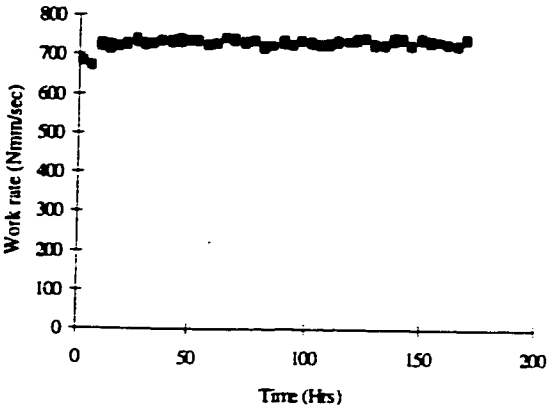

d

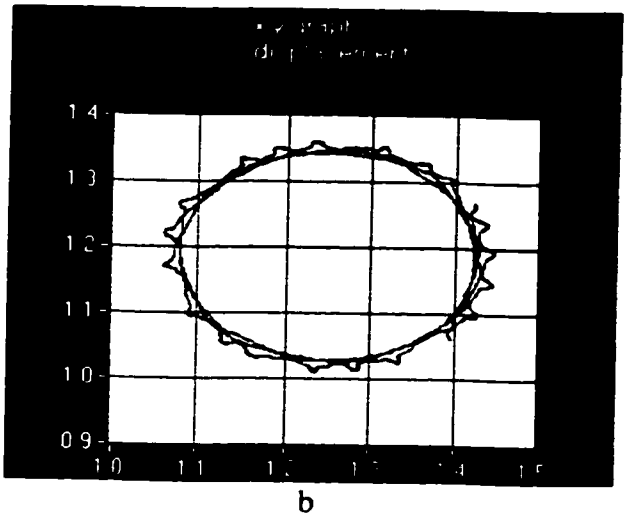

b

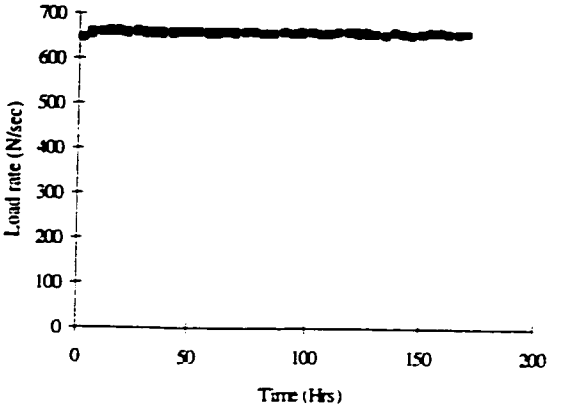

e

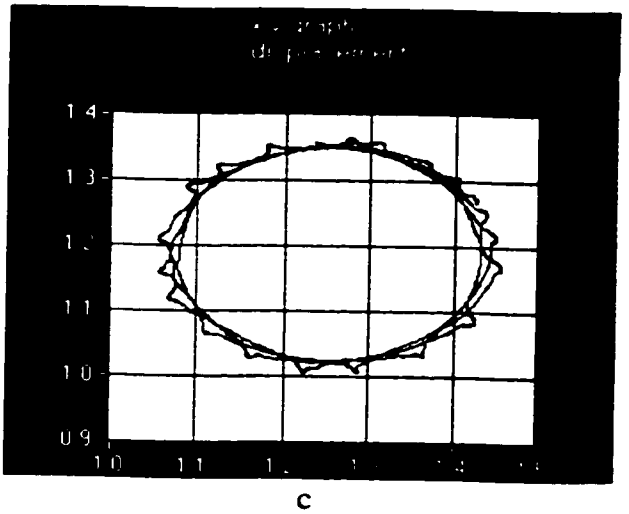

c

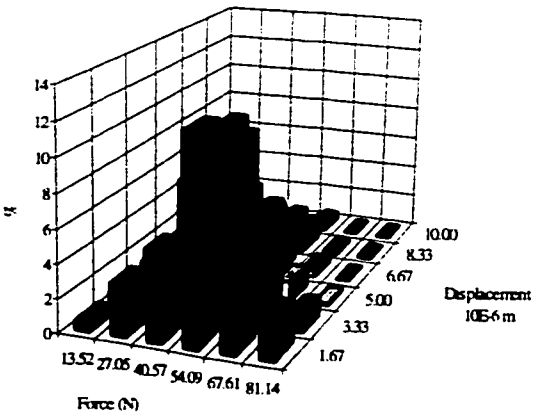

f

Figure 4.12a-f) Experimental data analysis for sliding contact Fx/Fy = 1

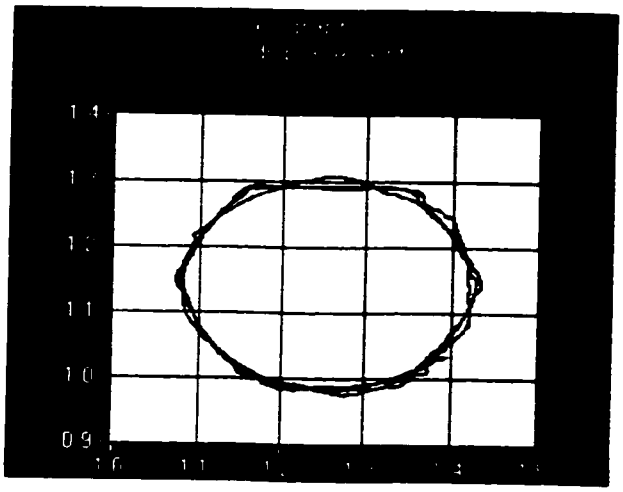

a

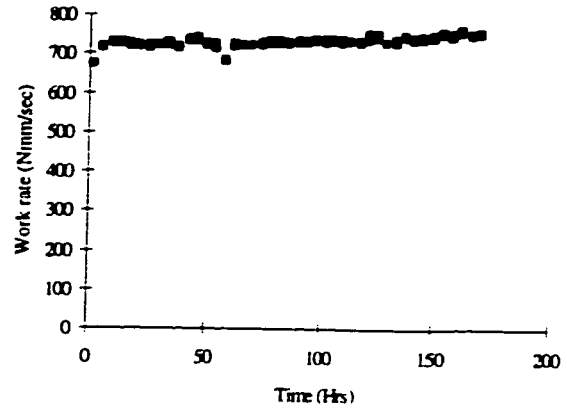

d

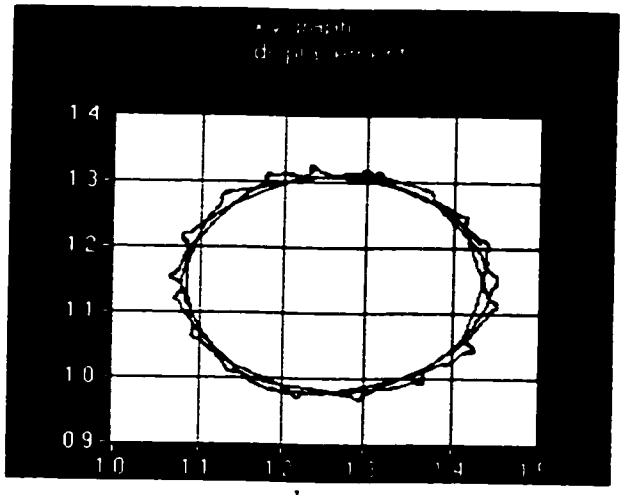

b

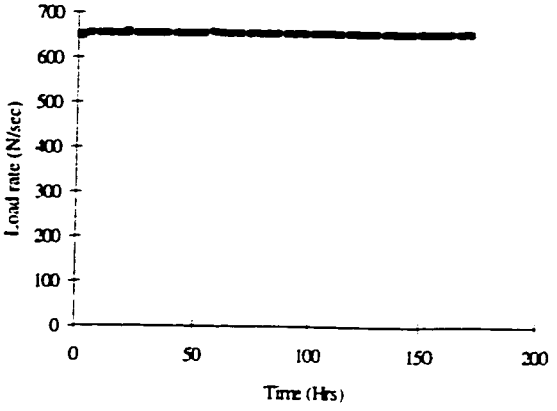

e

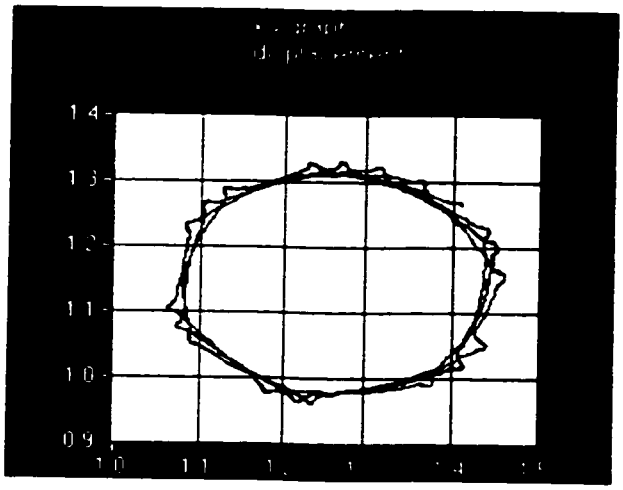

c

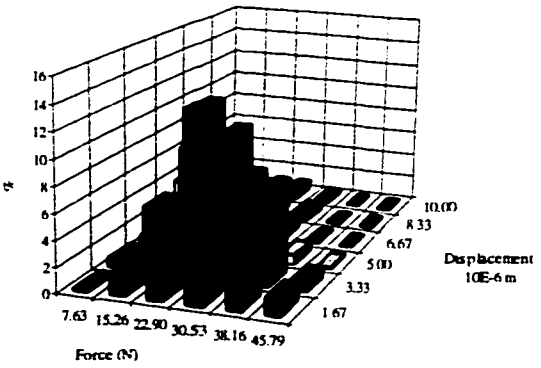

f

Figure 4.13a-f) Experimental data analysis for a purely sliding contact Fx/Fy = 1

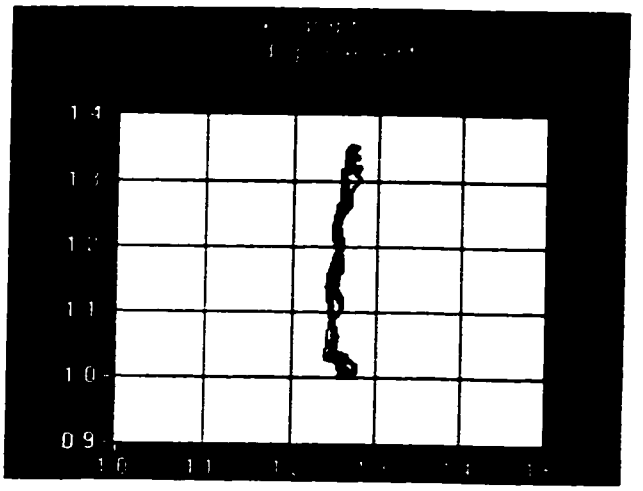

a

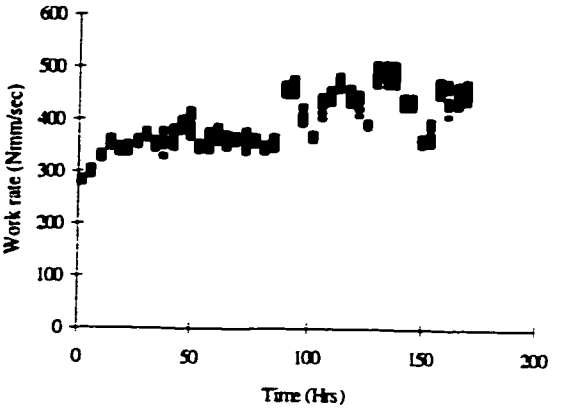

d

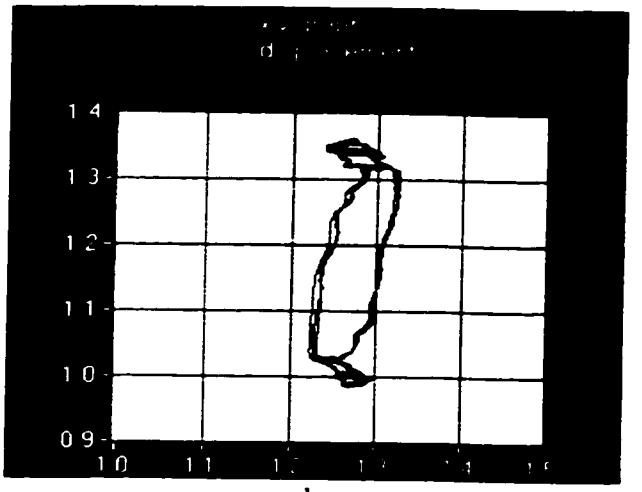

b

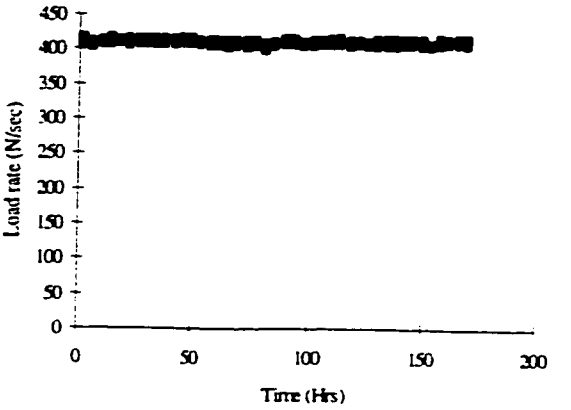

e

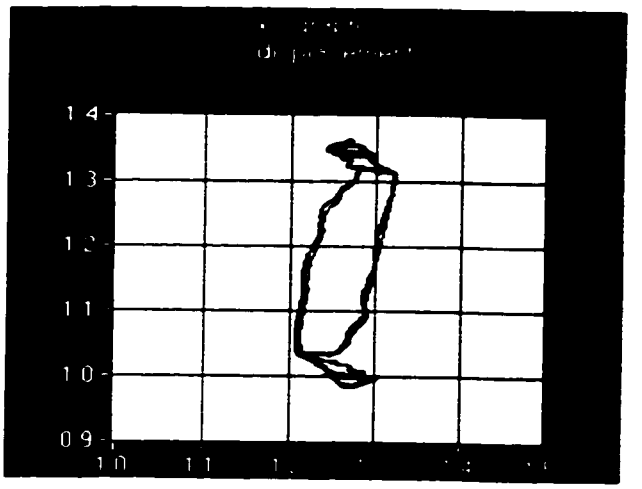

c

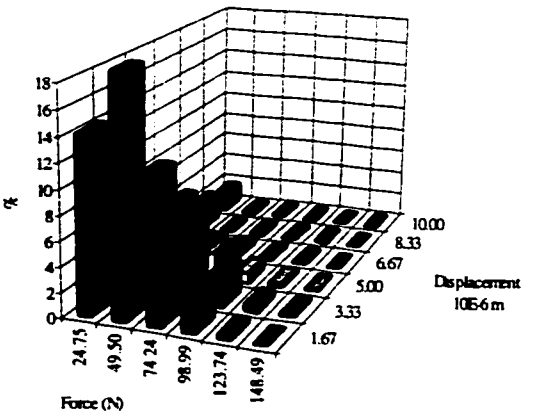

f

Figure 4.14a-f) Experimental data analysis for a normally impacting motion

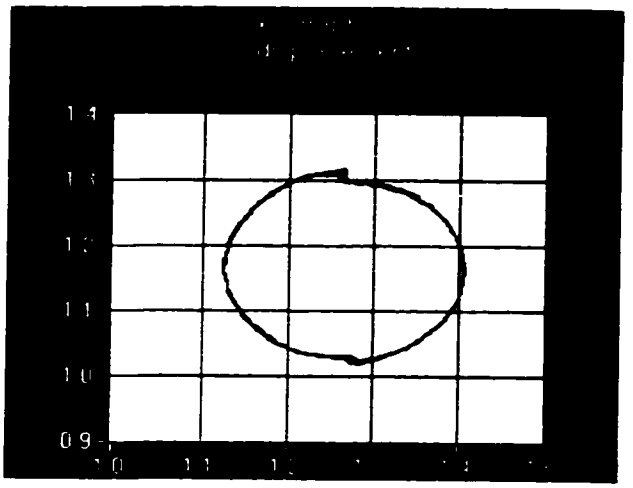

a

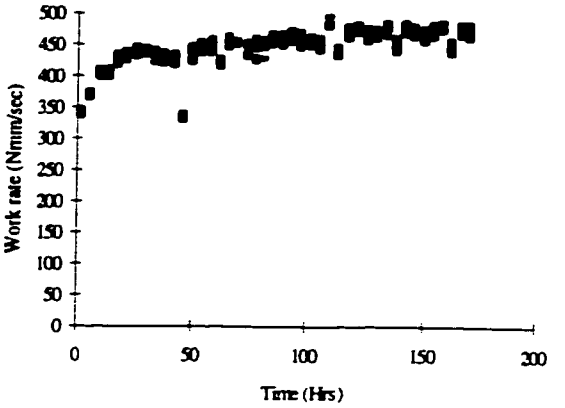

d

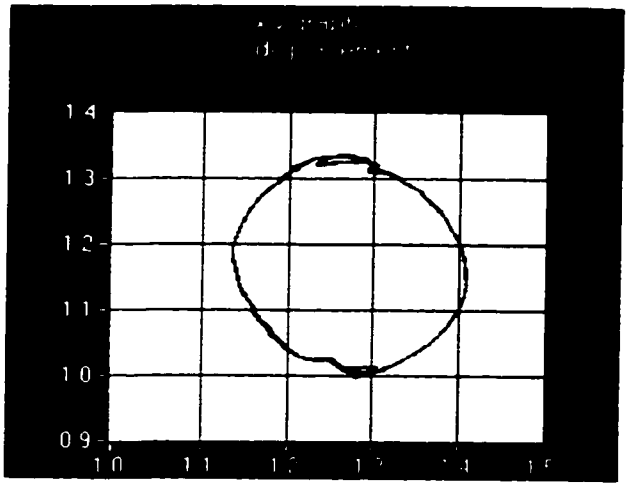

b

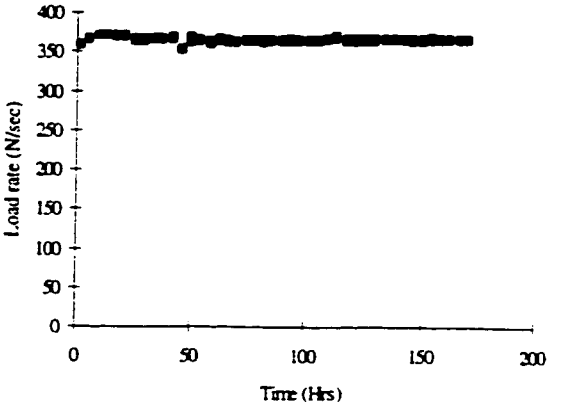

e

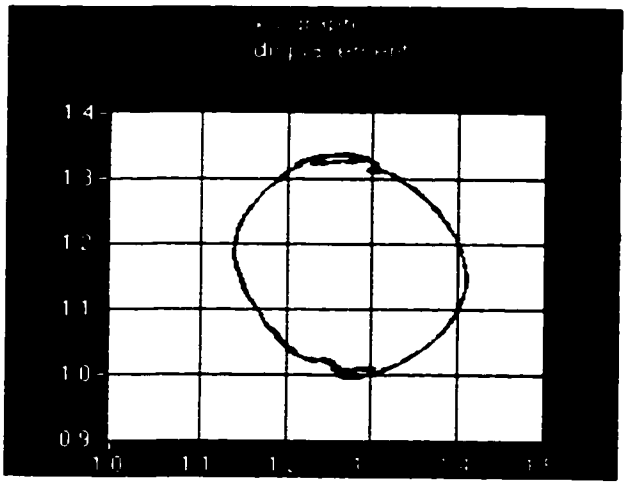

c

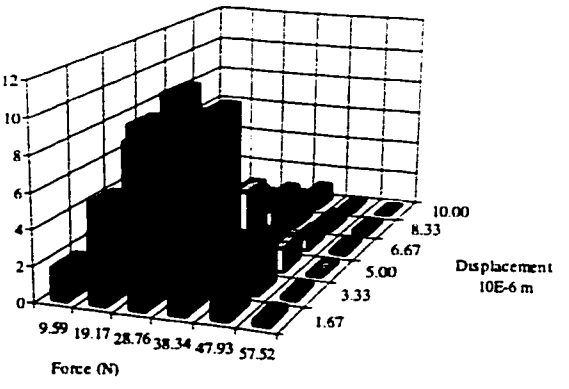

f

Figure 4.15a-f) Experimental data analysis for an Fx/Fy =0.35 (Oblique ratio)

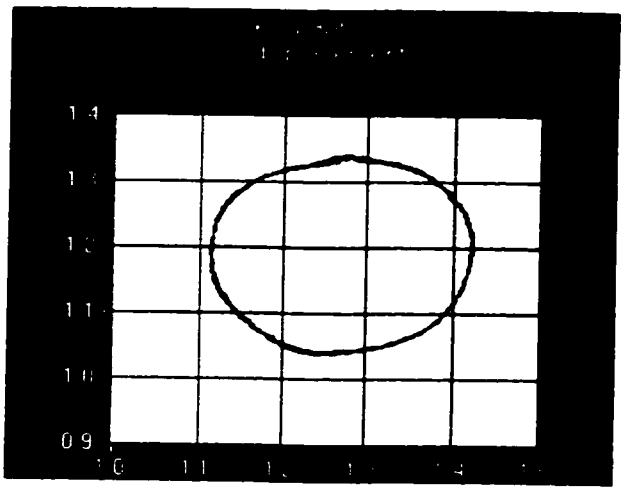

a

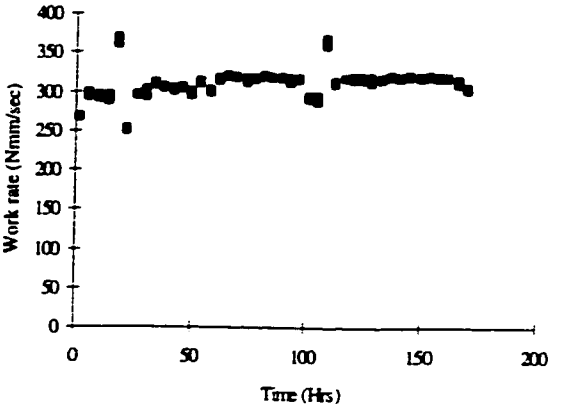

d

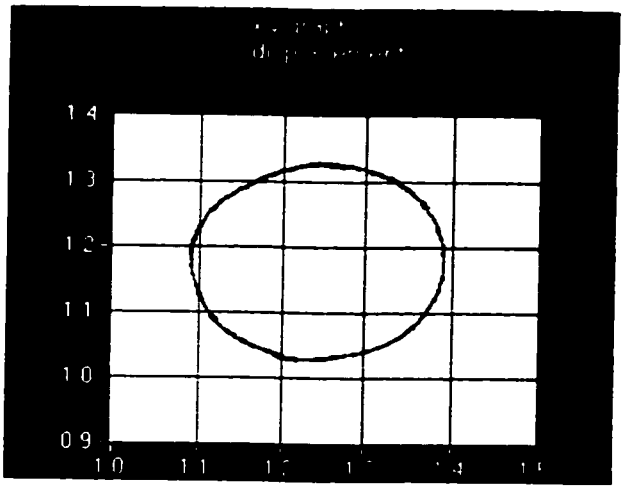

b

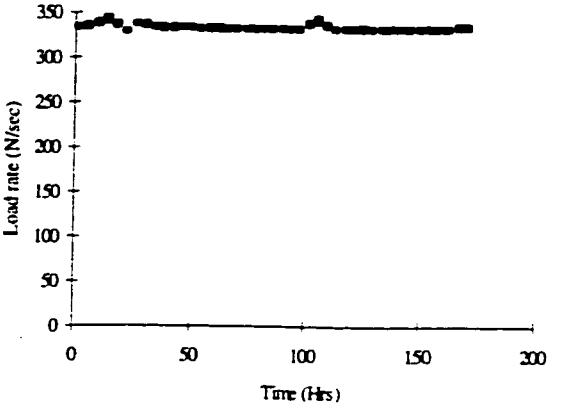

e

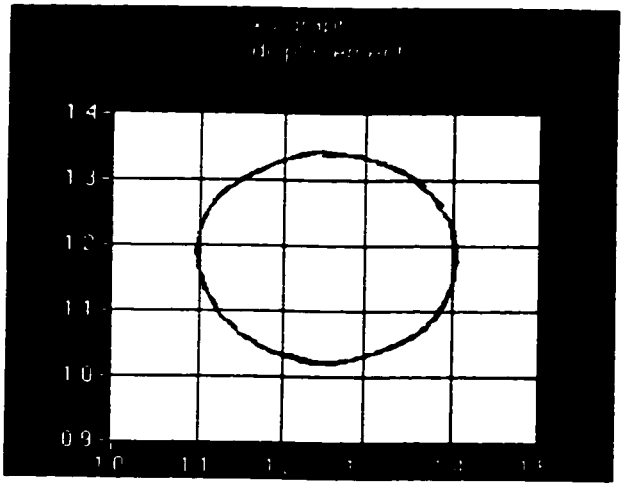

c

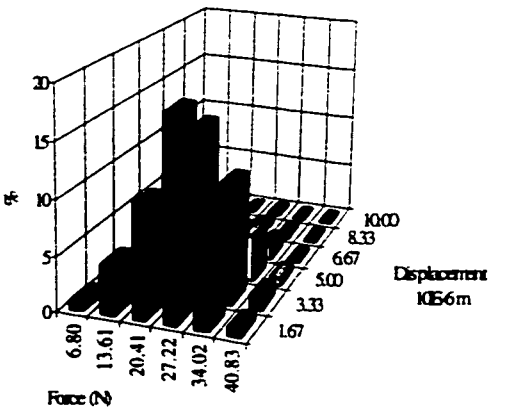

f

Figure 4.16a-f) Experimental data analysis for an Fx/Fy = 0.78 (Oblique ratio)

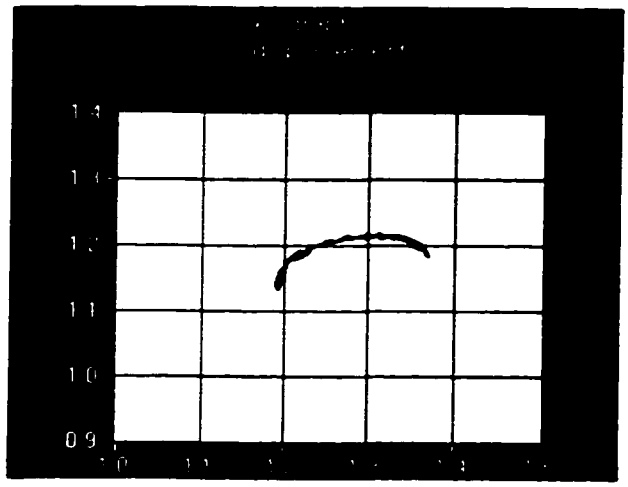

a

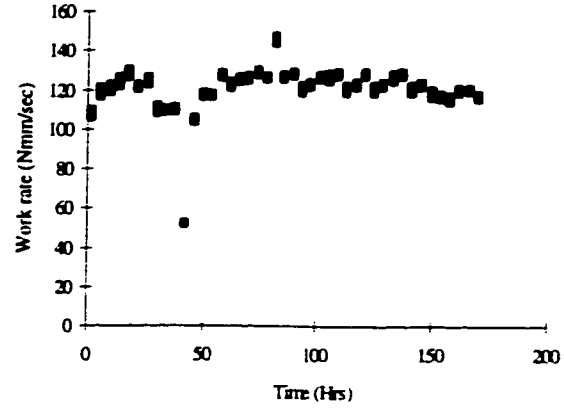

d

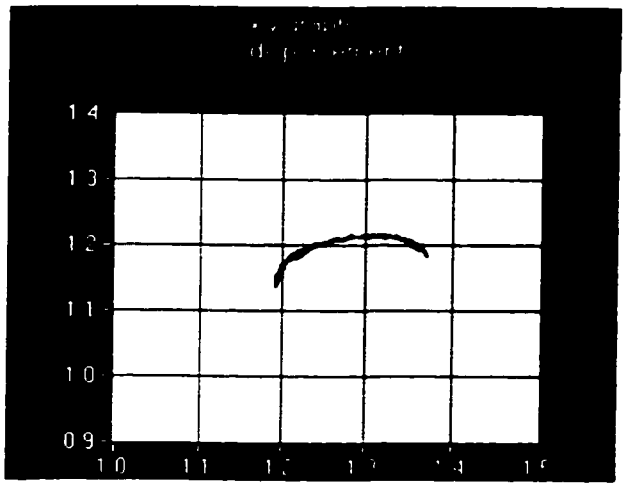

b

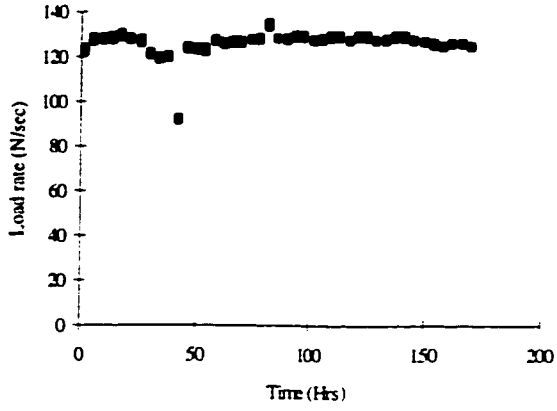

e

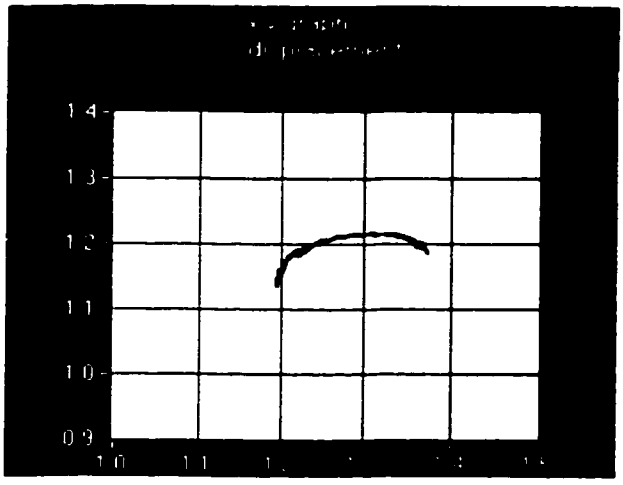

c

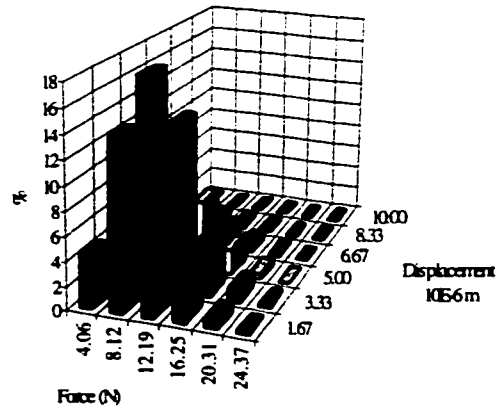

f

Figure 4.17a-f) Experimental data analysis for oscillatory sliding motion

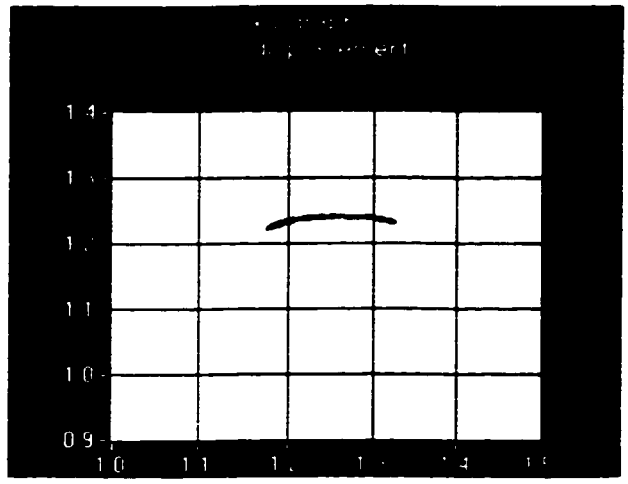

a

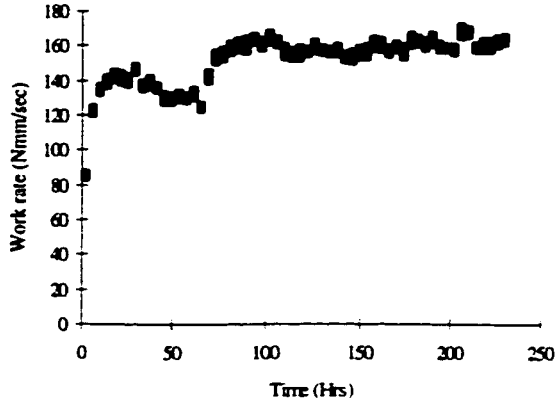

d

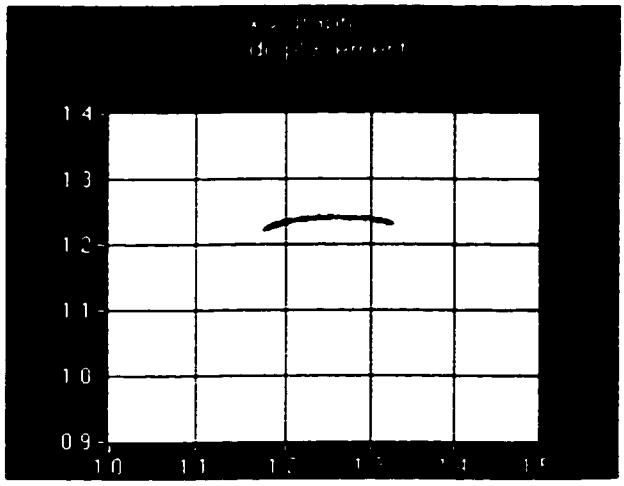

b

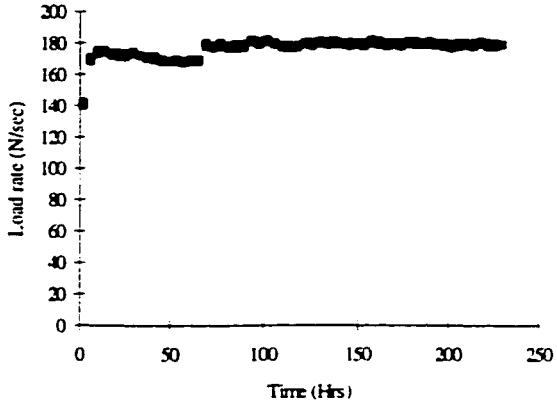

e

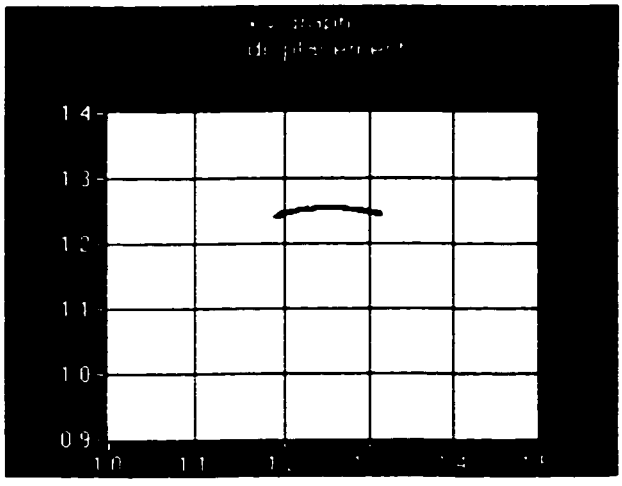

c

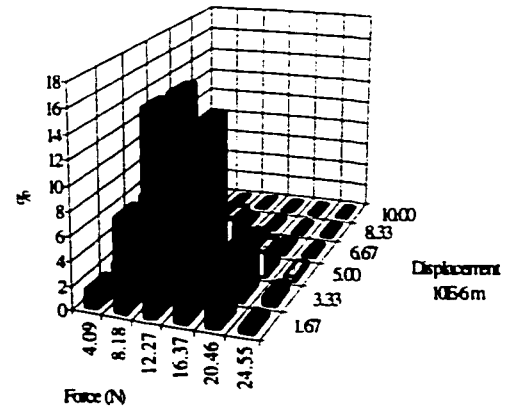

f

Figure 4.18a-f) Experimental data analysis for oscillatory sliding motion

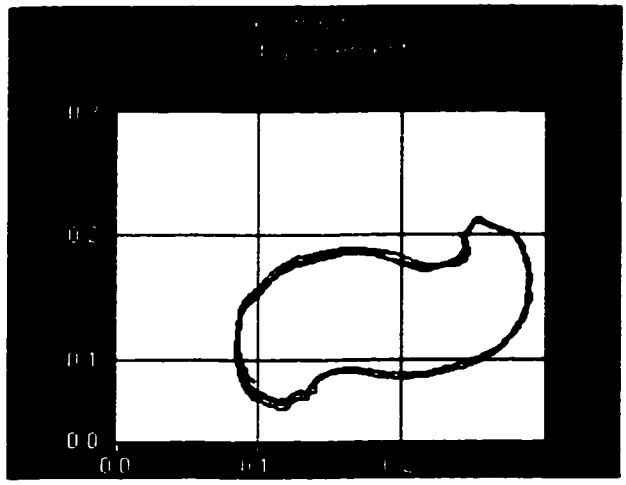

a

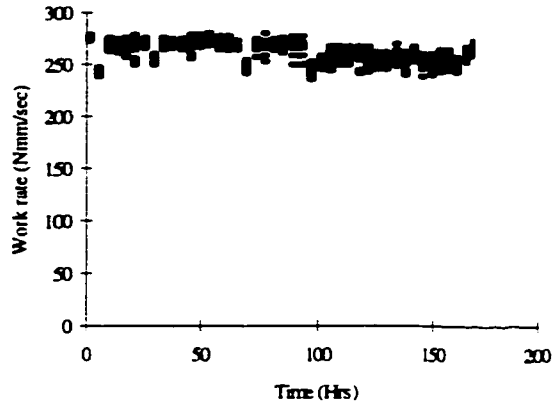

d

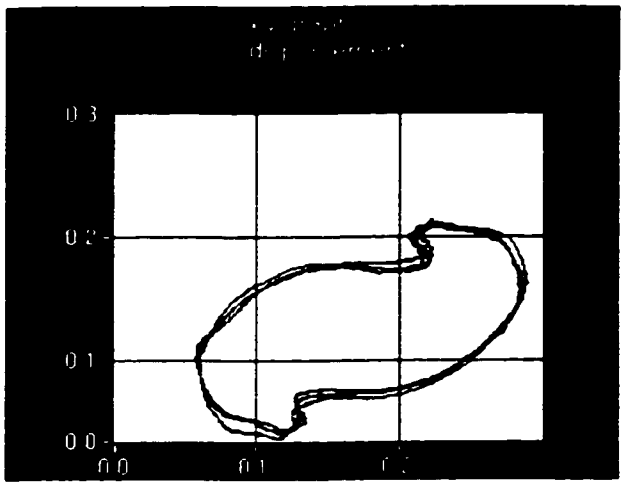

b

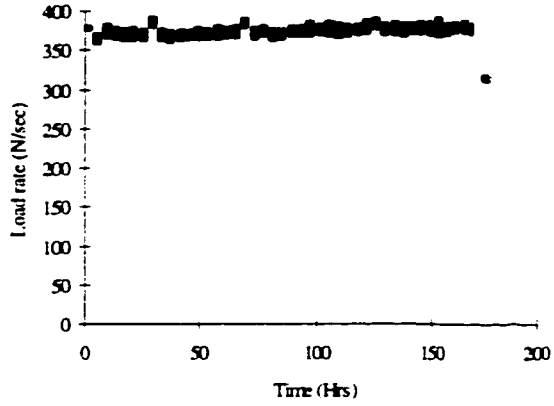

e

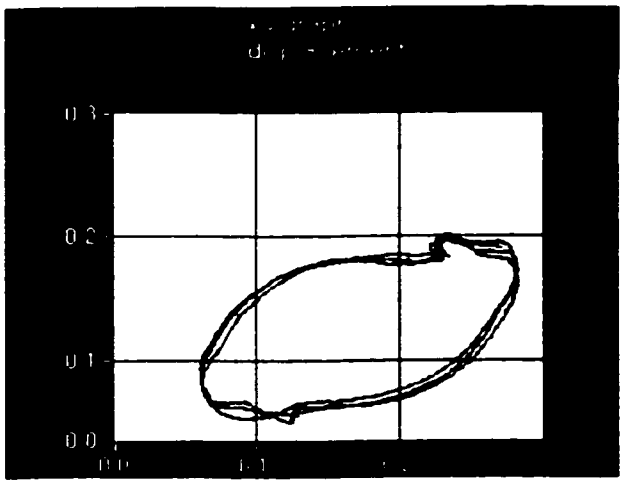

c

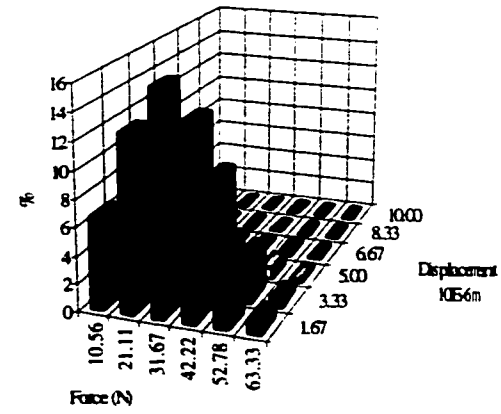

f

Figure 4.19a-f) Experimental data analysis for Fx/Fy = 0.35 (Oblique ratio)

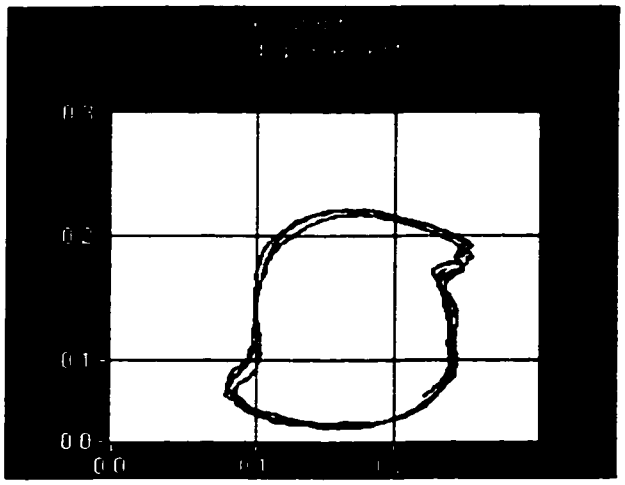

a

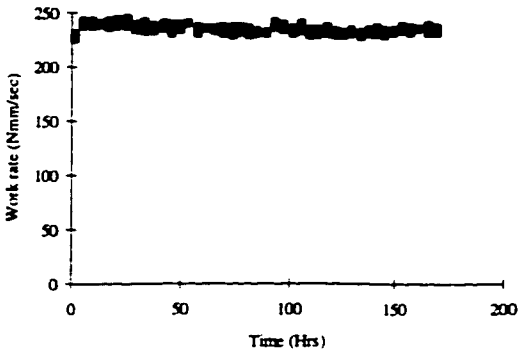

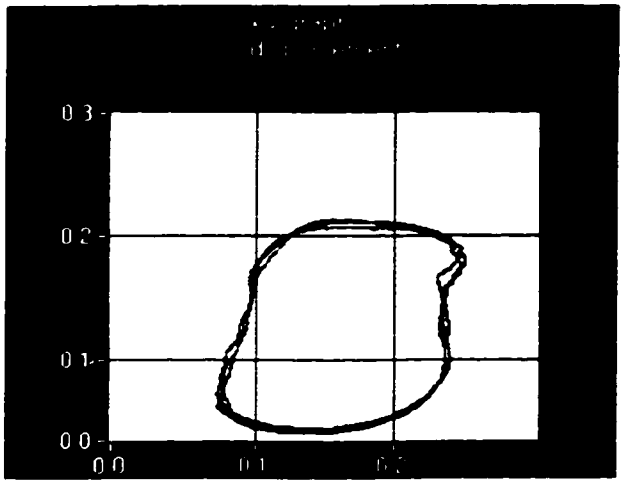

b

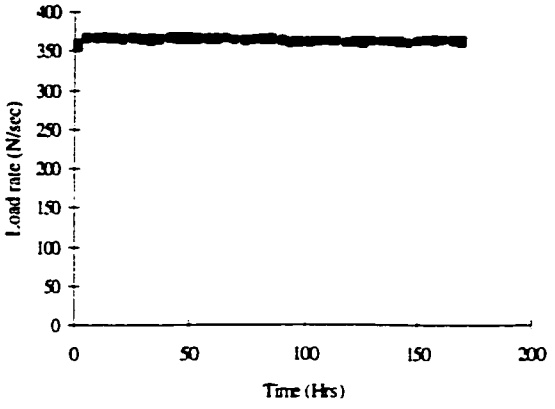

e

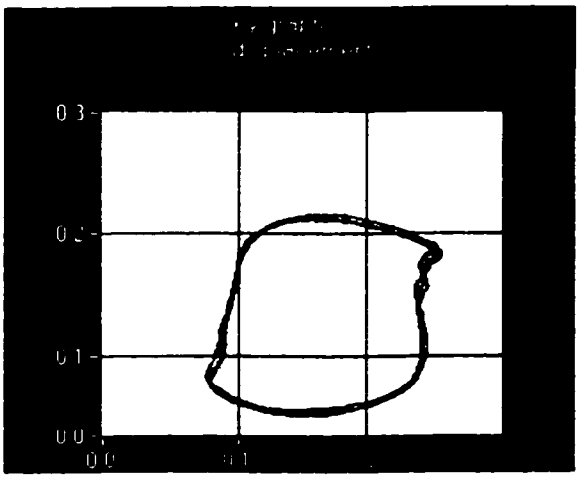

c

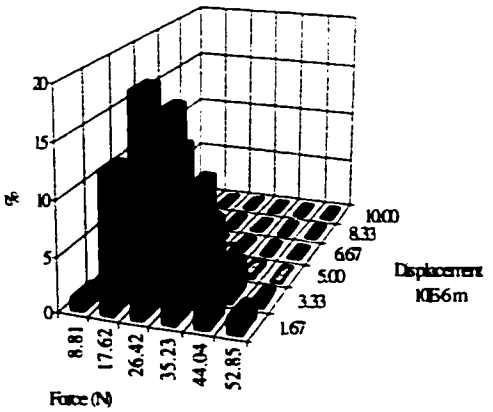

f

Figure 4.20a-f) Experimental data analysis for Fx/Fy =0.60 (Oblique ratio)

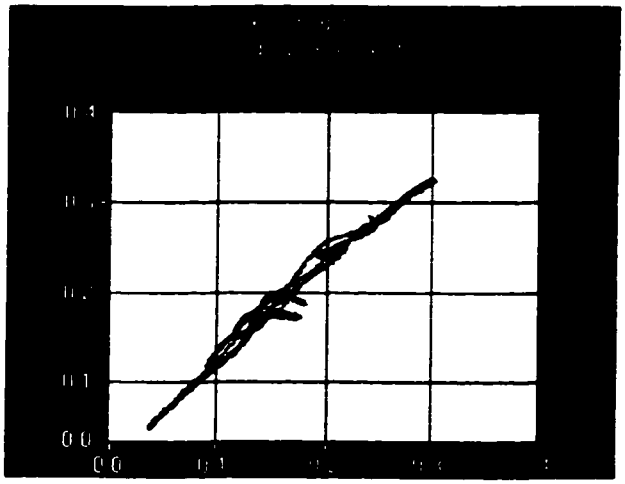

a

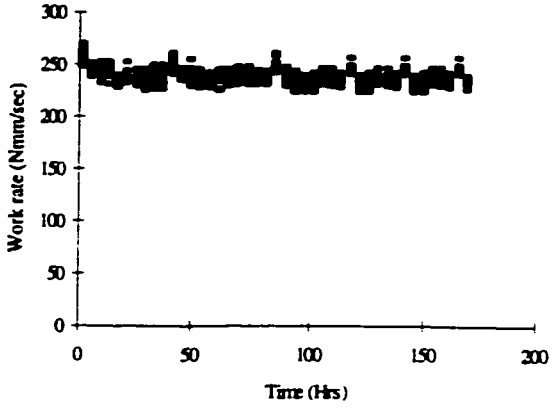

d

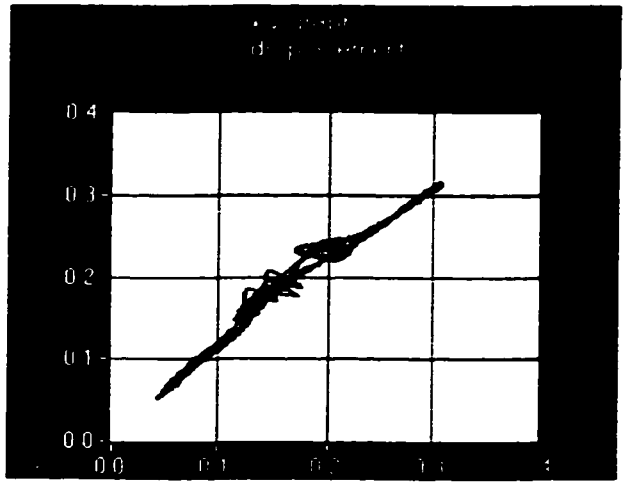

b

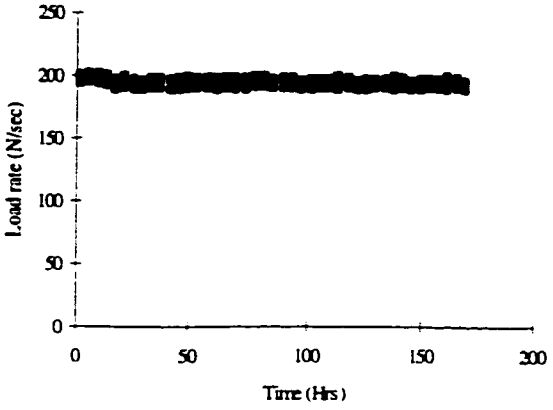

e

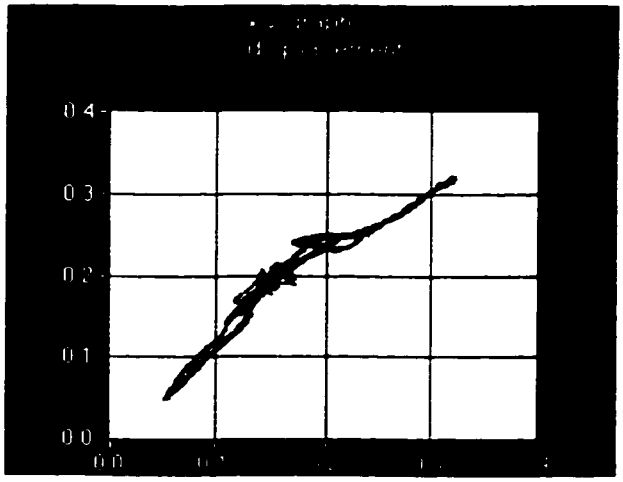

c

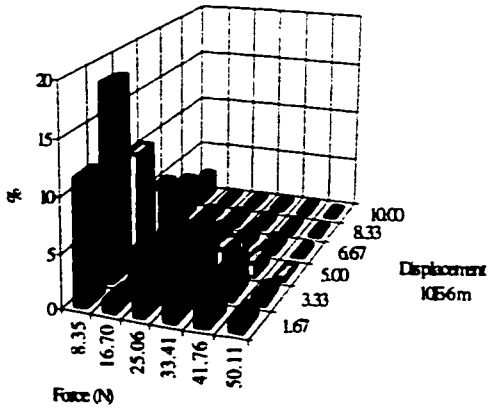

f

Figure 4.21a-f) Experimental data analysis for a normal impact motion

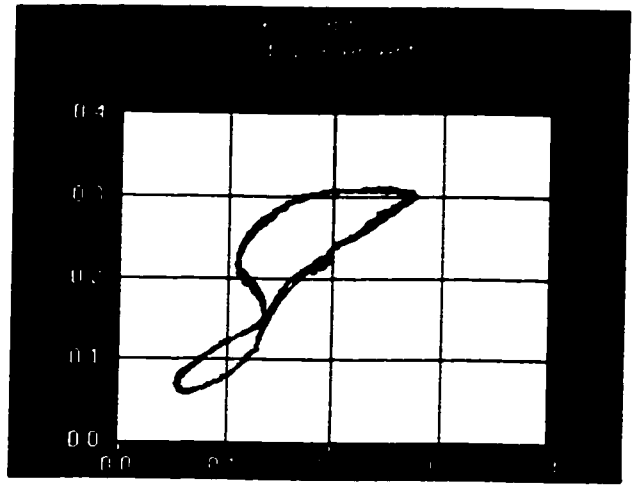

a

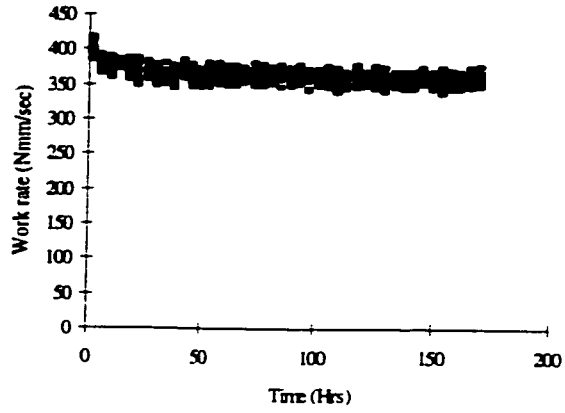

d

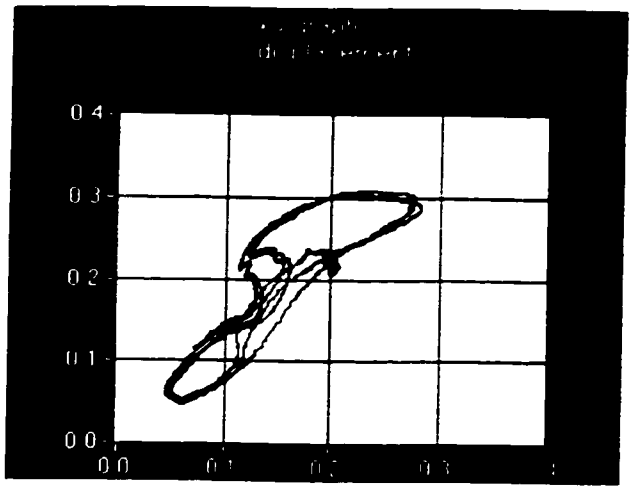

b

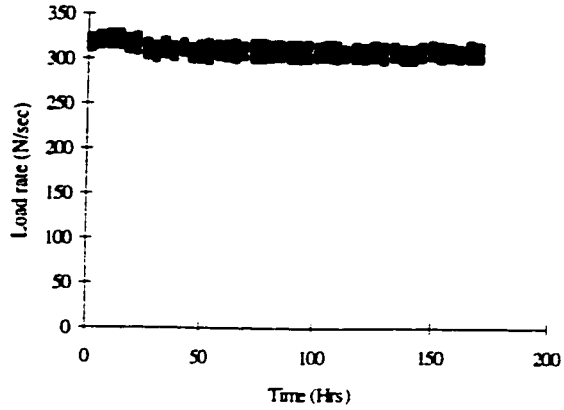

e

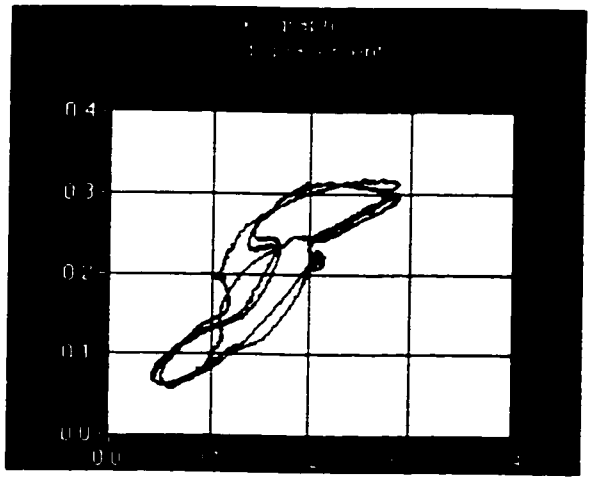

c

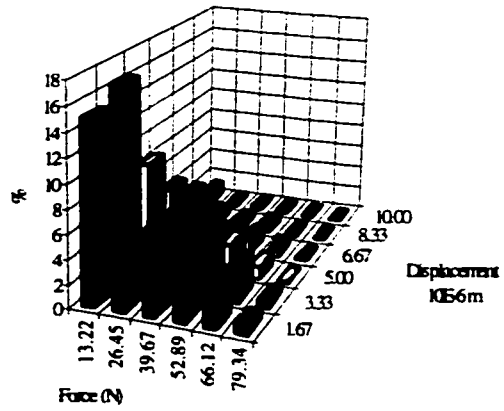

f

Figure 4.22a-f) Experimental data analysis for Fx/Fy = 0.05 (Oblique ratio)

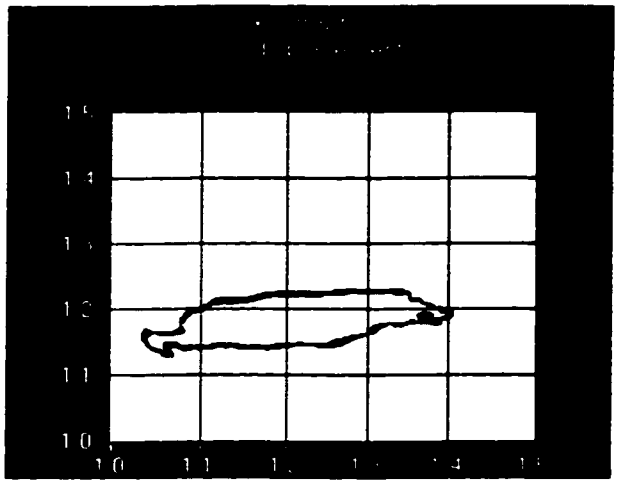

a

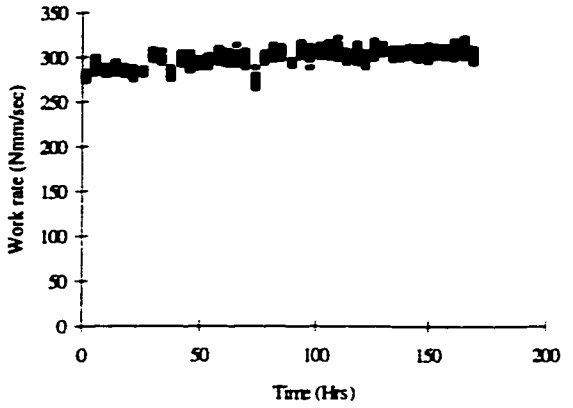

d

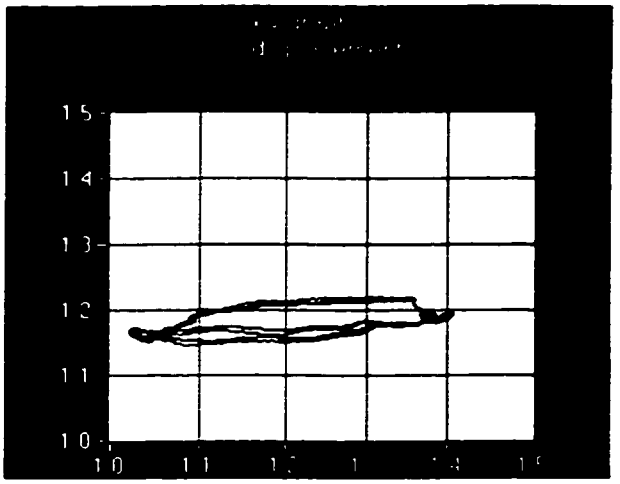

b

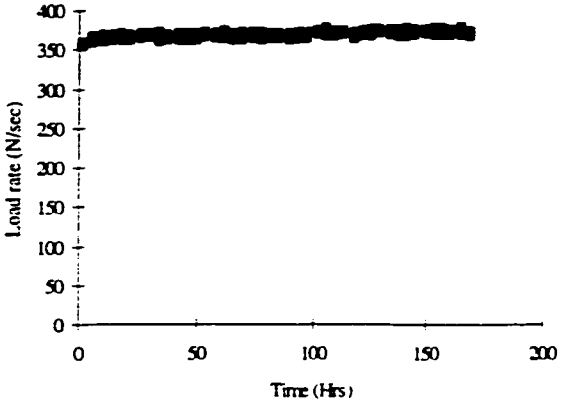

e

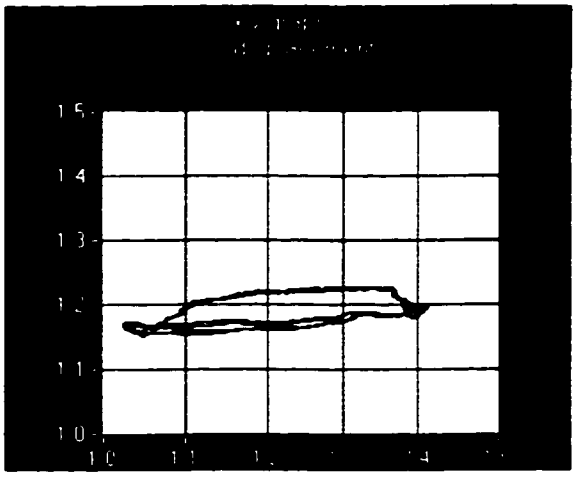

c

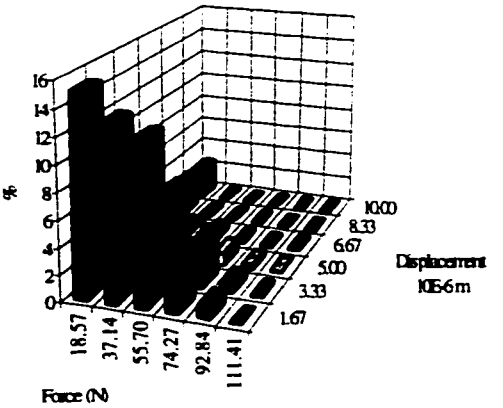

f

Figure 4.23a-f) Experimental data analysis for Fx/Fy = 0.05 (Oblique ratio)

CHAPTER 5

FRACTURE MECHANICS APPROACH FOR THE STUDY OF CRACK NUCLEATION AND PROPAGATION IN FATIGUE DOMINATED WEAR

5.1 Introduction

The wear model developed by Suh [10], based on delamination theory of wear requires the study of fracture mechanics, to analyse and justify experimental findings as well as quantify the wear volume due to the applied load. It has been established that crack nucleation and propagation are major factors in determining the wear rate [54]. In accordance with these arguments the state of the art survey conducted on crack nucleation and crack propagation will be, briefly examined. In this chapter, an extension to the delamination theory is introduced, by studying the crack nucleation and propagation phenomenon, using finite element modelling. [103, 109] (Author's Ref.)

5.1.1 Crack Nucleation

The nucleation of cracks at the subsurface level has been investigated by various prominent researchers, working in the area. It is approached from two different fronts. The dislocation mechanics approach is one and the continuum mechanics approach is the other. Based on the type of analysis performed, they could be in qualitative agreement pertaining to the various conditions affecting crack nucleation. If the material to be studied is considered to have impurities, then it will be advantageous to use the continuum mechanics approach, However,

if the material to be studied is assumed to be relatively pure with no impurity or inclusions, the dislocation mechanics is the right approach.

Researchers using dislocation mechanics for the study of cracks attribute its initiation to cumulative dislocation, for cyclic loading. Mura and Tanaka [55] identified the persistent slip band as the possible site for crack initiation due to the cumulative nature of dislocation on this plane. They proposed dislocation dipole models to explain significant physical phenomena apparent in cyclic loading and justified that damage accumulation of cyclic loading was due to dislocation. They attributed fatigue crack initiation to a critical value of cumulative self energy of dislocation. Following this research Tanaka and Mura [56] derived a relationship for the monotonic buildup of dislocation using the theory of continuously distributed dislocation. They associated crack nucleation with extrusion or intrusion, and stated that the critical value of the stored strain energy is reached when the crack size grows to the grain size of the metal.

Lin [57] developed a quantitative fatigue crack initiation theory. His analysis indicated that during cyclic loading of members, one thin slice of metal slips during forward loading and another closely located slice slides during the reverse loading. He also investigated the effects of local plastic strain, mean stress, grain size and strain hardening on the number of cycles required for fatigue crack initiation.

Mura and Nakasone [58] extended their research on crack initiation and arrived at a new model taking the form of a new nucleation theory similar to Griffith's theory. It was based

on the concept of Gibbs free energy change from the state of dislocation dipole accumulation on the persistent slip band to a state of crack initiation on this layer. A plot of the Gibbs free energy against cyclic numbers of loading indicates that it takes a maximum value at some critical number and progressively goes down after passing this number, implying that crack nucleation will occur at this critical value.

Cheng et al. [59] carried out an experimental study on surface crack initiation for contact fatigue by machining furrows using electric discharge machining (EDM) methods. The reason for using EDM is for avoiding built-up edge and associated residual stress for the purpose of stress analysis. They were able to conclude from their test results that the size of the furrow did not influence the crack initiation life. Following this investigation, Cheng et al. [60] extended the new crack initiation model derived by Mura and Nakasone [58] for sliding boundary conditions. This model was derived both for a surface and a substrate crack and the quantitative analysis they carried out showed that the life of a surface crack initiation is much lower than that of a substrate crack. They studied the influence of the various factors affecting the life of a crack initiation such as, residual stress, hardness, temperature, etc. They showed experimental verification of their analytical equations both for the surface as well as the substrate models.

The continuum mechanics approach for crack nucleation is based on the assumption that we are dealing with a non-pure metal containing inclusions at the substrate. The energy criteria was first proposed by Gurland and Plateau [61] while considering void nucleation from elastic spherical inclusions. The stress criteria was proposed by Ashby [62] and it states that

a void can be formed at a particle matrix interface if the tensile radial stress at that point exceeds the cohesive strength of the interface.

Argon et al. [24] proposed the conditions of cavity formation for equiaxed inclusions in ductile fracture. They found that the critical local elastic energy is necessary but not sufficient condition for crack nucleation. Therefore, the interfacial strength must also be reached for the other condition to be satisfied before particle matrix separation is to occur. Argon and Im [63] demonstrated experimentally that due to the high hydrostatic pressure at the contact interface the possibility of void nucleation is reduced. But further away from this region the effective stress is dominant enough to initiate crack.

Jahanmir and Suh [64] carried out an in depth analysis, studying the subsurface stress distribution of two contacting objects, sliding relative to one another, and showed the location of void formation, based on the summation of the steady state cumulative residual stresses and applied stresses. The analysis carried out in their investigation followed the Merwin and Johnson [23] method which utilized an approximate solution for the point in a semi-infinite body, loaded in compression and tension while being subjected to a rolling/sliding member.

Jahanmir and Suh [64] demonstrated that void nucleation can only occur below a certain depth, from the surface because of the large hydrostatic pressure at the contact. The depth of void nucleation from the surface was found to be more for higher normal contact pressure and friction coefficients. The crack nucleation criteria was based on the continuum

mechanics approach proposed by Argon et. al. [24], which states that the radial stress, which is equal to the summation of the von Mises (effective) stress and the hydrostatic stress, around an inclusion, should reach the particle matrix bond strength.

Salahizadeh and Saka [65] conducted an elasto-plastic analysis in order to study the mechanics of crack initiation in rolling contact. Using the continuum mechanics approach they had to insert hard particle inclusions in their model to study the crack nucleation criteria. They stated that for a particle matrix interface to debond, the stored elastic energy in and around the particle should be larger than the work of adhesion and the maximum residual radial stress should be greater than the cohesive strength of the particle matrix interface. An experimental analysis was conducted by Foltyn and Ravi-Chandar [66] for the crack nucleation of an interface crack in composite materials. Their analysis focused on the initiation process under mixed mode loading and they were able to conclude that under this type of loading, the interface fracture energy is a function of the extent of the mix.

5.1.2 Crack Propagation

The phenomenon of crack extension is identified as being dependent on the type of loading in its immediate vicinity. There are three modes of crack extension accepted in the fracture mechanics community. They are mode I, mode II and mode III, which are, opening mode encountered in symmetrical extension, sliding mode which occur in skew-symmetric plane loading and tearing mode which occur in skew symmetric bending of cracked plates respectively.

The state of the art survey conducted on crack propagation laws by Paris and Erdogan [67] covers the various models proposed for crack propagation. They studied the laws proposed by Head, Frost and Dugdale, McEvily and Illg, Liu, and Paris. They questioned the fact that only a few single specimen test results were used for verification purposes and showed that even though the laws are mutually contradictory they can be in agreement with the same sample of data. The authors concluded by saying that one should take extra precaution by ensuring that laws which correlate a wide range of test data for many specimens are properly examined before being accepted as laws.

Erdogan and Sih [68] conducted crack propagation analysis in plates under plane loading and transverse shear conditions. They found that under skew symmetric plane loading of brittle material the crack extension takes place at approximately 70^0 from the plane of the crack which is approximately equal to the value of the normal direction (70.5^0) of the maximum tangential stress at the crack tip.

Fleming and Suh [25,69] developed a subsurface crack propagation model in sliding contact. They showed the validity of linear elastic fracture mechanics approach for elasto-plastic materials because of the type of loading under sliding conditions. They argued that cracks on the subsurface level will close under sliding Hertzian type of loading, hence, leaving the trailing edge to be under purely elastic stress. Consequently they derived the distribution of the stress intensity factors for use in the Paris fatigue crack propagation law.

Application of the approach proposed by Paris, for contact conditions that involve severe

plastic deformation is questionable. Therefore, for contacts that involve high degree of plastic deformation at the crack interface, the Crack Tip Sliding Displacement (CTSD) approach is used [70]. Because the crack tip is subjected to high levels of stress, the CTSD is obtained from the residual relative displacement observed at the crack tip. The advantages of using this approach is that the crack propagation rate can be directly obtained from the analysis. Hence, there is no need for computation of the stress intensity factor.

Salahizadeh and Saka [71] used a finite element approach to calculate the stress intensity factors for straight and branched subsurface cracks subjected to Hertzian loading conditions. Their analysis considered interactions that could possibly occur between the two faces of the cracks and went on to investigate the type of stress intensity factor affecting the straight as well as the branched cracks. They were able to show that while straight cracks were subjected to mode II loading the branched cracks were subjected to both mode I as well as mode II type of loading. Their analysis also used the commonly accepted crack propagation law of Paris [72,73].

Crack nucleation and crack propagation have been identified as the two most important wear controlling factors in delamination wear. The different studies, analytical as well as experimental, conducted by Suh et al. [19,20] on crack nucleation and crack propagation give credence to this theory. Ensuing the proposal of the delamination theory of wear by N.P. Suh, an in depth analysis of this phenomenon was carried out by Jahanmir [11]. His analytical approach which was conducted for determining the crack nucleation employed the use of the Merwin and Johnson [23] approach for elastic-perfectly plastic material in rolling contact,

which later on was modified for sliding conditions. The two dimensional stress equation derived by Smith and Liu [74] was utilized for calculating the elastic plastic stress for plane strain condition.

The Smith and Liu's equation was developed for line contact of a semi-infinite body with Hertzian type elliptical contact distribution. However, since asperity contacts are better approximated by spherical or point contact, an axi-symmetric model will describe the problem more accurately than a line contact. Given the fact that a plane strain line contact model is similar in characteristics with regards to the subsurface stress distribution as shown by Hamilton and Goodman [75], utilizing line contact in plane strain is a reasonable assumption and would not give qualitative errors. Also, the analysis time required to obtain the stress distribution and its effects at the subsurface level is reduced tremendously. A comparison of the non-dimensional second stress invariant given by Hamilton and Goodman [75] indicates that the distribution is similar for both cases. The maximum value of the ratio of the second stress invariant to the maximum applied Hertzian contact pressure is seen to occur at a depth of 0.5a (value of 0.357) and 0.7a (value of 0.322) for spherical and cylindrical contacts respectively. Therefore, given the closeness of the numbers, the interchangeability of the two (subsurface stress due to spherical contact and plane strain cylindrical contact) is justifiable.

5.2 Validity of Hertzian Contact Mechanics for a Tube in a Conforming Support

The problem of analysing the wear of a heat exchanger tube should be studied by considering

the global or macro contact initially, to estimate the amount of asperity contact for a given load. The heat exchanger tube is resting in a scallop bar or a drilled hole support that has a radial clearance of 0.2-0.4 mm. Applying the Hertzian contact equation for this problem might introduce some errors in determining the overall contact length as given in Johnson [76,77]. Hence, a finite element model was developed to verify equation 5.1. This equation gives the half length (a) of a Hertzian contact width, for a line contact (contact of two conforming cylinders with radii of R_1 and R_2, Young's modulus of E_1 and E_2, and Poisson's ratio of ν_1 and ν_2 respectively) with an elliptical pressure distribution.

$$a = \sqrt{\frac{4P_0R}{\pi E^*}} \qquad \textbf{(5.1)}$$

where

$$E^* = E_1E_2/[(1-\nu_1)^2E_2+(1-\nu_2)^2E_1]$$

$$R = R_1R_2/(R_1+R_2)$$

The finite element model was developed for a two dimensional cylindrical contact using a quadrilateral four node (PLANE42) element with elasto-plastic hardening capabilities, in ANSYS [92] finite element program. Because of symmetry, only half of the tube and its support were modelled, assuming the support is fixed while a load is applied at the top of the half tube. The contact interface was modelled using a 2-D point to line contact element (CONTAC48) which has a stiffness of 10^{12} N/m. The modelling was carried out such that the dimensions of the contacting bodies are about 4 times higher than the estimated and finely meshed contact zone.

PLANE42 element was selected due to the fact that the generated 2D contact elements

(CONTAC48), are not compatible with elements that contain mid-side nodes. To carry out the analysis, the contact elements are generated on the line where it is predicted that contact will occur, and the load was applied for determining the total length of contact. The software has automatic load-step features which bisects the difference between the current time step and the total time step and accelerates the time of computation if numerous steps are selected. This bisection algorithm is activated only if the convergence is not satisfied in the first few iterations. Comparison of the results obtained from the finite element program was about 7% off than that of the Hertzian contact mechanics approach. The finite element analysis conducted supports the validity of the above equation (eq. 5.1) in determining the total contact length. This result is in agreement with that of Johnson's [76] which indicates the validity of the relationship even for closely conforming objects as long as the materials have high Young's modulus values.

5.3 Estimation of Micro-Contact Asperity Size

After establishing the validity of eq. 5.1, the next step is to estimate the number of asperity contact based on a fixed average area of contact per asperity. The contact pressure of each asperity is taken to be equal to the hardness or flow pressure of the softer material. Aramaki et al. [78] and Hisakado [80] have shown that the net effect of increasing the contact load is to increase the number of asperity contacts. The other assumption is that to maintain the Hertzian macro contact pressure distribution the asperity contact density is spaced accordingly.

The micro contact areas occurring between the two metals has been studied by different researchers. A number of studies have been carried out by Hisakado [81, 82] to properly determine the approximate asperity number and size, based on the surface finish. The findings from his research work are implemented in this thesis, to properly carry out the analysis for determining the number of asperity contacts based on the surface finish and applied load for the experiments conducted through the course of this research work. This approach is also utilized for a set of experimental data found in open literature giving an average asperity size.

The characteristic curve given by Hisakado [81] plots the relationships between the number of asperities in contact and applied apparent pressure, varying as a function of different maximum asperity height of the rough surface. He has given the results of experimental investigations to validate the theoretical approach proposed, and the chart provides both these results. The approximate average roughness of H = 10 μm (H is defined as the distance between the line parallel to the center line and passing through the lowest point on the surface and the line containing at least three of the highest peaks) is estimated for the experiments conducted. Based on this result and an average pressure of about 160 kg/cm^2 (this apparent pressure was an average value for the four sets of experiments, with an applied load of the order of 10 - 50 N) the number of asperities per unit area obtained is about 80 mm^{-2}. Using this value as the approximate figure for these experiments and taking $5k$ (k is the yield strength in shear) as the maximum Hertzian pressure value causing the flow pressure contact, an average asperity contact radius (a) of nearly 10 μm is obtained. After determining the average micro contact asperity size, the number of asperities per contact can

be obtained using the following relationship:

$$A_n = \frac{P_0}{A_s h} \tag{5.2}$$

where

A_n = number of asperities in contact per unit length

P_0 = total force per unit length

A_s = area of asperity contact

h = hardness of the soft material

From the above equation, one can estimate the distribution of asperity contacts based on an initial assumption of equal distance between the asperities which, at a later stage, will be modified to reflect the Hertzian elliptical pressure distribution cross-sectionally. This approach is assumed to be valid based on the fact that maintaining elliptical pressure distribution at the macro level is controlled by the number and distribution of asperity contact at the micro level.

5.4 Crack Nucleation Analysis

Study of the crack nucleation analysis requires contact mechanics to properly characterize the stress distribution in the members. Hence, it is essential to utilize a combination of numerical analysis (FEM) and analytical closed form approaches where possible to handle the problem. The validity of the Hertzian contact mechanics approach, which was derived for an elliptical contact, was verified for determining the contact conditions. Ensuing this analysis the crack nucleation criteria and zones shall be investigated.

5.4.1 Crack Nucleation Criteria

The crack nucleation criteria survey given at the beginning of this chapter indicates that of the two avenues, the one which attributes nucleation to impurities or inclusions in the metal matrix is amenable to fracture mechanics equations and can be analysed using continuum mechanics in general. Therefore, the crack nucleation criteria from inclusions which proposes the theory that since hydrostatic stress has an effect on the crack nucleation from inclusions, one should include their influence on the effective stress such that the summation of this two in addition to the residual stress, should reach a critical value before a crack is formed. However, since stress alone is not enough to produce crack nucleation one should also have a local strain criteria in combination with the stress criteria, implying the zone of crack nucleation should be in a plastically deformed zone, with the radial stress value equal to or above the material cohesive strength.

In this chapter, the same assumption taken by Jahanmir and Suh for calculating the stress values is followed. Namely, that the rigid inclusions in the material have the same properties like the parent material, while calculating the elasto-plastic stress distributions at the subsurface level. It is a reasonable assumption in that it will give a good understanding about the state of stress and its effects at the subsurface level. The residual stress distribution is taken as a function of the plastic stress and it is assumed that the principal shear strain and the principal shear stress are on the same plane, as indicated in Fig. 5.1.

The crack nucleation criteria indicates that for large diameter inclusions of 0.025 μm or

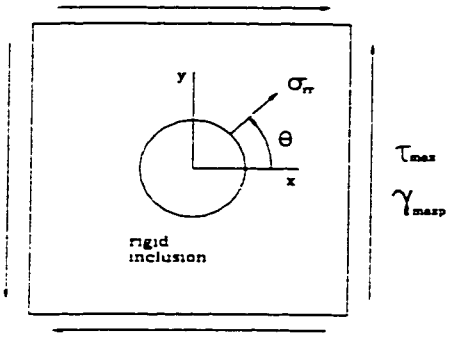

Figure 5.1 Critical interfacial stress around an inclusion

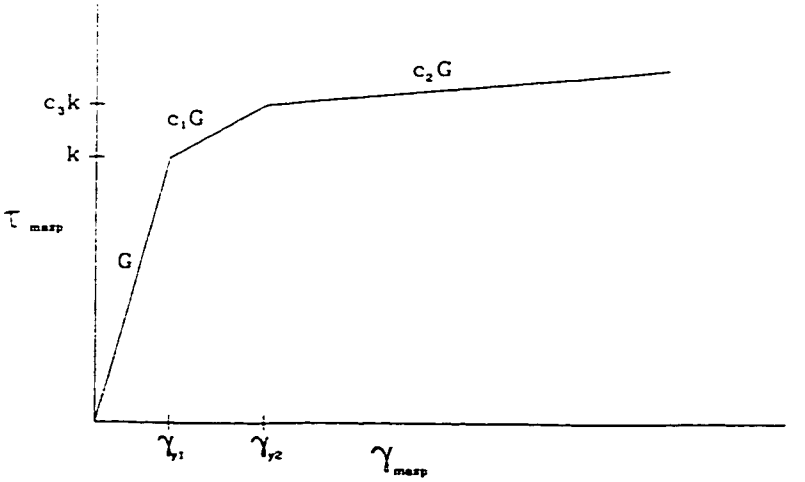

Figure 5.2 Residual stress - plastic strain relationship

bigger the strain criteria is always satisfied, hence the local stress criteria is sufficient to determine the crack nucleation positions. The study conducted by Jahanmir and Suh assumed the value of $2k$ to be the limiting case of the interfacial stress for the formation of crack. This estimate is rather conservative and the possibility of nucleation occurring at values lesser than $2k$ can not be discounted. Also, the study done by Argon and Im [63] indicates that without considering the effect of other inclusions in the neighbourhood, this critical stress is approximately $1.5k$. In addition Salahizadeh and Saka [65] have indicated that the stress which is obtained around an inclusion can be amplified if the inclusion is not smooth and round. It should be noted that this study does not consider hard inclusions that might initiate crack by particle fracture.

The analysis conducted by Jahanmir and Suh [64] carried out the stress calculation in a homogeneous medium and implemented the effect of the residual stress due to plastic deformation around the inclusion in the form of a stress, proportional to the shear strain and shear stress modulus. Hence, the need for the consideration of the stress from the calculated plastic strain. Verification of this approach was conducted in this thesis by implementing an inclusion in the finite element program and carrying out the complete analysis to determine the maximum stress around an inclusion.

In order to properly determine the relationship between the proposed critical value for crack nucleation using Jahanmir and Suh's [64] approach and the actual value calculated from the analysis carried out for a model with an inclusion in the material, it is essential to carry out a comparative study. This study is carried out by developing a FEM model of the problem

with the hard inclusion and the result arranged in the post processor to reflect the critical interfacial stress value. This critical interfacial stress is calculated from the applied stresses as follows:

$$\sigma_{rr} = \sqrt{3}\tau_{max} + \sigma_h \qquad (5.3)$$

where

σ_{rr} = maximum interfacial normal stress

τ_{max} = maximum shear stress

σ_h = hydrostatic stress

The finite element model was developed for a simple case of a symmetric problem with a 1 μm radius inclusion located at 10 μm (1*a*, probable position where crack is supposed to originate as will be seen) from the surface and subjected to a maximum Hertzian contact pressure of 4*k*. The inclusion (Figure 5.1) is assumed to have four times the amount of the Young's modulus of the parent material. The material chosen had a first and a second hardening modulus of 0.1E and 0.01E respectively (similar characteristics to what is shown in Figure 5.2). The element chosen was PLANE42 and the size of the symmetric model was 200 μm by 400 μm (Figure 5.3a) The finite element mesh shown in Figure 5.3b is zoomed in to show the critical zone which has a dimension of about 20 μm by 20 μm. The maximum interfacial stress value can be compared to the analysis conducted without the inclusion and a parallel can be drawn to validate the approach of the above procedure.

It should be noted that inserting an inclusion in the finite element model at various points to obtain the contour plots similar to those obtained using Jahanmir's approach is impractical. It is only utilized to observe if the method implemented by Jahanmir, over or under estimates

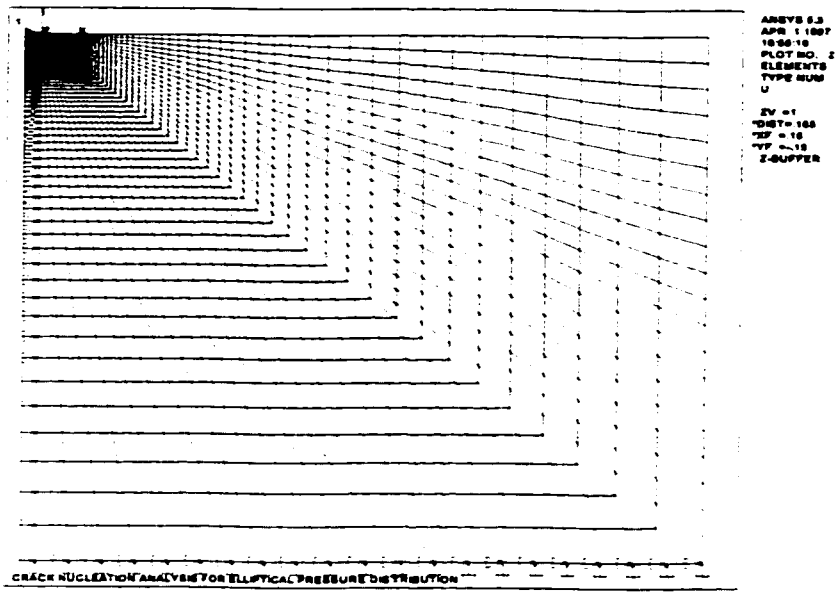

a)

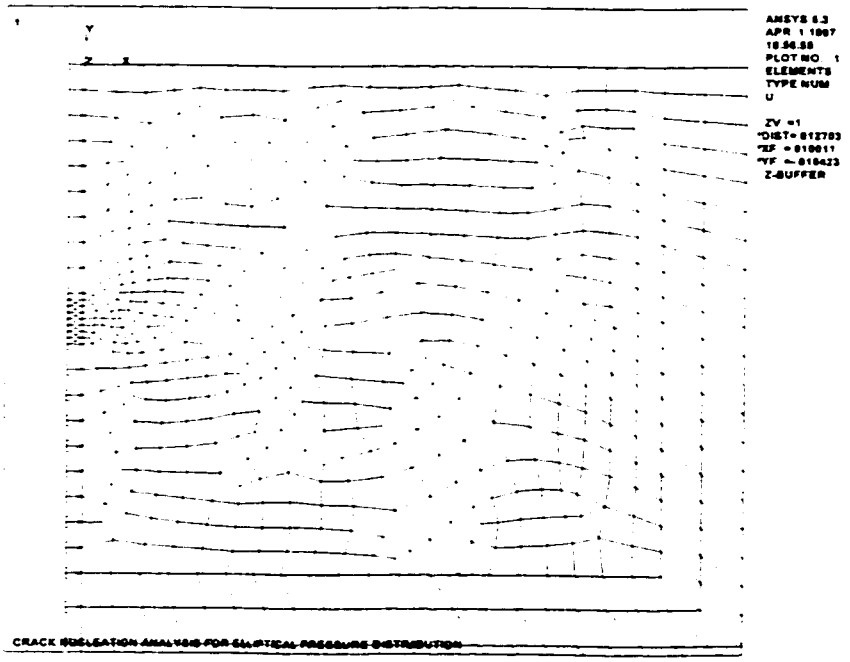

b)

Figure 5.3 Finite element mesh for a cylinderical inclusion a) with boundary conditions b) magnified near the inclusion

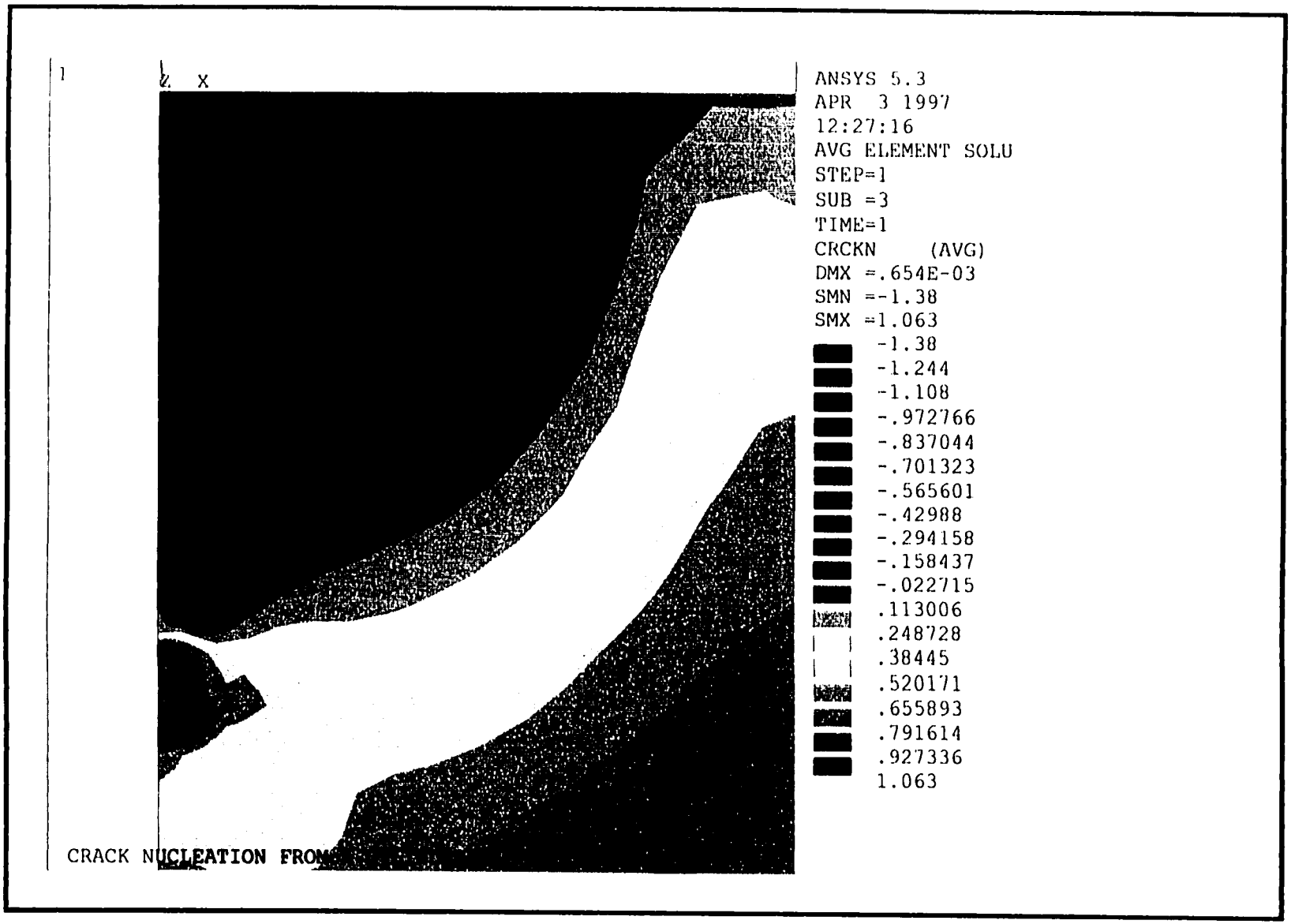

Figure 5.4 Contour plot of interfacial stress around an actual inclusion.

the actual value of the interfacial stress. Results of the finite element analysis for the model with the cylindrical inclusion, post processed to display the interfacial stress values can be observed in Figure 5.4. This figure shows that the value of the maximum interfacial stress obtained around the inclusion was almost $1k$, as opposed to $0.5k$ using Jahanmir's approach. This suggests that instead of taking the $2k$ as the critical value for the interfacial stress, it is safe to take $1k$ to be the critical value for crack nucleation, on the contours obtained using the Jahanmir and Suh's approach.

After establishing this fact, the next stage of the investigation is the quantitative study based on the plane strain cylindrical contact geometry, to assess the values at which crack will nucleate. The Argon criteria for crack nucleation is utilized here and a finite element program is developed to verify this.

Jahanmir has shown that for cylindrical inclusions the interfacial normal stress is a summation of the cumulative residual stress, applied stress and hydrostatic stress, given by the following equation [11]:

$$\sigma_{rr} = \sqrt{3}k\sin(2\theta_0) + \sqrt{3}\tau_{max}\sin2(\theta_0 - \phi) + \sigma_h \qquad \textbf{(5.4)}$$

where

θ_0 = angle at which σ_{rr} will be a maximum

ϕ = angle for τ_{max} from the two dimensional component stresses

The above equation was proposed for an elastic perfectly plastic solid, and the factor $\sqrt{3}$ comes into picture because of the yield criterion used (von Mises). The derivation was based on the fact that the maximum cumulative residual stress will have a maximum value of $\sqrt{3}k$

because of the nature of the stress / strain relationship [94]. In addition, it is assumed that cumulative residual stress will occur until steady state value is reached, beyond which further loading will have no effect in increasing the magnitude of the residual stress.[97, 98]

5.4.2 Finite Element Model for Crack Nucleation Analysis

The above relationship (eq. 5.4) was derived for a cyclically loaded object where each point in the loaded member was continuously subjected to tension as well as compression type of loading. Because of the nature of the cyclic loading it is apparent that there will be a continuous plastic deformation until a steady state value is reached. This model is further extended in this thesis to investigate the conditions that arise due to impact loading. The major difference between this approach and the one done by Jahanmir and Suh is that in this case the material is assumed to follow a more realistic stress strain curve which has a similar trend to that of Figure 5.2 (i.e. a multi-linear elasto-plastic material with isotropic work hardening properties). The value of the Young's modulus for the hardening section is assumed to vary between 0.1 and 0.2 for the first hardening modulus and between 0.01 and 0.02 for the second hardening modulus and that the direction of the maximum plastic shear strain is the same as that of the maximum shear stress. In the analysis conducted by Iyer and Ko [79], they had used a bi-linear hardening property which varied from 0.2E for 6061 aluminium to 0.001E for 410 steel. Salahizadeh and Saka [65], on the other hand have used 0.1E for their hardening modulus for steel. Therefore, given the fact that there is no absolute value for Inconel 600 in open literature, the above mentioned parametric study covers a reasonable range. It should be noted that for the case of a normally and obliquely impacting

objects, it is assumed that the load is going to be applied at the same point forcing steady state value right after the first loading.

Because of the loading condition, the residual stress is a function of the principal plastic shear strain, which is assumed to have its value according to the relationship of equation (5.5), which is also shown in Figure 5.2. The reason for selecting the value of 1.29 for c_3 as the limiting case for the first hardening modulus stems from the fact that shakedown will only occur beyond the onset of plastic deformation ($3.1k$) and until a maximum Hertzian contact pressure of $4k$ [23]. This indicates that the first hardening modulus (higher slope) is within this region. Beyond this point it is assumed that the hardening of the material drops dramatically, following the multi-linear elasto-plastic curve. This implies that a more gentler slope of the second hardening modulus will take effect after the shakedown value. The residual stress is given by one of the following relationships depending upon the value of the maximum plastic shear strain.

$$\begin{aligned} \tau_{maxp} &= \gamma_{maxp} G && for && \gamma_{maxp} \le \gamma_{y1} \\ \tau_{maxp} &= k + (\gamma_{maxp} - \gamma_{y1}) c_1 G && for && \gamma_{y1} < \gamma_{maxp} \le \gamma_{y2} \\ \tau_{maxp} &= c_3 k + (\gamma_{maxp} - \gamma_{y2}) c_2 G && for && \gamma_{maxp} > \gamma_{y2} \end{aligned} \qquad \textbf{(5.5)}$$

where

τ_{maxp} = residual principal shear stress

γ_{maxp} = residual principal shear strain

γ_{y1} = yield stress value in shear

γ_{y2} = hardened shear stress value

G = elastic shear stress

c_1 = plastic shear stress coefficient for first hardening modulus

c_2 = plastic shear stress coefficient for second hardening modulus

c_3 = constant corresponding to shakedown limit (1.29)

With this in mind an asperity contact with a Hertzian elliptical pressure distribution model was developed using the ANSYS finite element program (Figure 5.5a).Figure 5.5b shows the magnification of the freely meshed area near the contact area zone, of about 40 μm by 20 μm. The element chosen for this model was a four node 8 degrees of freedom (PLANE42) element. The half Hertzian contact length (a) was determined as 10 μm and in order to satisfy the semi infinite boundary condition without compromising computing time, it was decided that the contact zone will have at least a minimum rectangular size of 800 μm by 400 μm. The model utilized is a two dimensional plane strain problem to represent the axi-symmetric problems (spherical contact).

The area in the immediate vicinity of the contact zone was divided into 793 elements generated using the automatic meshing routine of the program. Total number of elements was almost 4000 and the Hertzian contact pressure was approximated by a series of linear pressure gradients that satisfy the elliptical pressure values at the element nodes and was applied using a two dimensional pressure element (SURF19). The remaining part of the model was meshed coarsely and post processing was confined to the elements selected in the immediate contact zone, a rectangular area of 40 μm by 20 μm.

Sequential verification of the finite element model was carried out to ensure the accuracy of the results obtained. The first step was to conduct a comparative study of the results obtained

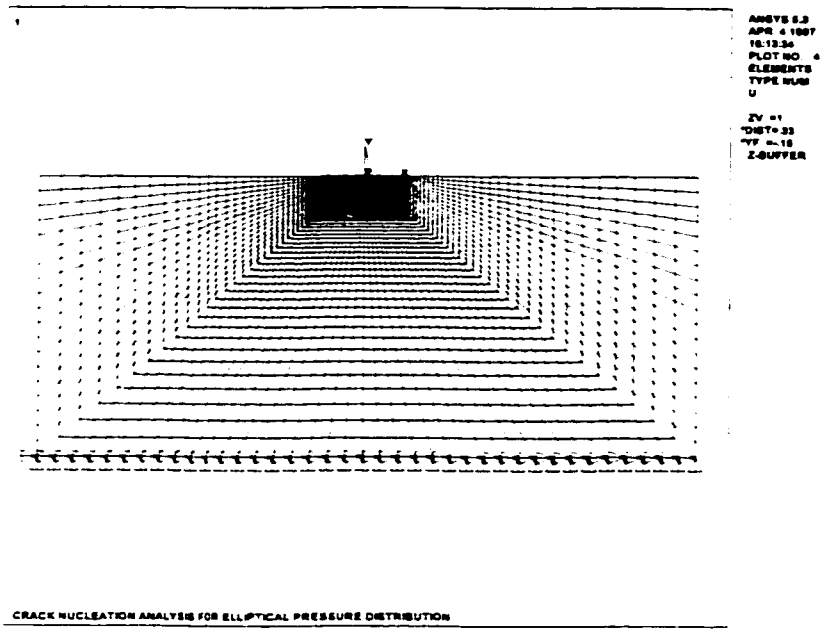

a)

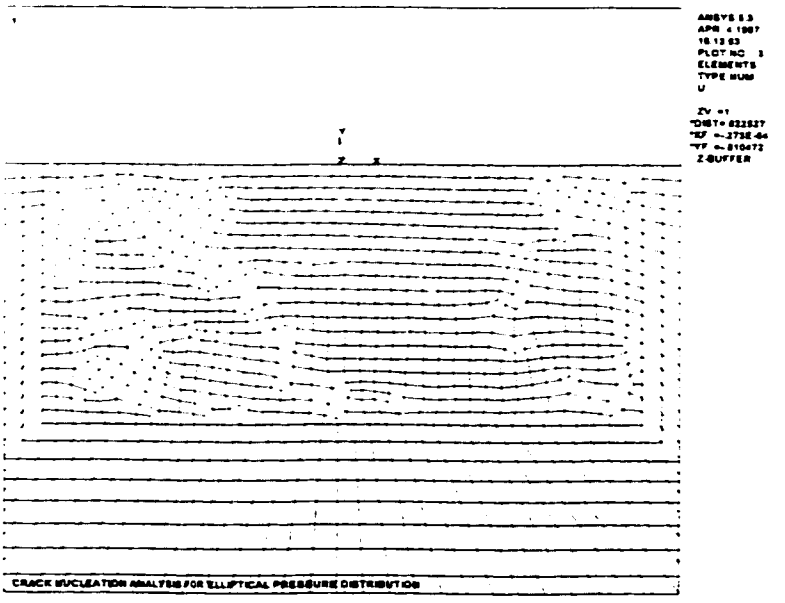

b)

Figure 5.5 Finite element mesh a) with boundary conditions and b) magnified near the contact zone

from the finite element model to the analytical results given by Hamilton and Goodman[75], which was carried out for cylindrical contact conditions subjected to sliding with a coefficient of friction of 0.25. Comparisons of the ratio of maximum effective stress over Hertzian pressure ($\sqrt{J_o}/P_o$) value gave the location on the *xy* plane to be the same for both analytical as well as numerical (finite element) approach and the percentage error for the magnitude was 0.85% (0.352 for the analytical result and 0.356 for the numerical result). Further the extent of plastically deformed zone was verified for this type of loading, by comparing the normalized contour plot (square root of the second stress invariant over the maximum Hertzian pressure) values and the limiting value for plastic deformation as given by Merwin and Johnson and a good agreement (< 10% discrepancy) was obtained between the finite element analysis and the estimated value. It should be noted that the extent of plastic deformation is estimated in the case of the published paper, by assuming that the contour of the second stress invariant (calculated for purely elastic stress) is valid after the fact that plastic loading has commenced in the material.

The other verification of the finite element program developed was carried out by using the results published by Jahanmir [11]. The analysis of the interfacial stress value was conducted for a problem having a maximum Hertzian value of $4k$ and a friction coefficient of 0.25 loaded repetitively until shakedown is reached. The finite element program was run such that the loading was moved from left to right for 20 μm in steps of 1 μm. This was repeated 9 times, simulating the motion of a sliding object loaded cyclically. This repetitive loading is done to compare the values given by Jahanmir, with the assumption that the plots given are for the maximum depth value (obtained for $4k$ and 0.25 friction coefficient) given in their

report. The contour obtained was comparable to the one published by Jahanmir and Suh [64] having a maximum interfacial stress value of 2.13k as opposed to nearly 2.2 in their report. There was a slight variation in the contour, which may be attributed to the difference in boundary conditions at the surface.

The equation followed in obtaining the critical normal interfacial stress is given by the following relationship:

$$\sigma_{rr} = \sqrt{3}\tau_{maxp} + \sqrt{3}\tau_{max} + \sigma_h \qquad \textbf{(5.6)}$$

The finite element model analysis results were post processed for the above equation after the solution was obtained using five sub-steps for the given load. The contour plot determined gives a good qualitative analysis with regards to probable positions of crack nucleation zone, from inclusions. It should be noted that a similar approach can be expanded, for the study of crack nucleation in a homogenous medium, as well.

5.4.3 Results and Discussion of the Finite Element Analysis

The plastic strain is the cause of the residual stress which in turn affects the formation of cracks. In order to observe the **extent of the plastically deformed zone** at the contact zone Figures 5.6-5.8 are plotted giving the variation of the principal shear strain in this zone for a maximum Hertzian pressure contact P_0 of 4k, 5k and 6k respectively. It can be seen from Figure 5.6 that the entire plastic deformation is under the surface for a Hertzian contact pressure of 4k. This zone grows in area and comes up to the surface for the Hertzian contact pressures of 5k and 6k. This result implies that the residual stress associated with the plastic

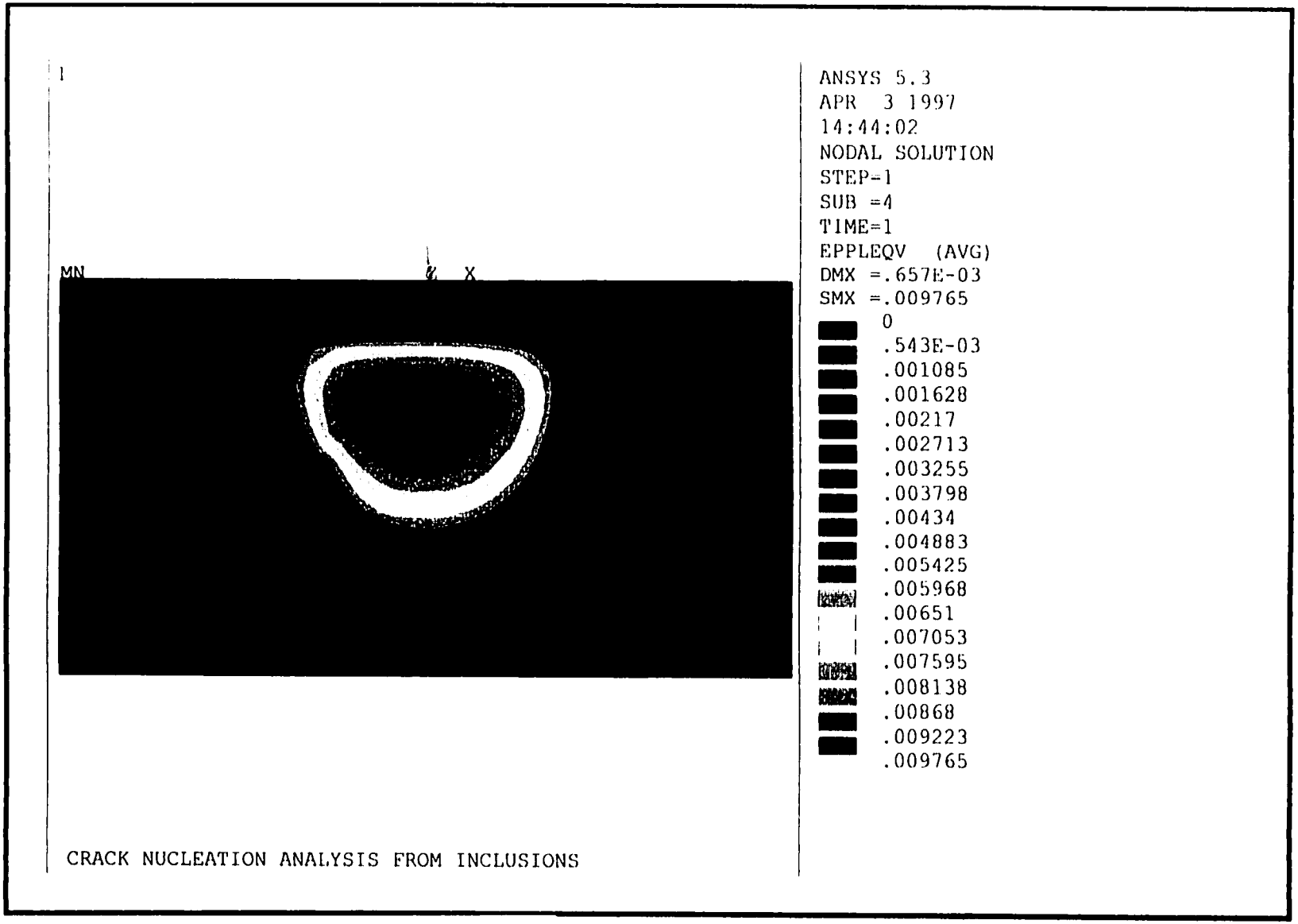

Figure 5.6 Plastic strain plot for 4k contact pressure

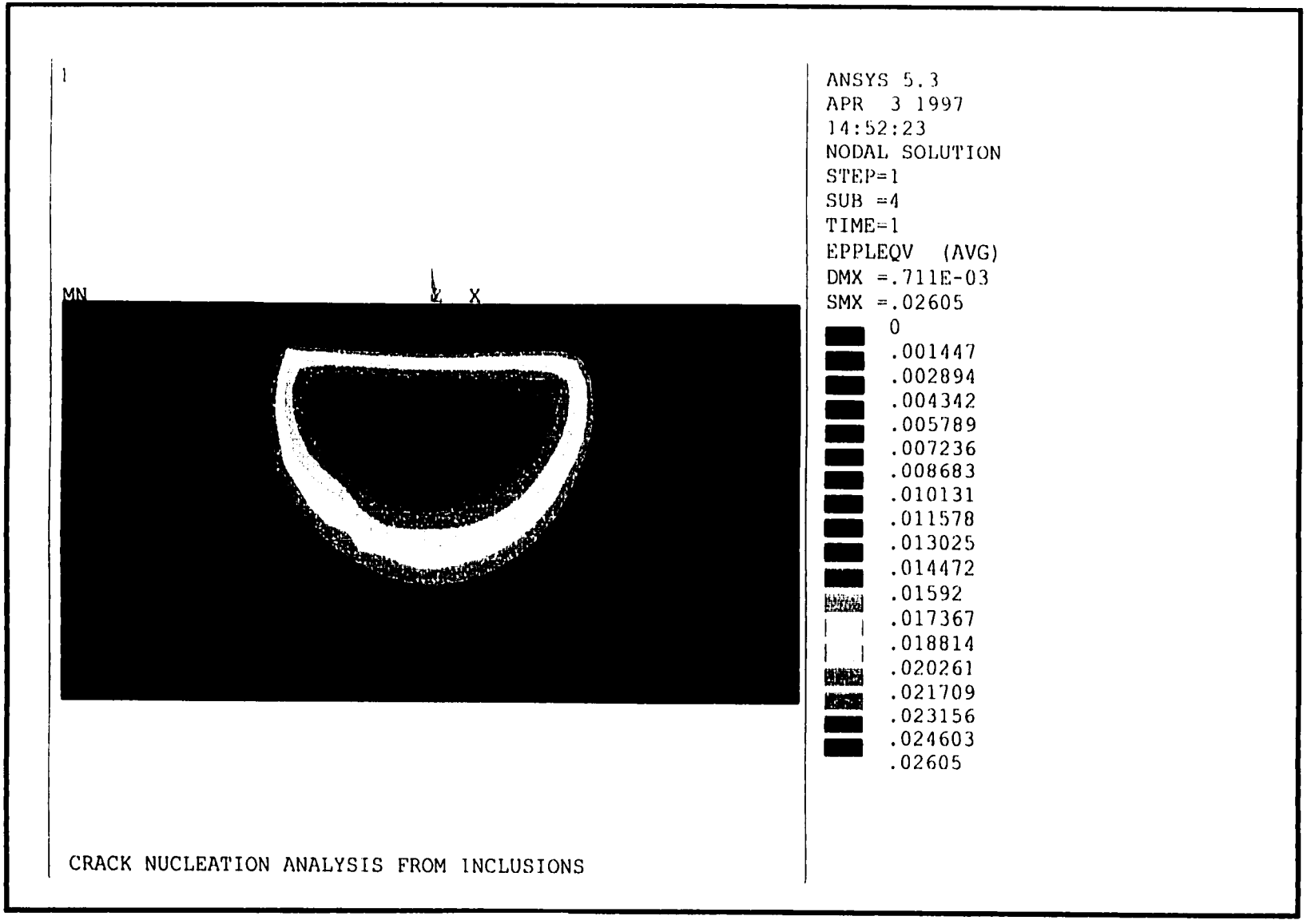

Figure 5.7 Plastic strain plot for 5k contact pressure

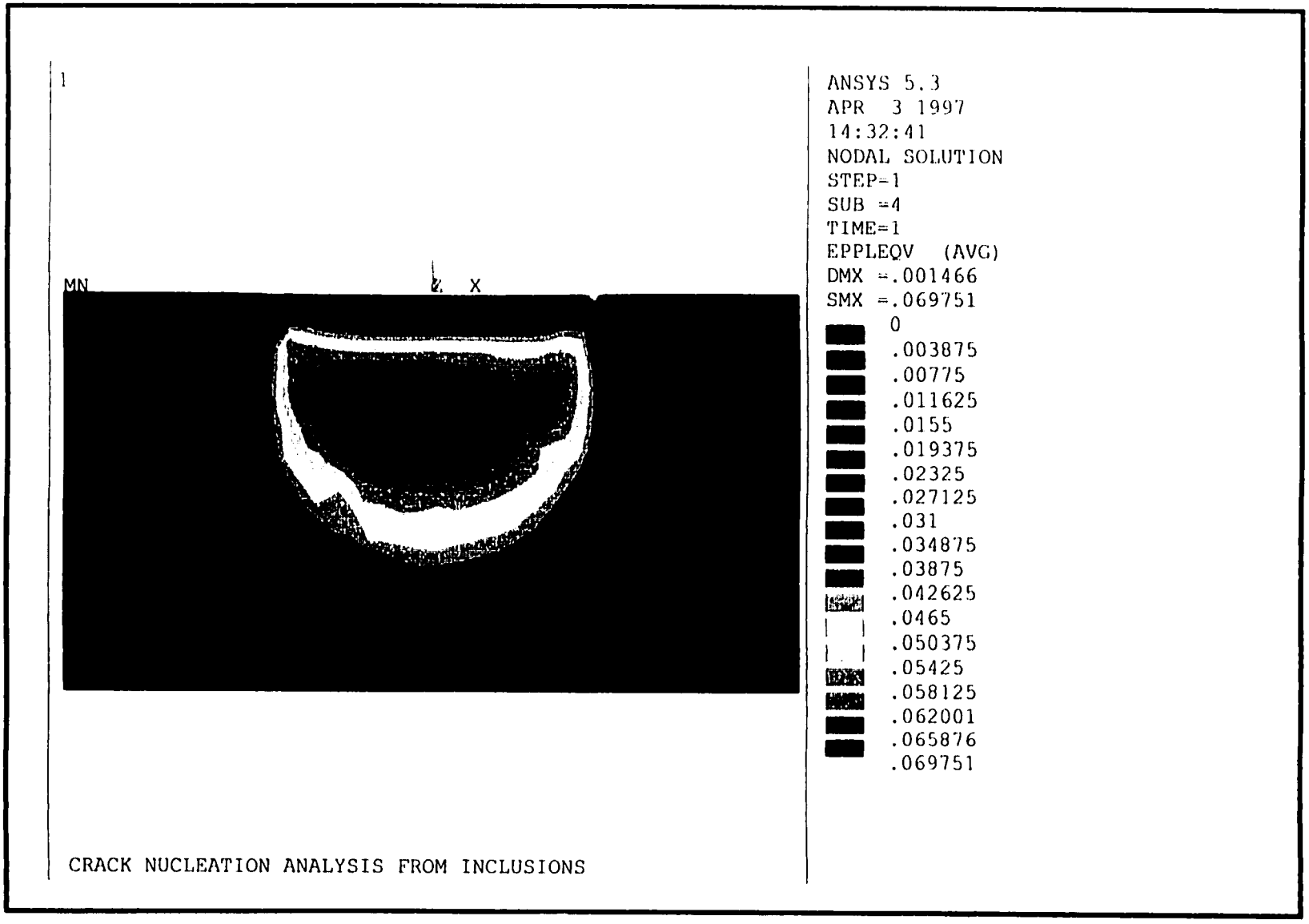

Figure 5.8 Plastic strain plot for 6k contact pressure

deformation is higher in the case of $5k$ and $6k$, and is the cause of the critical interfacial stress approaching the surface. The comparison of the plastically deformed zone was carried out using a similar approach as indicated in the previous section and it was done using the reference given by Merwin and Johnson [23]. It should be noted that the extent of plastic deformation is in good agreement with that estimated from Merwin and Johnson.

Comparison of this work with Jahanmir and Suh's [64] results gave a slight difference in the extent. It is assumed that this might have happened because of the boundary condition considered in their case. They had included constraints on the surface beside the loading zone which might have increased the rigidity of the material subjected to the loading condition.

The analysis was carried out for normal as well as oblique impact, using a quasi-static approach, where the possibility of cumulative plastic deformation after the first loading does not exist. The simulation carried out on the finite element model indicated that there was no appreciable difference in the plastic deformation observed, for a cyclical loaded member, after the first loading. This is mainly because of the elastic bulk material surrounding the deformed zone. Therefore, if there is a chance of the interfacial normal stress value reaching the critical limit (crack initiation from cylindrical inclusions), it will happen during the second cycle of the loading history.

The contour graphs displayed in Figures 5.9 to 5.22, for the various loading conditions, show the immediate contact zone, which has a dimension of $4a$ by $2a$. The data tabulated in Table 5.1 is represented by a colour coded contour of the interfacial stress value. These plots are

given in this chapter to indicate the fact that under the type of loading involved, the subsurface crack nucleation is a major factor causing the wear associated with the contact conditions.

Table 5.1 Parametric study of crack nucleation from inclusions

Test case No.	Coefficient of friction	Maximum Hertzian pressure (P_0)	First hardening modulus	Second hardening modulus	Maximum σ_n/k value	Range of crack initiation zone	Figure No.
1	0.0	4.0*k*	0.0E	0.0E	1.04	2*a*	5.9
2	0.0	4.0*k*	0.1E	0.0E	0.90	--	5.10
3	0.0	4.0*k*	0.1E	0.01E	0.90	--	5.10
4	0.0	4.0*k*	0.1E	0.02E	0.90	--	5.10
5	0.0	4.0*k*	0.2E	0.01E	0.83	--	5.11
6	0.0	4.0*k*	0.2E	0.02E	0.83	--	5.11
7	0.1	4.0*k*	0.1E	0.01E	0.92	--	5.12
8	0.2	4.0*k*	0.1E	0.01E	1.31	0.0 - 0.1*a* 1.4 - 1.9*a*	5.13
9	0.3	4.0*k*	0.1E	0.01E	2.34	0.0 - 1.6*a*	5.14
10	0.0	5.0*k*	0.1E	0.0E	1.37	0.5 - 2.8*a*	5.15
11	0.0	5.0*k*	0.1E	0.01E	1.37	0.5 - 2.8*a*	5.15
12*	0.0	5.0*k*	0.1E	0.01E	1.37	0.5 - 2.8*a*	5.15
13	0.0	5.0*k*	0.2E	0.02E	1.16	0.9 - 2.4*a*	5.16
14	0.1	5.0*k*	0.1E	0.01E	1.80	0.0 - 2.7*a*	5.17
15	0.2	5.0*k*	0.1E	0.01E	2.97	0.0 - 2.9*a*	5.18
16	0.0	6.0*k*	0.1E	0.0E	2.66	0.0 - 4.0*a*	5.19
17	0.0	6.0*k*	0.1E	0.01E	2.65	0.0 - 4.0*a*	5.20
18	0.0	6.0*k*	0.2E	0.02E	2.52	0.0 - 3.6*a*	5.21
19	0.1	6.0*k*	0.1E	0.01E	3.21	0.0 - 4.0*a*	5.22

* The half Hertzian contact width is 5 μm only for this case and 10 μm for all the rest

The parametric study included varying the friction coefficient (μ) (0.1,0.2 and 0.3),

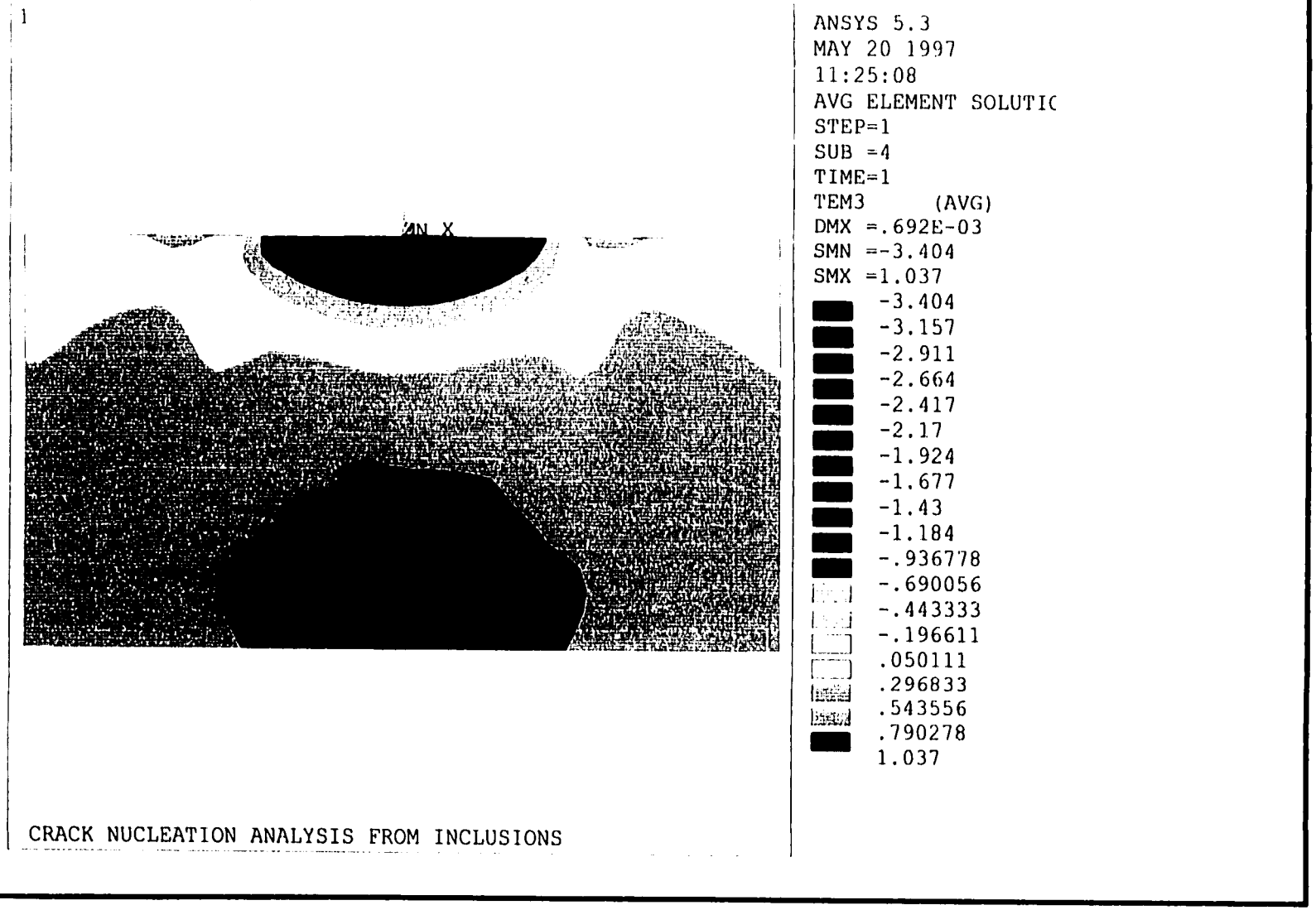

Figure 5.9 Contour plot of interfacial stress around an inclusion ((a = 10μm, μ=0.0, $P_0 = 4k$, $c_1 = 0.0$, $c_2 = 0.0$)

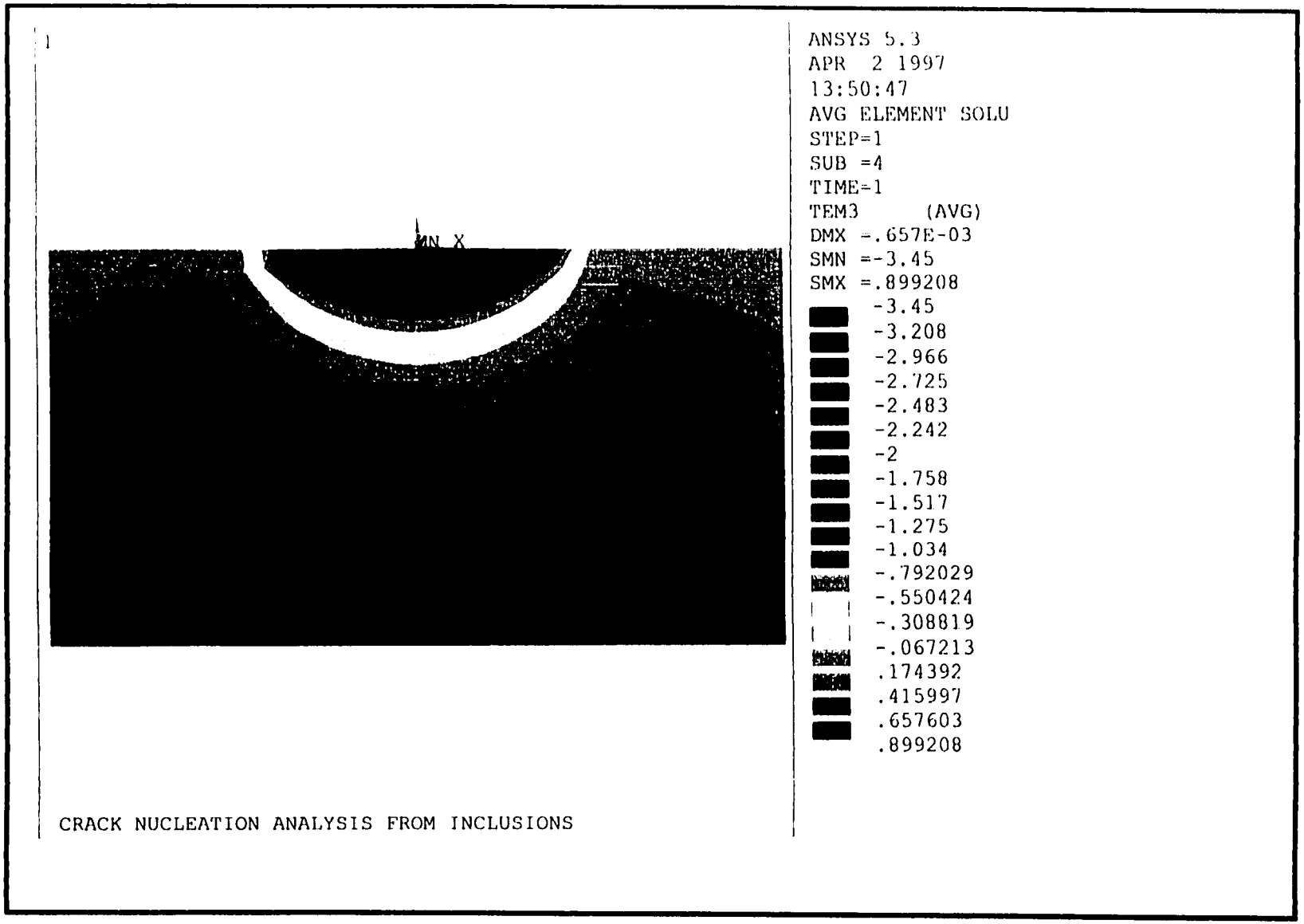

Figure 5.10 Contour plot of interfacial stress around an inclusion ((a = 10μm, μ=0.0, $P_0 = 4k$, $c_1 = 0.1$, $c_2 = 0.0$, 0.01 and 0.02)

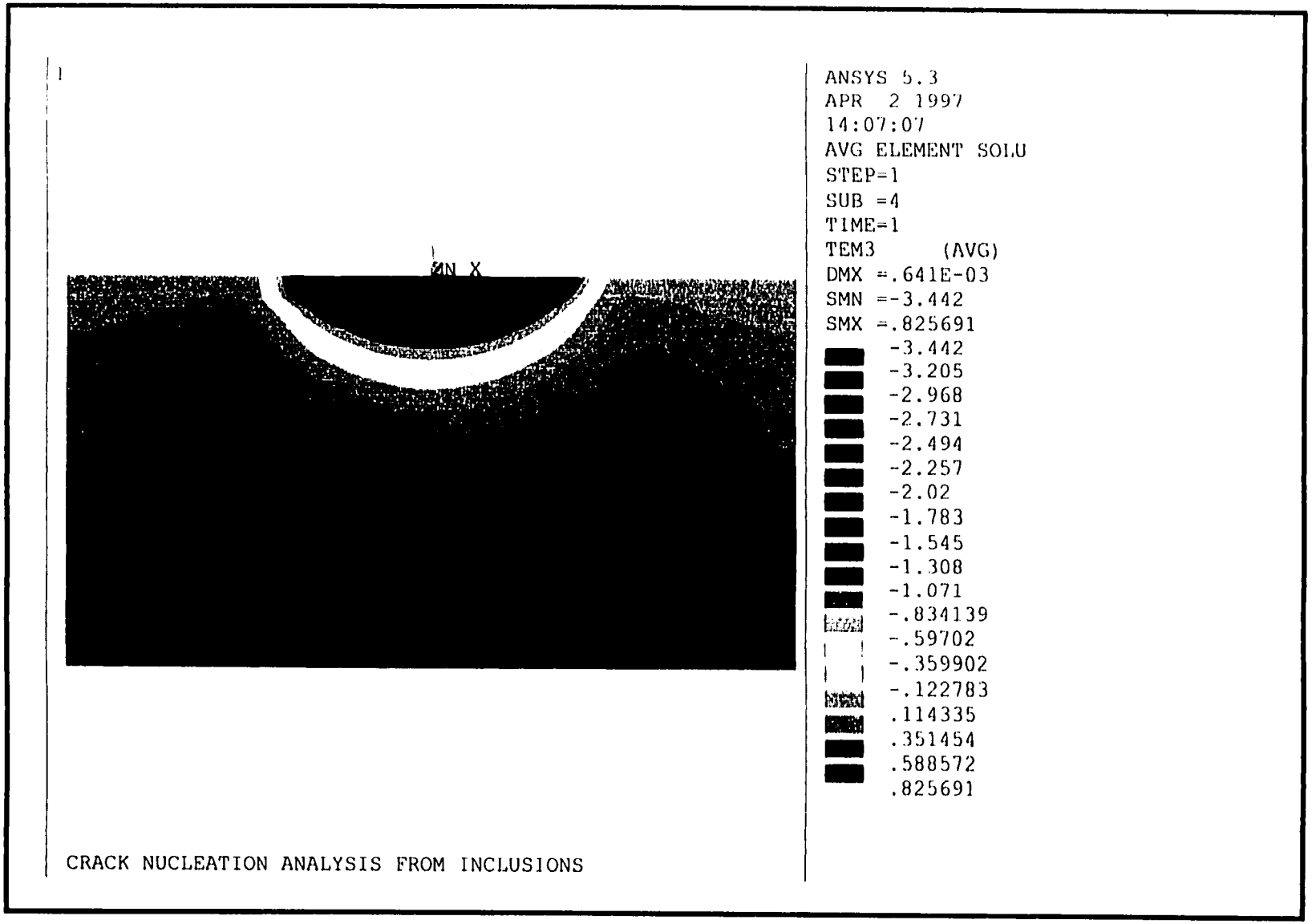

Figure 5.11 Contour plot of interfacial stress around an inclusion ((a = 10μm, μ=0.0, $P_0 = 4k$, $c_1 = 0.2$, $c_2 = 0.01$ and 0.02)

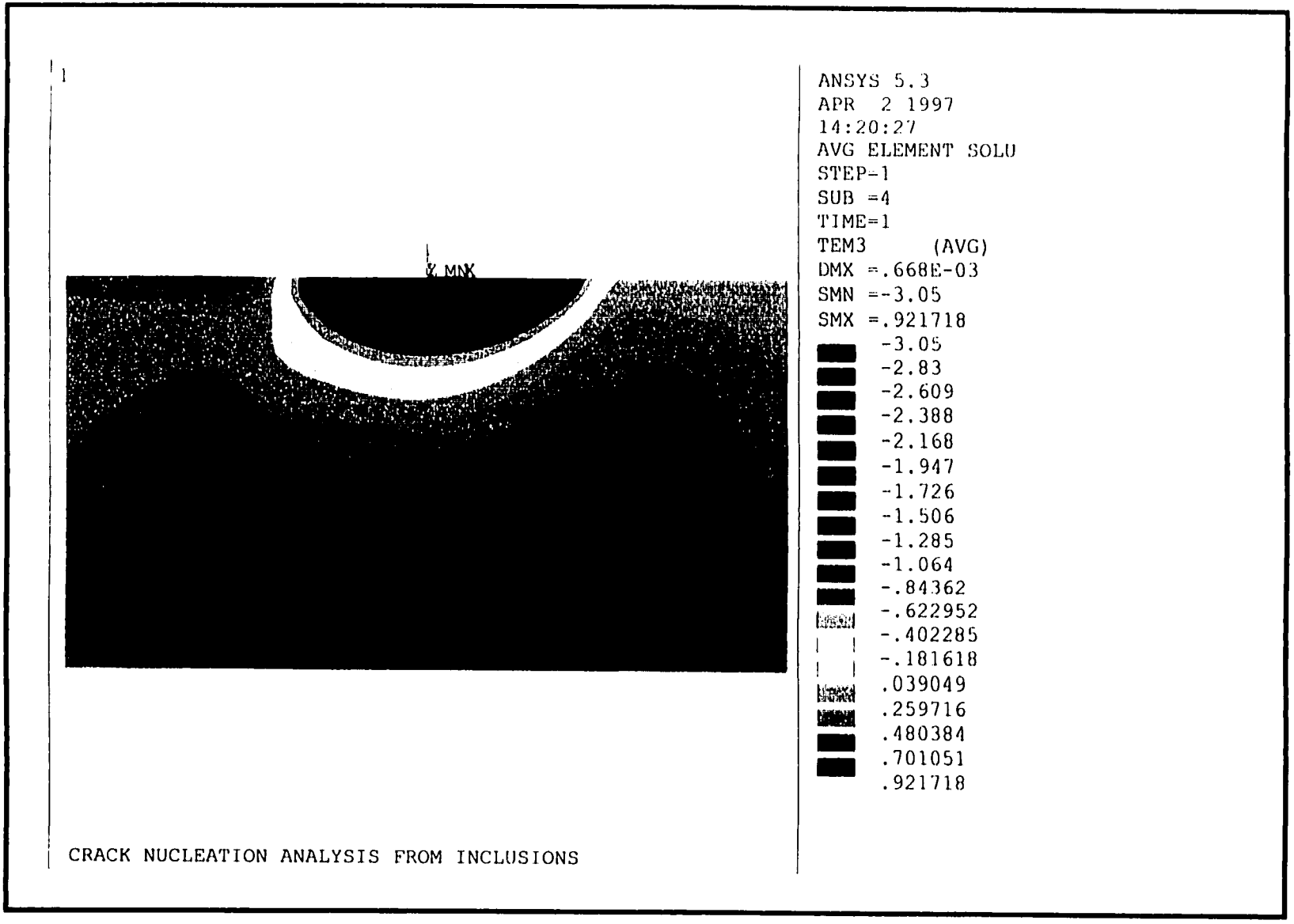

Figure 5.12 Contour plot of interfacial stress around an inclusion ((a = 10μm, μ=0.1, $P_0 = 4k$, $c_1 = 0.1$, $c_2 = 0.01$)

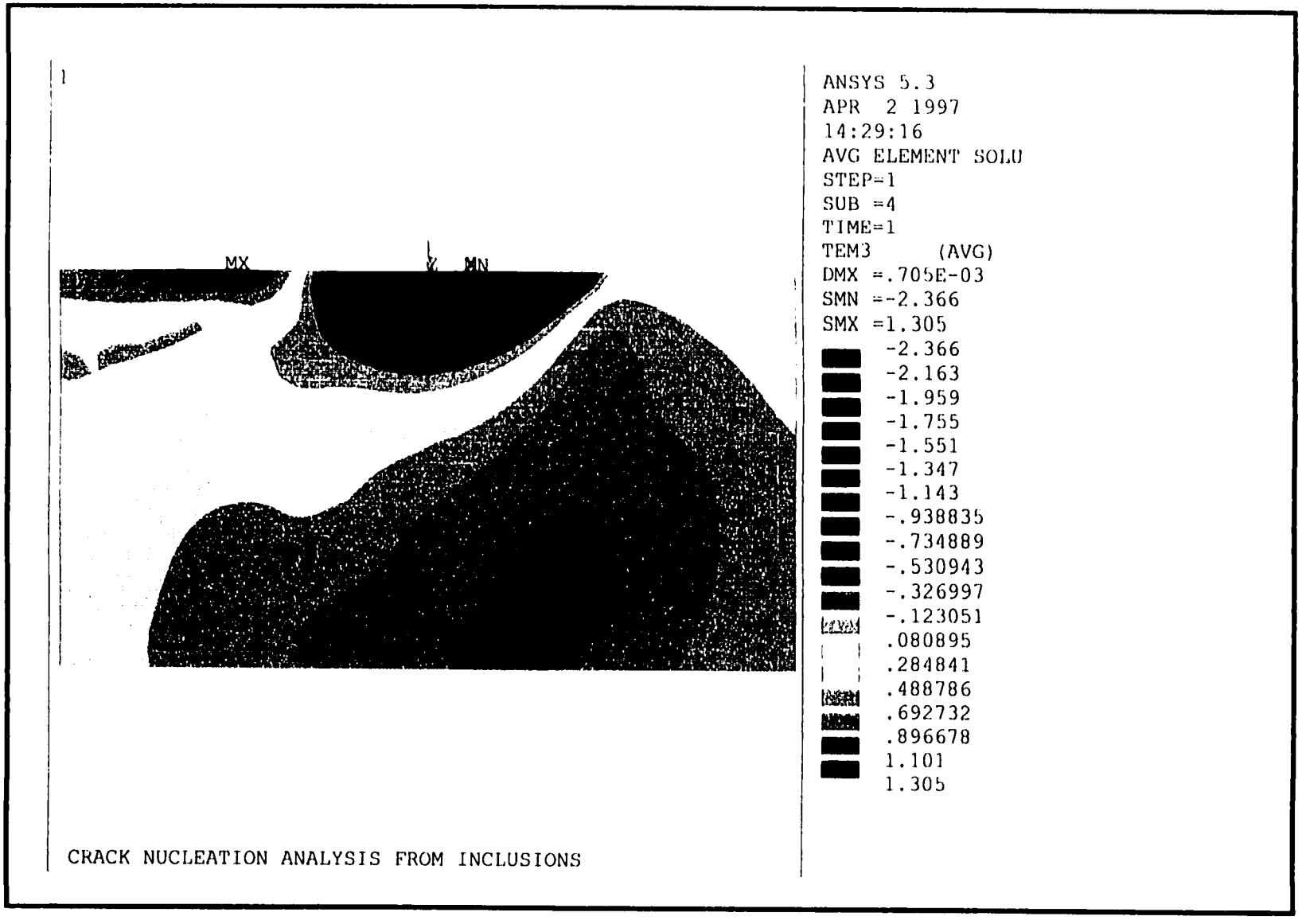

Figure 5.13 Contour plot of interfacial stress around an inclusion ((a = 10μm, μ=0.2, $P_0 = 4k$, $c_1 = 0.1$, $c_2 = 0.01$)

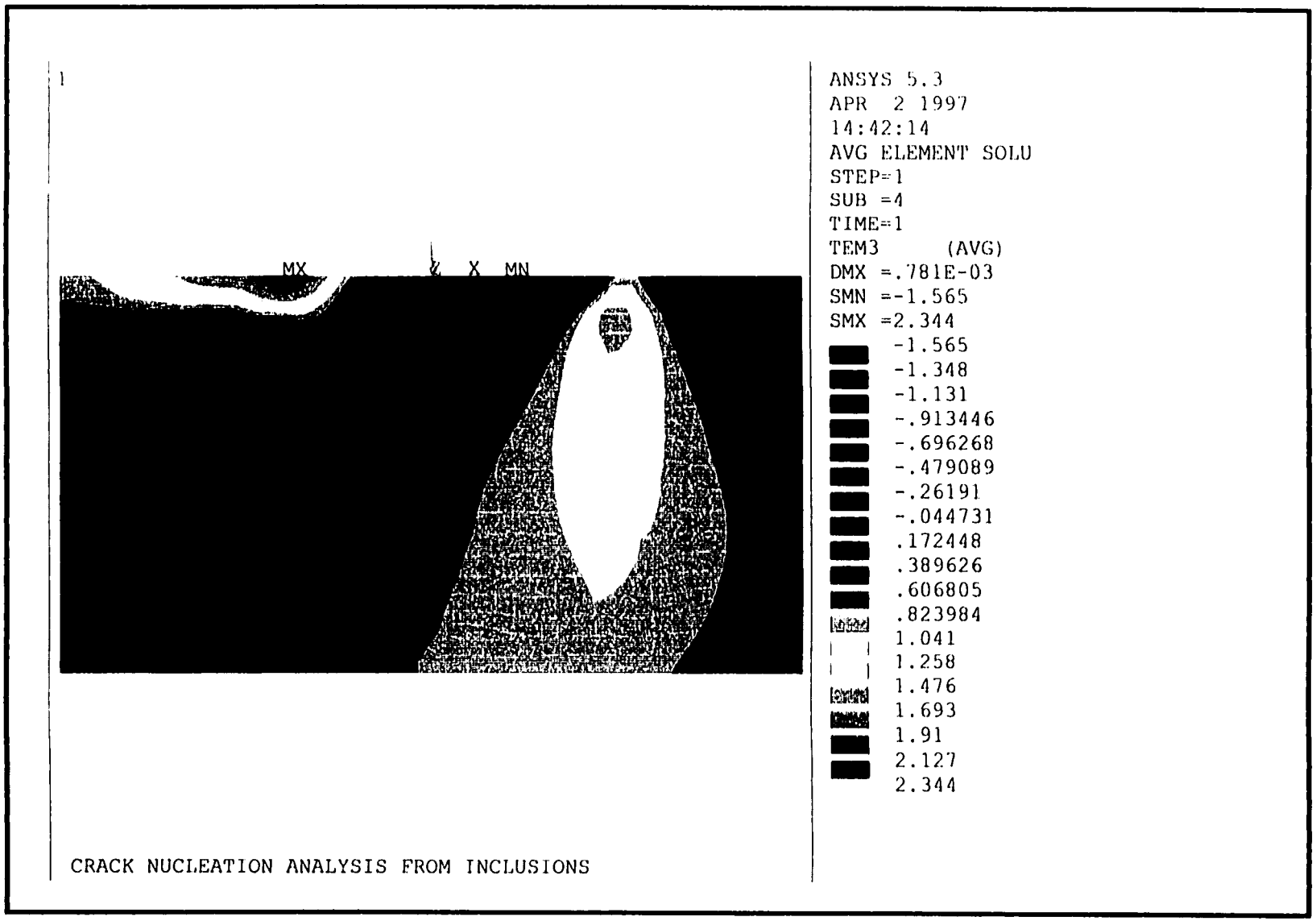

Figure 5.14 Contour plot of interfacial stress around an inclusion (a = 10μm, μ=0.3, $P_0 = 4k$, $c_1 = 0.1$, $c_2 = 0.01$)

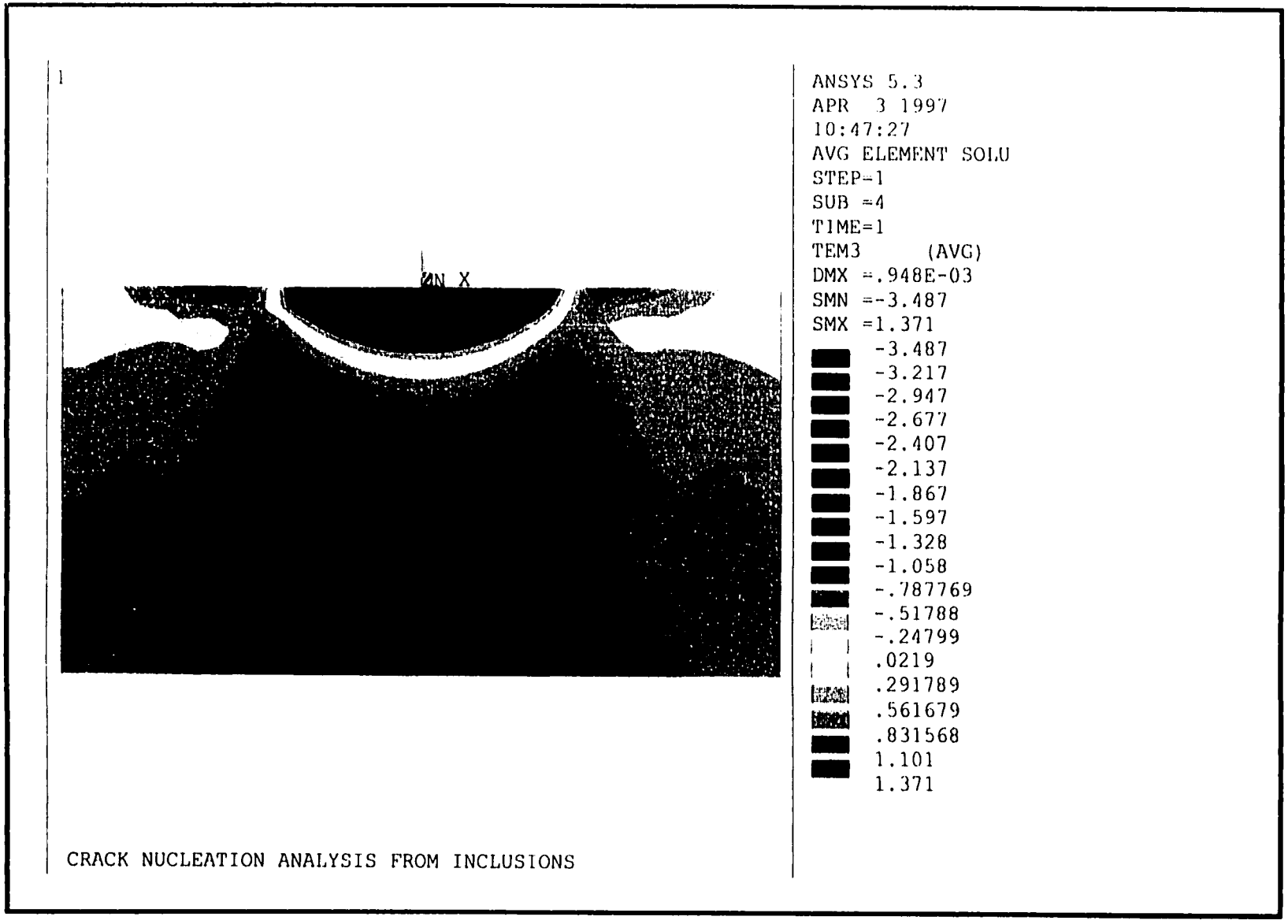

Figure 5.15 Contour plot of interfacial stress around an inclusion (a = 5 and 10 μm, μ=0.0, $P_0 = 5k$, $c_1 = 0.1$, $c_2 = 0.0$ and 0.01)

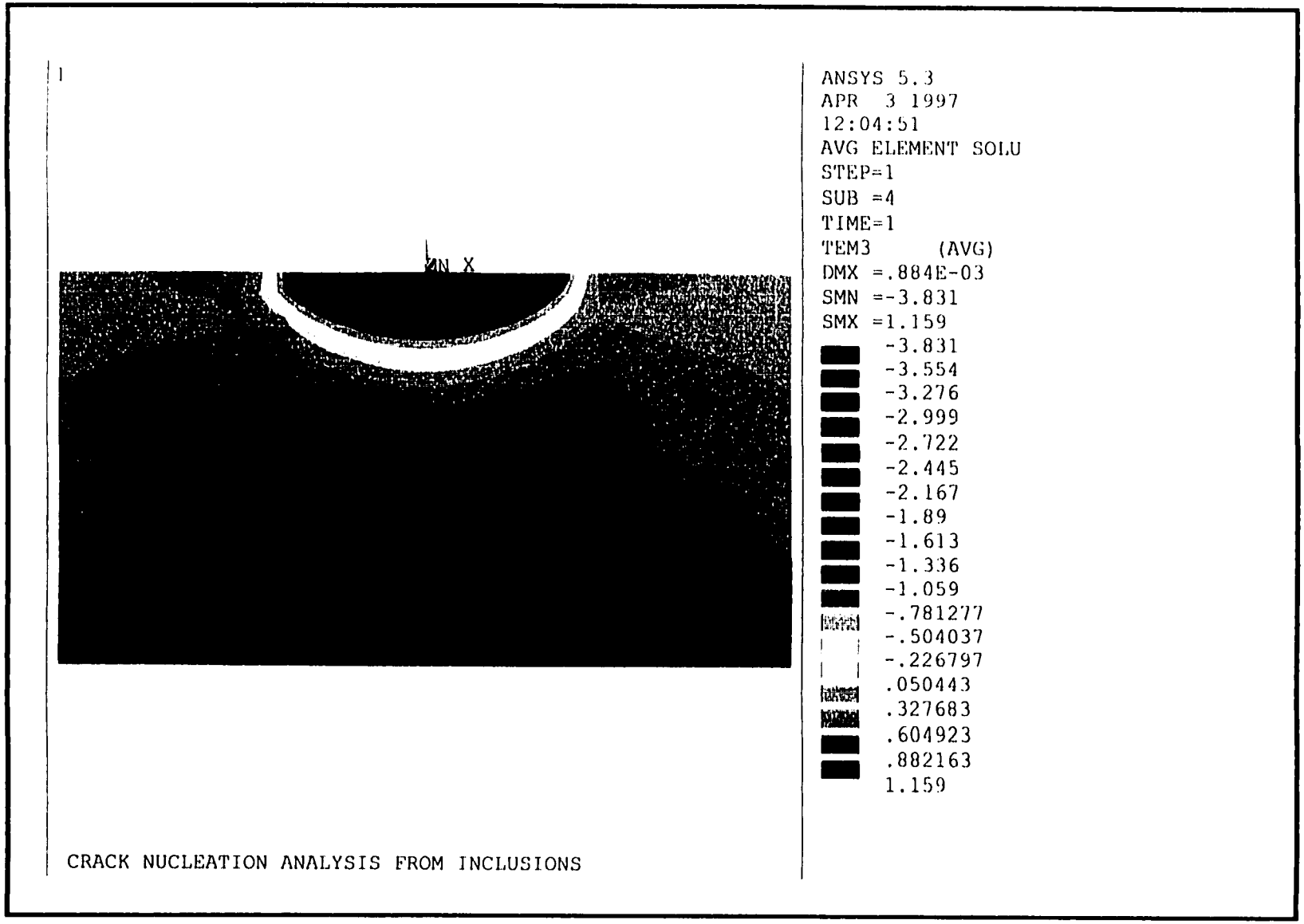

Figure 5.16 Contour plot of interfacial stress around an inclusion (a = 10μm, μ=0.0, $P_0 = 5k$, $c_1 = 0.2$, $c_2 = 0.02$)

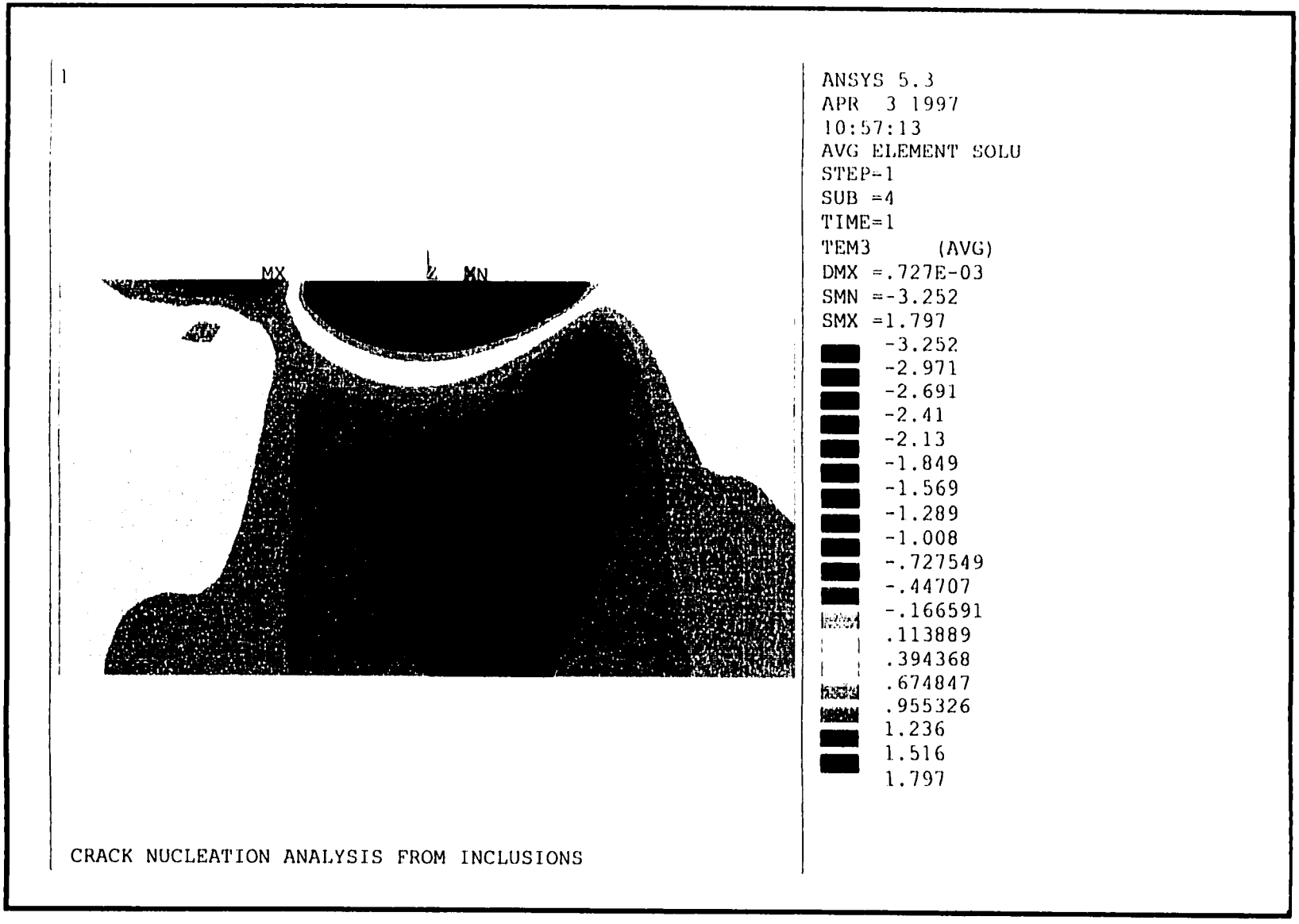

Figure 5.17 Contour plot of interfacial stress around an inclusion (a = 10μm, μ=0.1, $P_0 = 5k$, $c_1 = 0.1$, $c_2 = 0.01$)

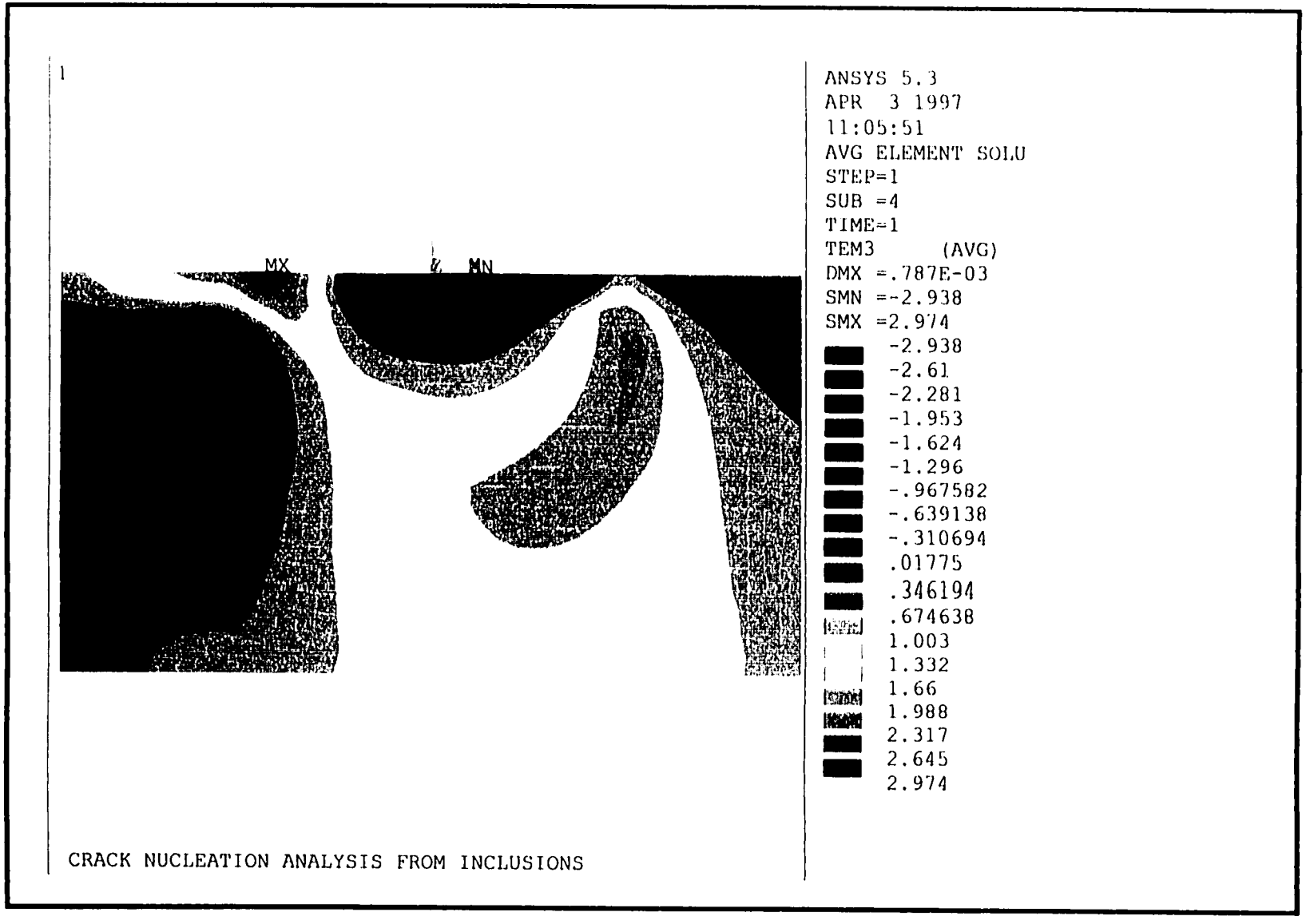

Figure 5.18 Contour plot of interfacial stress around an inclusion (a = 10μm, μ=0.2, $P_0 = 5k$, $c_1 = 0.1$, $c_2 = 0.01$)

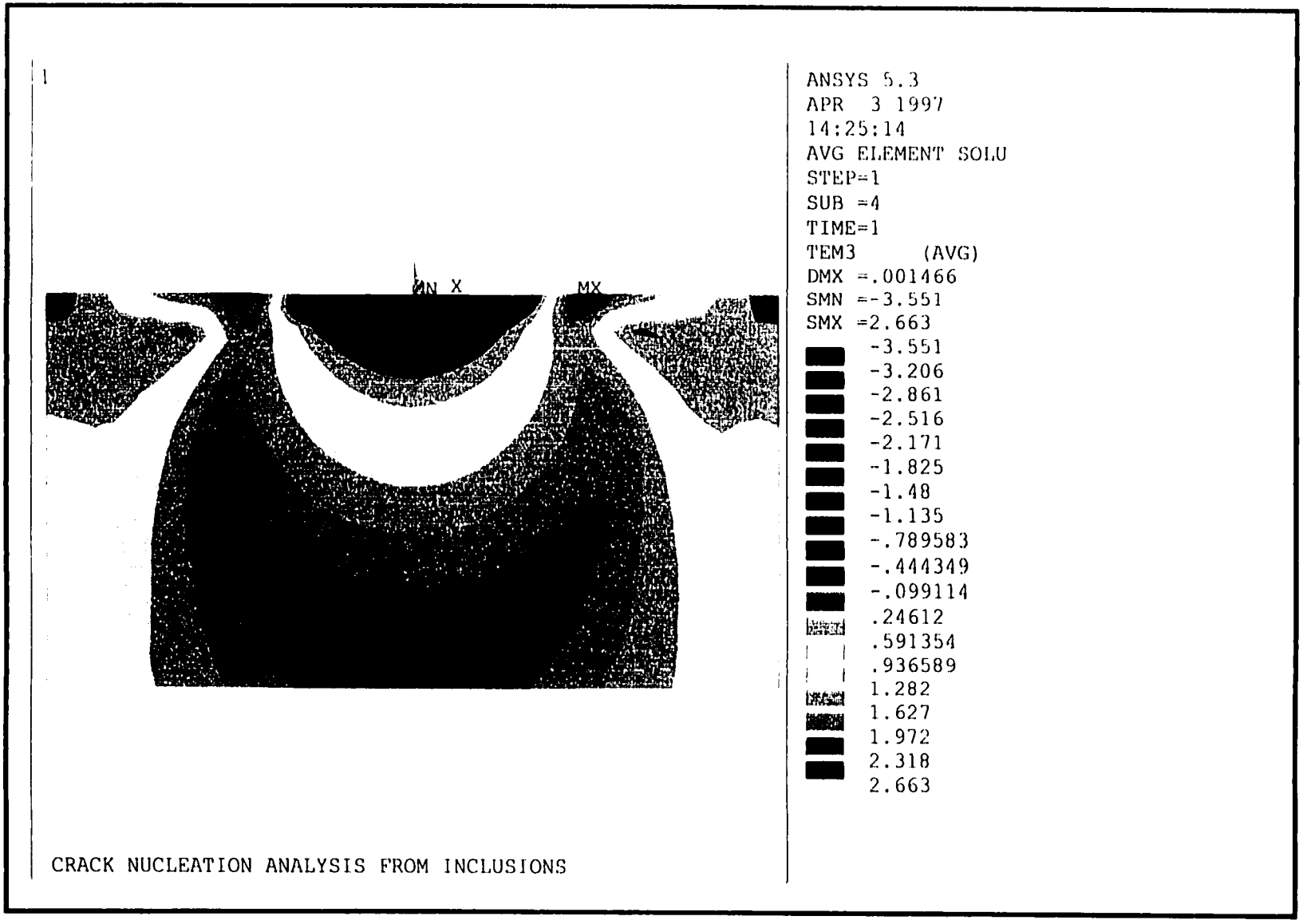

Figure 5.19 Contour plot of interfacial stress around an inclusion (a = 10μm, μ=0.0, $P_0 = 6k$, $c_1 = 0.1$, $c_2 = 0.0$)

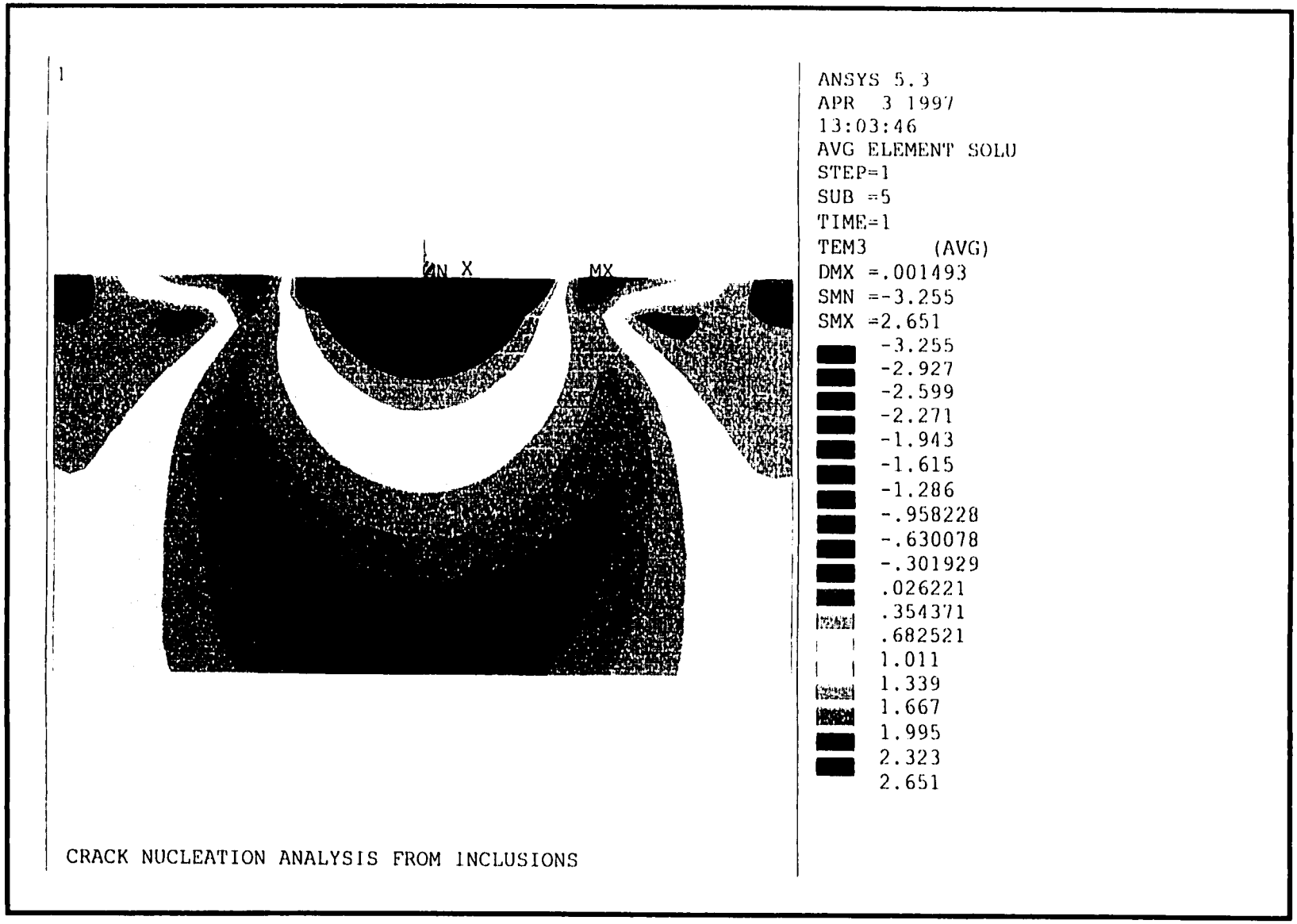

Figure 5.20 Contour plot of interfacial stress around an inclusion (a = 10μm, μ=0.0, $P_0 = 6k$, $c_1 = 0.1$, $c_2 = 0.01$)

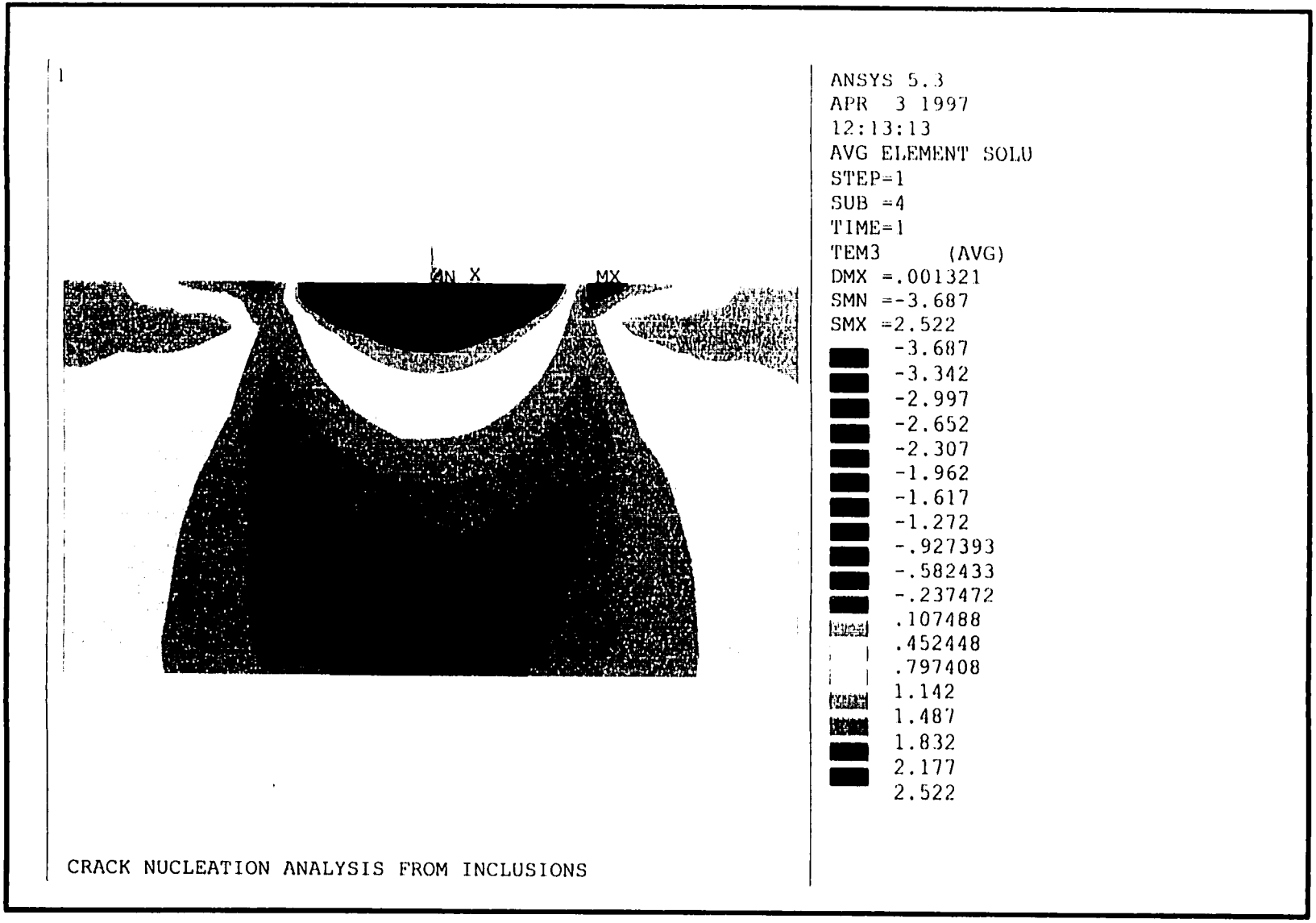

Figure 5.21 Contour plot of interfacial stress around an inclusion (a = 10μm, μ=0.0, $P_0 = 6k$, $c_1 = 0.1$, $c_2 = 0.01$)

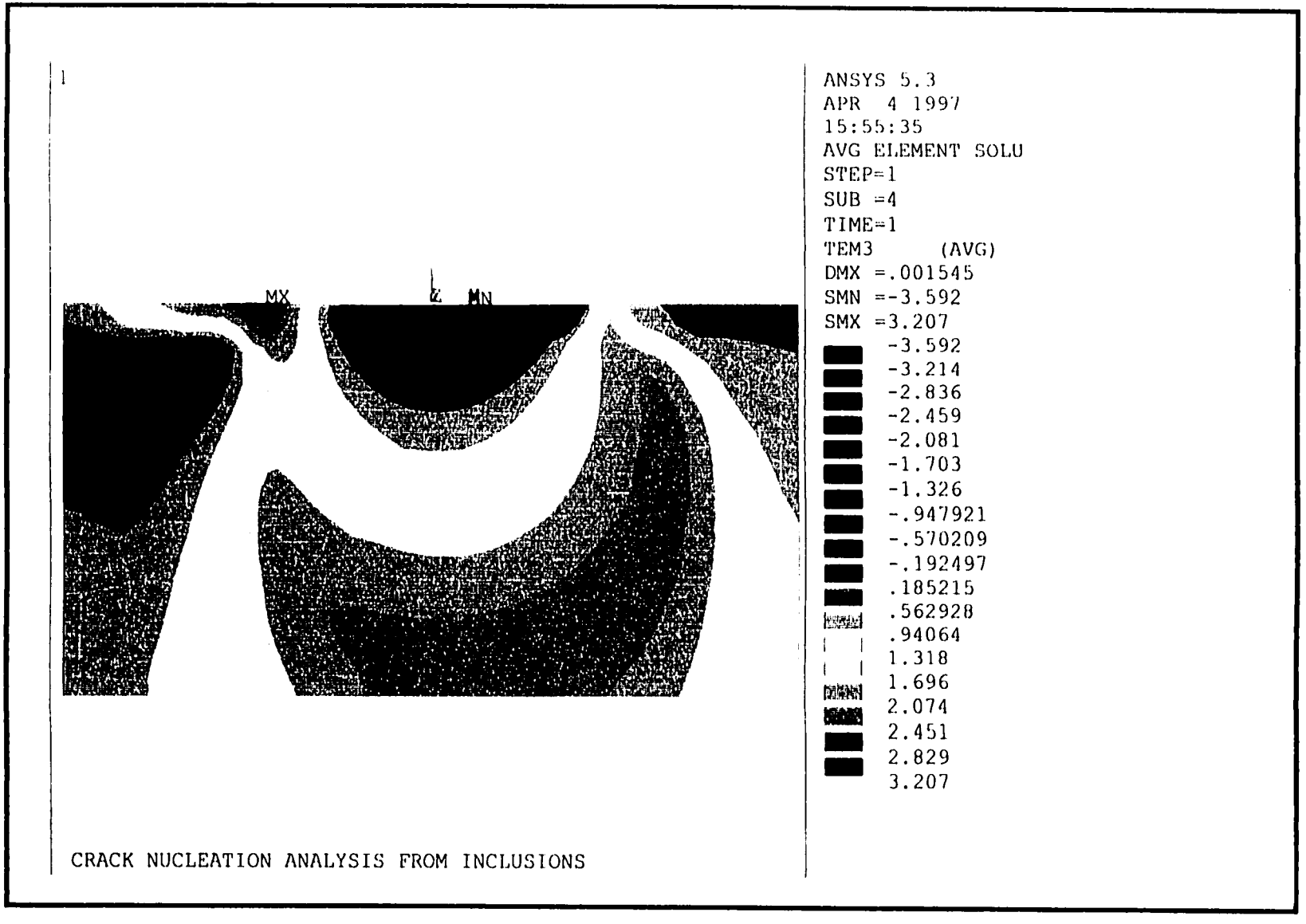

Figure 5.22 Contour plot of interfacial stress around an inclusion (a = 10μm, μ=0.0, $P_0 = 6k$, $c_1 = 0.2$, $c_2 = 0.02$)

maximum Hertzian pressure (P_0) ($4k$, $5k$ and $6k$) and the first (c_1) (0.1 and 0.2) and the second (c_2) (0.01 and 0.02) hardening moduli. The common denominator in all these cases is that an elliptical (Hertzian) pressure distribution was applied in plane strain condition.

It can be observed from Table 5.1 that the value of the **hardening moduli** c_1 and c_2 do not affect the outcome of the result significantly. The value of the critical interfacial stress, for the applied maximum Hertzian pressure of $4k$, varied from 0.8 to 1.0 depending upon the different values of the first hardening modulus (Figures 5.9 to 5.11). The position where the maximum value occurred is nearly $2a$ from the surface for all the cases, implying that at this values the formation of crack is marginal and that it is at a higher depth into the surface. It should be noted that for values of the maximum Hertzian contact below $4k$ crack nucleation from inclusions does not occur and that the mechanism of wear will be other than delamination wear.

One of the parametric study conducted was to observe the effect of **friction coefficient** on the distribution and value of the subsurface interfacial stress for crack nucleation. Unlike the study of Jahanmir and Suh [22], the analysis was limited to low friction coefficient values because of the gross plastic deformation occurring due to the lack of the surrounding elastic bulk material at the surface. This implies that for higher values of friction coefficient at the asperity level, abrasive or adhesive wear mechanism will be prevalent instead of delamination wear. This is due to the high level of stress occurring at the interaction zone, which will force the formation of the debris. The delamination process is not effective any longer, because the subsurface crack nucleation and propagation are not the wear controlling

mechanisms.

The critical value of the interfacial stress (σ_n/k) was observed for a coefficient of friction varying form 0.1 to 0.3, for $P_0 = 4k$, and the ratio of the normal interfacial stress (σ_n) to yield strength in shear (k) was plotted in Figures. 5.12-5.14. As is evident, the friction coefficient has a significant effect on the formation of cracks even at lower values of maximum Hertzian contact pressure. It was observed that the maximum value of σ_n/k exceeded the critical value of 1, for a coefficient of friction of 0.3. It was also observed that the maximum critical value shifted to the surface, for coefficient of friction of 0.2 and stayed at the surface beyond this value. Even though, the maximum value has gone to the surface, it does not mean that there are no critical zones underneath. Implication of this result is that wear associated with oblique impact has relatively high stress values which aid in the tearing of the surface for the formation of wear.

The finite element analysis conducted for different **asperity contact radius** of 10 μm and 5 μm (Fig. 5.15) indicates that provided all conditions (load and material properties) are kept constant the maximum interfacial stress value remained the same for both cases except for the position where it occurred. It was proportionately scaled down with respect to a (half Hertzian contact width), indicating that it can be non-dimensionalised with respect to it.

It can be seen from the Figures 5.15 to 5.22 that crack nucleation for a maximum Hertzian contact pressure (P_0) of $5k$ and $6k$, crack nucleation readily occurs. This is mainly because the effect of the residual stress which overcomes the negating effect of the hydrostatic

pressure. The high σ_{rr} values observed at the surface for the case of $6k$ (Figure 5.19 to 5.22) are a result of the high plastic strain generated and the lack of hydrostatic loading in these areas. However, in real contacts the chances of this type of a situation occurring are slim as the contacting body itself will deform to apply hydrostatic pressure, increasing the contact area and reducing the effect of the plastic strain and applied stress near the surface. Implications of these are again the continued sustenance of the critical zone, at the subsurface level.

The final study in the crack nucleation analysis took into account different maximum Hertzian pressure value and the distribution of the crack nucleation zone varied accordingly. It was at a distance of $2a$ from the surface for $4k$ loading, all the way up to the surface for $6k$. The contour of the maximum interfacial stress followed a similar pattern where the maximum value is below the surface gradually approaching to it near the end of the loading zone in the case of higher values of the maximum Hertzian pressure ($6k$). The plot of this critical interfacial stress zone which covers a range below the surface is shown in Fig. 5.23 for different maximum Hertzian pressure values ($4k$, $5k$ and $6k$). This zone is different than the one provided by Jahanmir and Suh [22], possible explanation could be, as mentioned earlier, the difference in boundary conditions.

The contact flow pressure of the asperity, which in this case is characterized by an approximate value of $5k$ for the maximum Hertzian contact pressure, should at least be equal to $4k$ of the flat surface material in order to initiate a crack, according to the above criteria for interface stress value. Therefore, for delamination to be the effective mechanism of wear,

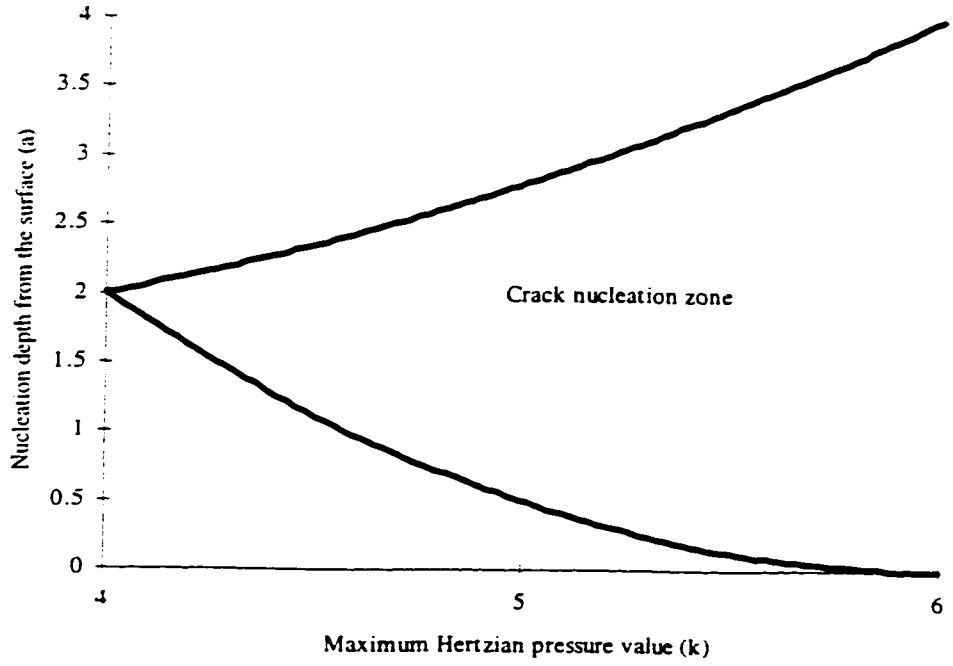

Figure 5.23) Crack nucleation zone for different maximum Hertzian contact pressure

the two metals in contact must have similar flow pressure or the wearing material must have lower flow pressure in contact.

5.5 Crack propagation Analysis

The crack nucleation analysis was done in the previous section to determine the possible locations of a crack and number of cyclic loading essential to initiate it. Similarly, it is essential to conduct a crack propagation analysis to determine the number of cyclic loading required to generate a wear debris and also to investigate the direction a crack, subjected to an elliptical pressure distribution at the contact interface, will follow. Therefore, a finite element model is generated to study the crack propagation direction and rate, in the next section.

5.5.1 Crack Propagation Direction Analysis of a Plastically Loaded Member

It is essential to study the contour of the effective stress around a crack front to establish the direction a propagating crack will follow. Also, the condition of this crack propagating towards the surface, instead of continuously propagating parallel to it, needs to be established. This goal is attained by carrying out a parametric study of a subsurface crack at the positions, where crack is estimated to occur and observing the trend of the effective stress distribution, for a progressively growing crack.

The finite element model developed for the analysis of crack propagation involved the use

of the quadrilateral eight node element (PLANE82), two node surface element (SURF19) and the 2-D contact element (CONTAC12). In the model, the use of a coarse and a fine mesh was implemented to ensure semi-infinite boundary conditions. This was attained by using extremely fine mesh near the crack zone and progressively increasing the mesh size further from this critical zone. The automatic mesh generating routine was used after identifying the line subdivisions (Fig. 5.24a-b). The analysis of stress distribution was carried out for a small crack existing in an elasto-plastic material which has a multi linear isotropic hardening property.

The contour plots given in Figures 5.25 to 5.34 show the effective stress around the crack front, which indicates the propagation trend for the above loading condition. The crack length for Figure 5.25 is $0.4a$ and grows progressively in steps of $0.2a$ for each figure, up to $2a$ for Figure 5.33. The last figure (5.34) shows the analysis carried out for a crack length of $3a$. Observation of the effective stress near the crack tip, can give a clear indication about the direction the crack propagation will follow.

Anderson [72] has shown that the effective stress is a maximum at either side of a growing crack subjected to mode I loading conditions. As per this argument the analysis carried out for the progressively growing crack indicates that the effective stress which was originally at either side of the crack gradually turns towards the crack front for a crack propagating straight, along the x-axis. The implication of this analysis is that the path a growing crack would follow, would have been towards the surface, after the crack has reached a width of $1.0\text{-}1.4a$ (Figure 5.28-5.30). There is a clear transition of the effective stress, which was

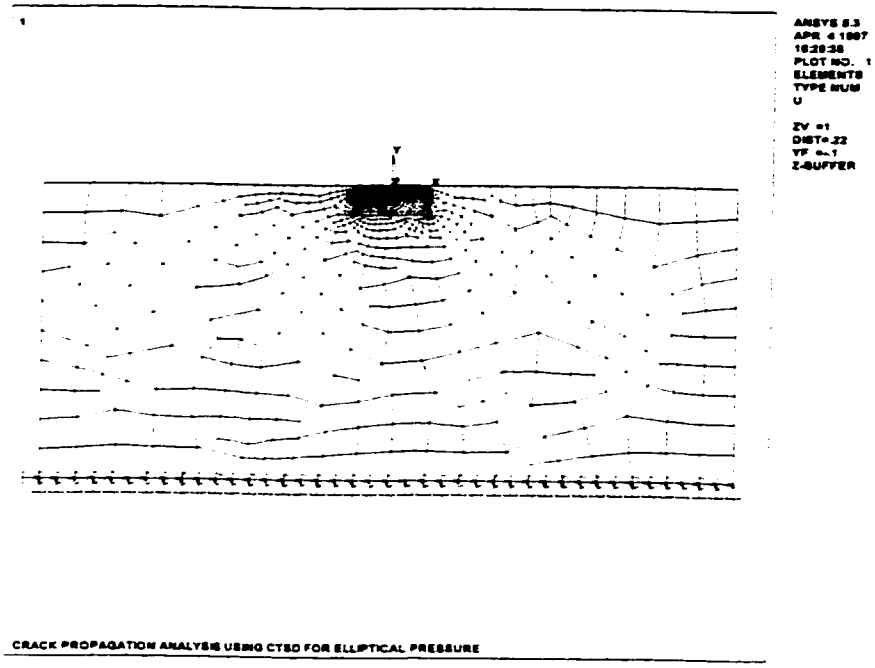

a)

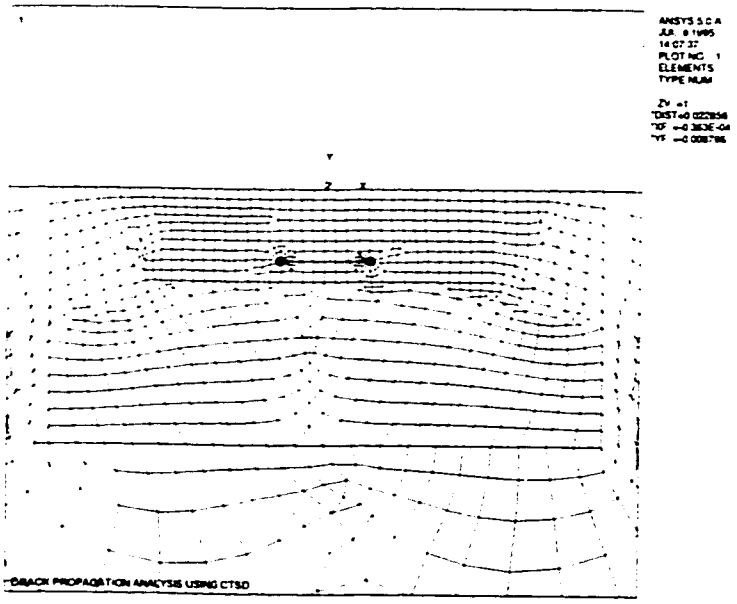

b)

Figure 5.24) Finite element mesh for crack propagation a) with boundary conditions b) magnified near the crack zone

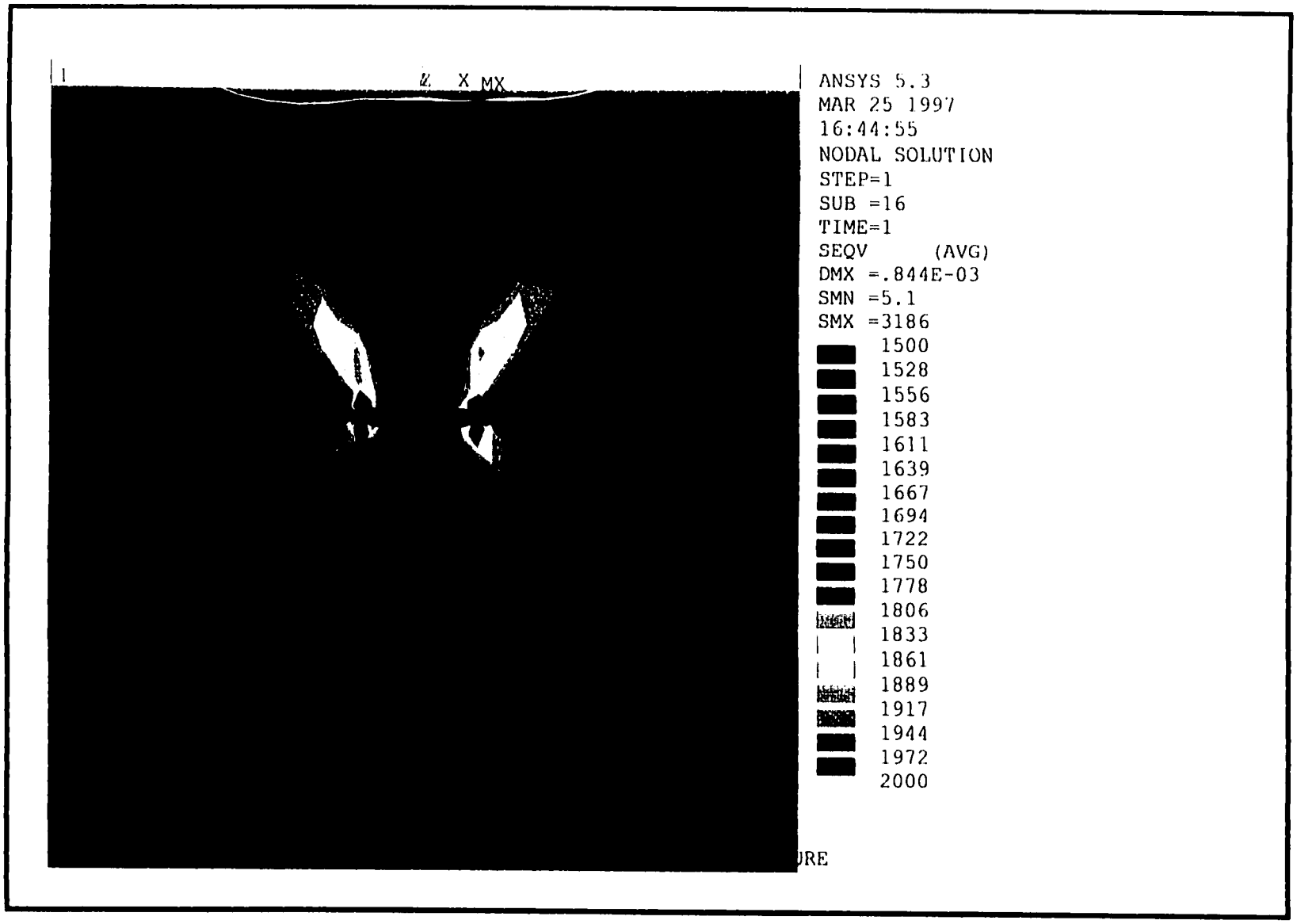

Figure 5.25 Contour plot of effective stress around a crack (crack length = 4μm)

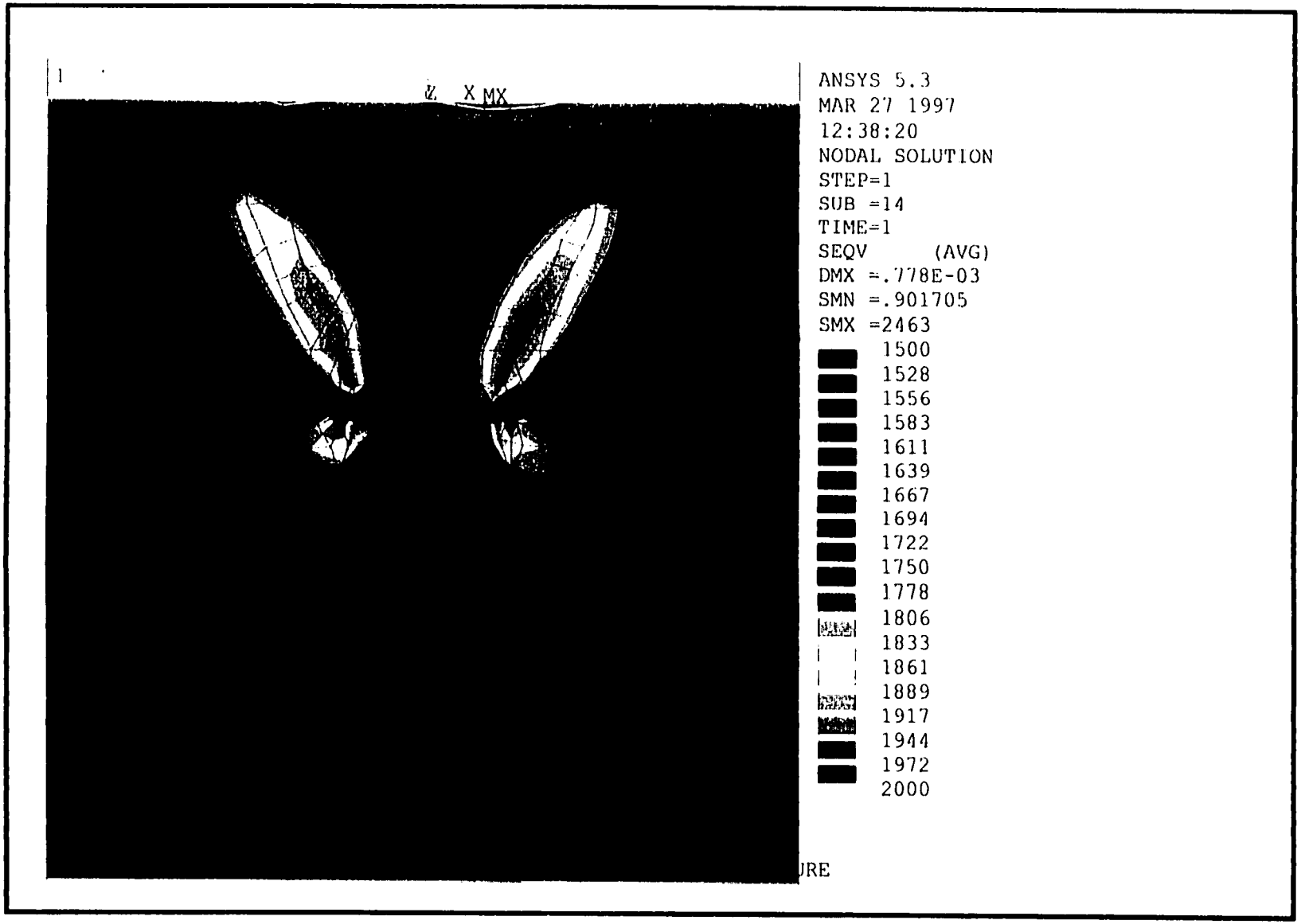

Figure 5.26 Contour plot of effective stress around a crack (crack length = 6μm)

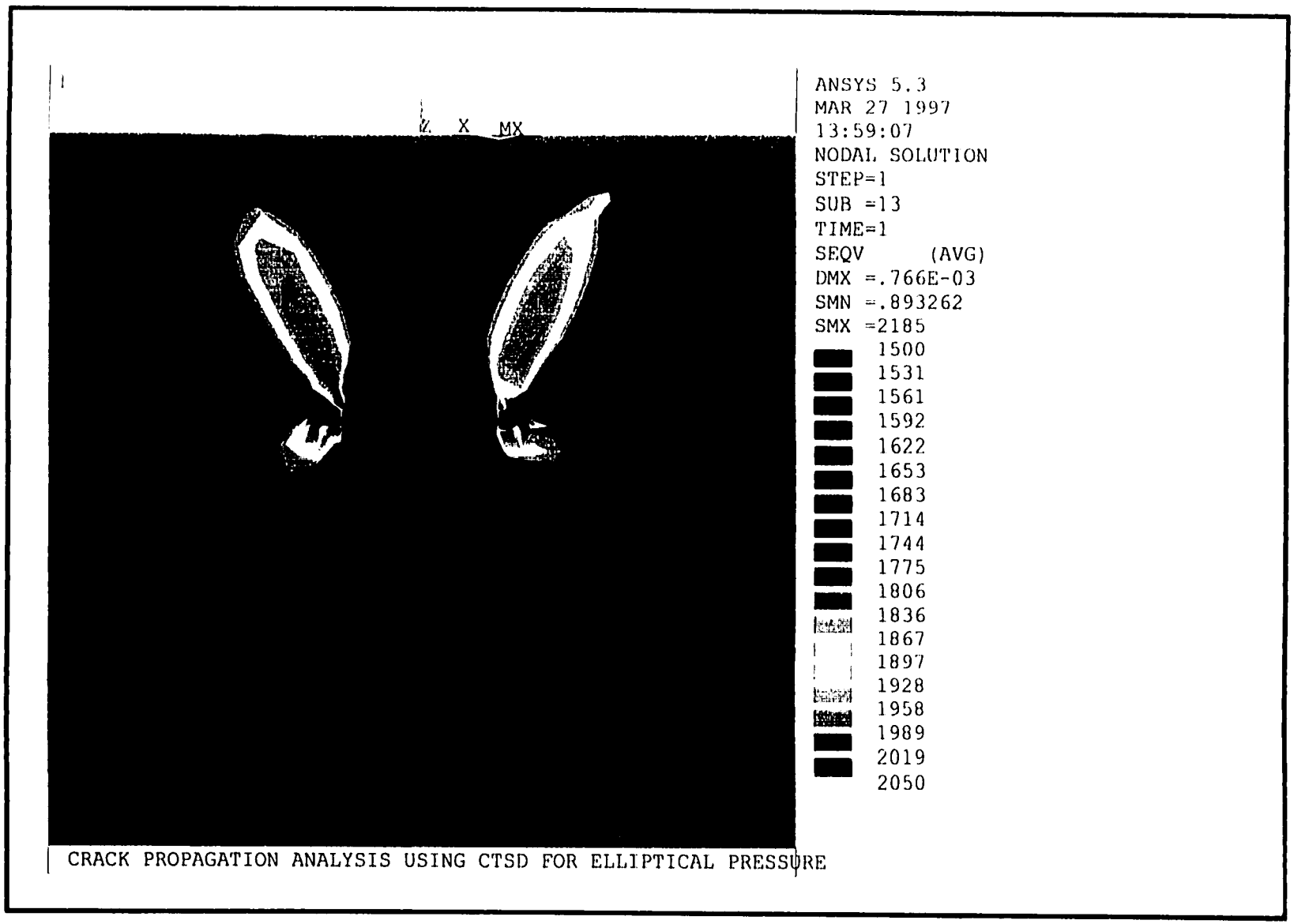

Figure 5.27 Contour plot of effective stress around a crack (crack length = 8μm)

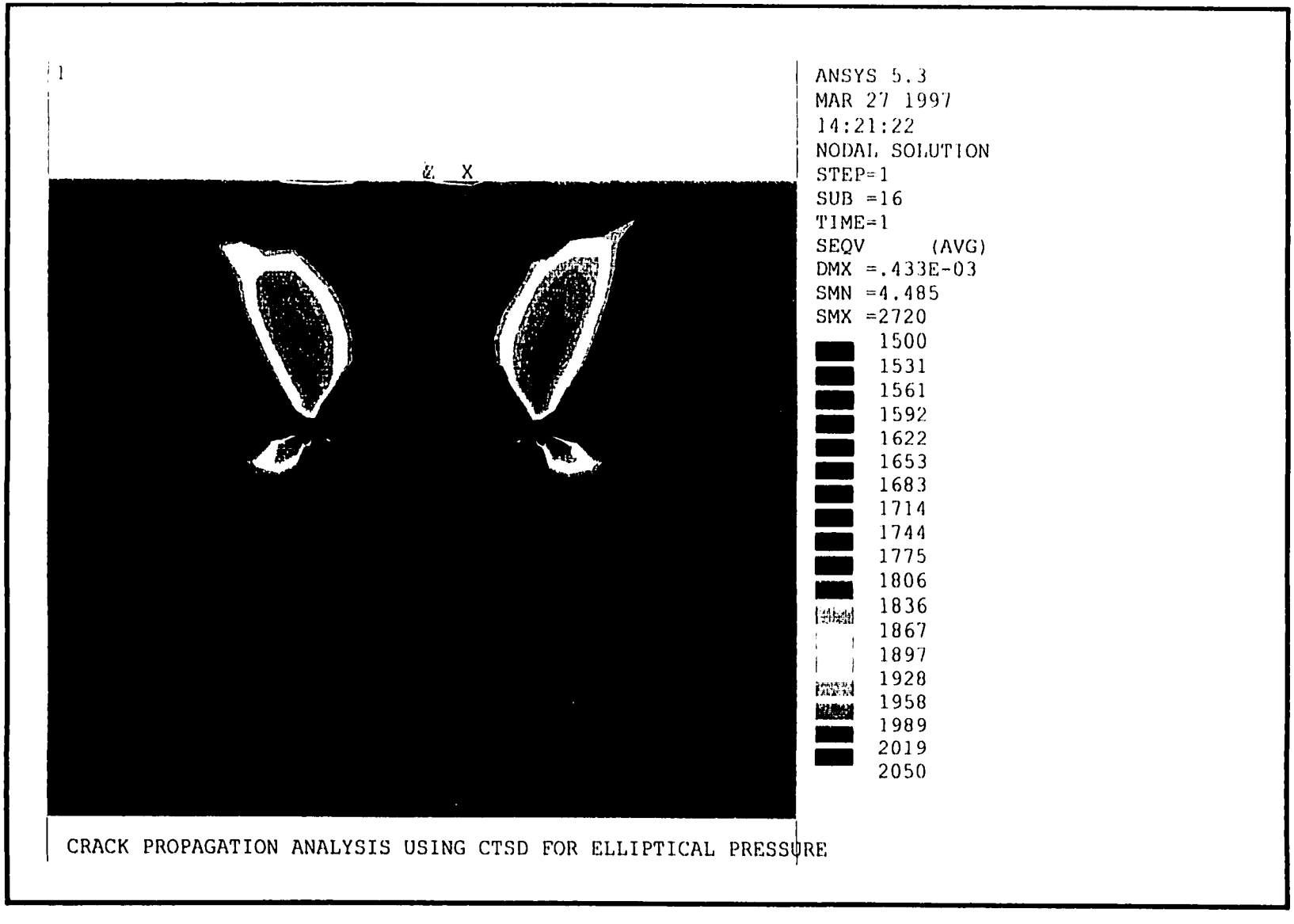

Figure 5.28 Contour plot of effective stress around a crack (crack length = 10μm)

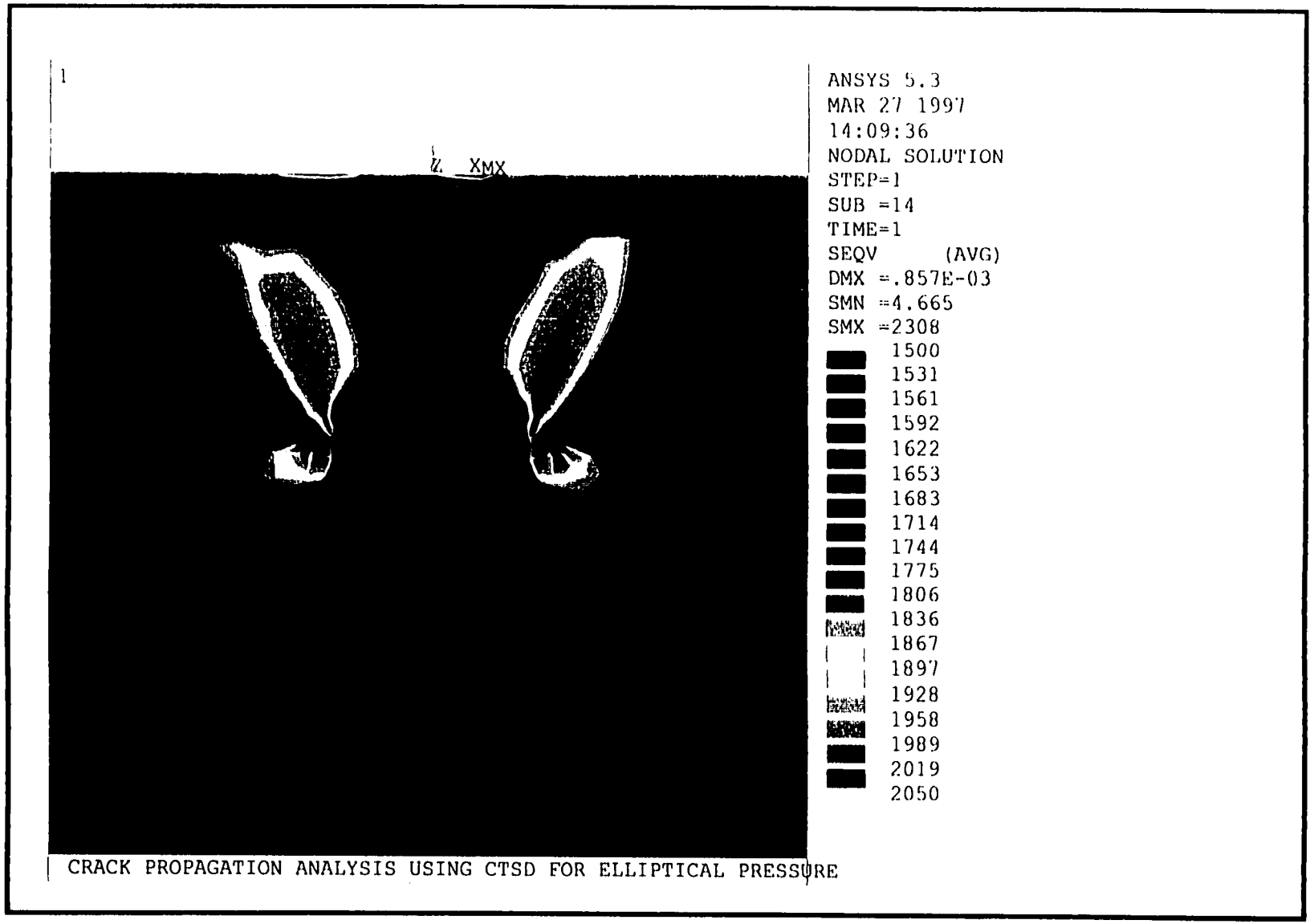

Figure 5.29 Contour plot of effective stress around a crack (crack length = 12μm)

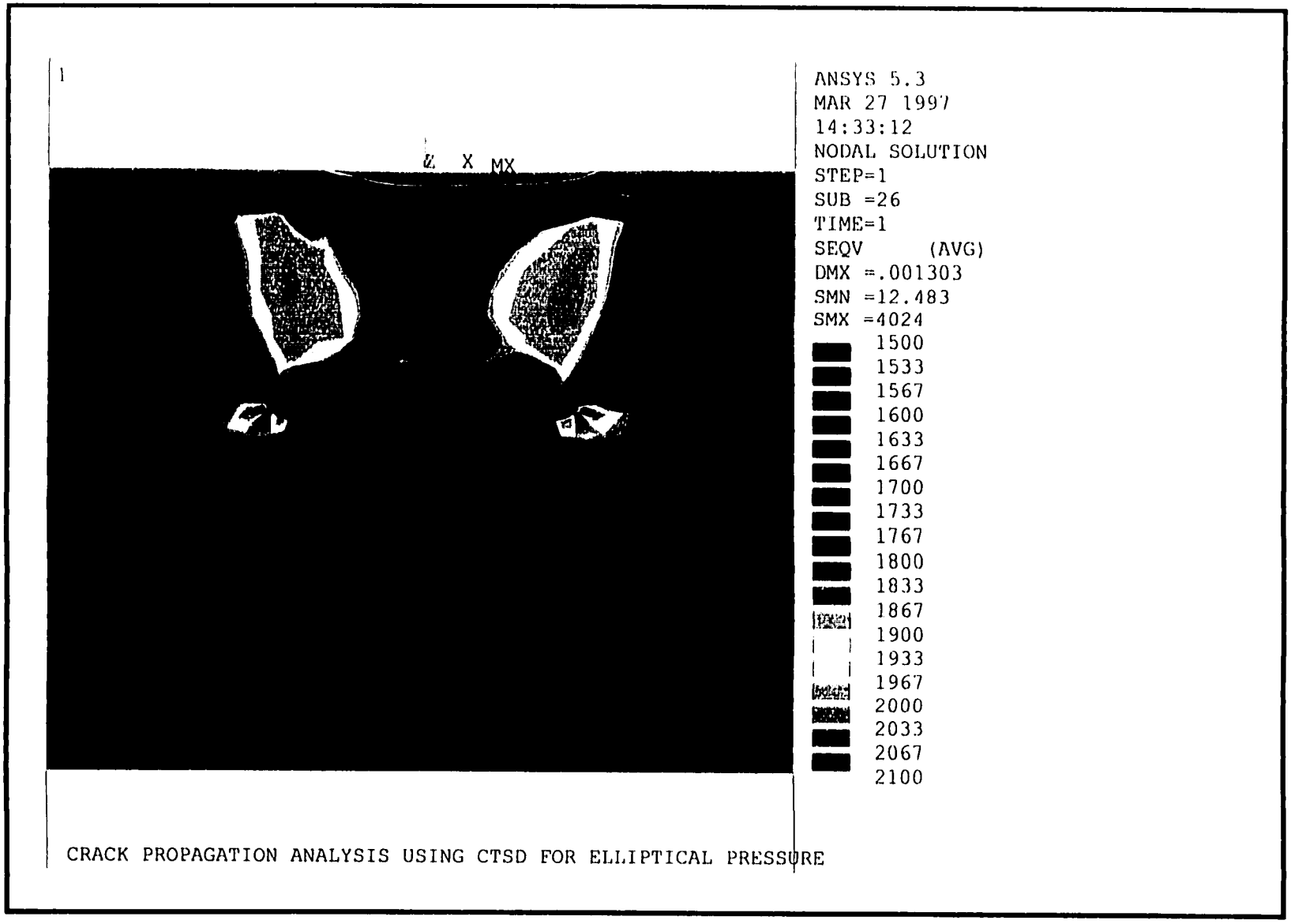

Figure 5.30 Contour plot of effective stress around a crack (crack length = 14μm)

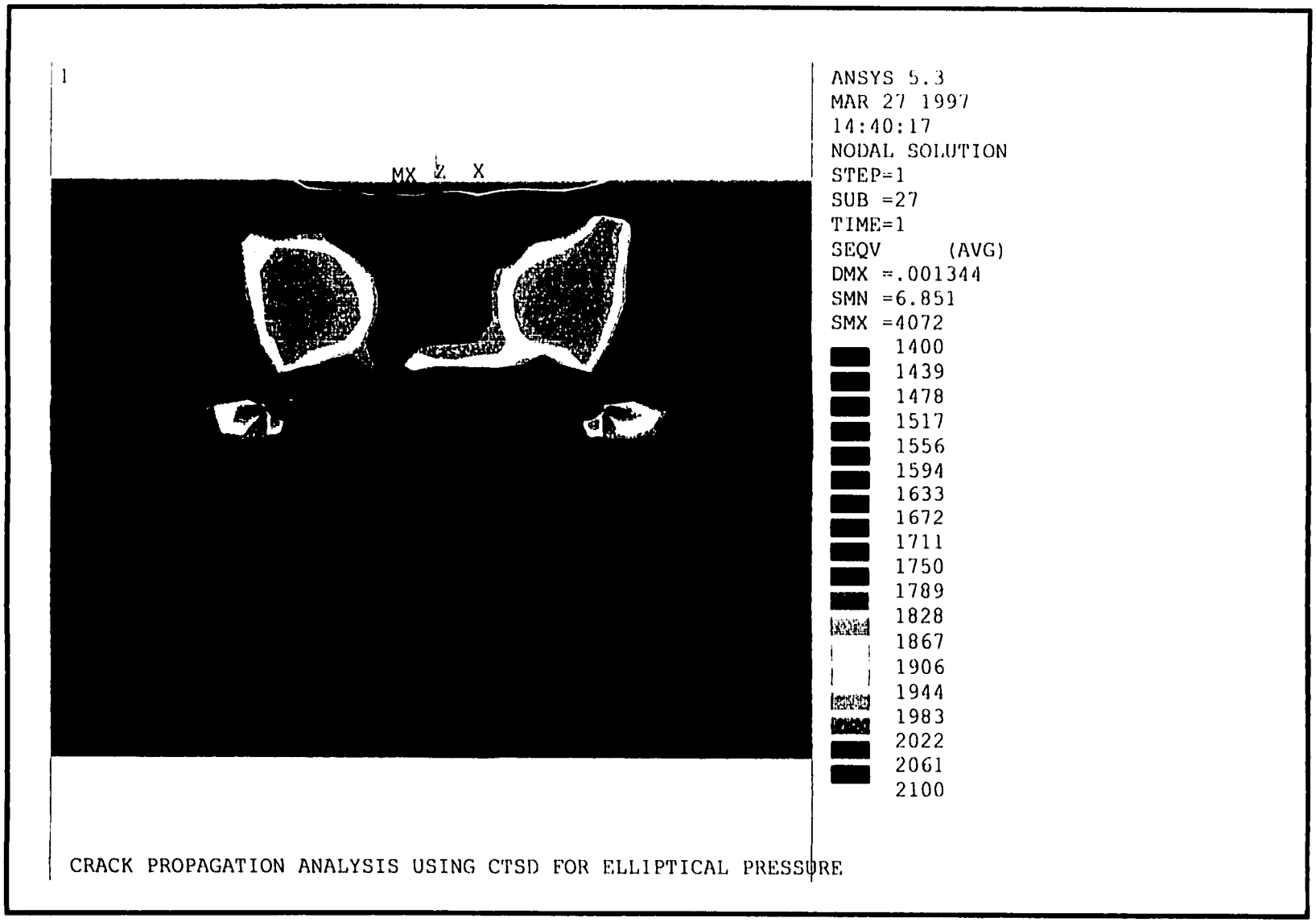

Figure 5.31 Contour plot of effective stress around a crack (crack length = 16μm)

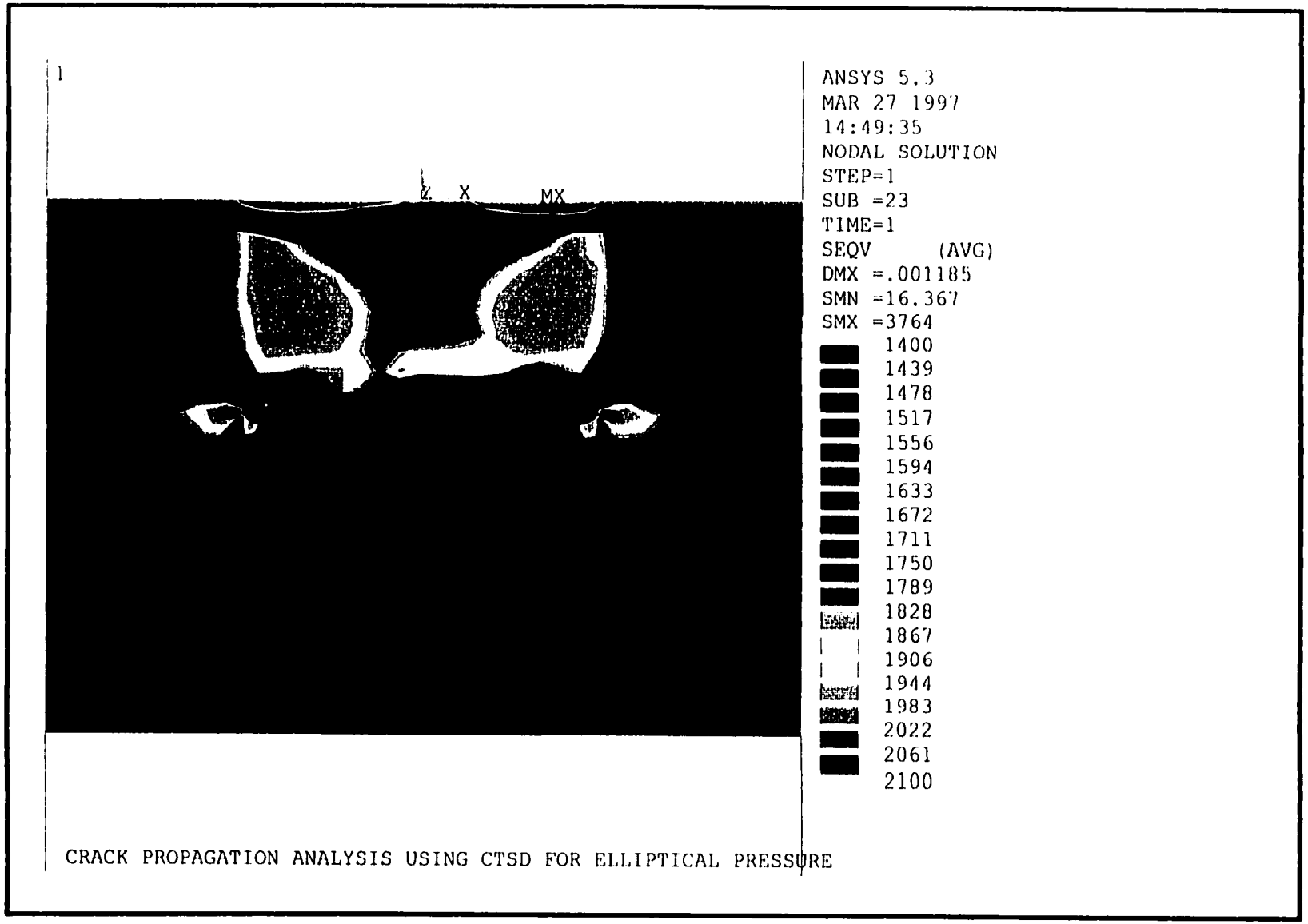

Figure 5.32 Contour plot of effective stress around a crack (crack length = 18μm)

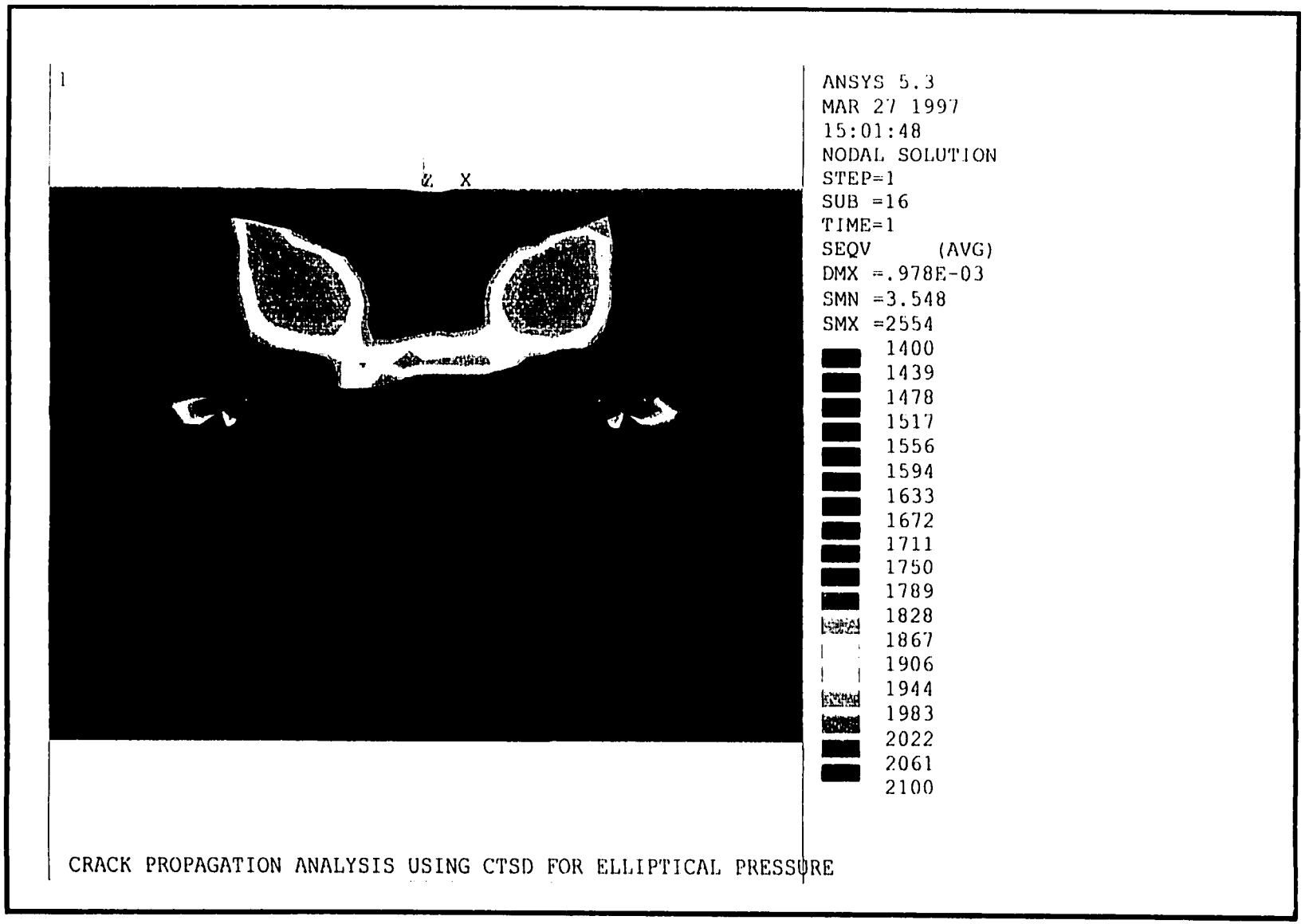

Figure 5.33 Contour plot of effective stress around a crack (crack length = 20μm)

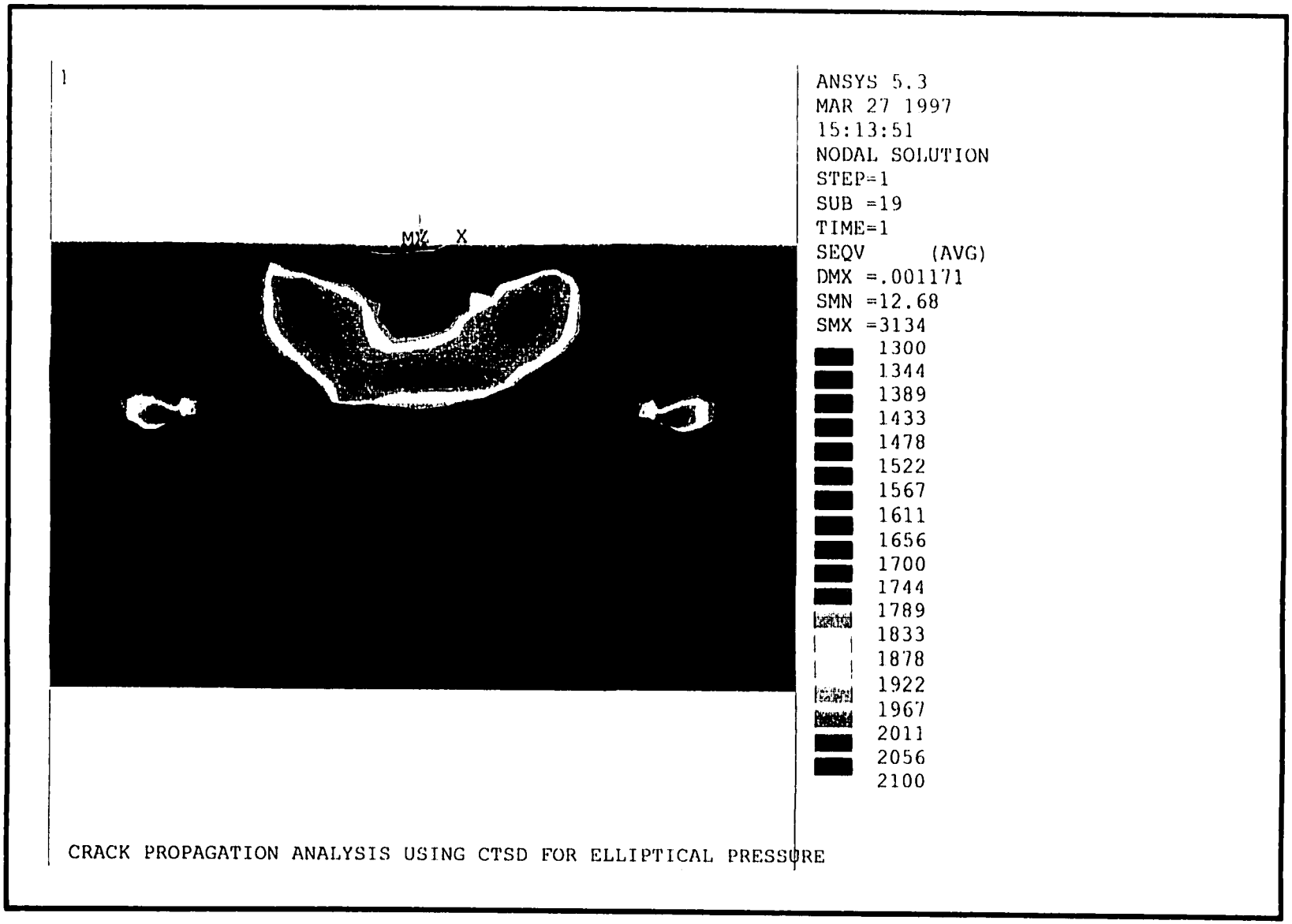

Figure 5.34 Contour plot of effective stress around a crack (crack length = 30μm)

evenly distributed in front of the crack (maximum values above and below the crack, Figure 5.25) to that of uneven distribution (maximum values above and in front of the crack, Figure 5.30). One should observe that due to the asperity contact, high stress values are limited to within the vicinity of this zone. Hence, the wear debris size can not be much more than the asperity size.

5.5.2 Crack Propagation Rate of a Plastically Loaded Member

The final stage in the analysis of the wear debris formation is the propagation rate of the subsurface crack. The finite element model is similar to the one described in the previous section. As part of the parametric study, the hardening moduli were varied to study their effect on the CTSD. The slope of the first hardening or plastic modulus is taken as 0.1 and 0.2 of the Young's modulus (E), and 0.01E and 0.02E for the second modulus slope. Because of the time duration (up to 4 hrs depending upon the type of analysis) required to run the finite element program, other than the hardening moduli, the parametric study was limited to four variables, friction coefficient (μ), maximum Hertzian pressure (P_0), crack length ($2l$) and depth (h).

The mesh of the finite element model developed to study the crack propagation using CTSD is given in Figure 5.24a. The zoomed view covering a square area of 40 μm by 25 μm is given in Figure 5.24b. The crack length selected for the parametric study was from 4 μm ($0.4a$) to 20 μm ($3.0a$). The position of the crack was from $0.7a$ to $2a$. It was essential to conduct this parametric study, in order to comprehend the effect of different variables

affecting the CTSD. This is an ideal condition where the load causing the crack nucleation which is applied at a particular point will continue to be applied at that same point until the formation of the wear debris. The following relationship describes the total CTSD per loading cycle.

$$C_{tot} = C_{CTSD} - C_{rwld} \tag{5.7}$$

where

C_{tot} = total crack propagated

C_{CTSD} = crack generated while being loaded

C_{rwld} = crack rewelded after the removal of the load

If one is to assume that the rewelding is zero then the total crack propagated per cycle will be equal to the CTSD. Based on this assumption an experimental validation for the wear rate will be conducted in Chapter 6, which will help in deducing the crack propagation rate.

The nature of the crack loading is such that the plastically deformed zone around the crack edge is relatively large and hence, the validity of the linear elastic fracture mechanics approach is questionable. Therefore, in accordance with this reasoning the next step is to consider the J integral or the Crack Tip Opening Displacement (CTOD) approach used by Sin and Suh [70] and Salahizadeh and Saka [60] in analysing a highly stressed contact zone. However, since the CTSD approach is an efficient approach provided a finite element model is available, it will be the appropriate path to follow.

The finite element analysis conducted by Salahizadeh and Saka [60] indicated that the crack tip sliding displacement (CTSD), because of the type of loading, is equivalent to the amount

of crack tip relative sliding distance minus the rewelding amount. Neglecting this rewelding amount, they got a good approximation of the crack tip propagation rate, in comparison to the experiment they used for verification purposes.

The results of the analysis are comparable with the values given by Salahizadeh and Saka [71]. The verification of the program was carried out by conducting the analysis for the conditions given in the above reference, a model which consists of a 400 μm half Hertzian contact width and a crack of 30 μm at 320 μm from the surface. An average difference of nearly 10% was calculated for the CTSD between the values given in the report and those obtained from the finite element program written, for both with and without interface friction. Considering the fact that it is a numerical method and the order of magnitude is 10^{-7}m it can be taken as a good approximation for the crack propagation values.

5.5.3 Results of Crack Propagation Analysis and Discussion

The study of the crack propagation analysis, which was conducted using the CTSD approach, was also studied parametrically, to see the effect of the different variables on the crack propagation rate of the metal. Similar to that of the crack nucleation analysis the first parameter that was varied was the **hardening moduli** to see the effect on the rate. For the given condition of depth of 0.7a and crack width of 0.6a the variation of the CTSD was from 0.009 μm to 0.013 μm. The values are of the same order of magnitude and the difference between them is not too high. This conclusion is similar to that reached in the crack nucleation case as well.

The other parametric study carried out, is to locate the maximum CTSD values, by varying the **maximum Hertzian pressure** applied. The study was conducted for the worst case scenario of a crack occurring at a depth of $2a$ and having a width of $2a$, with a maximum Hertzian pressure of $5.5k$ (A convergence problem was encountered for $6k$). The values of the CTSD for these cases, were found to be relatively high, ranging from 0.0098 μm to nearly 0.070 μm depending upon the load. These analysis were conducted for loadings that did not include friction at the crack interface.

The numerical analysis conducted on the CTSD, indicates that it is also dependent on the **length of the existing crack**. Following this, a parametric study was conducted by varying the crack length, while maintaining all the other variables the same. The result obtained shows that there is an almost linear relationship between the CTSD and the crack length (Figure 5.35). This property will be implemented in the next chapter while deriving the new wear model.

Part of the parametric study conducted, is to see the effect of introducing a **friction coefficient** at the **crack interface** and at the **contact surface**. It is considered that the shear stress is equal to the product of the normal stress and the friction coefficient at the interface. The results are dramatic drops in the value of the CTSD even for the those obtained for high surface loads (Figure 5.36). Therefore, since accurate determination of this quantity is highly dependent on the friction coefficient at the interface, it is crucial that one should ascertain the crack propagation rate obtained from this approach, describes the phenomenon properly.

Table 5.2 Parametric study of the CTSD values

No.	Coefficient of friction Surface/Interface	Maximum Hertzian pressure (P_0)	Crack depth (h μm)	Width of crack (C μm)	First hardening modulus	Second hardening modulus	Crack Tip Sliding Displacement (CTSD μm)
1	0.0 / 0.0	4.0*k*	0.7*a*	0.6*a*	0.1E	0.01E	0.01328
2	0.0 / 0.0	4.0*k*	0.7*a*	0.6*a*	0.1E	0.02E	0.00983
3	0.0 / 0.0	4.0*k*	0.7*a*	0.6*a*	0.2E	0.01E	0.01256
4	0.0 / 0.0	4.0*k*	0.7*a*	0.6*a*	0.2E	0.02E	0.00881
5	0.3 / 0.0	4.0*k*	0.7*a*	0.6*a*	0.1E	0.01E	0.01286
6	0.0 / 0.0	4.0*k*	2.0*a*	2.0*a*	0.1E	0.01E	0.00980
7	0.0 / 0.0	4.0*k*	2.0*a**	2.0*a**	0.1E	0.01E	0.00501
8	0.2 / 0.3	4.0*k*	1.0*a*	2.0*a*	0.1E	0.01E	0.00995
9	0.0 / 0.1	4.0*k*	2.0*a*	2.0*a*	0.1E	0.01E	0.00565
10	0.0 / 0.3	4.0*k*	2.0*a*	2.0*a*	0.1E	0.01E	0.00190
11	0.0 / 0.3	5.0*k*	1.0*a*	2.0*a*	0.1E	0.01E	0.02490
12	0.0 / 1.0	5.0*k*	1.0*a*	2.0*a*	0.1E	0.01E	0.00409
13	0.2 / 1.0	5.0*k*	1.0*a*	2.0*a*	0.1E	0.01E	0.00364
14	0.0 / 0.0	5.0*k*	1.0*a*	0.4*a*	0.1E	0.02E	0.00569
15	0.0 / 0.0	5.0*k*	1.0*a*	1.0*a*	0.1E	0.02E	0.02273
16	0.0 / 0.0	5.0*k*	1.0*a*	2.0*a*	0.1E	0.02E	0.05072
17	0.0 / 0.0	5.0*k*	2.0*a*	2.0*a*	0.1E	0.01E	0.04596
18	0.3 / 0.3	5.0*k*	2.0*a*	2.0*a*	0.1E	0.01E	0.00656
19	0.0 / 0.0	5.5*k*	2.0*a*	2.0*a*	0.1E	0.01E	0.07004
20	0.0 / 0.0	6.0*k*	2.0*a*	0.6*a*	0.1E	0.01E	0.02484

* the value of "*a*" is 5 μm in this case only and it is 10 μm for all the rest

Due to the complexity of the problem, the results of the theoretical model will be plotted with respect to the experimental results and the value for the CTSD will be adjusted accordingly, for a sub-set (3 per each set) of experiments, as will be seen in Chapter 6.

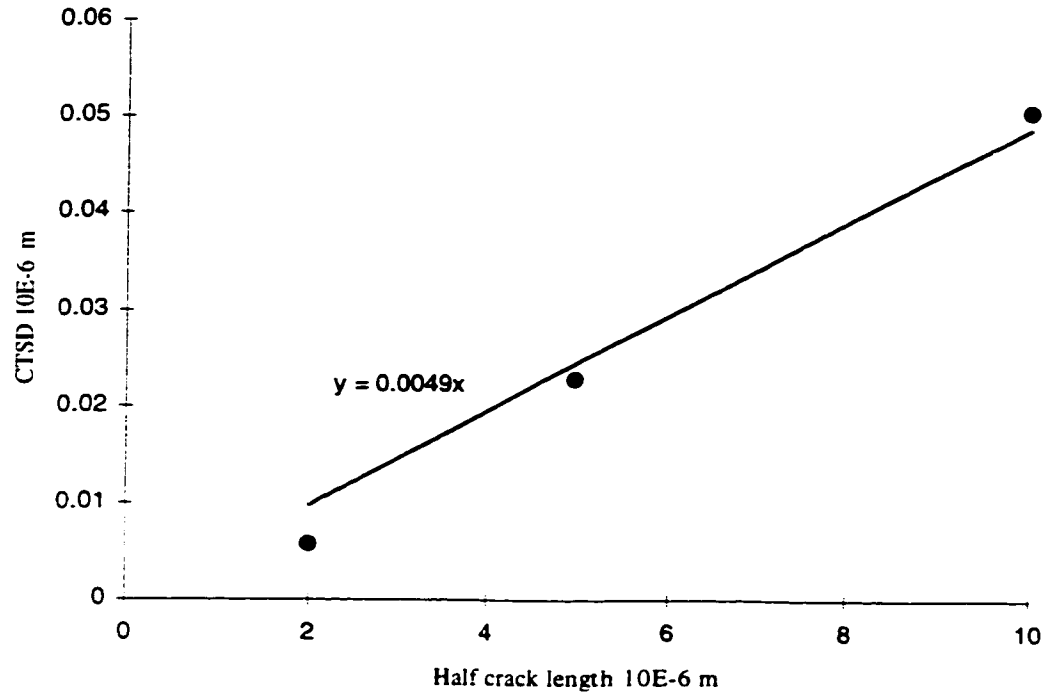

Figure 5.35 CTSD growth relative to the subsurface crack length

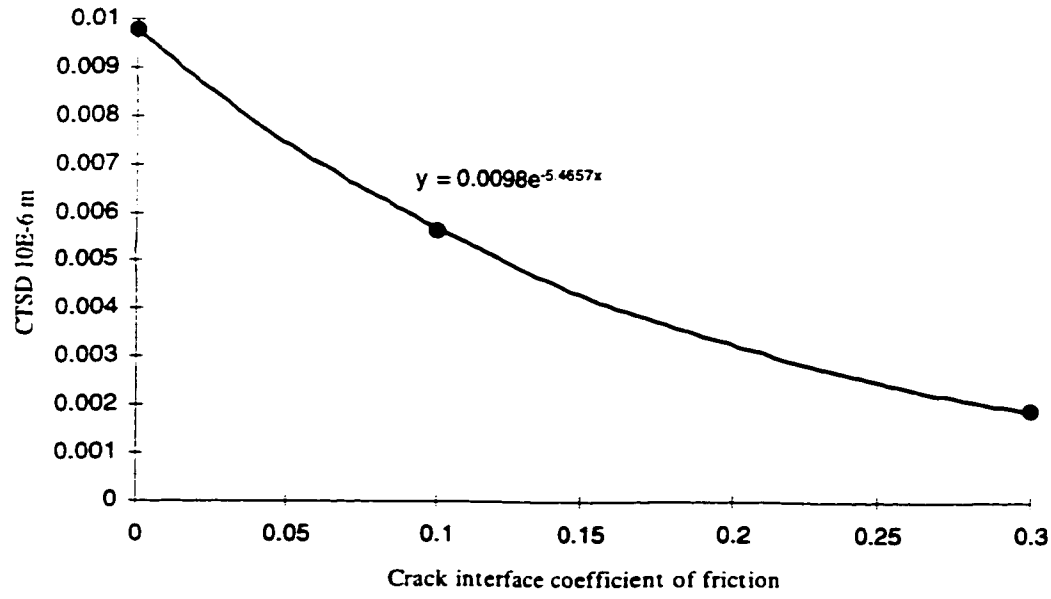

Figure 5.36 Effect of interface friction coefficient on the CTSD values

The CTSD approach was used in obtaining the total crack propagation rate by assuming that the rewelding after the removal of the load is zero. The parametric analysis conducted indicated that a number of factors such as coefficient of fiction, maximum Hertzian pressure, depth of crack, width of crack and the hardening properties of the material as well, affect the magnitude of the CTSD. It was apparently observed that higher values of the hardening moduli reduced the magnitude of the CTSD while increasing the value of the maximum Hertzian contact pressure increased it. It was also seen that for longer cracks the value of the CTSD was higher and for cracks located deeper from the surface the CTSD is smaller in magnitude.

Even though the above general trend was observed for the various loadings and properties, the magnitude of the CTSD had a variation of one order (0.0019 - 0.070 μm). However, determination of the right value is rather difficult at this juncture. Hence, an average value (for $5k$ maximum Hertzian pressure) can be employed to study the wear process, for this type of debris formation process and properly calibrated experimentally.

5.6 Conclusion

This analysis shows that crack nucleation from cylindrical inclusions does not readily form for pure impact contact conditions, loaded elliptically by a maximum pressure value of $4k$. From the analysis carried out it can be observed that the effect of increasing the pressure value results in an increase in the extent and amount of plastic deformation which effectively translates into a combined high value of residual as well as applied stress in comparison to

the hydrostatic stress. Therefore, this is the main reason why values of σ_n/k pass the critical limit of 1, for higher values of P_o. This critical value is also bypassed at the surface near the end of the asperity contact mainly due to the lack of high hydrostatic pressure. This gives a clue about the size of fatigue wear debris, magnitude of which could be approximated to be similar to the contact asperity length. Application of friction force will move this maximum interfacial stress value progressively to the surface as well. This also strengthens the theory that was proposed earlier about the size of the wear debris. The effect of hardening has been observed for the maximum Hertzian pressure value of $4k$ and it was found that the maximum value of the interfacial stress was obtained for the non-hardening material. This is again a result of the amount of residual stress due to the high plastic strain. However, this effect might not be the same for the various maximum contact pressure values given here. Even though, Jahanmir and Suh [64] have reported that crack nucleation in the case of rolling contact can occur only after nearly 70 passes, it seems that the analysis taken here indicates that crack nucleation can occur only after the second loading. This may be due to the hardening of the material, which in turn will increase the value of the residual stress as well as the applied stress values, and also the fact that their boundary condition is different may play a role as well.

The parametric study conducted for the crack propagation rate, implemented the variation of the different quantities affecting it. Because of the nature of the problem, accurate determination of the CTSD for the actual conditions is difficult. It is especially hard to obtain the real value of the interface friction coefficient, which may involve interlocking of the top and bottom surfaces. Even though, the value of the CTSD was in the range of 0.002 μm to

0.070 μm, it could introduce significant errors while calculating the wear volume. In accordance with this argument, a reasonable value for the CTSD corresponding to the applied flow pressure (maximum Hertzian pressure of $5k$) and maximum interfacial friction coefficient (1), is taken as a valid initial starting value to calculate the wear volume.

Following the analysis given in this chapter, a step by step justification and derivation of a new wear model for impact motion (oblique and normal), is carried out in the next chapter. This model will be extended to sliding wear as well, and the CTSD value calibrated for impact and sliding, based on the total wear loss.

CHAPTER 6

DEVELOPMENT OF NORMAL & OBLIQUE IMPACT WEAR MODELS BASED ON PRINCIPLES OF DELAMINATION THEORY

6.1 Introduction

Various empirical and semi-empirical wear models have been proposed by different researchers in the area of tribology, as discussed in Chapter 2. Among the diverse theories put forth so far, the delamination theory of wear has helped to forward one of the most important mathematical models, which has effectively employed a fracture mechanics approach to determine the wear rate occurring near the interface of two interacting objects. This theory essentially addresses the phenomenon which occurs in sliding of two objects by considering the critical values of the stress distribution at the contact interface. However, further investigation reveals that similar arguments used for sliding wear can be justifiably employed to extend this theory to impacting conditions as well. [106, 110] (Author's Ref.)

6.2 Extension of Delamination Theory to Obliquely and Normally Impacting Objects

Among the various impact wear models surveyed, none has utilized a fracture mechanics approach extensively, to arrive at a mathematical representation of the wear volume. Even though the investigation conducted by Engel [28] involved rigorous contact mechanics approach, it still did not address the microscopic interaction, which describes the wear. The inherent difference between the Engle's approach and the delamination theory of wear is that the first deals with the macro contact, while the latter deals with the micro contact of the

interacting materials.

Most of the derivations of the wear models existing thus far are highly empirical, relying heavily on experimental investigations, to predict the wear. Even though the mathematical wear models vary from each other, there is a consensus among the various researchers that fatigue is the dominant wear mechanism for low contact force conditions. Hence, the derivation of this impact wear model needs to address the various steps involved in wear debris formation. It is based on a similar principle as the delamination theory of wear[21]. The applicability of delamination wear to impact motion, is supported by leading tribologists such as Rice[4], Ko[84] and Jahanmir[85]. Jahanmir investigated the problem of erosion during impact and indicated the applicability of a similar analysis, like the one done for delamination wear under sliding. However, there were some differences between his work and this one, in quantifying the fracture mechanics dependant quantities (crack nucleation and propagation), as mentioned earlier in the previous chapter. Therefore, the following reasoning can be justifiably argued to establish the wear model proposed in this research work:

1. The transmission of normal and tangential loads are carried out through the asperity points of two impacting surfaces. Due to the repetitive application of loading, asperities of the softer material are easily deformed and flattened out, or form minor wear particles in some instances. Further impacting action between these two objects will result in a smooth surface for the softer material and rougher asperity for the harder material. Therefore, the contact between the two objects will no longer be asperity to asperity, but rather asperity to surface (Figure 6.1). However, due to the

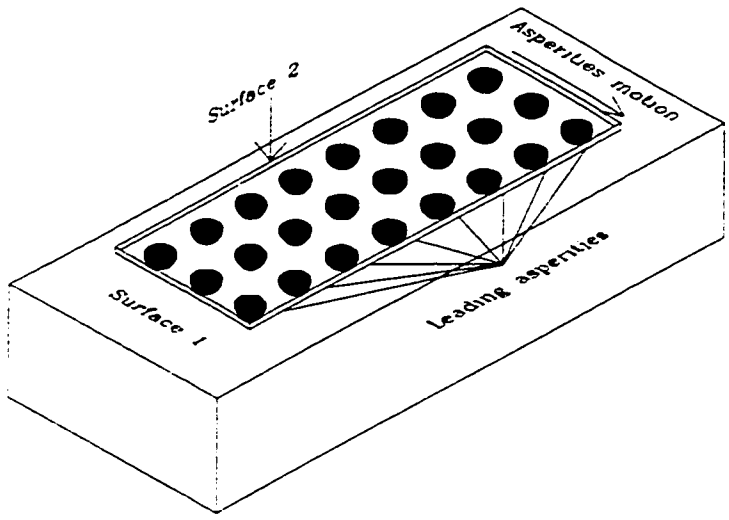

Figure 6.1 Idealisation of the contact of two surfaces, asperity on flat

distribution of asperity it can safely be stated that the global contact conditions (geometry and force) are also responsible for the final shape that the wearing body will have.

2. The quasi-static subsurface stress distribution carried out assuming smooth surface contact, indicates that the maximum of the summation of the principal shear stress (residual as well as applied) and hydrostatic stress values, for an applied maximum elliptical pressure of $5k$, will occur at some distance away from the surface, at a location where the effect of the subsurface effective stress is greater than the triaxial compressive stress. There are two negating stress effects in the formation of wear, the triaxial compressive stress or hydrostatic stress and shear stress. The triaxial compressive stress reduces the crack initiation process while the shear stress aids in the initiation and propagation of crack. Favorable conditions with reduced triaxial compressive stress and increased shear stress arise, as the distance from the contact surface increases further into the material. The result, as was seen, is to initiate crack from inclusions at this depth rather than at the surface. The crack initiation will be followed by crack propagation.
3. Cyclic loading of the softer material will cause the subsurface stresses to propagate the crack, initiated around an inclusion, parallel to the surface following the weakest shear resistance direction. The crack propagation process continues parallel to the contacting surface until the formation of a debris or the effect of contact pressure is not considerable enough to influence its growth. The direction of propagation is parallel to the surface until it reaches a certain length and then proceeds at an angle to reach the surface. Observing the plot of the effective stress around the crack tip

indicates that there is a tendency for the axes of the maximum value to be inclined to the surface, which implies that crack propagation will tend to go towards the surface as it goes on growing in size. This phenomenon is indicated in the previous chapter which deals with the finite element modeling. The crack propagation rate is governed by the material properties and amount of cyclic force applied on the object near the crack.

4. Finally, the material will wear in the form of thin circular sheets, thickness of which will be dependent on the location of the maximum sum of the shear and hydrostatic stress within the vicinity of an inclusion. This depth is estimated in Chapter 5, where extensive finite element analysis is conducted to determine this position. This argument effectively extends the delamination theory of wear to impacting conditions. It is complimentary to the theory that fatigue is the main cause of wear for impacting objects.

The difference between delamination theory for sliding wear and the above justifications for impact wear within the context of delamination are:

1. Because of the relative motion associated with impact, the crack nucleation process is assumed to initiate immediately upon contact, within the first two to three cycles of loading. The incubation period as described by Engel is the time required for crack to propagate parallel to and eventually towards the surface resulting in the formation of a wear debris. There is no incubation period in sliding wear due to the fact that abrasive and adhesive wear mechanisms dominate at the beginning of the wear process.

2. The shake down principle implemented for an elastic perfectly plastic material in the case of sliding for delamination wear, was based on the material's continuous plastic deformation for cyclical loading, until a steady state value is reached. This is not applicable here because of the hardening of the elastoplasic material chosen and the assumption that the point of application and magnitude of the impact load remain the same over the duration of the debris formation process.
3. The crack nucleation analysis is conducted following Jahanmir and Suh's[22] approach where as the crack propagation rate is estimated from the crack tip sliding displacement (CTSD) as described by Shih and Suh[70] and Salahizadeh and Saka[71]. It should be noted that the result for both sliding and impact is qualitatively the same implying that crack nucleation does not control the wear process but rather the crack propagation does.
4. The major difference between this research work and that of delamination for sliding is the deduction that the critical crack length is equivalent to or is of the same order of magnitude as the asperity length. This is inherently different than the delamination theory of wear where this value was not identified explicitly. However, as will be explained later this value is not very critical in the wear volume calculation.

Following the above approach for impact wear, which is analogous to the sliding wear reasoning, sequential assumptions relating the macroscopic nature of the contact mechanics to the microscopic character of the physical phenomenon, will be listed to arrive at a reasonable wear model for impact. It is apparent that two relatively smooth objects that are in contact transmit the load through the asperity as explained earlier. Hisakado[82] and

Tsukada et al.[86-90] have shown that the contact of two surfaces through their asperity can be the analyzed by assuming the contact to be between a perfectly smooth surface and a rough one.

Even though the derivation of a purely analytical model describing the wear process is rather difficult at this juncture, an attempt is made to arrive at a theoretical oblique impact wear model that heavily relies on fracture mechanics, starting with the following reasonable assumptions:

a. The force between the interacting bodies is transmitted through spherical asperities distributed at the contact interface such that the macro-contact pressure distribution is elliptical.

b. The contact pressure of each asperity in turn is considered to be elliptical and average pressure is equivalent to the hardness of the softer material.

c. The effect of one asperity on an adjacent one is considered to be negligible.

d. Since the wear debris is of the same order of the asperity contact length, it is estimated that the subsurface crack comes to the surface resulting in a wear debris, after axisymmetrically propagating for a distance of L, which is the same as the asperity contact radius 'a_{asp}'.

e. The material elastoplastic properties are considered by including a multi-linear isotropic hardening and neglecting strain-rate effects over the wear process.

f. The point of application of the cyclical impact force is repeated at the same point (Figure 6.2) until the wear debris is formed which will result in another set of asperity contact until the whole layer on the global level is worn.

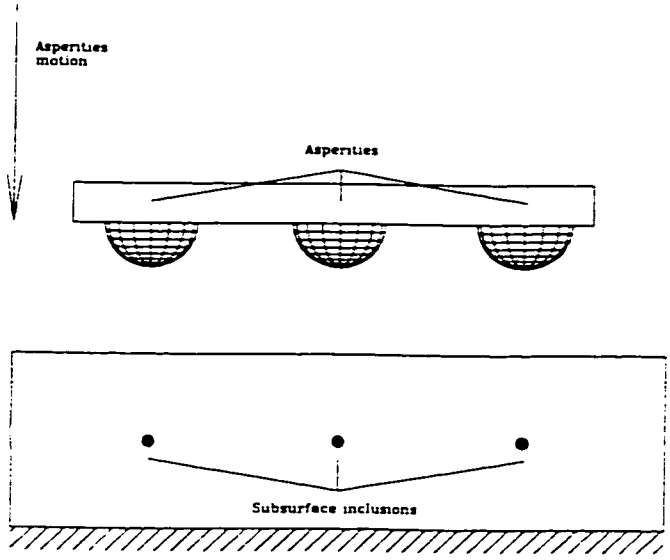

Figure 6.2 Idealisation of Impact surfaces along with inclusions causing crack nucleation

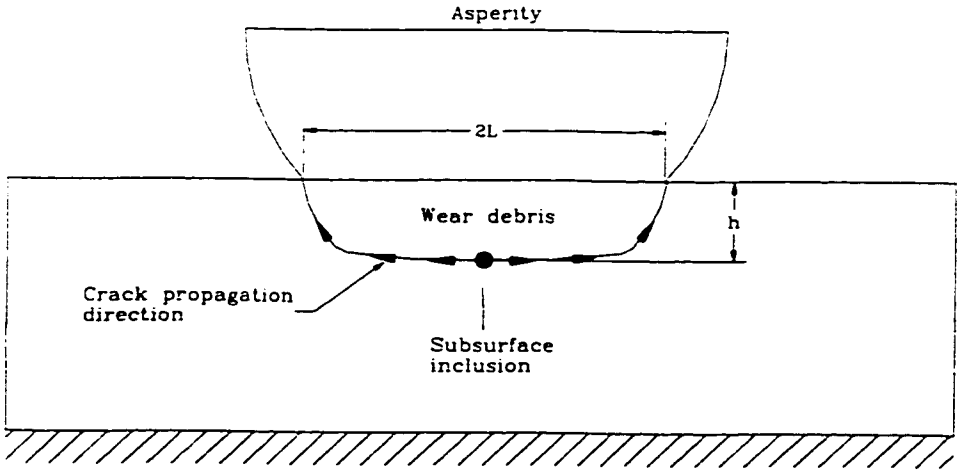

Figure 6.3 Wear debris formation under impact loading

g. The total number of asperity contacts remain constant for the entire wear process provided the maximum impact force is maintained constant.

From the above oblique impact wear process description and assumptions, it can be inferred that wear is a result of the crack nucleation and propagation, due to the asperity contacts of two interacting materials. The delamination theory of wear derived for sliding conditions has resulted in an equation which has a wear volume proportional to the applied load and sliding distance. The derivation of the impact wear equation is analogous to the sliding model except instead of the sliding distance, the number of impacts are taken. The justification of this equation has already been given and the fracture mechanics approach employed in the previous chapter has shown its validity. The wear volume derivation is schematically represented in Figure 6.3. Therefore, from the above reasoning the rate of change of wear volume for an asperity repetitively impacting a particular area, can be formulated as follows $[h\pi(2l\Delta l + \Delta l^2)]$, by neglecting small terms (Δl^2):

$$\frac{dw_a}{dn} = 2\pi h(p_{o\alpha sp}, E, \nu, \mu, \sigma_y)\, l(p_{o\alpha sp}, E, \nu, \mu, \sigma_y, n)\Delta l(p_{o\alpha sp}, E, \nu, \mu, \sigma_y, n) \qquad \textbf{(6.1)}$$

where,

h = crack nucleation depth

p_{0asp} = maximum Hertzian contact pressure of the asperity

w_a = wear volume corresponding to one asperity loading

σ_y = yield stress of the material

n = number of cyclic loading

Δl = crack propagation rate for a crack length of (l)

The crack propagation rate (Δl) is a crucial quantity in the determination of the wear volume. This quantity can be expressed in terms of the cyclic loading as:

$$\Delta l = \frac{dl}{dn} \tag{6.2}$$

Substituting for Δl in equation (6.1) and integrating it all the way up to the critical axi-symmetric crack length L (= a_{asp}), the total wear volume due to one asperity contact can be derived as follows:

$$w_a = 2\pi h(p_{oasp}, E, \nu, \mu, \sigma_y) \int_0^L l(p_{oasp}, E, \nu, \mu, \sigma_y, n)\, dl \tag{6.3}$$

The total wear volume w, after the total number of cyclic loading required to produce this critical crack length is applied, is the summation of all the wear particles due to all the asperities in contact. This is given by:

$$w = \sum_{i=1}^{i=n_a} w_{ai} = n_a w_a \tag{6.4}$$

where,

n_a = number of asperities

The latter part of equation (6.4) is valid, provided that the asperities in contact have the same area and cause equal volume of wear particles, in addition to producing wear debris equal to the asperities in contact, n_a. This quantity n_a is given by the following relationship in terms of the maximum applied contact force and the load on each asperity:

$$n_a = \frac{3\tilde{P}_0}{2\pi p_{0asp} a_{asp}^2} \tag{6.5}$$

where,

$\bar{P}_0$ = the applied load (N)

a_{asp} = radius of the asperity in contact

The volume of wear due to an asperity was obtained by integrating equation (6.3). This geometrical quantity does not indicate the variation of the wear, with respect to the cyclically applied load (time). In order to introduce the wear volume variation wit respect to time, one needs to express the critical crack length as a function of time, and substitute for the wear volume in equation (6.4). The total number of cyclic loading required for the formation of one $2L$ diameter asperity (N_{cpf}) can be obtained from the crack propagation relationship (equation 6.2). This can only be done provided, that the crack propagation rate is expressed as a function of the crack length l.

The parametric study conducted in the previous chapter helps to express the crack propagation rate as a function of the crack length. This was plotted in Figure 5.35 of the previous chapter, and it can be observed that there is an almost linear relationship between the two values.

$$\Delta l = k_s l \tag{6.6}$$

Therefore, taking into account the fact that the crack initiation position is at some distance from the zero value (initial condition of l_0), the differential relationship given by equation (6.2) can be integrated, to give the cyclic loading for the final crack propagation value (N_{cpf}) as a function of the critical crack length (L), initial value l_0 and slope value k_s. This integration is given as:

$$\frac{1}{k_s}\int_{l_0}^{L}\frac{dl}{l} = \int_{N_{cnf}}^{N_{cpf}} dn$$

$$N_{cpf} = \frac{1}{k_s}\ln\left(\frac{L}{l_0}\right) \qquad \textbf{(6.7)}$$

where,

$N_{cpf} \gg N_{cnf}$ and $N_{cnf} \approx 0$ compared to N_{cpf}

Since the crack nucleation criteria assumes the inclusion diameter to be more than 0.025μm, the initial condition, i.e., position where crack nucleation will occur, is taken as half of the inclusion diameter (0.0125 μm). This is because the center of the inclusion is assumed to be on the y axis. The total critical axi-symmetric crack length is equal to 10 μm as indicated, and the slope of equation (6.6) is dependent on the maximum crack propagation rate (Δl) at this crack length. The maximum crack propagation rate which is taken to be the CTSD at L=10 μm, is therefore, obtained for an applied maximum Hertzian pressure of $5k$, and an estimated critical depth of 10 μm.

The crack nucleation number of cyclic loading (N_{cnf}) is already determined from the relationship giving crack nucleation criteria, for an elasto-plastic material, which obeys the multi-linear isotropic hardening law. It is seen that crack nucleation is not the wear controlling factor. This is an already established fact by various researchers, such as Suh and Jahanmir. The total number of load application is therefore, a sum of the number of load application for crack initiation and number of load application for crack propagation, which is almost equal to the N_{cpf}, as shown by:

$$N_{tc(m)} = N_{cnf} + N_{cpf} \approx N_{cpf} \qquad \textbf{(6.8)}$$

where,

$N_{tc(m)}$ = total crack nucleation and propagation number for 'm' type motion

$m = i$ => impact, $m = o$ => oblique impact and $m = s$ => sliding motion

This value of $N_{tc(m)}$ and the linear crack growth assumed for the crack propagation rate will be used to calculate the wear volume. The critical crack length can be written as:

$$L = l_0 e^{k_s N_{tc(m)}} \tag{6.9}$$

The total wear volume can be written as a function of time, in terms of the total number of times the load is applied, and can be expressed by the following equation:

$$w = n_a w_a \frac{n N_n}{N_{tc(m)}} \tag{6.10}$$

where,

N_n=number of loading during each excitation cycle n

The volume of each debris w_a is given by:

$$w_a = \pi h L^2 = \pi h \left(l_0 e^{k_s N_{tc(m)}} \right)^2 \tag{6.11}$$

Because the total wear is a function of the number of times the cyclic loading is applied, for conditions involving oblique type of impact, N_n depends upon the number of times the asperities pass over the crack nucleation zone for each excitation. Hence, the number of cyclic loading per excitation is given by:

$$N_n = \left(1 + \frac{s}{s_a} \right) n_{cl} = \left(1 + \frac{v_s t^*}{s_a} \right) n_{cl} = \left(1 + \frac{v \cos(\theta) t^*}{s_a} \right) n_{cl} \tag{6.12}$$

where,

s = total sliding distance per impact

s_a = average distance between two asperities

n_{cl} = number of columns of asperity

v = velocity of impact

θ = angle of impact

t^* = duration of contact

The duration of contact for a cylinder impacting in a conforming support was derived in Chapter 3 and is written as (equation3.84):

$$t^* = \pi \sqrt{\frac{\bar{m}_c}{2a_{wh}E^*} \ln\left(\frac{8a_{wh}^3 E^*}{R\bar{P}_0}\right)} \qquad \textbf{(6.13)}$$

where,

$\bar{m}_c$ = mass of the cylinder (kg)

a_{wh} = half the axial contact length

$\bar{P}_0$ = the impact force (N) = $P_0/(2a_{wh}) = P_0/a_{wt}$

E^* = equivalent Young's modulus

R = equivalent radius

It should be noted that the impact force is expressed as the actual applied force and not normalised with respect to the axial distance. This is following the elastic compliance equation used to derive the impact time, given by Dubowsky and Freudenstein [53]. Following a similar approach for obtaining the wear volume, the actual applied force will be used. further in this chapter. In equation (6.12), the sliding velocity v_s is given as the cosine function of the impact angle θ (the angle made between the impacting surface and the force). The value of N_n has a limiting case between 1 (for normal impact) and $n_{cl}\pi d_c/2a$ (for pure sliding motion). n_{cl} is defined as the number of columns in contact and d_c is the diametral clearance. The above derivations are carried out for a cylinder supported in a conforming

support, with a diametral clearance of d_c. The number of columns of asperities (Figure 6.4) is determined from the ratio of the Hertzian contact width and the average spacing between asperities. It is given by:

$$n_{cl} = \frac{2a}{s_a} = \sqrt{\frac{2an_a}{a_{wt}}} = \sqrt{\frac{6\bar{P}_0}{a_{wt}\pi p_{0asp}a_{asp}^2}\left(\frac{\bar{P}_0 R}{\pi E^* a_{wt}}\right)^{1/2}} \tag{6.14}$$

Equation (6.12) is written with the assumption that the total contact time is also the total slip time, which indicates that sticking is neglected. The average distance between the asperities (s_a), is given by equation (6.15). It is a function of the number of asperities in contact, the half Hertzian contact width a and the axial contact length a_{wt}, as follows:

$$s_a = \sqrt{\frac{2aa_{wt}}{n_a}} \tag{6.15}$$

Taking the values of s_a, t^*, w_a and n_a and substituting them into equation (6.9), the final wear equation is obtained. All the variables in this equation can be theoretically obtained, either from the fracture mechanics analysis conducted in Chapter 5, or as shown in this chapter from contact mechanics analysis. Therefore the final oblique impact wear equation is given by:

$$w = \frac{3\bar{P}_0 L^2 h}{2p_{0asp}a_{asp}^2}\sqrt{\frac{6\bar{P}_0}{a_{wt}\pi p_{0asp}a_{asp}^2}\left(\frac{\bar{P}_0 R}{\pi E^* a_{wt}}\right)^{1/2}} \left[\frac{n}{N_{tc(o)}}\right]\left(1+\frac{\nu\cos(\theta)\sqrt{\pi^2\bar{m}_c\ln(8a_{wh}^3E^*/R\bar{P}_0)/2a_{wh}E^*}}{\sqrt{4\pi aa_{wt}p_{oasp}a_{asp}^2/3\bar{P}_0}}\right) \tag{6.16}$$

Therefore given the fact that all the above quantities can be determined from the finite element model developed for this problem, the wear volume can be calculated analytically

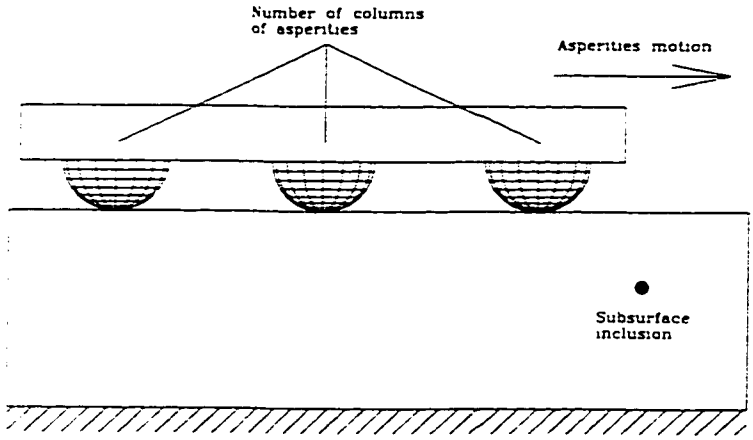

Figure 6.4 Cyclic loading of the subsurface due to asperity sliding motion

assuming all the conditions stated are valid for describing the wear phenomenon. It should be noted, however, that there are a number of assumptions that are taken to simplify this complex phenomenon. Hence, discrepancies occurring should not come as a complete surprise to the reader. Therefore, based on the deviation of the theoretical wear values from the actual ones, the CTSD can be modified for normal impact, oblique impact and sliding wear separately. Finally, results obtained from these validations are used in Chapter 7, to characterize the wear, using the appropriate parameter.

The flow chart of Figure 6.5, indicates the approach taken to derive the wear model. The input parameters are the material properties and type of contact condition while the final output is the result. The contact mechanics approach implemented in the analysis is used to first get an initial estimate of the asperity size which is in turn used to conduct the analysis for crack nucleation. After the crack nucleation position is estimated the next procedure is to determine the crack propagation direction and also the crack propagation rate from the CTSD. The other input given to the system is the total wear volume which is in turn used to validate the value of the CTSD to appropriately find a reasonable value to the wear. In other words the wear process is calibrated based on a physical understanding of the mechanism

The wear of cylinder impacting normally against a conforming cylinder support can be derived in a similar fashion assuming the wear will follow the pattern described in the optimal wear path principle. The arguments utilized for the pure impact wear model will still hold in this case as well. The only exception will be in the position of the crack nucleation point from the surface and the crack propagation quantities will differ depending upon the

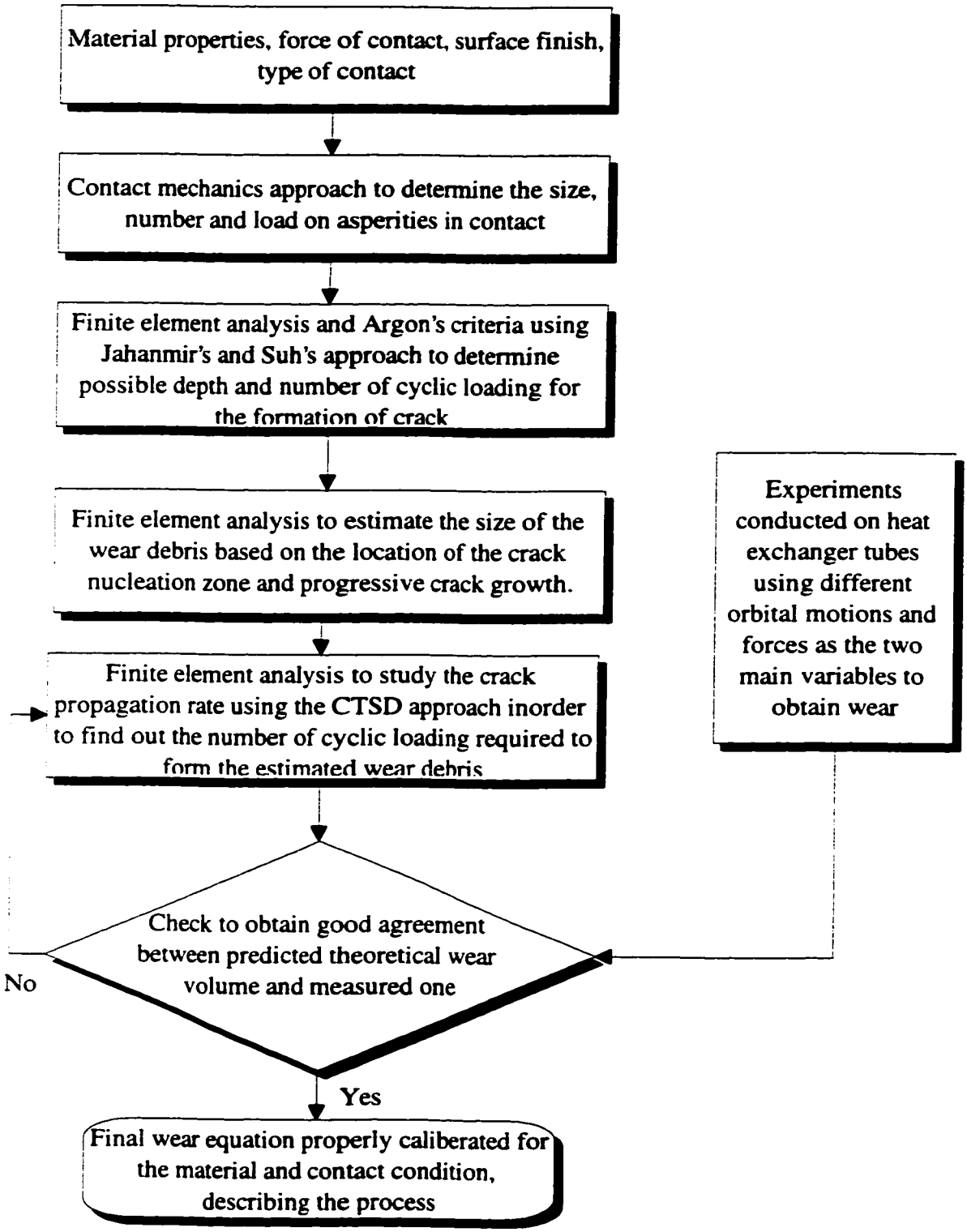

Figure 6.5 Flow chart of the wear model

value of the force and total duration of contact as well as the ratio of normal to tangential force.

The wear of cylinder impacting normally against a conforming cylinder support can be derived in a similar fashion, assuming the wear pattern will follow the rationales described in the optimal wear path principle. The arguments utilized for the oblique impact wear model still holds in this case as well. Due to the loading condition the position of the crack nucleation point from the surface and the crack propagation quantities may vary slightly. This will be taken into consideration, during the calibration of the model. From the general oblique impact wear model, a normal impact wear equation can be formulated. This equation which heavily relies on fracture mechanics, is derived, with the subsequent reasonable assumptions listed (similar to that of the oblique impact):

a. All the conditions stated for oblique impact except condition (g) are valid here as well.

b. The total number of asperity contacts remain constant for the entire wear process provided the maximum impact force is maintained constant.

$$w = \frac{3\bar{P}_0 L^2 h}{2p_{0asp} a_{asp}^2}\left[\frac{n}{N_{tc(i)}}\right] \tag{6.17}$$

where,

$N_{tc(i)}$ = total number of impacts to obtain a wear debris of volume w_a

This equation implies that the debris formation is not a continuous process, but rather one that involves an incubation period after the complete removal of a layer. This observation is

analogous to the one given in the delamination theory of wear, where debris formation is layer by layer, controlled by the crack propagation rate. Therefore, the total wear depth is calculated from the equation relating the total wear volume to the summation of the individual volume of wear and the wear geometry is assumed to follow Engle's optimal wear path principle [28].

Given the fact that asperity contact distribution is more, where the macro-pressure distribution is high, the wear of the surface will not be even. This is in agreement with Engle's experimental observations for impacting bodies, where the wearing body curvature will continuously vary until conformance of the two bodies are reached. This process will be enforced even though wear is said to form layer by layer. The implication of this occurrence is that more layers will be worn at the position where the asperity distribution is denser than at the edge of the contact.

The different terms in the wear equation are calculated from contact mechanics taking into account the microscopic contact of asperities of the of rough surfaces and fracture mechanics. The number of asperity contacts is calculated based on the assumption that the average contact interface pressure is taken as the hardness of the softer material (plastic flow pressure) [79-81], even though each asperity contact has elliptical pressure distribution. The macro contact of the cylinder in a conforming support is calculated using the Hertzian contact equation which was verified using a finite element model developed using ANSYS in the previous chapter.

The position where crack nucleation is most likely to occur is calculated using a finite element method employing Argon's criteria. The crack propagation rate is estimated using the Crack Tip Sliding Displacement (CTSD), where the overall relative crack tip sliding displacement is calculated from the model for the applied load. The analysis is carried out for the complex loading condition using the finite element model developed for a subsurface crack. All the above stress calculations for crack nucleation and propagation for all the three cases of normal and oblique impact are shown in the previous chapter.

The determination of the wear profile for the given geometry can be calculated by using Engel's approach of wear model of a cylinder within a cylinder. According to the optimal wear path principle the wear curvature surface is equal to the geometric Hertzian contact of the two objects and proceeds in a manner which will conform the shape of the wearing object to the curvature of the hard object.

The equations for determining the progressive wear is given in Chapter 3. However, it is observed in this chapter that since the amount of wear depth is far more than that which can be described using this equation the wear will be assumed to follow the radius of the support, in accordance with the rationales of the optimal wear path principle. Hence, following this justification, a purely geometrical approach is used to obtain a relationship between the wear depth and the total wear volume as (Figure 6.6):

$$w = (h_t + R_2 - R_1)R_2 \sin(\theta_2) + \theta_1 R_1^2 - \theta_2 R_2^2 \qquad \textbf{(6.18)}$$

The value of θ_1 is given from the geometry as:

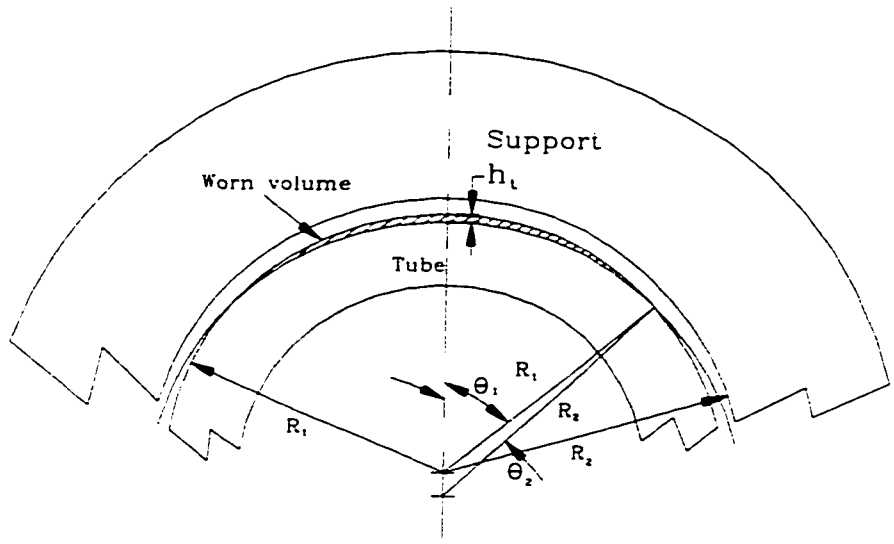

Figure 6.6 Geometry of a worn volume for oblique and normal impact

$$\theta_1 = \cos^{-1}\left(\frac{R_2^2 - R_1^2 - [R_2 - R_1 + h_t]^2}{2(R_2 - R_1 + h_t)R_1}\right) \tag{6.19}$$

and that of θ_2 is given by:

$$\theta_2 = \cos^{-1}\left(\frac{R_2^2 - R_1^2 + [R_2 - R_1 + h_t]^2}{2(R_2 - R_1 + h_t)R_2}\right) \tag{6.20}$$

Using the above equation (6.17), the wear depth can be expressed as an approximate function of the wear volume. Substituting this value of R_1 into the previous equation relating the wear depth and volume following Engle's optimal wear path principle, one obtains the overall wear depth which is critical in determining the life of a tube in a heat exchanger.

$$h_t = f^n(w) \tag{6.21}$$

A typical plot of this relationship is shown in Figure 6.7, giving the approximate relationship that exists between the wear volume and the depth, for a cylinder of 9.15 mm radius support and 8.73 mm radius tube. Using this relationship good results were obtained for the experimental wear depth, obtained from a tube impacting and sliding in a cylindrical support as reported by Hofmann et al. [83]. A typical result for a case of impact gave 40 μm as opposed to 38 μm for the estimate.

The next step is to derive the wear model of a tube sliding purely in a cylindrical support with a diametral clearance of d_c. This model can be derived using a similar approach like the oblique and normal impact models derived earlier, in this sections. The contact mechanics approach supported by the geometric approach, can be utilized to arrive at a sliding wear model that heavily relies on fracture mechanics, with the following reasonable assumptions similar to the ones given in oblique and normal impact:

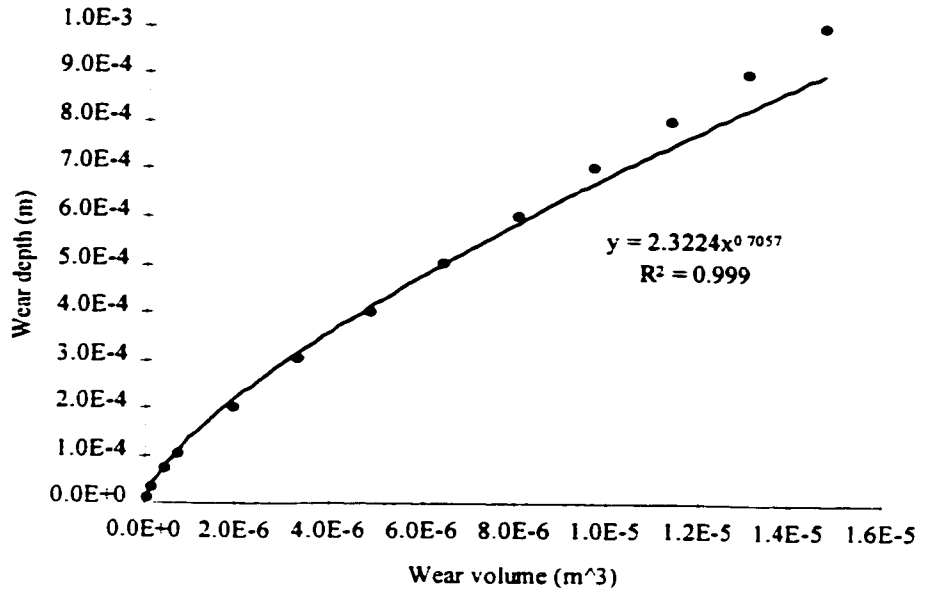

Figure 6.7 Relationship of wear depth vs wear volume for impact wear

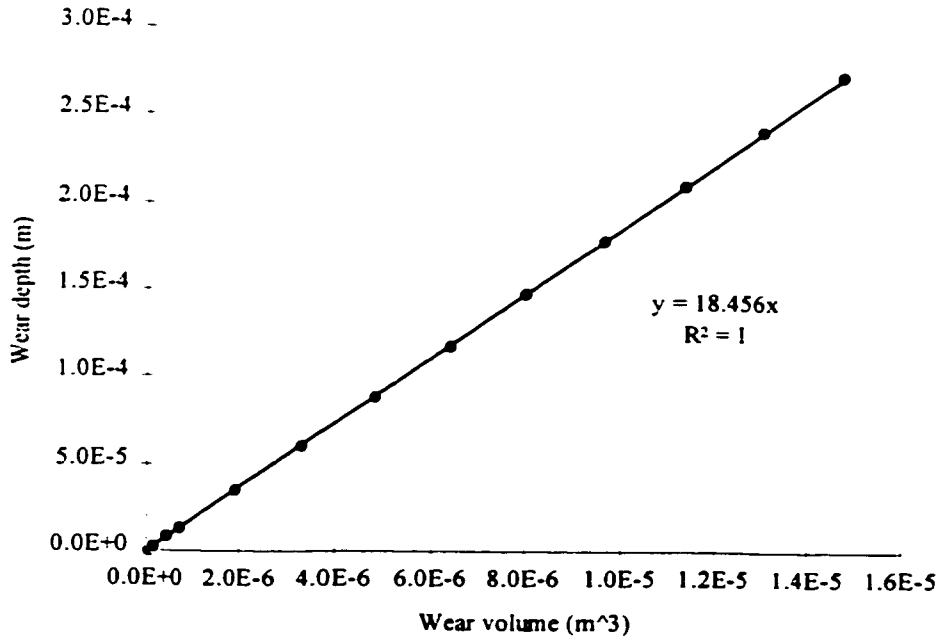

Figure 6.8 Relationship of wear depth vs wear volume for sliding wear

a. All the assumptions stated for the case of oblique impact are taken to be valid here as well, except for condition (g).

b. The total number of asperity contact remains constant for the entire wear process provided the maximum contact force is maintained constant.

c. The number of wear particles is proportional to the number of leading asperities in contact assuming these asperities are evenly spaced over the surface

Since the total sliding distance of a tube inside a cylindrical support with a diametral clearance of d_c is πd_c, the wear equation can be written as:

$$w = \pi L^2 h n_a n_{cl} \left(\frac{\pi d_c}{2a} \right) \left[\frac{n}{N_{tc(s)}} \right] \tag{6.22}$$

In the above equation, the value of cyclic loading depends on the number of times a cracked zone is passed by an asperity. Therefore the final wear equation is given by:

$$w = \frac{3L^2 h \bar{P}_0}{2 p_{0asp} a_{asp}^2} \sqrt{\frac{6\bar{P}_0}{a_{wt} \pi p_{0asp} a_{asp}^2} \left(\frac{\bar{P}_0 R}{\pi E^* a_{wt}} \right)^{1/2}} \left[\frac{\pi (R_2 - R_1)}{2} \left(\frac{\pi E^* a_{wt}}{\bar{P}_0 R} \right)^{1/2} \right] \left[\frac{n}{N_{tc(s)}} \right] \tag{6.23}$$

The only difference between the equation for normal and oblique impact and the one for sliding above, is that the radius of the wearing cylinder does not try to conform to the radius of the support but rather decreases continuously resulting in the following equation for the volume worn:

$$w = \pi \left(R_{1org}^2 - R_1^2 \right) = \pi \left(2 h_t R_{1org} - h_t^2 \right) \tag{6.24}$$

where

$$R_1 = R_{1org} - h_t \tag{6.25}$$

The above two equations can be used to express the wear depth in terms of the wear volume. Therefore the wear depth equation can be expressed as:

$$h_t = R_{1org} - \sqrt{R_{1org}^2 - \frac{w}{\pi}} \tag{6.26}$$

This equation is plotted in the form of a chart (Figure 6.8) for a typical case and it can be seen that there is an almost linear relationship between wear depth and the total wear volume. The remaining aspect of the wear equation is to quantify the fracture mechanics quantities required to initiate a crack and propagate it until a critical length is reached and a debris is formed. This analysis was already performed in the previous chapter which dealt with the stress analysis for complex type of loading and non linear material properties. A comparative analysis of the three wear models will be provided in the next section.

6.3 Theoretical Model for Wear

The three wear equations used in calculating the wear volume are derived in the previous section of this chapter. They are rewritten here to show the structure of the models and their relative differences and similarities. The models are also arranged by lumping up some of the parameters, to demonstrate the relationship of the wear volume to the applied load. Therefore the wear models corresponding to the three contact conditions are given by the following equations respectively:

$$w = K\bar{P}_0\left[\frac{n}{N_{tc(i)}}\right] = K_{ni}\bar{P}_0 n \tag{6.27}$$

for normal impact,

$$w = K\bar{P}_0\sqrt{\frac{6\bar{P}_0}{a_{wt}\pi p_{0asp}a_{asp}^2}\left(\frac{\bar{P}_0 R}{\pi E^* a_{wt}}\right)^{1/2}}\left[\frac{n}{N_{tc(o)}}\right]\left(1+\frac{\nu\cos(\theta)\sqrt{\pi^2\bar{m}_c\ln(8a_{wh}^3E^*/R\bar{P}_0)/2a_{wh}E^*}}{\sqrt{4\pi a a_{wt}p_{oasp}a_{asp}^2/3\bar{P}_0}}\right)$$

$$= K_{oi}\bar{P}_0^{7/4}[1+k_{oi1}\bar{P}_0^{1/2}\ln(k_{oi2}/\bar{P}_0)^{1/2}]n \qquad \textbf{(6.28)}$$

for oblique impact and

$$w = K\bar{P}_0\sqrt{\frac{6\bar{P}_0}{a_{wt}\pi p_{0asp}a_{asp}^2}\left(\frac{\bar{P}_0 R}{\pi E^* a_{wt}}\right)^{1/2}}\left[\frac{\pi(R_2-R_1)}{2}\left(\frac{\pi E^* a_{wt}}{\bar{P}_0 R}\right)^{1/2}\right]\left[\frac{n}{N_{tc(s)}}\right]$$

$$= K_{ps}\bar{P}_0^{5/4}n \qquad \textbf{(6.29)}$$

for sliding wear.

K is taken to be the same for the same material combination, surface finish and magnitude of loading. The type of loading and interaction between the contacting materials, dictates the equation to be used. The difference in the above three equations is the fact that the crack propagation rate is not the same for all three, because of the effect of friction at the surface, and also the fact that far field stress will cause some amount of propagation as the asperity slides over the subsurface crack. The three sets of equations given above for normal impact, oblique impact and sliding motions are expressed in terms of the load and cycle. From the experimental validation it can be seen that the crack propagation rate for oblique impact and sliding is more or less similar and that of impact is slightly lower than these two.

The final equations are, among other factors, a linear function of the critical debris length L. This is mainly due to the fact that the wear volume of a debris is assumed to grow axisymmetrically beginning at the crack nucleation center. This argument is valid as long as the applied load is large enough to ensure that the crack propagation is in a uniform axisymmetric fashion. As the crack grows in size the critical stress zone is limited to within the vicinity of the contacting asperity. Therefore, in the case of sliding where the critical crack length could subsequently grow parallel to the sliding motion (not axi-symmetrically), the wear model is insensitive to the critical length, because the volume will no longer be proportional to L^2. This is also the case where the asperity impact point is not the same for subsequent cyclic loading, implying a debris cross section that is not circular (axi-symmetric) but rather rectangular. The values of the CTSD given in Table 5.2 are listed for different parameters. The one corresponding to $5k$ with an interface friction coefficient of 1 is taken as the CTSD for this analysis. The value of the friction coefficient is taken this high to account for the possibility of asperities getting interlocked at the interface.

All the input parameters in the wear model are estimated theoretically from the finite element analysis or are measured from the transducers (force and displacement). The results ensuing the identification of the crack nucleation region and number of cyclic load required to generate a crack, and the crack propagation values to estimate the total number of cyclic loading to produce one debris, are all required in the equation. The number of asperities in contact are estimated from the applied force and the average maximum Hertzian contact pressure value of $5k$.

6.4 Experimental Validation of the Theoretical Wear Model

Since the ultimate goal of this research work is to properly characterize wear, the new mathematical model is used to verify experimental results in this section. The verification of the proposed wear model is crucial in substantiating the validity of this approach. Hence, in accordance with the derived wear equations and various analytical as well as numerical results describing the wear process, an attempt was made, to compare the predicted wear volume using purely theoretical approach. All the quantities were estimated from the finite element analysis or the input given to the setup. The impact or sliding force value for estimating the wear is taken from the measured force value (rms) and the number of excitation and average sliding distances are estimated from the input and display respectively. The quantities L, h, n_a, d_c, n_{ct}, a and $N_{tc(m)}$, were estimated theoretically or taken from the geometry of the tube and support, to arrive at the wear volume.

Taking into account the difference between the theoretical and experimental values, a best fit line is chosen for the theoretical vs actual wear volume and adjusted accordingly. The study was conducted by introducing a linear regression analysis to plot this relationship. The equation utilized for this analysis was using the least square approximation method, where the value of the slope m and intercept b is given by:

$$m = \frac{n_d \Sigma xy - \Sigma x \Sigma y}{n_d \Sigma (x^2) - (\Sigma x)^2}$$

$$b = \frac{\Sigma y \Sigma (x^2) - \Sigma x \Sigma xy}{n_d \Sigma (x^2) - (\Sigma x)^2} \qquad \textbf{(6.30)}$$

where,

x = independent variable

y = dependent variable of x

n_d = number of pairs of data (x, y)

The error indicator which is known as the R^2 value is given by the following equation:

$$R^2 = 1 - \frac{\Sigma(y-y_{new})^2}{\Sigma(y^2) - (\Sigma y)^2/n_d} \tag{6.31}$$

where,

y_{new} = value of the dependent variable obtained from the best fit equation

It should be noted that if the equation contains all the discrete data, then R^2 will be unity. This implies that the more R^2 approaches unity, the better the equation approximates the actual curve. However, since the linear approximation for some of the data forced the origin to be the intercept point, the quantity b is taken to be zero. This implies that the new equation for the slope of the regression result, is given by:

$$m = \frac{\Sigma xy}{\Sigma(x^2)} \tag{6.32}$$

The above equations were used to obtain a best fit curve and the error estimation quantity in a spread sheet program (Microsoft Excel). Therefore, the CTSD can be adjusted until the independent and dependent variables are the same (slope of unity). The CTSD is assumed to be the same for initial contact conditions, and the value properly calibrated for oblique and normal impact, and sliding motions.

There are three sets of experimental results investigated in this research work, each

categorised for impact and sliding motions. This analysis for the verification of the model, was conducted in three stages. The first one was to obtain the theoretical wear volume by assuming a CTSD value of $4.0*10^{-3}$ μm for normal impact and $8.0*10^{-3}$ μm (assumed because of the effect of loading from far field as it slides over the crack) for sliding and oblique impact. This results in a trend line which shows the relationship between the theoretical wear volume and actual wear volume. The next stage was to randomly select three data points spaced at the maximum, minimum and in between.These values were used to fit a linear trend line, which was used to caliberate the CTSD value, such that the theoretical wear volume is equal to the actual one. The final stage was to select all the experimental data, and adjust the CTSD using the trend line that best approximates all the data point.

The plots of the three lines given in each graph represents the result of the theoretical model, the calibrated model using three data points and the final result obtained from the calibration of all the data. The first three sets depicted in Figures 6.9, 6.10 and 6.11 are results found in open literature [48,83,84] where as the last one shown in Figure 6.12 is from experiments conducted at Concordia University by the author for this research work. In Figure 6.10 a and b the three point calibration is not conducted as the total number of experiments were only three. Hence, the data was plotted only for the theoretical model and calibrated one. It should be noted that the margin of error for the results is not given in the above literature.

The results indicate that the maximum value of the trend line, among all the theoretical cases was nearly 3.7. This is a rather good estimate of the wear volume from first principles. Similar analysis reported in open literature [100] required a factor of about 5000 used to

scale the wear appropriately. It can be observed that the model calibrated using three random data points and all the data points are almost the same for most of the experimental results. This implies that the model can actually be calibrated using some data and use the CTSD obtained from this results. The maximum error occurred at experiments where the wear volume was relatively small, introducing the possibility of errors being magnified. Even though every possible precaution was taken to avoid errors, small wear volumes will have a higher percentage error compared to higher wear volumes.

Results of the theoretical wear model was shown to improve by adjusting the CTSD value for normal impact, oblique impact and sliding motions based on the trend line which relates the theoretical predicted wear volume, to the actual wear volume separately. Figures 6.9-6.12 show the validity of CTSD calibration. Calibration of the result ended up in giving a CTSD value of a minimum of 0.0011 μm in the case of pure impact and a maximum of 0.0071 μm for pure sliding contact conditions. It should be noted that there were no experimental constants. The actual wear volume is used to properly calibrate a quantity that would have been difficult to determine otherwise. Even though most of the wear models on fretting wear data, normally require experimental investigations to determine some experimental constants for the proper characterization of the wear volume, this model does not. This is mainly because it is based on a physical understanding of the process.

6.4 Conclusion

This chapter presented a wear model which is applicable to low level force contact condition

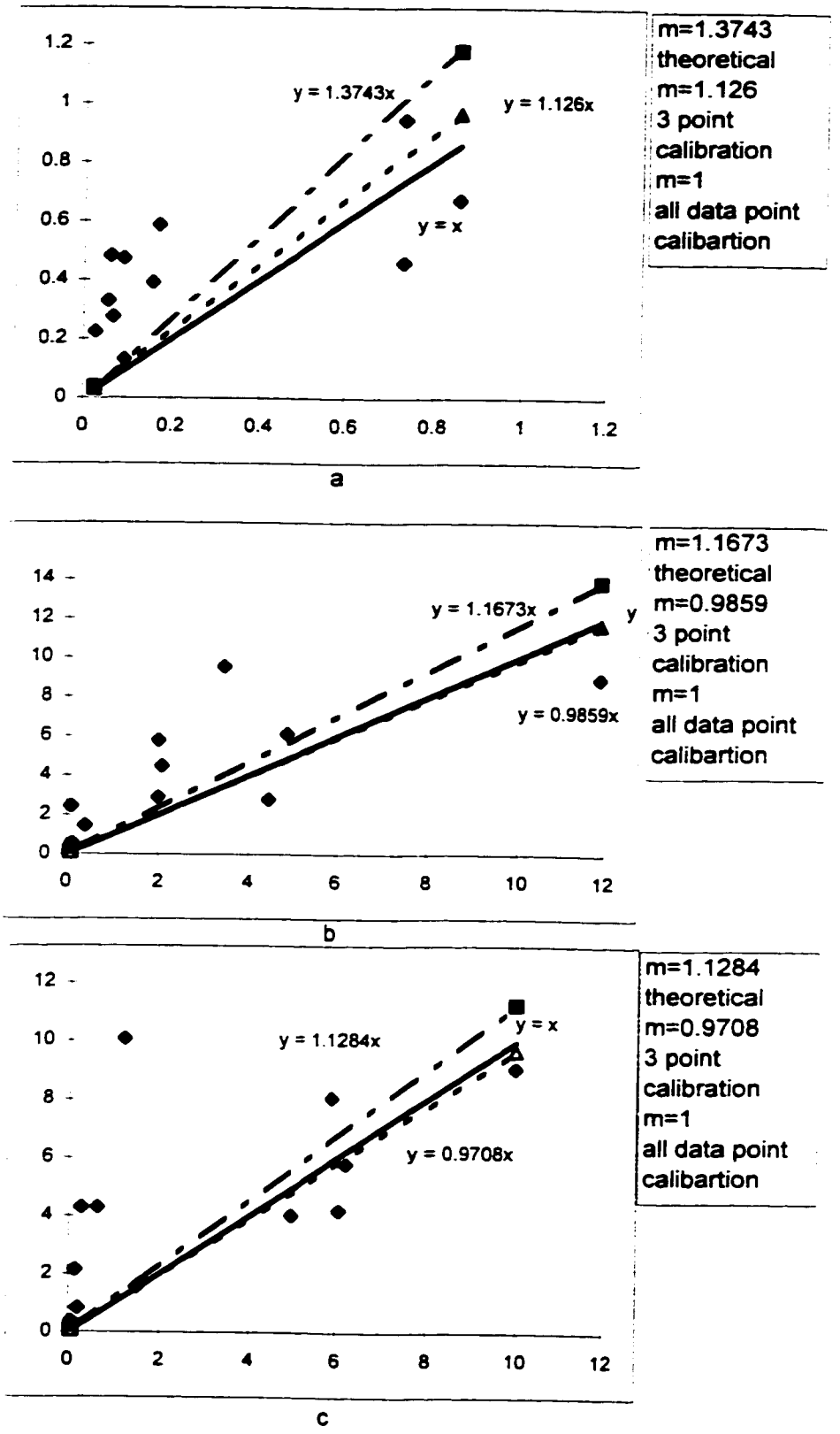

Figure 6.9 Theoretical vs actual wear for a) normal impact b) sliding and c) oblique impact [84]

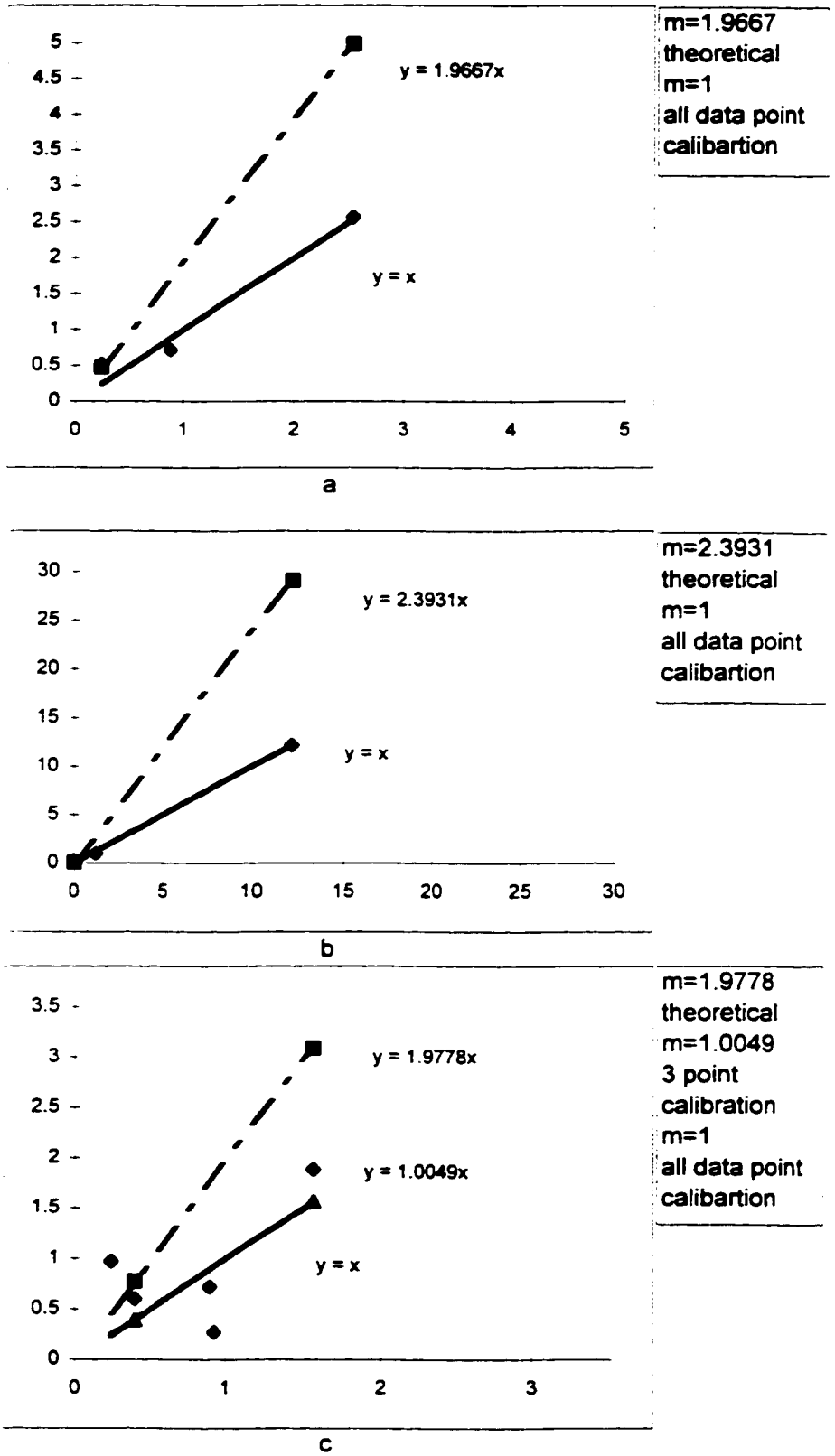

Figure 6.10 Theoretical vs actual wear for a) normal impact b) sliding and c) oblique impact [83]

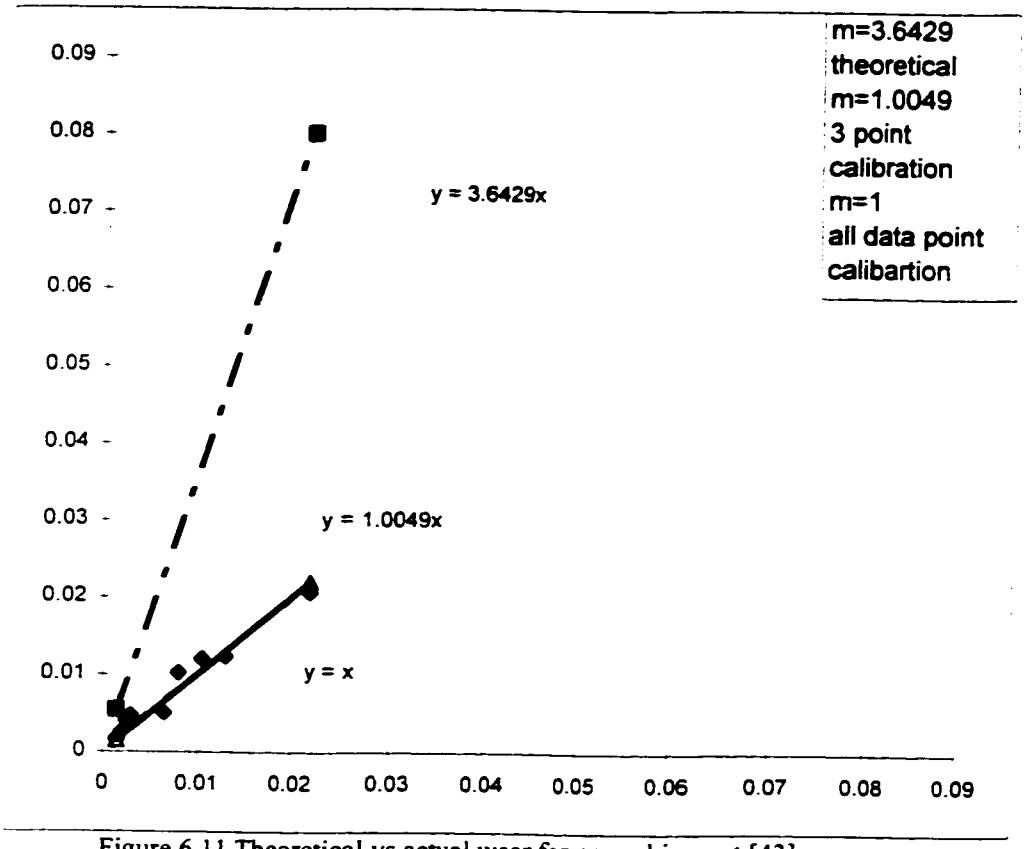

Figure 6.11 Theoretical vs actual wear for normal impact [43]

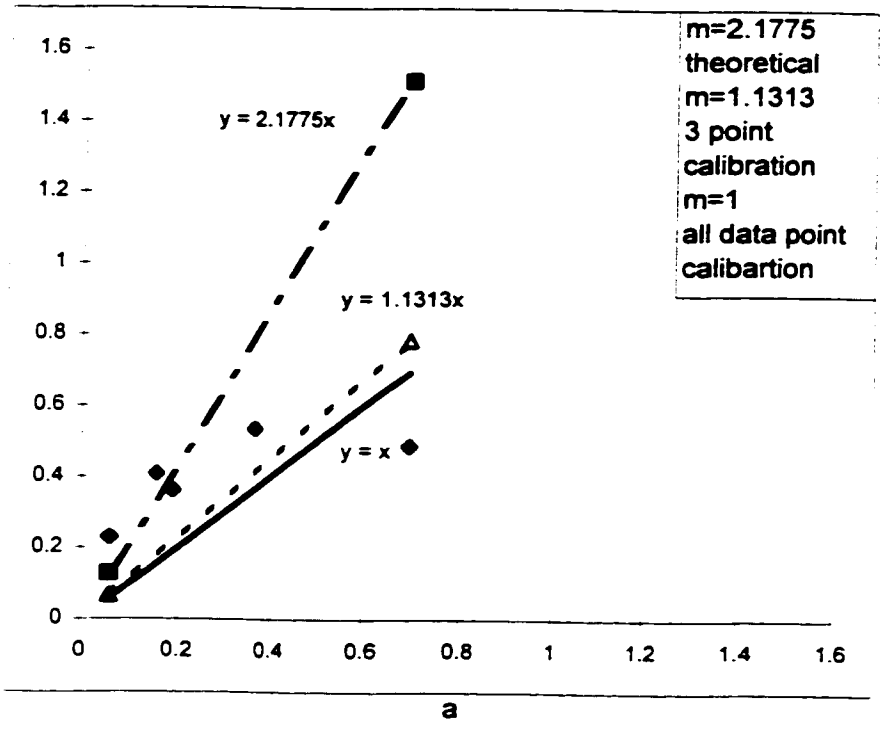

a

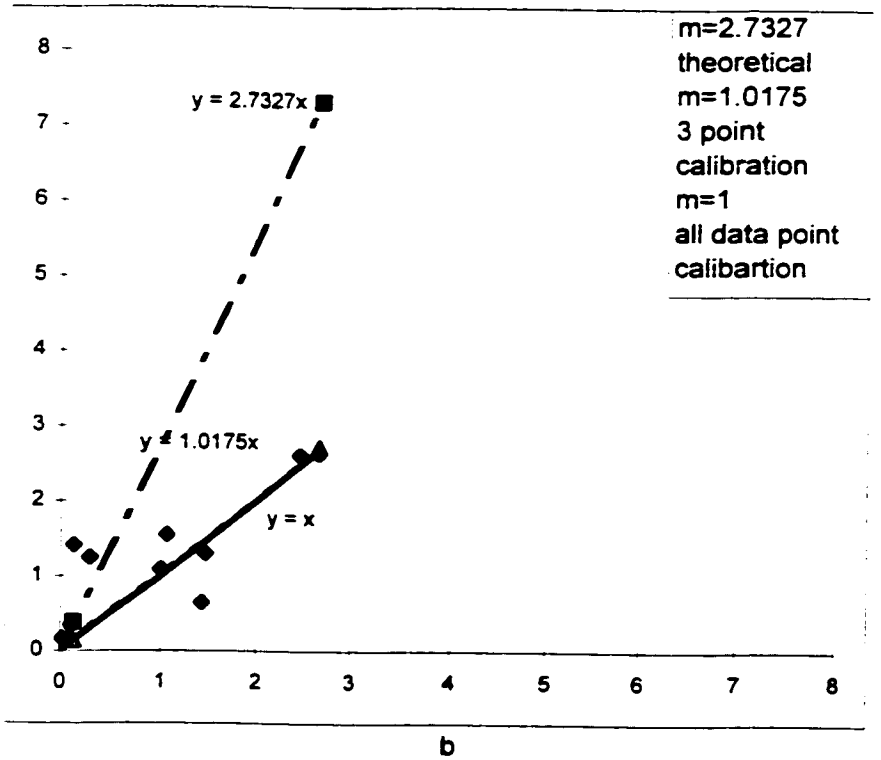

b

Figure 6.12 Theoretical vs actual wear for a) normal impact and b) sliding

(force does not cause global plastic deformation at the contact) involving normal impact, oblique impact and sliding type of relative motions. It is evident that the appropriate characterization parameter should include a combination of the applied load and number of cyclic loading. However, it should be noted that depending upon the type of motion, geometry could play a crucial role as well.

If the motion of contact is normal or oblique impact, then the wear will proceed in a manner such that the two radii will try to conform, implying an increase in the number of asperities in contact which in turn will reduce the subsurface shear stress which is responsible for the formation of wear. If on the other hand the wear is of pure sliding type the radius of the wearing tube will continuously reduce implying a reduction in the average area of contact which will further result in an increased shear stress at the subsurface level responsible for the formation of wear debris.

It is apparent that accurate determination of the wear volume requires validation of the theoretical model. Following this study, the next step is to analyse the experimental results using known characterization parameters, and a new characterization parameter which will implement the above new wear model. The theoretical model will be expanded to handle the problem for better results as will be seen in the next chapter. The characterization parameter of the wear rate in nuclear power plant heat exchangers will be investigated using existing parameters and proposed ones against the conducted long term experiments.

CHAPTER 7

WEAR CHARACTERIZATION PARAMETER

7.1 Characterization of Wear

Work rate is the commonly accepted characterization parameter for wear rate. This parameter was introduced by Frick [44] and is defined as the product of the normal force and sliding distance per unit time. However, there were some discrepancies with regards to the validity of this quantity as an appropriate scaling parameter. This has been indicated in the literature survey of Chapter 2 as well as in the theoretical analysis conducted using existing generalized wear model in Chapter 3, for the various orbital motion and geometry combination. This chapter will present a new characterization parameter based on the wear model derived in Chapter 6, and also give a comparison with the conventional work rate and the modified work rate derived by Hofmann et al. [5]. A flow chart for this procedure is given in Figure 7.1. [107, 111] (Author's Ref.)

7.2 Conventional Characterization Parameter

The conventional quantity used to characterize the wear rate involved in a nuclear power plant heat exchanger, as mentioned earlier, is the work rate. The work rate is defined as the product of the normal force and sliding distance divided by the time. While using discrete approach it is crucial to ensure sufficient sampling rate of the required data, in order to

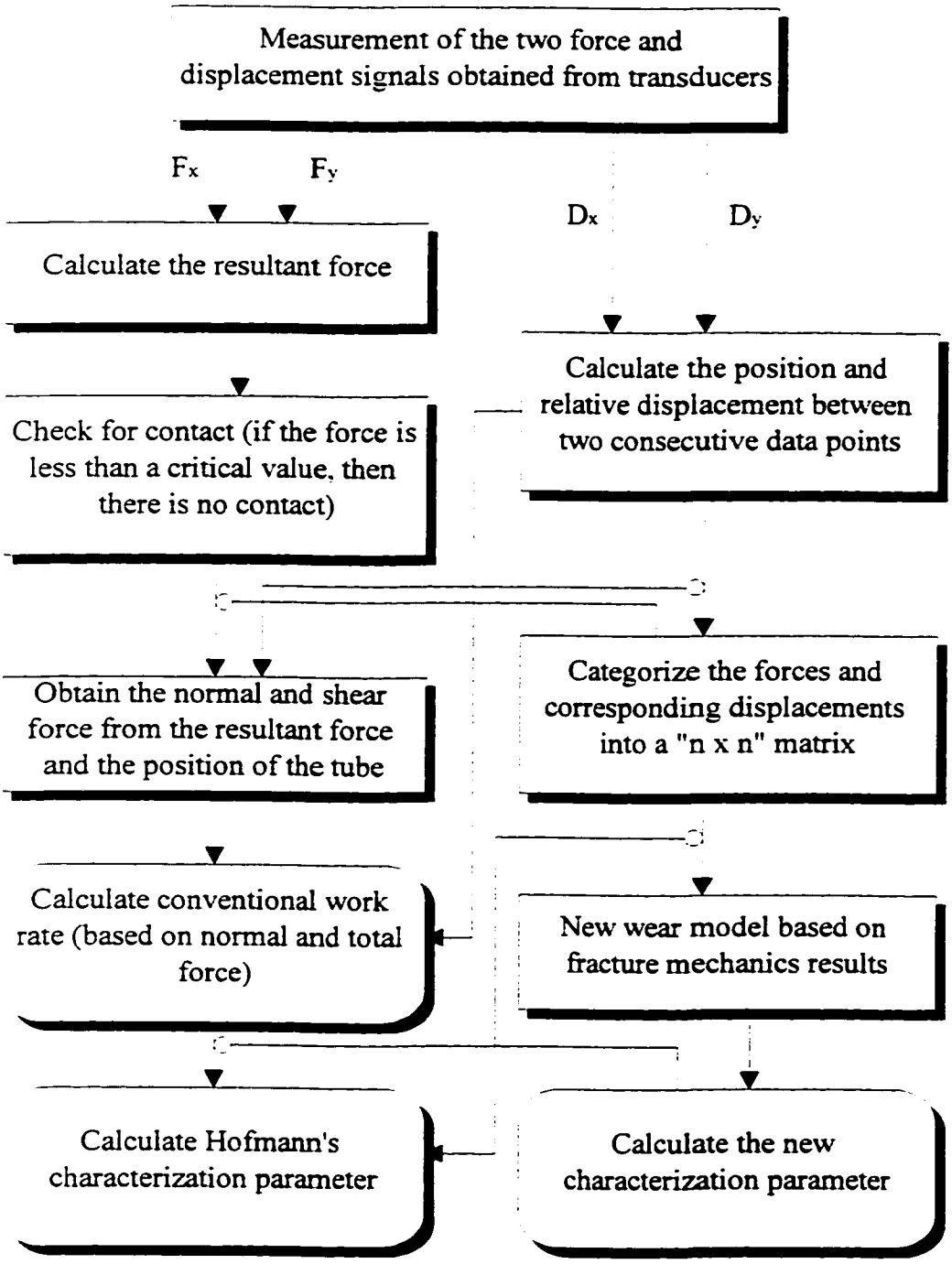

Figure 7.1 Flow chart of the characterization model

increase the accuracy of the experiment. If there are n_f measured displacement and force signals scanned at a rate of n_s Hz then the work rate is:

$$W_R = \frac{n_s}{n_f} \sum_{i=1}^{i=n_f-1} \frac{F_{ni} + F_{n(i+1)}}{2} (D_{i+1} - D_i) \qquad (7.1)$$

where,

F_{ni} = normal force at time i corresponding to displacement D_i at time i

This characterization parameter can be utilized to investigate the wear occurring on heat exchanger tubes. However, as mentioned earlier direct use of this quantity could introduce significant errors that could lead to faulty results. The measurement of the normal force is determined from the phase difference between the resultant force vector and the resultant displacement vector. Since this may introduce some experimental error, it is appropriate to consider the measured (resultant) force multiplied by the distance for the work rate. The plot of the conventional work rate (based on the resultant force) vs wear rate, obtained from both experimental setups (The single span heat exchanger tube fretting rig borrowed from Ontario Hydro as well as the one built at Concordia University) is given by Figure 7.2. As can be seen from this plot, the scatter is considerable. The R^2 quantity which is a measure of the overall scatter indicates that there is room for improvement. Because of this type of scatter evident in the experimental data, Hofmann et al. [5] expanded their work to better characterize wear using the work rate quantity, by introducing empirical scaling factors.

7.3 Hofmann's Characterization Parameter

The empirical derivation of the new characterization parameter by Hofmann et al.[5]

S = 3, 4 ($F_x/F_y = 1$)
Osc S = 8, 9 (Oscillatory sliding motion)
I = 1, 5, 12 ($F_x/F_y = 0$)
O = 2, 6, 7, 10, 11, 13, 14 ($0 < F_x/F_y < 1$)

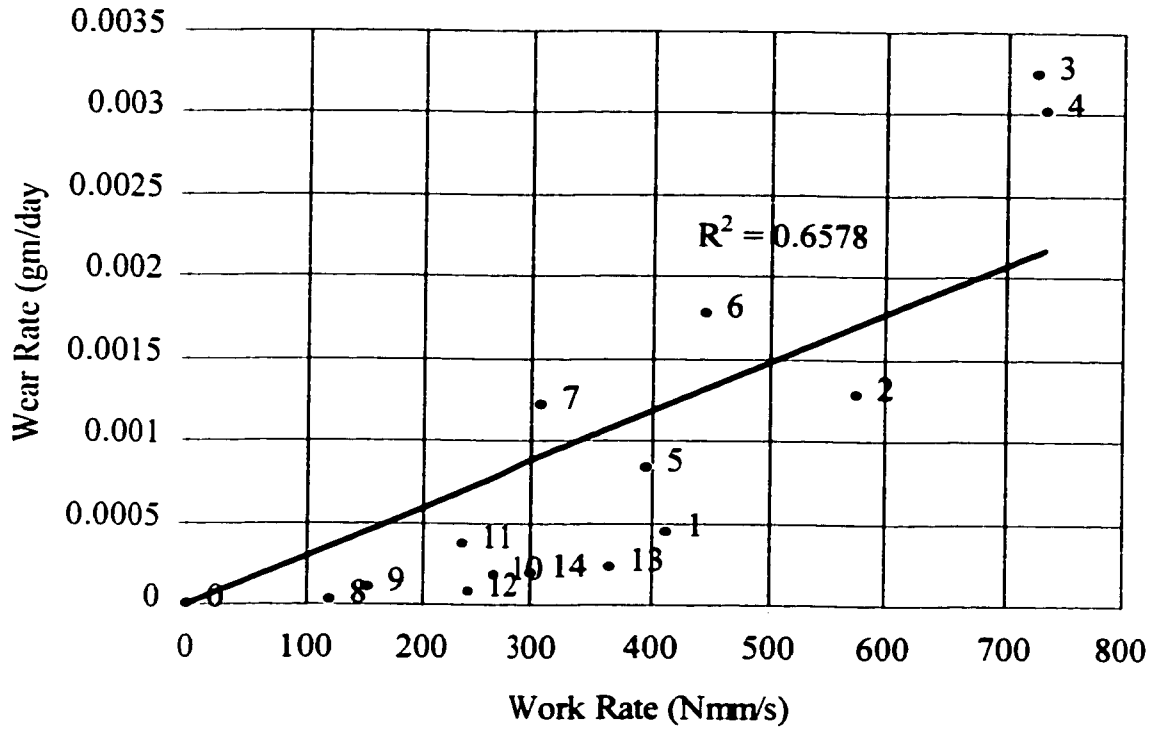

Figure 7.2 Wear rate vs work rate analysis for the experimental data collected from the single span heat exchanger fretting wear rigs, borrowed from Ontario Hydro and also built at Concordia University.

revolves around the introduction of a wear intensity factor into the conventional wear rate / work rate equation to scale its value for the type of orbital motion involved in the wear process. They carried out a well controlled experimental study to investigate the wear rate of Inconel 600 as a function of work rate, in simulated steam generator environments and excitation conditions. The tests were carried out in pressurized water at 200^{0}C, with excitation frequency in the range of 33-46 Hz. During the course of their tests, contact forces and tube displacement were directly measured, with high sampling rate for accurate estimation of the work rate.

Hofmann et al. [5] suggested that for a pure impacting motion, where the contact time is less than 0.5 ms, some type of non-linear correlation must exist, and that wear rate prediction requires the introduction of a third independent variable, in addition to work rate. In their attempt to understand the non uniqueness of the wear rate / work rate relationship, they carefully examined the impact forces and sliding distances of those tests which have approximately the same work rate but have an order of magnitude difference in their wear rates. To characterize the stresses and interactions introduced into these two cases, they used the following approach.

Their approach utilizes the data on frequency of contacts with certain sliding velocity and contact force classes. Examples of the three dimensional graphs, low and high wear rate tests (under the same work rate input) were given in reference[5]. They concluded that the high wear rates were obtained when high sliding velocities were measured. They also made an interesting observation regarding the wear reducing effect of interspersed perpendicular

contacts with high contact forces and extremely small sliding velocities. They argued that in the case of impact/sliding the contribution of these two types of motion operate in opposite directions. While sliding motion is a wear enhancing factor as it induces tensile stresses in the contact zone, impact with small contact forces can act as a wear reducing factor. The beneficial effect can be attributed to work hardening, and the elastic and plastic compressive stresses induced in the surface asperities without wear. This argument explains in part that when these two types of motion are combined, the resultant tensile stresses will be reduced, and may lead to smaller wear rates. With this understanding, Hofmann et al. developed a wear model which is based on the following assumptions:

1. In sliding wear, the wear rate is proportional to the square of the sliding velocity and is directly proportional to the normal contact force
2. In impact induced fatigue wear, the wear rate is proportional to the cube of the impact force and to the number of impact cycle N, after reaching the incubation period. This assumption is based on Engle's analysis and experimental observations.

Consequently Hofmann et al. suggested to modify the conventional wear rate/work rate relationship by introducing an additional "overall wear intensity factor" to accommodate the wear enhancing and wear reducing effects. These factors were lumped up into the multiplication factor known as the wear intensity factor. This approach is shown in Table 7.1, which indicates how the categorization is performed.

$$w_r = k_3 W_{int} W_R \tag{7.2}$$

where,

k_3 = specific wear rate (estimated by means of a reference test under oscillating sliding condition)

sliding condition)

W_{int} = overall wear intensity factor

W_R = average work-rate

Table 7.1 Weighted multiplication factor for the characterization of work rate

$MF_{S1I} \setminus MF_{I1I}$	MF_{I12}	MF_{I13}	MF_{I14}	MF_{I15}
MF_{S21}	MF_{S22}	MF_{S23}	MF_{S24}	MF_{S25}
MF_{S31}	MF_{S32}	MF_{S33}	MF_{S34}	MF_{S35}
MF_{S41}	MF_{S42}	MF_{S43}	MF_{S44}	MF_{S45}
MF_{S51}	MF_{S52}	MF_{S53}	MF_{S54}	MF_{S55}

The multiplication factors are defined for sliding and impact separately and the weighted percentage of impact and sliding wear are given respectively as follows:

$$MF_I = \sum_{i=1}^{i=5} M_{I1i} = \sum_{i=1}^{i=5} k_{H1}(F_i/k_{H2})^3 p_{1i} \tag{7.3}$$

and

$$MF_S = \sum_{i=1}^{i=5}\sum_{j=2}^{j=5} M_{Sij} + M_{S11} = \sum_{i=1}^{i=5}\sum_{j=2}^{j=5} F_i(D_j)^2 p_{ij} + F_1(D_1)^2 p_{11} \tag{7.4}$$

where,

k_{H1} and k_{H2} are material dependant constants

p_{ij} = percentage of F_i D_j category (class of F_i=0-0.2F_{max}, class of D_j=0-0.2D_{max}, etc.)

F_i = average normal force category ($F_1 = 0.1F_{max}$, etc.)

D_i = average displacement for sliding category ($D_1 = 0.1D_{max}$, etc.)

The overall wear intensity factor is formulated in terms of the frequency in percent of sliding and impacting. For impacting conditions (small sliding velocity class), a non-dimensional

wear reducing factor. In contrast, for sliding conditions (high sliding velocity classes), a non-dimensional sliding wear weighing factor which is proportional to the square of the sliding velocity, is used as the wear enhancing factor. Hofmann et al. presented in [5] an empirical method for obtaining the weighted percentage of work hardening and the weighted percentage of sliding wear in terms of the respective weighing factors. Some of the constants in this formulation are material dependent and should be obtained experimentally. The overall wear intensity factor which can be considered as a correction factor of the average work rate is the given by the following relationship:

$$W_{int} = \frac{[MF_S]^2}{MF_I + MF_S} \tag{7.5}$$

In their analysis, Hofmann et al.[5] used 100N for F_{max} and 10μm for D_{max} to calculate the wear intensity factor. In the analysis of the experimental results obtained from the fretting wear tests conducted at Concordia University, the errors obtained for the characterization parameter (modified work rate) by following the procedure were too high. Hence, the force -displacement weighted percentage matrix was obtained by taking the maximum value of the applied force and measured displacement and dividing these values into five to obtain the 5x5 matrix for each experiment. The calculation of the wear intensity factor was done using a spread sheet program after obtaining the percentage distribution using the program which was developed on the G code compiler (LabView).

The value of W_{int} was optimized for the linear curve, until the highest R^2 value was obtained. The work rate / wear rate relationship plot along with its R^2 value can be seen in Figure 7.3a. Since the error was found to be very high, a variation of the wear intensity factor (equation

7.5) was implemented by changing the power of the numerator to unity. A considerable improvement was obtained (Figure 7.3b). This implies that the sliding weighted percentage ratio should be taken with respect to the sum of sliding and impact weighted percentages. It should be noted that, this process is in violation of the proposed methodology as given in the reference[5]. Because of the failure of the proposed methodology, a new analysis will be derived based on the wear models derived in chapter 6 and result will be examined in relation to the above models.

7.4 The Proposed Asperity Contact Dependent Characterization Parameter

A new wear model which is applicable to low level force contact condition involving oblique impact, normal impact and sliding type of relative motions was derived in Chapter 6. The proper characterization parameter can be derived from this model ensuing some mathematical simplifications. It is apparent that the appropriate characterization parameter is evidently a combination of the load applied and the frequency this load is applied at. However. it should be noted that depending upon the type of motion, geometry could play a crucial role as well.

Because of the nature of the experiment it is not uncommon to have a complex motion of the tube within the support involving impact as well as sliding conditions. The wear models derived using the appropriate assumptions in Chapter 6 will be used as a basis for arriving at a generalized characterization parameter better suited to describe the wear occurring due to the complex motions evident in this situation. The experiment conducted showed that even

S = 3, 4 ($F_x/F_y = 1$), Osc S = 8, 9 (Oscillatory sliding motion),
I = 1, 5, 12 ($F_x/F_y = 0$) O = 2, 6, 7, 10, 11, 13, 14 ($0 < F_x/F_y < 1$)

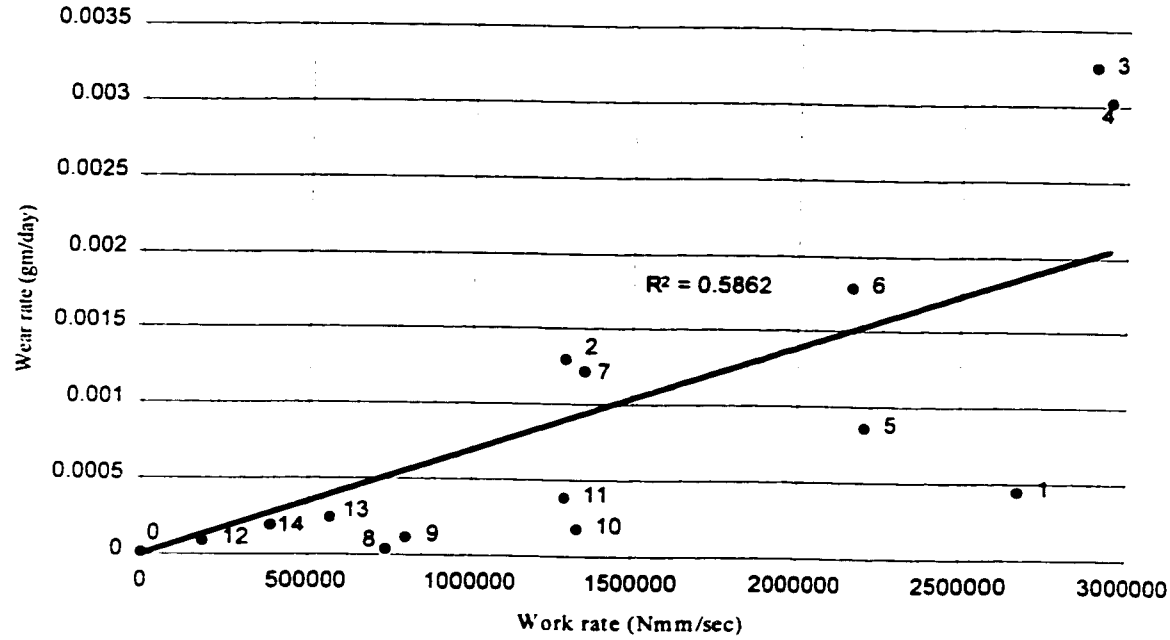

a)

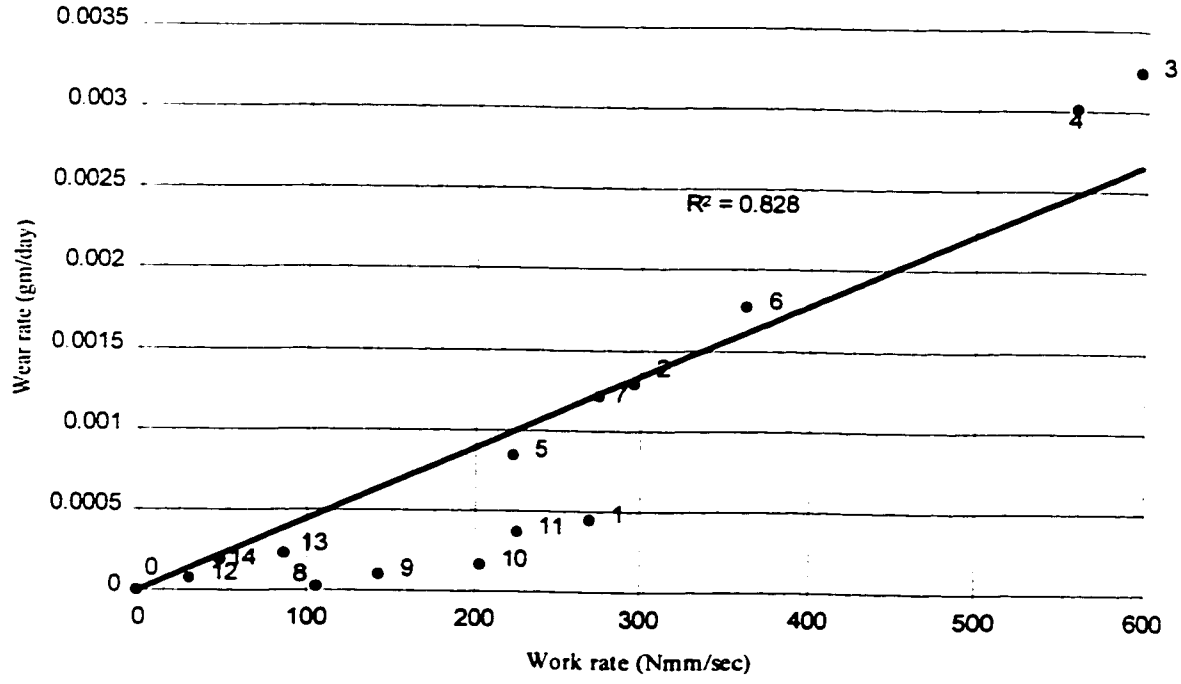

b)

Figure 7.3 Wear rate vs modified work rate relationship as a) given by Hofmann and b) modifying Hofmann's Wear intensity factor

to the complex motions evident in this situation. The experiment conducted showed that even for normal impact type of excitation there was some amount of sliding witnessed in the displacement measurement taken. Hence the generalised sliding wear equation, which as a limiting case, describes the wear due to impact alone will be used in this section to describe the wear process (equation 6.22):

$$w = \pi L^2 h n_a n_{cl} \left(\frac{\pi d_c}{2a} \right) \left[\frac{n_f}{N_{tc(s)}} \right] \tag{7.6}$$

where,

n_f = total excitation cycle

The equation which is given by equation (7.6) can be modified to account for the different percentage of contact force and displacement occurrences. Even though the above equation was derived for pure contact conditions (pure sliding), it is not uncommon to come across real occurrences and experimental investigations involving different motion types with certain percentage combinations. Therefore, the equation can be rewritten to include the effect of impact as well as sliding in a generalized model by considering the percentage of occurrence of impact dominated and sliding dominated wear.

$$w = \pi L^2 h n_a \left[\frac{n_f}{N_{tc(m)}} \right] \left(\frac{\pi d_c}{2a} n_{cl} p_S \right) \tag{7.7}$$

where,

n_{cl} = number of column of asperities parallel to the sliding distance

p_S = percentage of sliding

$N_{tc(m)}$ = Critical cyclic loading applied for impact (m=i) or sliding (m=s)

Since a discrete approach is utilized, the quantity describing the orbital motion πd_c needs to

problem, it is essential to describe the total displacement per cycle associated with the sliding part in terms of the average sliding distance per measurement and total number of data collected per cycle. It should be noted that depending on the type of dominant motion, the critical number of load application has to be set to that corresponding to either impact or sliding from the onset.

$$w = \pi L^2 h n_a \left[\frac{n_f}{N_{tc(m)}}\right]\left(\frac{v_s t^* s_r}{2af} n_{cl} p_S\right) \tag{7.8}$$

The above equation can be further simplified by substituting for n_a (it is a ratio of the applied force to the product of the asperity area A_s and hardness H_d of the softer material) to give:

$$w = \frac{\pi h L^2 P_0 n_f}{A_s H_d N_{tc(m)}}\left(\frac{v_s t^* s_r}{2af} n_{cl} p_S\right) \tag{7.9}$$

where,

s_r = sampling rate

f = frequency of motor excitation

Given the fact that the area of asperity contact is assumed to be equal to the area worn debris which is in the form of a layer, the above equation can be further simplified to the following:

$$w = \frac{h P_0 n_f}{H_d N_{tc(m)}}\left(\frac{v_s t^* s_r}{2af} n_{cl} p_S\right) \tag{7.10}$$

The above equation can be written in the rate form as follows:

$$\dot{w} = \frac{h}{H_d N_{tc(m)}}\left(\frac{v_s t^* s_r}{2af} n_{cl} p_S\right)\frac{P_0 n_f}{T} \tag{7.11}$$

The symbol T in the above equation is the total duration of the wear process. Since the actual experiment involves a total force which is not constant one should substitute the maximum

experiment involves a total force which is not constant one should substitute the maximum measured force by the average or mean force over the duration of the experiment. Therefore the above equation can be rewritten in terms of the average or mean load rate (P_m) defined in Chapter 4 as $\int P(t)dt/T$. From the above equation it is apparent that the appropriate characterization quantity is the mean force rate, scaled properly by the percentages of impact occurrence and sliding motion occurrence. However, from Figure 7.4 and 7.5 it can be seen that the mean force rate and the total work rate are proportional to each other. Hence one can use the conventional work rate quantity in lieu of the mean force rate. This approach can be substantiated using the work rate calculations for an idealised condition of a purely sliding contact of a tube in a hole and partial sliding contact as seen in the figure, for the case of an oblique impact. The work rate and load rate are given by equation (7.12) for the case of pure sliding condition and equation (7.13) for the case of oblique impact conditions.

$$W_R = \frac{2\pi r_c P}{T} \qquad and \qquad P_m = \frac{2\pi P/n}{(2\pi/n)T} = \frac{P}{T} \tag{7.12}$$

where,

r_c = the radial clearance

and also,

$$W_R = \frac{2\theta_1 r_c P}{T} \qquad and \qquad P_m = \frac{2\theta_1 P/n}{(2\pi/n)T} = \frac{\theta_1}{\pi T}P \tag{7.13}$$

It can be seen that a ratio of the work rate to the mean load rate gives a relatively constant value equal to $2\pi r_c$. This is due to the variation of r_c being considerably small, over the duration of the experiment. Therefore substituting the work rate instead of the mean load rate one would obtain the following relationship:

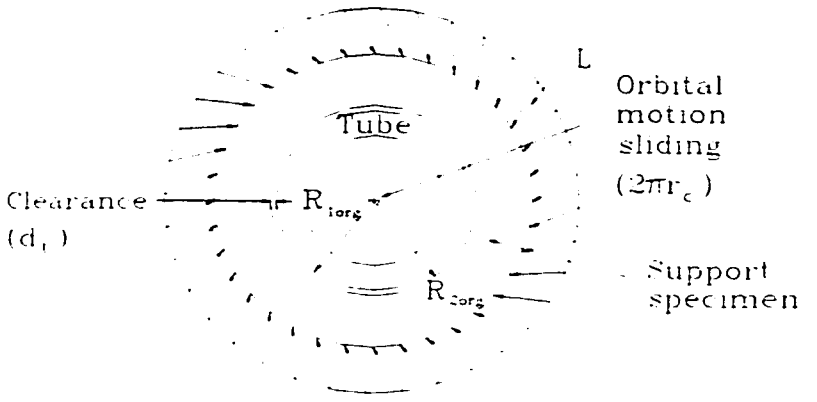

a)

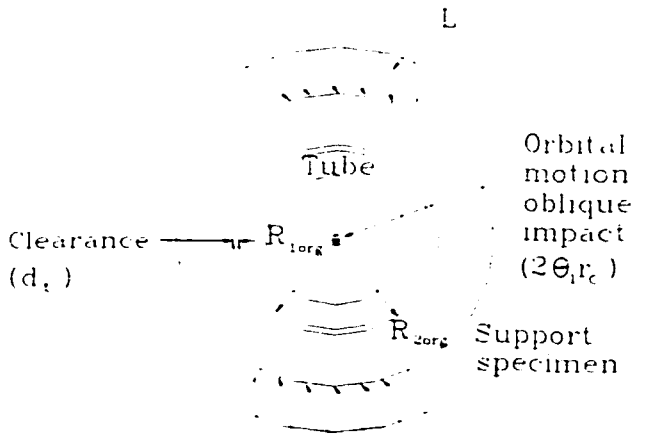

b)

Figure 7.4 representation of idealised force for a) sliding motion and b) oblique impact

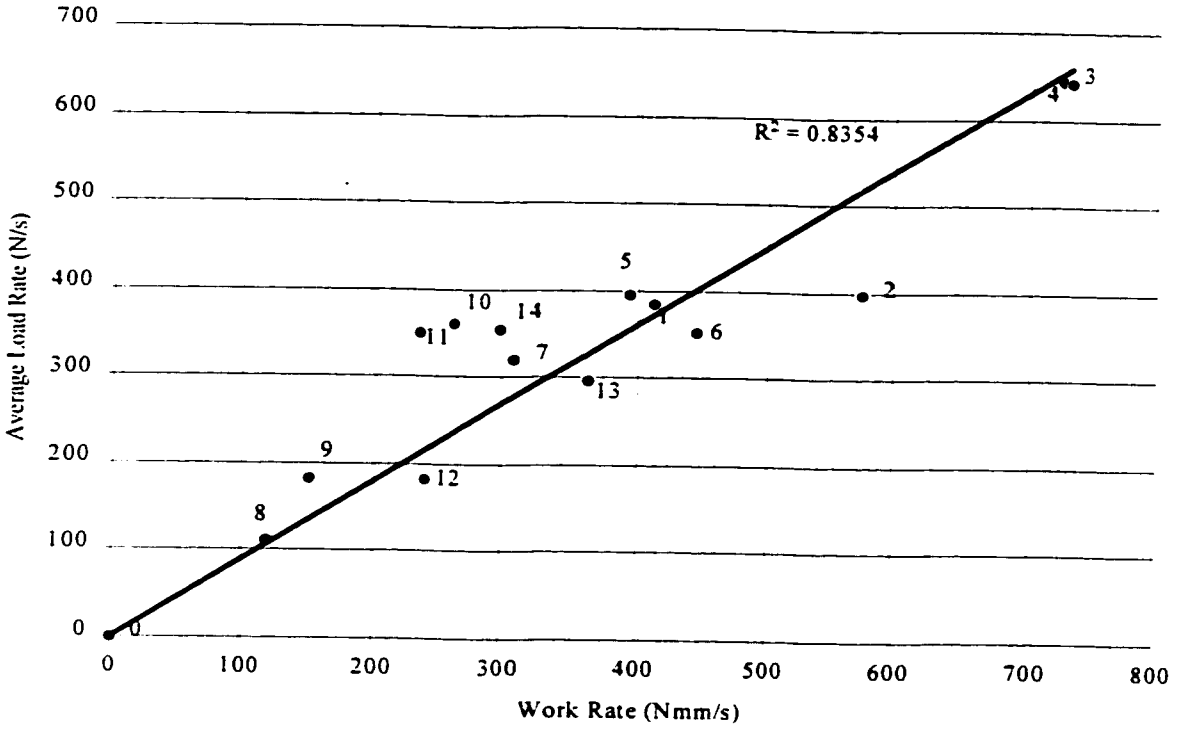

Figure 7.5 Average (mean) load rate vs work rate indicating the possibility of inter substitution

$$\dot{w} = \frac{h}{H_d N_{tc(m)}} \left(\frac{v_s t^* s_r}{2af} n_{cl} p_S \right) k_w W_R \tag{7.14}$$

The constant k_w is introduced to account for the conversion factor from load rate to work rate, as well as to account for the experimental error that could be introduced as a result of the improper measurement of $v_s t^*/2a$.

The characterization quantity which is defined as the modified work rate is multiplied by a factor normalized with respect to the maximum value so as not to deviate from the accepted characterization parameter by much, and is given as:

$$W_{Rm} = \frac{\left(\frac{v_s t^* s_r}{2af} n_{cl} p_S \right)}{\max \left| \frac{v_s t^* s_r}{2af} n_{cl} p_S \right|} W_R \tag{7.15}$$

Therefore the final wear equation which will be used for the characterization of the wear is given by the following relationship:

$$\dot{w} = K_w W_{Rm} \tag{7.16}$$

where,

$$K_W = \frac{h}{H_d N_{tc(m)}} \max \left| \frac{v_s t^* s_r}{2af} n_{cl} p_S \right| k_w \tag{7.17}$$

It is assumed that the depth at which the wear will originate, the hardness of the material and the total number of cycles required to originate and propagate crack until wear debris forms are constant but not the same for sliding wear and impact wear.

The analysis considered here takes into account the percentage categories of force and sliding distance. Therefore the percentage of sliding and force are divided into a six by six matrix describing the force variation in one direction and the displacement variation on the other (Table 7.2). The overall multiplication factor is given by:

$$Mf = \sum_{i=1}^{i=6} \sum_{j=1}^{j=6} \frac{v_s t^* s_r}{2af} n_{cl} p_{ij} \qquad \textbf{(7.18)}$$

It is the summation of the product of weighted percentage of applied force and equivalent number of asperity columns through out the duration of the experiment. The above formulation can be easily visualized in a tabular form consisting of the percentage force and displacement distribution and the multiplication factors as well. The product in Table 7.4 is obtained by multiplying the contents of the same cells in the two tables, Table 7.2 and Table7.3.

Table 7.2 Percentage distribution of force and sliding combination.

	0-0.166F_{max}	0.16-.33F_{max}	0.33-0.5F_{max}	0.5-0.66F_{max}	.66-0.83F_{max}	0.83-1.0F_{max}
0-.16D_{max}	p_{11}	p_{12}	p_{13}	p_{14}	p_{15}	p_{16}
.16-.33D_{max}	p_{21}	p_{22}	p_{23}	p_{24}	p_{25}	p_{26}
.33-.5D_{max}	p_{31}	p_{32}	p_{33}	p_{34}	p_{35}	p_{36}
.5-0.66D_{max}	p_{41}	p_{42}	p_{43}	p_{44}	p_{45}	p_{46}
.66-.83D_{max}	p_{51}	p_{52}	p_{53}	p_{54}	p_{55}	p_{56}
.83-1.0D_{max}	p_{61}	p_{62}	p_{63}	p_{64}	p_{65}	p_{66}

where,

D_{max} = constant at 10μm and F_{max} take the maximum value for each experiment.

Table 7.3 Percentage distribution matrix multiplier.

R \ C	$0.083n_{climax}$	$0.250n_{climax}$	$0.416n_{climax}$	$0.583n_{climax}$	$0.750n_{climax}$	$0.916n_{climax}$
$0.083As_{max}$	R_1*C_1	R_1*C_2	R_1*C_3	R_1*C_4	R_1*C_5	R_1*C_6
$0.250As_{max}$	R_2*C_1	R_2*C_2	R_2*C_3	R_2*C_4	R_2*C_5	R_2*C_6
$0.416As_{max}$	R_3*C_1	R_3*C_2	R_3*C_3	R_3*C_4	R_3*C_5	R_3*C_6
$0.583As_{max}$	R_4*C_1	R_4*C_2	R_4*C_3	R_4*C_4	R_4*C_5	R_4*C_6
$0.750As_{max}$	R_5*C_1	R_5*C_2	R_5*C_3	R_5*C_4	R_5*C_5	R_5*C_6
$0.916As_{max}$	R_6*C_1	R_6*C_2	R_6*C_3	R_6*C_4	R_6*C_5	R_6*C_6

where,

n_{climax}= maximum number of asperity contact perpendicular to the sliding direction

As_{max} = maximum equivalent number of contact length for one cycle $[v_s t^* s/(2af)]$

Table 7.4 Multiplication factor for conventional work rate

$P_{11}*0.083n_{climax}*0.083As_{max}$	$P_{12}*0.250n_{climax}*0.083As_{max}$	$P_{13}*0.416n_{climax}*0.083As_{max}$	$P_{14}*0.583n_{climax}*0.083As_{max}$	$P_{15}*0.750n_{climax}*0.083As_{max}$	$P_{16}*0.916n_{climax}*0.083As_{max}$	$\sum C_{11\text{-}16}$
$P_{21}*0.083n_{climax}*0.250As_{max}$	$P_{22}*0.250n_{climax}*0.250As_{max}$	$P_{23}*0.416n_{climax}*0.250As_{max}$	$P_{24}*0.583n_{climax}*0.250As_{max}$	$P_{25}*0.750n_{climax}*0.250As_{max}$	$P_{26}*0.916n_{climax}*0.250As_{max}$	$\sum C_{21\text{-}26}$
$P_{31}*0.083n_{climax}*0.416As_{max}$	$P_{32}*0.250n_{climax}*0.416As_{max}$	$P_{33}*0.416n_{climax}*0.416As_{max}$	$P_{34}*0.583n_{climax}*0.416As_{max}$	$P_{35}*0.750n_{climax}*0.416As_{max}$	$P_{36}*0.916n_{climax}*0.416As_{max}$	$\sum C_{31\text{-}36}$
$P_{41}*0.083n_{climax}*0.583As_{max}$	$P_{42}*0.250n_{climax}*0.583As_{max}$	$P_{43}*0.416n_{climax}*0.583As_{max}$	$P_{44}*0.583n_{climax}*0.583As_{max}$	$P_{45}*0.750n_{climax}*0.583As_{max}$	$P_{46}*0.916n_{climax}*0.583As_{max}$	$\sum C_{41\text{-}46}$
$P_{51}*0.083n_{climax}*0.750As_{max}$	$P_{52}*0.250n_{climax}*0.750As_{max}$	$P_{53}*0.416n_{climax}*0.750As_{max}$	$P_{54}*0.583n_{climax}*0.750As_{max}$	$P_{55}*0.750n_{climax}*0.750As_{max}$	$P_{56}*0.916n_{climax}*0.750As_{max}$	$\sum C_{51\text{-}56}$
$P_{61}*0.083n_{climax}*0.916As_{max}$	$P_{62}*0.250n_{climax}*0.916As_{max}$	$P_{63}*0.416n_{climax}*0.916As_{max}$	$P_{64}*0.583n_{climax}*0.916As_{max}$	$P_{65}*0.750n_{climax}*0.916As_{max}$	$P_{66}*0.916n_{climax}*0.916As_{max}$	$\sum C_{61\text{-}66}$
						$\sum C_{17\text{-}67}$

The quantities described in the above table are used to multiply the percentage distribution table which categorizes the applied force and sliding distance. Because the percentage category is the same for the sliding category, the average value of the number of columns, for all the experiments, is utilized to process each matrix, however since the force category is different for all of them the average or mean force of each experiment is utilized for the individual matrix of each experiment. The total multiplication factor is added and used to scale the work rate value to obtain a better result.

The final quantity $\Sigma C_{17\text{-}67}$ is the multiplying factor which is normalized by the maximum value, maintaining the scaling parameter values between 0 and 1. A combination of a spread sheet program and the G code were used to properly obtain the percentage distribution of the various force and displacement category. Following this work, the result of the wear rate/modified work rate relationship was plotted with satisfactory results as shown in Figure 7.6.

7.5 Discussion of Results

The modified Hofmann approach did not describe the work rate / wear rate relationship as expected, for the various contact conditions which included pure sliding and normal impact conditions. But it should be noted that the modification incorporated to their equation did reduce the scatter. It should also be noted that there was the introduction of an experimental constant physical interpretation of which was not provided adequately. The scaling or multiplication factor addresses the difference between sliding and impact dominated wear.

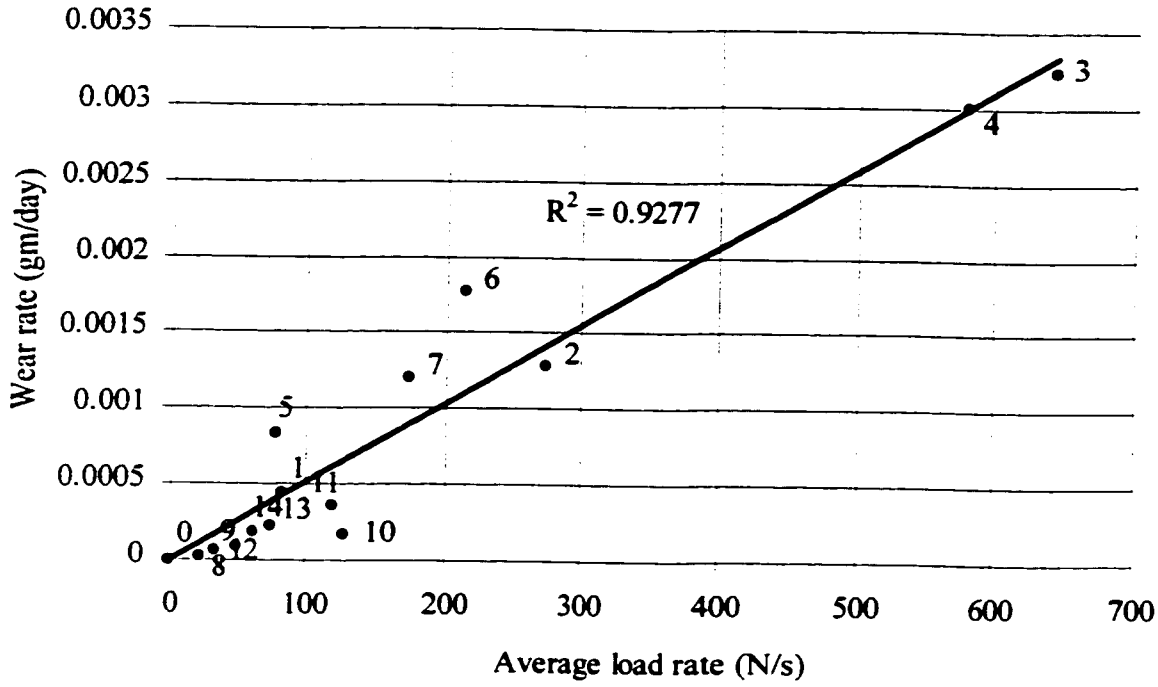

a)

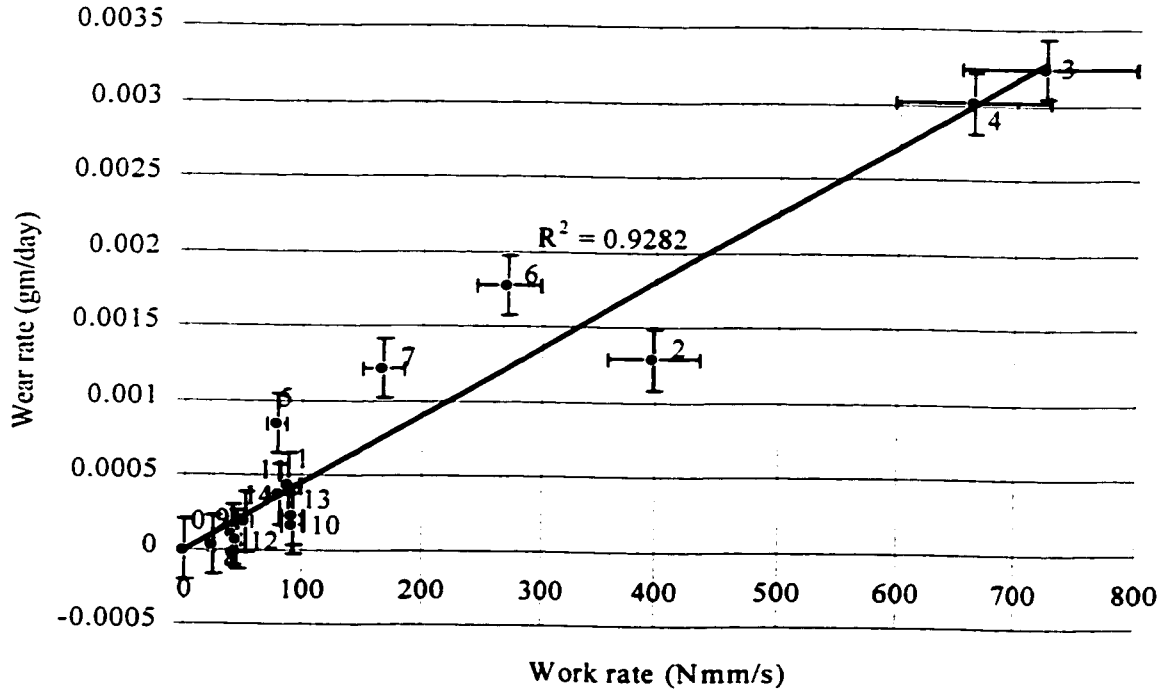

b)

Figure 7.6 New wear rate characterization parameter, a) average load rate b) modified work rate, derived using the new asperity contact dependent wear model.

As the formulation was highly empirical, and impact was seen as wear reducing instead of a factor that causes wear at a slower rate, the error may have occurred as a result.

The new method which was developed based on the fatigue related approach to wear mechanics, was better suited to describe the relationship between wear rate and work rate. The reduction in the scatter was significant compared to the two approaches (conventional and Hofmann's). This is mainly because, the relationship was derived based on a fundamental approach, which describes the phenomenon accurately. It should also be noted that the new approach does not involve the use of many experimental constants and relies only on the measured force and displacement data and the fracture mechanics results.

The difference between the conventional work rate and new characterization parameter is considerable. It can be seen that the wear rate is better described with the new approach. Implementation of this data can be incorporated using theoretical analysis (commercially available softwares), developed to describe the force and motion interaction of a heat exchanger tube. The errors, as discussed earlier, tend to be more at the lower levels of wear. This is mainly due to the fact that measurement errors will be relatively higher at lower rather than at higher wear volumes. However, the scatter was reduced tremendously, even at these low wear volume experiments. Therefore, this approach can be effectively utilized to characterize the wear rate/work rate relationship using the multiplication factor introduced in this section.

7.6 Conclusion

The results of the experimental analysis indicate that the work rate characterization parameter by itself is not sufficient to identify wear accurately. Hence a new and improved characterization parameter is proposed based on the fact that fatigue dominated wear is responsible for the bulk of wear debris formed. Comparative studies carried out have indicated that the best fit with minimum error was obtained using the new approach. The theoretical basis for this approach was the delamination theory of wear and its extension to impact type of conditions.

CHAPTER 8

CONCLUSIONS AND RECOMMENDATIONS FOR FUTURE WORK

8.1 Conclusions

The state of the art survey conducted on generalized as well as specific (heat exchanger tube related) wear models, indicated that the available relationships for describing the wear were highly empirical and hardware dependent. The overall consensus was that, even though there were a few mechanisms at work in wearing objects, subsurface stress effect was found to be highly critical in the debris formation process, under fretting conditions of heat exchanger tubes. This phenomenon was especially true for impacting objects, where lateral relative motion between the two is rather limited. Therefore, the applicability of an extended delamination theory of wear for impacting objects, was unquestionable.

Using existing generalized wear models, an attempt was made to co-relate the wear-rate to the commonly used characterization parameter, work-rate. However, the draw back of this parameter was that, for purely impacting bodies the theoretical value is extremely small, (elastic compliance of the two contacting objects). The use of this characterization parameter indiscriminately led to erroneous results, leaving the problem of characterization unresolved with regards to the wear-rate / work-rate relationships. In addition, the proposed linear relationship of the above quantities, by some researchers, was invalidated following the

detailed derivations for different contact conditions (force and motion) as shown in the third chapter.

Fretting wear is a complex phenomenon which requires experimental verification of any model, developed to predict the wear volume. An experimental setup was borrowed from Ontario Hydro Technologies, while another one was designed and built at Concordia University, to ensure the applicability of the new wear model developed in this research work. This procedure was adopted to show that the wear model was a generalized one, capable of estimating the wear rate, irrespective of the setup. After proper calibration and commissioning of the rigs, a set of experiments were conducted in house to obtain some relevant data. These data were collected and stored on optical disks for off-line analysis. An important link was established experimentally, between the average work rate and "load rate" showing the possibility of substituting one with other.

The stress analysis utilized in this research work relied heavily on the finite element modelling approach, due to the unavailability of closed form solutions for elasto-plastic, multi-linear isotropic hardening materials. This finite element method was also used to verify a closed form solution for an elliptical pressure load, validity of which was questionable for the given geometry of the interacting bodies (Hertzian contact for closely conforming objects). Following this, an extensive parametric study was conducted to determine crack nucleation positions for an elliptically loaded surface, with a cylindrical inclusion. The possible direction of the crack propagation rate was also investigated by observing the stress conditions around a growing crack. The final set of parametric studies was conducted to

determine the crack propagation rate using the CTSD approach. This fracture mechanics study was highly crucial in the derivation of the new theoretical wear model.

The elaborate work conducted in extending the delamination theory, was successfully implemented towards the derivation of a new mathematical model for wear, under impact conditions (normal and oblique). The model essentially takes advantage of the quantities obtained from the fracture mechanics studies. The derivation of this model was albeit to the conditions enlisted for the extension of the delamination theory of wear for impacting objects, as listed in Chapter 6. The step by step procedure, described in the formation of a wear debris, is supported by the micro structural analysis conducted by researchers, as indicated. Validity of the wear equations was verified using experimental investigations on the two separate setups, with different dynamic characteristics. This theoretical model was also verified using experimental data from different sources, found in some unclassified publications. It was deemed essential to calibrate the CTSD in the wear model, using only three data points, for a more accurate wear volume prediction.

The calibrated wear model was accurate in giving an approximate value for the trend line of the total wear. However, because of the nature of the experiment, the force and displacement values can not be fully controlled through out the duration. This results in a considerable scatter of the actual data from the linear trend line. Therefore, it was essential to introduce a characterization parameter, which categorizes the percentages of occurrence of forces and displacements. Result of this characterization parameter was a substantial improvement over the conventional work rate parameter, used for characterization of the wear rate. The validity

of this new characterization parameter affirms the accuracy of the new motion dependent theoretical wear model, which was derived from a fundamental understanding of the process.

8.2 Recommendations for future work

Wear is a complex phenomenon which involves a deep knowledge of contact mechanics, material science, thermodynamics and fluid mechanics. Most of the wear models proposed so far, have not attempted to study the effects of the fluid squeeze film behaviour on the heat exchanger tubes. Also the effects of the friction induced thermal stresses, are neglected. It is the author's recommendation that further work in this area incorporate the study of thermal stresses and fluid squeeze film effect in the formation of wear debris.

From the study conducted in this thesis, it is apparent that asperity contact is critical in the debris formation process. As a means of reducing the wear, investigations can concentrate on the development of new materials capable of withstanding the adverse operating conditions, at the asperity level. Material study can concentrate on means of increasing the ratio of actual to apparent area of contact. This may include surface treatment using laser technology or surface coating.

The finite element study carried out for the crack propagation analysis needs to be expanded for actual sliding conditions. It is essential to traverse the load across the subsurface crack in order to obtain a good estimate of the crack propagation rate per loading cycle for a sliding object. The crack propagation rate should be investigated to reflect a more realistic value of

the CTSD for sliding conditions.

To strengthen the validity of this research work, it is crucial to increase the experimental data base using multiple tube and multi-span support, simulating actual operating conditions before the implementation of this theory in the actual design process. The effect of residual stresses should be studied on the overall wear process.

It has been observed that the support of the tube is crucial in the wear process. Therefore, it is essential to conduct an in-depth analysis on the type of support and the relative merit. The use of different geometry support such as broached hole and lattice geometry should be carefully investigated.

REFERENCES

[1] Waterhouse, R.B., "Fretting Corrosion", *Pergamon Press*, Toronto, 1972.

[2] Lewis, E.E., "Nuclear Power Reactor Safety", *John Wiley & Sons*, New York, 1977.

[3] Ko, P.L., "Metallic Wear-A Review, with Special References to Vibration-Induced Wear in Power Plant Components", *ASME Pressure Vessels and Piping Conferences*, Chicago, Illinois, July 21-24, 1986.

[4] Rice, S.L., "Variation in Wear Resistance Due to Microstructural Condition in High Strength Steel Under Repetitive Impact", *Tribology International*, Vol. 12, No. 1, pp. 25-29, 1979.

[5] Hofmann, P.J., Schettler, T. and Steininger, D.A., "PWR Steam Generator Tube Fretting and Fatigue Wear Phenomena and Correlations", *ASME International Symposium on Flow Induced Vibration and Noise*, 1992.

[6] Archard, J.F., "Contact and Rubbing of Flat Surfaces", *ASME Transactions, Journal of Applied Physics*, Vol. 24, No. 8, pp. 981-988, Aug. 1953.

[7] Palmgren A., "Ball and Roller Bearing Engineering, 3rd edn.", *SKF Industries Corporation*, Philadelphia, 1959.

[8] Rice, S.L., Nowotny, H. and Wayne, S.F., "Formation of Subsurface Zones in Impact Wear", *ASLE 35th annual meeting*, Anaheim, California, May 5-8, 1980.

[9] Rice, S.L., Nowotny, H. and Wayne, S.F., "Characteristics of Metallic Subsurface Zones in Sliding and Impact Wear", *Wear of Materials*, San Fransisco, California, 1981.

[10] Suh, N.P., "The Delamination Theory of Wear", *Wear*, Vol. 25, pp. 111-124, 1973.

[11] Jahanmir, S., "A Fundamental Study on the Delamination Theory of Wear", *Ph. D. Thesis*, Massachusetts Institute of Technology, 1977.

[12] Rosenfeld, A.R., "A Fracture Mechanics Approach to Wear", *Wear*, Vol. 61, pp. 125-132, 1980.

[13] Hills, D.A. and Nowell, D., "Mechanics of Fretting Fatigue", Kluwer Academic Publishers, 1994.

[14] Bayer, R.G., Clinton, W.C. and Sirico, J.L., "A Note on the Application of the Stress Dependency of Wear in the Wear Analysis of an Electrical Contact", *Wear*, Vol. 7, pp. 282-289, 1964.

[15] Rabinowicz, E., "Friction and Wear of Materials", *Wiley and Son*, New York, pp. 113-119, 1965.

[16] Bayer, R.G. and Ku, T.C., "Handbook of Analytical Design for Wear", *Plenum Press*, New York, 1964.

[17] Bayer, R.G. and Schumacher, R.A., "On The Significance of Surface Fatigue in Sliding Wear", *Wear*, Vol. 12, pp. 173-183, 1968.

[18] Bayer, R.G., Clinton, W.C., Nelson, C.W. and Schumacher, R.A. "Engineering Model for Wear", *Wear*, Vol. 5, pp. 378-391, 1962.

[19] Suh, N.P., Jahanmir, S. and Abrahamson, E.P., "The Delamination Theory of Wear, Progress Report", *Materials Processing Laboratory, Department of Mechanical Engineering*, M.I.T., 1974.

[20] Suh, N.P., Jahanmir, S., Fleming, J., Abrahamson, E.P., Saka, N. and Teixeira, J.P., "The Delamination Theory of Wear-II, Second Progress Report", *Materials Processing Laboratory, Department of Mechanical Engineering*, M.I.T., 1975.

[21] Suh, N.P., "An Overview of the Delamination Theory of Wear", *Wear*, Vol. 44, pp. 1-16, 1977.

[22] Jahanmir, S. and Suh, N.P., "Mechanics of Surface Void Nucleation in Delamination Wear", *Wear* Vol. 44, pp. 39-56, 1977.

[23] Merwin, J.E. and Johnson, K.L., "An Analysis of Plastic Deformation in Rolling Contact", *Proceeding of the Institution of Mechanical Engineers*, Vol. 177, No. 25, pp. 676-690, 1963.

[24] Argon, A.S., Im, J. and Safoglu, R., "Cavity Formation from Inclusion in Ductile Fracture", *Metallurgical Transactions A*, Vol. 6A, pp. 825-837, April 1975.

[25] Fleming, J.R. and Suh, N.P., "The Relationship Between Crack Propagation Rates and Wear Rates", *Wear* Vol. 44, pp. 39-56, 1977.

[26] Uhlig, Herbert H., "Mechanics of Fretting Corrosion", *ASME Transactions, Journal of Applied Mechanics*, Vol. 21, pp. 401-407, 1954.

[27] Feng, I-Ming and Uhlig, Herbert H., "Fretting Corrosion of Mild Steel in Air and in Nitrogen", *ASME Transactions, Journal of Applied Mechanics*, Vol. 21, pp. 395-400, 1954.

[28] Engel, P.A., "Impact Wear of Materials", *Elsevier*, New York, 1978.

[29] Rabinowicz, E. and Hozaki, K., "Impact Wear of Ductile Metals", *Proceedings of the JSLE International Conference*, Tokyo, Japan, pp. 263-268, July 8-10, 1985.

[30] Engel, P.A., Lyons, T.H. and Sirico, J.L."Impact Wear Model for Steel Specimens", *Wear*, Vol. 23, pp. 185-201, 1973.

[31] Engel, P.A., "Analysis and Design for Zero Impact Wear", *ASME Transactions, Journal of Lubrication Technology*, pp. 455-463, July 1974.

[32] Engel, P.A., "Impact on a Worn Surface", *Proceedings of the IUTAM Symposium on the Mechanics of the Contact Between Deformable Bodies*, Enschede, The Netherlands, August 1974.

[33] Engel, P.A., "Percussive Impact Wear: A Study of Repetitively Impacting Solid Components in Engineering", *Tribology International*, pp. 169-176, June 1978.

[34] Engel, P.A., "Experimental and Analytical Approaches in Impact Wear", *Wear of Materials*, pp. 401-412, 1977.

[35] Hofmann, P.J., Schettler, T., Wieling, N. and Steininger, D.A., "Influence of Contact Conditions on Vibration Induced Wear of Metals", Nuclear Engineering and Design, Vol. 119, pp. 439-445, 1990.

[36] Cha, J.H., Wambsganss, M.W. and Jendrzejczyk, J.A., "Experimental Study on Impact/Fretting Wear in Heat Exchanger Tubes", *ASME Transactions, Journal of Pressure Vessel Technology*, Vol. 109, pp. 265-274, August 1987.

[37] Ko, P.L., Tromp, J.H. and Weckwerth, M.K., "Heat Exchanger Tube Fretting Wear: Correlation of Tube Motion and Wear", *ASTM Symposium on Materials Evaluation Under Fretting Conditions*, Gaithersburg, MD, June 3, 1981.

[38] Ko, P.L., "Heat Exchanger Tube Fretting Wear: Review and Application to Design", *Third Keswick International Conference: Vibration in Nuclear Plant*, Log. No. 48, 11-14 May, 1982.

[39] Blevins, R.D., "Fretting Wear of Heat Exchanger Tubes, Part I: Experiments", *ASME Transactions, Journal of Engineering for Power*, pp. 625-629, Oct. 1979.

[40] Blevins, R.D., "Fretting Wear of Heat Exchanger Tubes, Part II: Models", *ASME Transactions, Journal of Engineering for Power*, pp. 630-633, Oct. 1979.

[41] Connors, H.J., "Flow-Induced Vibration and Wear of Steam Generator Tubes", *Nuclear Technology*, Vol. 55, Nov. 1981.

[42] Levy, G. & Morri, J., "Impact Fretting Wear In CO_2-Based Environments", *Wear*, Vol. 106, pp. 97-138, 1985.

[43] Blevins, R.D., "Vibration-Induced Wear of Heat Exchanger Tubes", *ASME Transactions Journal of Engineering Materials and Technology*, Vol. 107, pp. 61-67, Jan. 1985.

[44] Frick, T.M., Sobek, E. and Reavis, J.R., "Overview on the Development and Implementation of Methodologies to Compute Vibration and Wear of Steam Generator Tubes", *ASME Special Publication, Symposium on Flow-Induced Vibrations in Heat Exchangers*, Edited by M.P. Paidoussis, J.M. Chenoweth and M.D. Bernstien, New Orleans, Louisiana, Dec. 9-14, 1984.

[45] Pettigrew, M.J., Carlucci, L.N., Taylor, C.E. and Fisher, N.J., "Flow-Induced Vibrations and Impact Fretting-Wear in Nuclear Steam Generators and Heat Exchangers", *Canadian Nuclear Society Conference on Steam Generators and Heat Exchangers*, Toronto, Ontario, April 1990.

[46] Fisher, N.J., Guérout, F.M., Weckwerth, M.K. and Grandison, D.A., "Fretting-Wear of Nuclear Steam Generator Tube and Support Materials", *CANCAM Conference*, Victoria, BC., June 3-7, 1995.

[47] Hofmann, P.J., Schettler, T. and Steininger, D.A., "Pressurized Water Reactor Steam Generator Tube Fretting and Fatigue Wear Characteristics", *ASME Pressure Vessel and Piping Conference*, Chicago, Illinois,July 21-24, 1986.

[48] Hofmann, P.J., Friedrich, B.C. and Schröder, H.-J., "Prediction of PWR Steam Generator Tube Material Loss Caused by Perpendicular Impacting", *ASME International Symposium on Flow Induced Vibration*, 1996.

[49] Axisa, F., Desseaux, A. and Gibert, R.J. "Experimental Study of Tube/Support Impact Forces in Multi-Span PWR Steam Generator Tubes", *ASME Special Publication, Symposium on Flow-Induced Vibrations in Heat Exchangers*, Edited by M.P. Paidoussis, J.M. Chenoweth and M.D. Bernstien, New Orleans, Louisiana, Dec. 9-14, 1984.

[50] Rao, M.S.M., Steininger, D.A., Ahluwalia, K.S. and Eisinger, F.L., "Simulation of PWR Steam Generator Tubes Undergoing Turbulence and Fluidelastic Excitation for Wear Prediction", *ASME International Symposium on Flow Induced Vibration and Noise*, 1992.

[51] Poritsky, H., "Stresses and Deflections of Cylindrical Bodies in Contact With Application to Contact of Gears and Locomotive Wheels", *ASME Transactions Journal of Applied Mechanics*, pp. 91-201, June 1950.

[52] Weber, J.R., Stippes, M.C. and Costello, G.A., "Elastic Impact of Cylinders", *ASME Transactions, Journal of Applied Mechanics*,, pp. 1137-1138, December 1974 (Brief Notes).

[53] Dubowsky, S. and Freudenstein, F., "Dynamic Analysis of Mechanical Systems With Clearances, Part 1: Formation of Dynamic Model", *ASME Transactions, Journal of Engineering for Industry*, pp. 305-309, February 1971.

[54] Fan, H., Keer, L.M., Cheng, W. and Cheng, H.S., "Competition Between Fatigue Crack Propagation and Wear", *ASME Transactions, Journal of Tribology*, Vol. 115, pp. 141-147, Jan. 1993.

[55] Mura, T. and Tanaka, K., "Dislocation Dipole Models for Fatigue Crack Initiation", *ASME, AMD-Vol. 47*, pp. 111-131, 1981.

[56] Tanaka, K. and Mura, T., "A Dislocation Model for Fatigue Crack Initiation", *ASME Transactions, Journal of Applied Mechanics*, Vol. 48, pp. 97-103, March 1981.

[57] Lin, T.H., "Micromechanics of Fatigue Crack Initiation: Theory and Experimental Observations", *ASME, AMD-Vol. 47*, pp. 91-109, 1981.

[58] Mura, T. And Nakasone Y., "A Theory of Fatigue Crack Initiation in Solids", *ASME Transactions, Journal of Applied Mechanics*. Vol. 57, pp. 1-6, 1990.

[59] Cheng, W., Cheng, H.S., Keer, L.M. and Ai, X., "Surface Crack Initiation Under Contact Fatigue: Experimental Observation and Contact Analysis", *ASME Transactions, Journal of Tribology*, Vol. 115, pp. 658-665, 1993.

[60] Cheng, W., Cheng, H.S., Mura, T. and Keer, L.M., "Micromechanics Modeling of Crack Initiation Under Contact Fatigue", *ASME Transactions, Journal of Applied Mechanics*, Vol. 116, pp. 2-8, 1994.

[61] Gurland, J. And Plateau, J., "The Mechanism of Ductile Rupture of Metals Containing Inclusions", *ASM Transactions*, Vol. 56, 1963, pp. 54-65.

[62] Ashby, M.F., "Work Hardening of Dispersion Hardened Crystals", *Phil. Magazine*, Vol. 14, 1966, pp. 1157-1178.

[63] Argon, A.S. and Im, J., "Separation of Second Phase Particles in Spheroidized 1045 Steel, Cu-0.6Pct Cr Alloy, and Maraging Steel in Plastic Straining", *Metallurgical Transactions A*, Vol. 6A, pp. 839-851, April 1975.

[64] Jahanmir, S. and Suh, N.P., "Mechanics of Surface Void Nucleation in Delamination Wear", *Wear* Vol. 44, pp. 39-56, 1977.

[65] Salahizadeh, H. and Saka, N., "The Mechanics of Crack Initiation at Hard Particles in Rolling Line Contacts", *ASME Transactions, Journal of Tribology*, Vol. 114, pp. 341-347, April 1992

[66] Foltyn, P.A. and Ravi-Chandar, K., "Initiation of an Interface Crack Under Mixed-Mode Loading", *ASME Transactions, Journal of Applied Mechanics*, Vol. 60, pp. 227-229, March 1993 (Brief Notes).

[67] Paris, P. and Erdogan, F., "A Critical Analysis of Crack Propagation Laws", *ASME Transactions, Journal of Basic Engineering*, pp. 528-534, December 1963.

[68] Erdogan, F. and Shih, G.C., "On the Crack Extension in Plates Under Plane Loading and Transverse Shear", *ASME Transactions, Journal of Basic Engineering*, pp.519-527, December 1963.

[69] Fleming, J.R. and Suh, N.P., "Mechanics of Crack Propagation in Delamination Wear", *Wear* Vol. 44, pp. 39-56, 1977.

[70] Sin, H.-C. and Suh, N.P., "Subsurface Crack Propagation Due to Surface Traction in Sliding Wear", *ASME Transactions, Journal of Applied Mechanics*, Vol. 51, pp. 317-323, June 1984.

[71] Salehizadeh, H. and Saka, N., "Crack Propagation in Rolling Line Contact", *ASME Transactions, Journal of Tribology*, Vol. 114, pp. 690-697, October 1992.

[72] Anderson, T.L., "Fracture Mechanics; Fundamentals and Application", *CRC Press*, Inc., Florida, 1991.

[73] Kanninen, M.F. and Popelar, C.H., "Advanced Fracture Mechanics", *Oxford University Press*, New York, 1985.

[74] Smith, J.O. and Liu, C.K., "Stresses Due to Tangential and Normal Loads on an Elastic Solid With Application to Some Contact Stress Problems", *ASME Transactions, Journal of Applied Mechanics*, pp. 157-166, June 1953.

[75] Hamilton, G.M. and Goodman, L.E., "The Stress Field Created by Circular Sliding Contact", *ASME Transactions, Journal of Applied Mechanics*, pp. 371-376, June 1966.

[76] Johnson, K.L., "Contact Mechanics", *Cambridge University Press*, 1987.

[77] Johnson, K.L., "One Hundred Years of Hertz Contact", *Proceedings of the Institution of Mechanical Engineers*, Vol. 196, pp. 363-378, 1982.

[78] Aramaki, H., Cheng, H.S. and Chung, Y.-W., "The Contact Between Rough Surfaces With Longitudinal Texture-Part I: Average Contact Pressure and Real Contact Area", *ASME Transactions, Journal of Tribology*, Vol. 115, pp. 419-424, July 1993.

[79] Iyer, S.S. and Ko, P.L., "Finite Element Modelling of Plastic Deformation, Crack Growth and Wear Particle Formation for Sliding Wear of Power Plant Components", *ASME International Symposium on Flow Induced Vibration*, 1996.

[80] Hisakado, T., "On the Mechanism of Contact Between Solid Surfaces (1st Report, The Initial Separation and Distributions of Slopes of Facetes on Surfaces and on Profile Curve)", *Bulletin of JSME*, Vol. 12, No. 54, pp. 1519-1527, 1969.

[81] Hisakado, T., "On the Mechanism of Contact Between Solid Surfaces (2nd Report, The Real Area of Contact , the Separation and the Penetrating Depth)", *Bulletin of JSME*, Vol. 12, No. 54, pp. 1528-1536, 1969.

[82] Hisakado, T., "On the Mechanism of Contact Between Solid Surfaces (3rd Report, The Number and the Distributions of Radii of Contact Points)", *Bulletin of JSME*, Vol. 12, No. 54, pp. 1537-1545, 1969.

[83] Hofmann, P.J., Schettler, T. and Steininger, D.A., "Pressurized Water Reactor Steam Generator Tube Fretting and Fatigue Wear Characteristics", EPRI, Palo Alto, CA, USA Final Report NP-6341, 1989.

[84] Ko, P.L. and Basista, H., "Correlation of Support Impact Force and Fretting-Wear for a Heat Exchanger", *ASME Transactions, Journal of Pressure Vessel Technology*, Vol. 106, pp. 69-77, February 1984.

[85] Jahanmir, S., "The Mechanics of Subsurface Damage in Solid Particle Erosion", *Wear* Vol. 61, pp. 309-324, 1980.

[86] Tsukada, T. and Anno, Y., "An Analysis of the Deformation of Contacting Rough Surfaces (2nd Report, Estimation of the Initial Contact Positions)", *Bulletin of JSME*, Vol. 15, No. 86, pp. 989-995, 1972.

[87] Tsukada, T. and Anno, Y., "An Analysis of the Deformation of Contacting Rough Surfaces (3rd Report, Introduction of a New Contact Theory of Rough Surfaces)", *Bulletin of JSME*, Vol. 15, No. 86, pp. 989-995, 1972.

[88] Tsukada, T. and Anno, Y., "An Analysis of the Deformation of Contacting Rough Surfaces (4th Report, Formulae for Practical Use on Deformation of Plane Joints Making the Directions of Surface Asperities Parallel to Each Other)", *Bulletin of JSME*, Vol. 15, No. 89, pp. 1448-1456, 1972.

[89] Tsukada, T. and Anno, Y., "An Analysis of the Elastic and Plastic Deformations of Machined Surfaces in Contact (1st Report, Deformations of Contacting Rough Surfaces when the Directions of Surface Asperities Cross Each Other)", *Bulletin of JSME*, Vol. 17, No. 105, pp. 376-384, 1974.

[90] Tsukada, T. and Anno, Y., "An Analysis of the Elastic and Plastic Deformations of Machined Surfaces in Contact (2nd Report, Comparison Between Calculated and Experimental Results on the Deformations of Rough Surfaces in Contact)", *Bulletin of JSME*, Vol. 17, No. 105, pp. 385-392, 1974.

[91] Tsukada, T. and Anno, Y., "An Analysis of the Elastic and Plastic Deformations of Machined Surfaces in Contact (3rd Report, On the Contact of Surfaces whose Asperities do not have Directional Qualities)", *Bulletin of JSME*, Vol. 17, No. 105, pp. 393-400, 1974.

[92] ANSYS User's Manual, Volume I - IV, for Revision 5.0, *Swanson Analysis System*, Inc. Houston PA., 1994.

[93] Aramaki, H., Cheng, H.S. and Chung, Y.-W., "The Contact Between Rough Surfaces With Longitudinal Texture-Part II: Flash Temperature", *ASME Transactions, Journal of Tribology*, Vol. 115, pp. 425-431, July 1993.

[94] Montmitonnet, P., Edlinger, M.L. and Felder, E., "Finite Element Analysis of Elastoplastic Indentation: Part I- Homogeneous Media", *ASME Transactions, Journal of Tribology*, Vol. 115, pp. 10-14, January 1993.

[95] McDowell, D.L., "An Evaluation of Recent Developments in Hardening and Flow Rules for Rate-Independent, Nonproportional Cyclic Plasticity", *ASME Transactions, Journal of Applied Mechanics*, Vol. 54, pp. 323-334, 1987.

[96] Schenck, H. Jr., "Theories of Engineering Experimentation", *McGraw Hill*, 1968.

[97] Hattori, T., Nakamura, M. and Watanabe, T., "Fretting Fatigue Analysis by Using Fracture Mechanics", *ASME paper No. 84-WA/DE-10,* pp. 1-10, 1984.

[98] Johansson, L., "Numerical Simulation of Contact Pressure Evolution in Fretting", ASME Transactions, Journal of Tribology, Vol. 116, pp. 247-254, April 1994.

[99] Taponat, M.-C., Ko, P.K. and Robertson, M.F., "Wear Studies of Materials for Tubes and Anti-Vibrations Bars in Nuclear Steam Generators", *CANCAM Conference*, Victoria, BC., June 3-7, 1995.

[100] Magel, E.E., "Experimental and Theoretical Studies of the Wear of Heat Exchanger Tubes", *Thesis,M.App. Sc.*, University of British Columbia, March 1990.

[101] Wu, S. and Cheng, H.S., "Sliding Wear Calculations in Spur Gears Contacts", *ASME Transactions, Journal of Tribology*, Vol. 115, pp. 493-500, July 1993.

[102] Gessesse, Y.B., Attia, M.H. and Osman, M.O.M., "Assessment of the Concept of Work-Rate in Impact/Sliding Fretting: Contact Mechanics Approach", *ASME Winter Annual Meeting (WAM)*, New Orleans, La., Nov. 28-Dec. 3, 1993.

[103] Gessesse, Y.B., Attia, M.H. and Osman, M.O.M., "Crack Initiation in Elasto-plastic Materials Under Normal and Oblique Impact", *CSME FORUM, 13th Symposium on Engineering Applications of Mechanics*, Hamilton, Ontario, May 7-9, 1993.

[104] Gessesse, Y.B., Attia, M.H. and Osman, M.O.M., "Theoretical Validation of the Work Rate Characterization Parameter for Fretting Wear",to be submitted for review to *Wear Journal* in July.

[105] Gessesse, Y.B., Attia, M.H. and Osman, M.O.M., "Crack Initiation and Propagation in Elasto-plastic Materials for Complex Dynamic Loading Conditions", submitted for review to *Wear Journal*, 1997.

[106] Gessesse, Y.B., Attia, M.H. and Osman, M.O.M., "A New Theoretical Wear Model Under Fatigue Dominated Contact Conditions", to be Submitted for review to *Wear Journal* in July.

[107] Attia, M.H., Gessesse, Y.B. and Osman, M.O.M., "Proposal of a New Characterization Parameter Based on a New Theoretical Wear Model", submitted to *ASME Transactions, Journal of Tribology*, 1997.

[108] Gessesse, Y.B. and Attia, M.H., "Critical Analysis of the Work Rate Concept for Predicting Fretting Wear Rate of Steam Generator Tubes", Ontario Hydro Internal Report, 1996.(Draft copy)

[109] Gessesse, Y.B. and Attia, M.H., "Finite Element Study of an Inconel 600 tube, for Quantifying Various Wear Parameters for the Derivation of A New Wear Model", Ontario Hydro Internal Report, 1996.(Draft copy)

[110] Gessesse, Y.B. and Attia, M.H., "Development and Validation of a Normal and Oblique Impact Wear Models Based on the Principles of Delamination Theory of Wear", Ontario Hydro Internal Report, 1997.(Draft copy)

[111] Attia, M.H. and Gessesse, Y.B., "Experimental Investigations of a New Theoretical Wear Characterization Parameter for Nuclear Power Plant Heat Exchanger Tubes", Ontario Hydro Internal Report, 1997.(Draft copy)

APPENDIX A

A.1 Wear Pattern Radius Variation of Closely Conforming Objects

The equation of a circle gives

$$R_1^2 = x^2 + (y + k)^2 \tag{A.1}$$

From the geometry of a wearing cylinder following conformance of the two contacting radii the following table can be obtained:

at	A	B
x	0	a
y	$R_{1org} - h$	$(R_{1org}^2 - a^2)^{1/2}$

form the above equation

$$\begin{aligned} R_1^2 &= (R_{1org} - h + k)^2 \\ R_1^2 &= a^2 + (\sqrt{R_{1org}^2 - a^2} + k)^2 \end{aligned} \tag{A.2}$$

solving for the value of k which satisfies both equations in (A2)

$$k = \frac{hR_{1org} - 0.5h^2}{R_{1org} - h - \sqrt{R_{1org}^2 - a^2}} \tag{A.3}$$

Therefore, R_1 is given as

$$R_1 = R_{1org} - h + \frac{hR_{1org} - 0.5h^2}{R_{1org} - h - \sqrt{R_{1org}^2 - a^2}} \tag{A.4}$$

APPENDIX B

B.1 Relative Sliding Length Under Impact Conditions

The final length of two objects (cylinder and flat) in elastic contact can be derived by beginning from the equation describing the line of contact. The equation describing the profile of the contact surface is given by:

$$y_x = \frac{4P_0}{\pi E^*}\left[\left(\frac{x}{a}\right)^2 + K\right] \qquad 0 \le x \le a \qquad \textbf{(B.1)}$$

The length of the elastically deformed bodies in contact is therefore:

$$S_y = \int_0^a \sqrt{1 + \left(\frac{dy_x}{dx}\right)^2}\, dx \qquad \textbf{(B.2)}$$

which gives the result:

$$S_y = \frac{2K_y\sqrt{4K_y + a^2} + a^2 \ln\left(2K_y + \sqrt{4K_y^2 + a^2}\right) - a^2 \ln(a)}{4K_y} \qquad \textbf{(B.3)}$$

where

$$K_y = \frac{4P_0}{\pi E^*} \qquad \textbf{(B.4)}$$

The total elongation of the surface is:

$$\delta x = S_y - a \qquad \textbf{(B.5)}$$

which is in the order of 10^{-10} m.,

APPENDIX C

C.1 Error Analysis of the Measurement System

The error analysis for the experimental data is conducted by taking into account the standard deviation error of each component individually and [1] estimating their combined effect using the following equation to obtain the standard deviation of the total quantity:

$$\sigma_{W_R} = \left[\left(\frac{\partial W_R}{\partial F} \sigma_F \right)^2 + \left(\frac{\partial W_R}{\partial s} \sigma_s \right)^2 \right]^{1/2} \qquad \textbf{(C.1)}$$

where

W_R = work rate [$= Fs/T$] averaged over total time T

F = resultant force [$= \sqrt{(F_x^2 + F_y^2)}$] with standard deviation of σ_F

s = resultant displacement [$= \sqrt{(s_x^2 + s_y^2)}$] with standard deviation of σ_s

The standard deviation of the individual quantities can be obtained from the calibration curve of the force and displacement transducers. It is given by:

$$\sigma_i = \frac{1}{N} \Sigma \left(x^2 - \bar{x}^2 \right) \qquad \textbf{(C.2)}$$

where

σ_i = standard deviation of $i=F$ => force and $i=s$ => displacement

x = measured value of true quantity $\bar{x}$ for N data points

After obtaining the standard deviation of each quantity individually, the standard deviation

---

[1] Thrasher, L.W. and Binder, R.C., "A Practical Application of Uncertainties Calculations to Measured Data". Transactions of the ASME, Feb. 1957.

for the total work rate can be obtained from the ratio of:

$$\frac{\sigma_{W_R}}{W_R} = \left[\left(\frac{\partial W_R}{\partial F}\frac{\sigma_F}{W_R}\right)^2 + \left(\frac{\partial W_R}{\partial s}\frac{\sigma_s}{W_R}\right)^2\right]^{1/2} \quad \textbf{(C.3)}$$

For the work rate given above, this will reduce to:

$$\frac{\sigma_{W_R}}{W_R} = \left[\left(\frac{\sigma_F}{F}\right)^2 + \left(\frac{\sigma_s}{s}\right)^2\right]^{1/2} \quad \textbf{(C.4)}$$

After determining the relative standard deviationthe confidence level of the error margin of 95% is obtained for using 2σ. From the caliberation measurements a standard deviation of 12.03 N and 0.7 μm, were obtained for the force and displacement transducers, respectively. Provided a typical force value of 200 N and 10.0 μm are used in the above equation, it will result in a relative error of 9.23%. This value is used for indicating the upper and lower bounds of the work rate.

Similarly the 2σ error was calculated (equation C.5) for the weight loss measurements using the measured value and the maximum error[2], giving a value of 0.0002gm.

$$\sigma = \left[\frac{1}{N-2}\Sigma(w_v - m\,\bar{w}_v - b)^2\right]^{1/2} \quad \textbf{(C.5)}$$

where

w_v = wear volume

m and b are least square approximation constants of the best fit linear line for $\bar{w}_v$.

[2]Bevington, P.R. "Data Reduction and Error Analysis for the Physical Sciences ", McGraw-Hill, 1969.